Selected physical properties of liquid grystallime polysiloxanes

Haws, Christine Margaret

SELECTED PHYSICAL PROPERTIES OF LIQUID CRYSTALLINE POLYSILOXANES

A thesis submitted for the Degree of Doctor of Philosophy
in the School of Engineering and Applied Science,
University of Durham

by

Christine Margaret Haws, BSc (Dunelm)

May 1989

DECLARATION

The results described in this thesis are my own work and no part of this thesis has been submitted for any degree in this or any other University.

The following papers have been accepted for publication during the period of study described in this thesis:

1. Dielectric Spectroscopy of Side Chain Siloxane Liquid Crystal Copolymers
   C M Haws, M G Clark, C B McArdle
   Proc. Int. Conf. on Liquid Crystal Polymers, Bordeaux, 6P8, (1987).
   Mol. Cryst. Liq. Cryst., 153, 537-546 (1987)

2. Laser Addressed Thermo-Optic Effect in a Novel Dyed Liquid-Crystalline Polysiloxane.
   C B McArdle, M G Clark, C M Haws, M C K Wiltshire, A Parker, G Nestor, G W Gray, D Lacey, K Toyne
   Liquid Crystals, 2 (5), 573-584 (1987)

3. Information Storage and Erasure Processes in Liquid Crystal Polymer Films
   C B McArdle, M G Clark, C M Haws
   Proc. Eurodisplay, IEE London, 160-163, 15-17 Sept. (1987)

4. Dielectric Spectroscopy of Side Chain Liquid Crystal Copolymers
   C M Haws, M G Clark, C B McArdle
   Proc. Solid State Physics Conference, IoP Bristol, PF, 16-18 Dec. (1987)

5. Dielectric Relaxation Spectroscopy of Liquid Crystalline Side Chain Polymers
   C M Haws, M G Clark, G S Attard
   "Side Chain Liquid Crystal Polymers", Chapter 7, Ed. C B McArdle, (Blackie) (1989)

ABSTRACT

SELECTED PHYSICAL PROPERTIES OF LIQUID CRYSTALLINE POLYSILOXANES

A thesis submitted for the Degree of Doctor of Philosophy by Christine Margaret Haws, May 1989.

The static and dynamic electrical behaviour, the electrical conductivity, the macroscopic viscosity and the optical transmission characteristics of side chain polysiloxane liquid crystal polymers (LCPs) have been studied. Particular emphasis has been placed on the study of the molecular dynamics using dielectric relaxation spectroscopy and the low field (AC) and high field (DC) conductivity, with the intention of relating structural variations to the behaviour of these materials, and of identifying the most appropriate LCPs for use in practical optical storage devices.

The effect on the molecular dynamics of the polymer backbone and the core, spacer and end groups of the mesogenic units was investigated. The LCP responses were shown to be broadly similar to those of low molar mass liquid crystals, though with longer relaxation times. The dynamic responses of structurally different LCPs were shown to be related when these were observed at a temperature referenced to the glass transition temperature. Values of the static permittivity of several LCPs have also been measured and tabulated.

Low field electrical conductivity measurements were used to show that the magnitude of the conductivity was comparable to that of commercial liquid crystals. A method was identified whereby the conductivity of different LCPs could be compared. The texture of the measuring electrode surface was found to play an important role in determining the impedance of electrical double layers formed near the surface of the sample, with smooth polymer based surfactants reducing the formation of space charge. High field DC conductivity measurements showed that Schottky-type charge emission occurred at the electrodes at elevated temperatures, except when the smooth polymer based surfactants were present. This was probably a result of the reduction in the local field near the electrode due to a better physical match at the LCP/surfactant interface.

The bulk viscosity of mixtures of an LCP and commercial liquid crystal were also measured and the results extrapolated to the viscosity of the LCP. The relationship between electrical conductivity and bulk viscosity was examined.

The optical absorption spectra of blue pleochroic dyes have been measured to identify appropriate dyes for use with LCPs in laser written optical memories. The stability of the alignment of selected LCPs with time and temperature was also observed optically.

ACKNOWLEDGEMENTS

I would like to thank Professor M G Clark, my industrial supervisor, and Dr M Petty, my supervisor at the University of Durham, for all their valuable contributions and guidance during the course of this work.

Many members of the Display and Imaging Research Laboratory at the GEC Hirst Research Centre have helped me with suggestions and practical assistance and I gratefully acknowledge their help. I would particularly like to thank Miss Anita Russ for her skilful fabrication of the glass sandwich measurement cells used in this work.

I am grateful to Professor G W Gray and the Liquid Crystal Group at the University of Hull (especially Dr G Nestor and Dr W Hawthorne) for supplying the Liquid Crystal Polymers used in this work. Thanks are also due to BDH Chemicals Ltd. for supplying the liquid crystal C6CN and the dye D102, as well as for dying the mixtures of S2 and GN3/14 referred to in Chapters 6 and 7 of this thesis.

I would also like to thank Dr G Attard, Professor G Williams and Dr A Price (University College of Wales) for useful discussions regarding the measurement and interpretation of the dielectric relaxation spectra of liquid crystals.

GEC Hirst Research Centre gave me permission to undertake this work and has provided generous financial support throughout. The Materials Science Division carried out mass spectrometry analysis and scanning electron microscope photography. I am grateful to Mrs L Ball at HRC for her efficient typing of this thesis.

Finally I would like to thank Ms. J Duncan, Mrs S Wallington and my husband, Stephen, for their moral support during this period of study.

CONTENTS PAGE

APPENDICES

Chapter One

Introduction

This thesis describes a study of selected physical properties of a variety of side chain liquid crystal polymers (LCPs) having polysiloxane backbones. The work was undertaken as part of a programme of collaborative research to assess the properties and applications of these materials. The collaborative partners were GEC Hirst Research Centre, Laser Scan Laboratories and the University of Hull and the programme was partially funded by the Department of Trade and Industry under the Joint Opto-Electronics Research Scheme (Ref:GR/C/8484.2).

The primary application perceived for these LCPs was as the storage medium in high density optical memory devices. Thus, the aims of the work described in this thesis have been the following:

i) To identify the most appropriate LCPs for use in these devices from the wide variety of novel materials that were available.

ii) To measure some of the physical parameters of the LCPs in order to provide information for the development of effective devices.

iii) To understand the influence of structure on the physical properties of the LCPs.

Two main characterisation techniques have been used: dielectric relaxation spectroscopy and DC and AC conductivity measurements. A brief survey of the optical and viscosity behaviour of selected LCPs has also been undertaken.

Dielectric relaxation spectroscopy was used to investigate the effect of structure on the ability of LCPs to reorient in an electric field. These measurements also provided information regarding the anisotropic dielectric permittivity of the LCPs; this determines the electric field strength needed to produce an aligned film. The tendency of these LCPs to mesogenic as opposed to polymeric behaviour has also been investigated.

The mechanism of electrical conduction in high and low field conditions has been studied, as well as the relative magnitude of the conductivity of several LCPs. The conductivity determines the threshold field for dielectric breakdown and influences the design of practical devices. The electric field strengths required to produce well aligned films of these LCPs were ten to twenty times larger than are generally needed for conventional liquid crystals and a tendency to breakdown had been detected in initial samples. Since there was little discussion of the electrical conductivity of LCPs in the literature, a systematic study of this property was considered to be particularly useful.

The main advantages of LCPs over low molar mass liquid crystal as optical storage media are their mechanical flexibility and film forming properties. The bulk viscosity of a typical LCP has been studied to aid the development of effective manufacturing techniques. A preliminary optical investigation of the stability of aligned samples of LCP with respect to temperature and time was also undertaken.

Chapter Two

Liquid Crystals and Liquid Crystal Polymers

2.1 Liquid Crystals

2.1.1 A General Introduction

Matter is usually considered to exist in three phases: solid (amorphous and crystalline), liquid and gas. The liquid crystalline phase is a fourth phase which exists between the solid crystalline phase and the isotropic liquid phase. Materials which can exhibit liquid crystalline phases are often called mesomorphic.

In the nineteenth century organic materials were observed which had no sharp transition temperature between the solid phase and the isotropic liquid phase, even after extensive purification procedures had been carried out. In 1888, Reinitzer observed two distinct melting points for a derivative of cholesterol and subsequently Lehmann (1890) suggested the name "liquid crystal" because of the crystal-like molecular structure of these fluids. Several thousand compounds have now been identified which exhibit mesophases and an essential requirement in all cases is that the constituent molecules have a highly anisotropic shape. The influence of molecular structure on liquid crystalline properties has been discussed by Gray (1966), (1983). Generally the molecules have fairly rigid rod-like structures, but disc shaped molecules can form discotic mesophases.

In moving from the solid phase to a mesophase, a crystal loses its translational order while retaining its orientational order. The degree of order remaining determines the characteristics of the mesophase. According to the classification system proposed by Friedel (1922), three main types of mesophase may be distinguished; these are called nematic, cholesteric and smectic. They are described in more detail in the

following sections. If the transitions between the solid phase, one or more mesophases and the isotropic phase occur over a range of temperatures, the liquid crystal is described as thermotropic. If the mesophase is formed from amphiphilic molecules in an isotropic solution by increasing their concentration in a suitable solvent, then it is described as lyotropic. In this work only thermotropic liquid crystals composed of rod-like molecules have been studied.

The mesophase characteristics are usually best determined by X-ray diffraction (de Vries, 1985) but considerable information can also be obtained by observing the appearance of a thin film of the liquid crystal using a polarising microscope. This appearance is generally termed the 'texture' of the liquid crystal. Each type of mesophase has a distinctive texture, which can also indicate the uniformity of molecular orientation over the sample. This uniformity is prerequisite in many of the applications of liquid crystals (for example, displays, shutters and optical storage devices). The boundary between areas of different orientation is characterised by disclinations (Demus and Richter, 1978).

The anisotropic nature of liquid crystals plays an important role in determining their physical characteristics. The optical, electrical, magnetic and viscoelastic properties are different when measured parallel and perpendicular to the long molecular axis. Several texts are available which review the physical behaviour of liquid crystals (see, for example, de Gennes (1974), Chandrasekhar (1977), Gray (1979), de Jeu (1980)). The

relationship between the values of physical parameters in the mesophase and in the isotropic phase can provide information on the nature of the forces acting between the molecules.

2.1.2 Nematic Liquid Crystals

Nematic liquid crystals exhibit a high degree of long range orientational order, but no long range translational order, as illustrated in Figure 2.1. The long axes of the rod shaped molecules align approximately parallel to one another, the direction of alignment being specified by a unit vector $\underline{n}$ (the director). The long molecular axes are not perfectly aligned but are distributed about $\underline{n}$ due to random thermal fluctuations opposing the orientational ordering. The strength of the orientational ordering can be quantified in terms of an order parameter, S. S=1 for perfectly aligned molecules and S=0 for randomly oriented molecules, such as those in an isotropic liquid. Assuming the molecules to be rigid rods with cylindrical symmetry and the distribution of molecular orientations to be cylindrically symmetric about $\underline{n}$, then the order parameter is an average function of θ, the angle between the long molecular axis and the director:

$$S = \langle 3/2\cos^2\theta - 1/2 \rangle \qquad [2.1]$$

where the angular brackets denote an average over all molecules. In this frame of reference a molecule is oriented at angled (θ,ϕ) with respect to the laboratory axes (x,y,z), where z is parallel to $\underline{n}$ (see Figure 2.2). Nematic mesogens exhibit uniaxial symmetry about the director and the

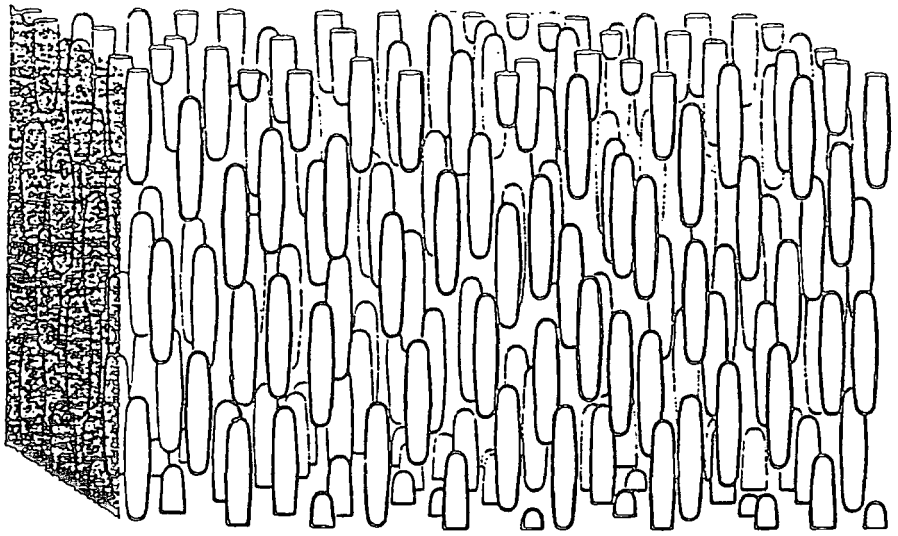

FIGURE 2.1
The nematic liquid crystal structure

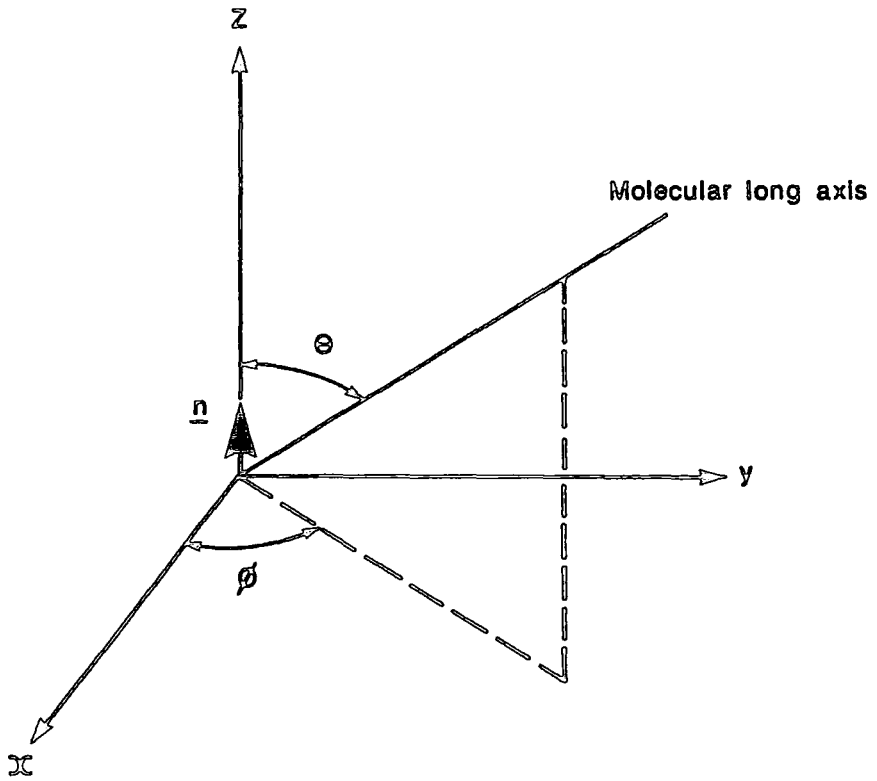

FIGURE 2.2
Molecular orientation (θ,ϕ) with reference to Laboratory axes (x,y,z)

molecules are distributed equally in the "up" and the "down" states (n is equivalent to -n). An example of a nematic liquid crystal is 4-cyano-4-pentylbiphenyl (supplied commercially by BDH Chemicals Ltd as K15):

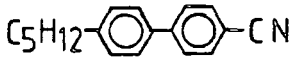

K 24 N 35.3 I

where K,N and I indicate the crystalline, nematic and isotropic phases, respectively, and the figures between these symbols are the phase transition temperatures in degrees Celsius.

2.1.3 Cholesteric Liquid Crystals

The cholesteric mesophase is a special case of the nematic phase and arises when the molecules possess a chiral centre. The system may be envisaged as being composed of parallel planes, in each of which there is a nematic arrangement of the molecules. The director of each sheet is turned through a small angle with respect to adjacent ones. The constant progressive rotation through several sheets results in a helical arrangement (see Figure 2.3). The pitch of the helix depends on the nature of the molecule and external forces and is defined as the distance over which the director rotates through an angle of 2π. Cholesteric structures may also be formed by adding optically active compounds to nematics, in which case the pitch is determined by the amount of additive.

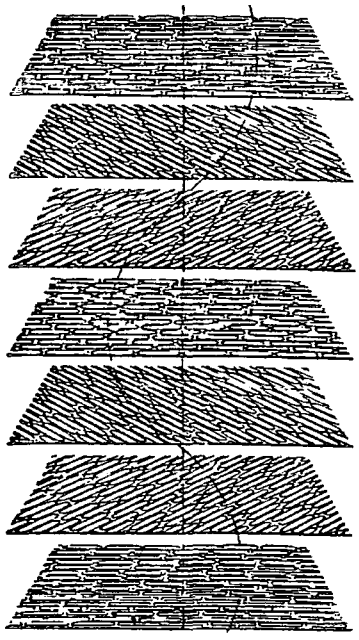

FIGURE 2.3
The cholesteric liquid crystal structure

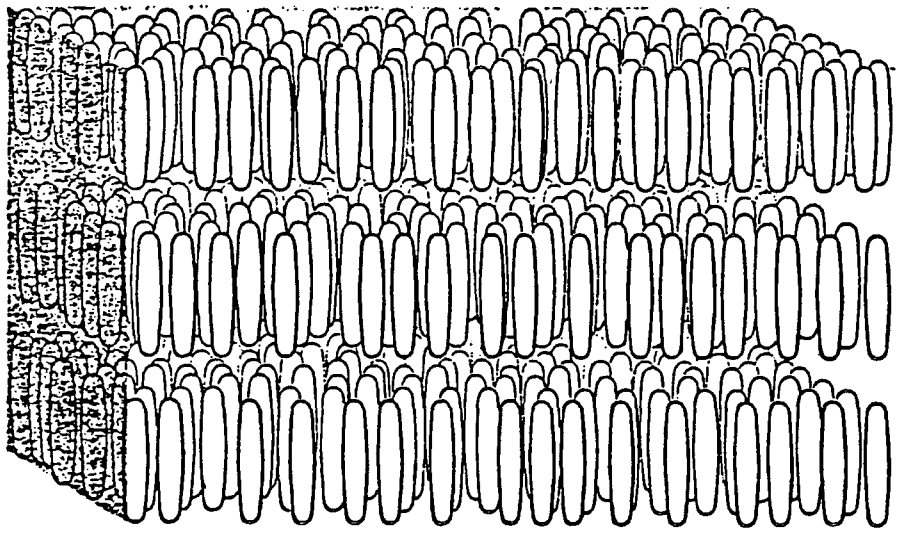

FIGURE 2.4
The smectic liquid crystal structure

An example of a cholesteric liquid crystal is D (or L)-4-methoxybenzylidene-4- (2-methylbutyl)aniline:

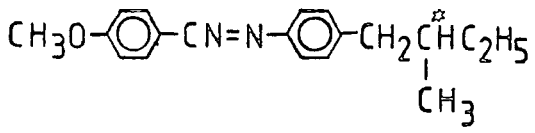

K 21 Ch 24 I

2.1.4 Smectic Liquid Crystals

Smectic phases are generally the most ordered liquid crystal phases. As well as exhibiting orientational order of the long molecular axes, they exhibit translational ordering such that the centres of the molecules tend to align to form layers, see Figure 2.4. There is always a degree of correlation between the layers, but in most cases it is extremely small. Smectic subgroups are distinguished according to the tilt, twist and long range translational ordering of the molecules. They are termed S_A,S_B, S_C...S_K. Smectic A (S_A) and Smectic C (S_C) liquid crystals are the least ordered as there is no regular arrangement of the molecular positions within the layers. The director is parallel to the layer normal in the S_A phase and tilted in the S_C phase. The other subgroups exhibit some degree of crystalline ordering within the layers and so are much less fluid than the S_A and S_C phases. Each smectic phase has a characteristic optical texture.

Generally the more ordered phases occur at lower temperatures. As well as applying to the individual smectic phases, this means that the less ordered nematic or cholesteric phase may occur at higher temperatures. Hence a possible phase sequence is:

solid →← smectic →← nematic or cholesteric →← isotropic liquid

However, under some circumstances re-entrant nematic phases have been observed at temperatures below that required for the smectic phase (Cladis, 1975).

An example of a smectic liquid crystal is 4-cyano-4′-octylbiphenyl (supplied commercially by BDH Chemicals Ltd as K24):

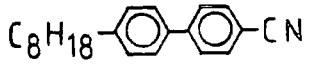

K 21.5 S_A 33.5 N 40.5 I

2.2 Liquid Crystal Polymers

The preparation of comb-like polymers which form thermotropic mesophases was first reported in the late 1970's by Shibaev and Platé in the USSR (Shibaev et al, 1979) and by Ringsdorf, Finkelmann and coworkers in West Germany (Finkelmann et al, 1978a,b). By attaching mesogenic monomers to a flexible polymer backbone, usually via a flexible spacer group, hybrid materials are formed. They exhibit long range orientational ordering of the mesogenic moities and hence the optical, electrical and magnetic behaviour of classical low molar mass liquid crystals (lmmLCs). However,

they retain the good film - forming properties and mechanical advantages of polymers. Many hundreds of liquid crystal polymers (LCPs) have now been synthesised and their properties are summarised in the following reviews: Blumstein (1978); Ciferri, Krigbaum, Meyer (1982); Finkelmann, Rehage (1984); Shibaev, Platé (1984); McArdle (1989).

A polymer can be made to exhibit liquid crystalline behaviour in either (or both) of two ways. If mesogenic monomer units are tied together in a "head-to-tail" arrangement such as to retain the structure of the individual units, then a main chain liquid crystal polymer is produced. If the mesogenic monomer units are tied together in a "head-to-head" arrangement, then a side chain liquid crystal polymer is produced. It is important in both types of structure that flexible elements are present between the mesogenic moieties in order to allow reorientation. This classification of liquid crystal polymers is summarised in Table 2.1.

Liquid crystal polymers exhibit the same mesophase behaviour as lmmLCs, that is they exhibit smectic, nematic and cholesteric phases. The positional and orientational long range order of lmmLCs are related to those of a single molecule, whereas for LCPs they can be related to either the monomer unit or to the macromolecule. A schematic illustration of the chain structure and organisation in nematic and smectic A phases of a side chain liquid crystal polymer is shown in Figure 2.5.

Monomer Unit	
Main Chain Polymer	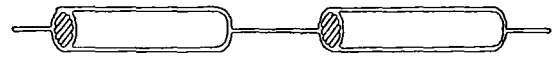
Side Chain Polymer	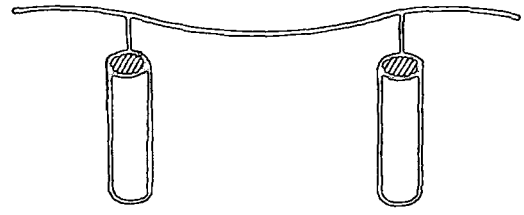
Side Chain and Main Chain (Mixed) Polymer	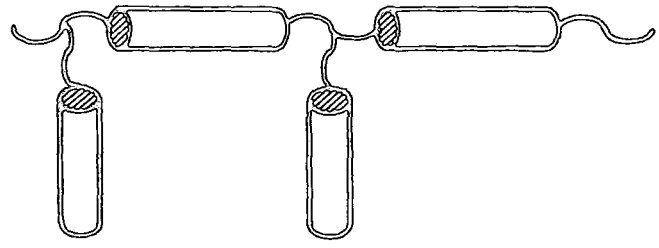

TABLE 2.1
Classification of liquid crystalline polymers

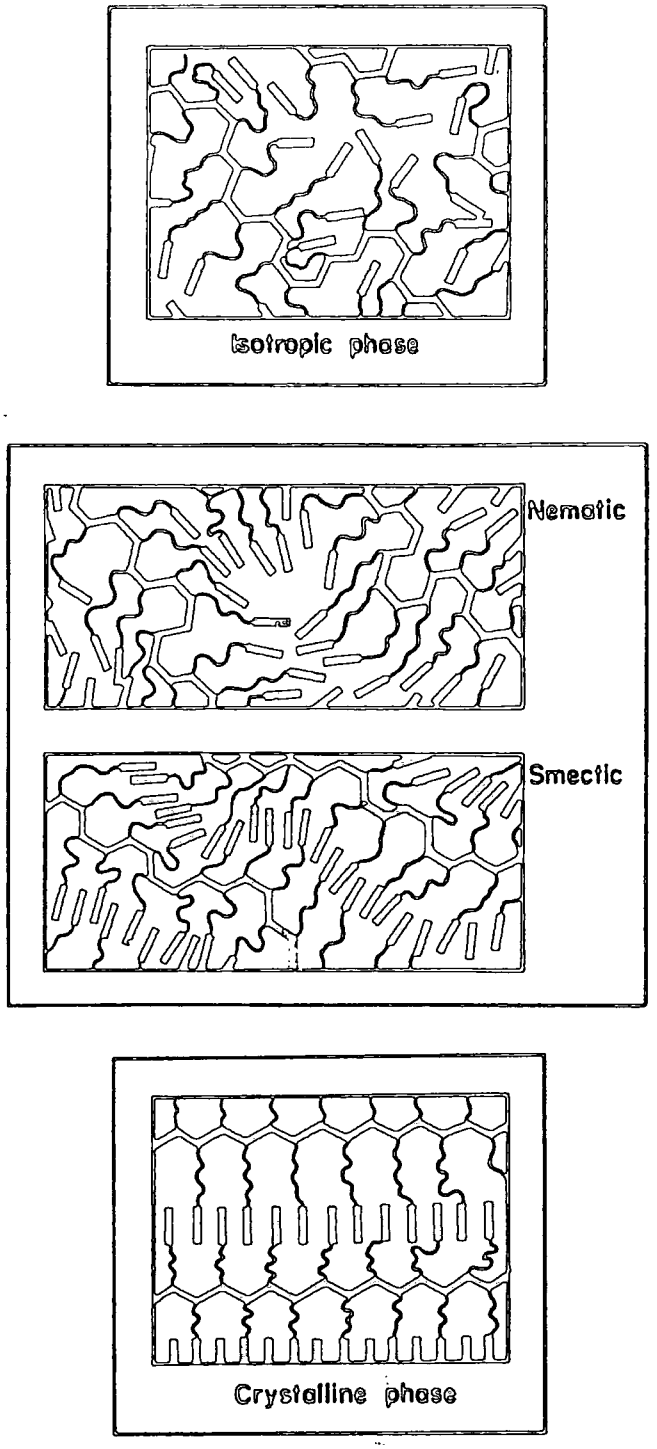

FIGURE 2.5
Schematic illustration of the chain structure and organisation in different phases of a liquid crystalline side chain polymer (from Attard et al (1986a))

2.3 Liquid Crystal Polymers used in this Study

The LCPs used in this work were all thermotropic side chain polymers produced by an addition reaction of a reactive monomer to a polymer backbone in the presence of an appropriate platinum catalyst. In all cases the backbone was a siloxane macromolecule. A wide variety of mesogenic side groups were available for substitution onto the backbone. All materials were synthesised by the Liquid Crystal Group at the University of Hull and their synthetic techniques have been described by Gray et al (1986) and Nestor (1988). Most LCPs were subjected to a rigorous purification procedure involving repeated precipitation from dichloromethane as described by Nestor et al (1987). This procedure removes any unreacted alkene side-chain precursor which had been shown to have a plasticising effect on the LCP (Attard et al, 1987c). The LCPs which were not subjected to this procedure will be clearly indicated in the following Chapters. The LCPs were usually used without further chemical treatment. Again, it will be indicated when this was not the case.

The structures and transition temperatures of the LCPs are summarised in Tables 2.2 to 2.5. The classifications of the LCPs as Methyl-Copolymers, Methyl-Homopolymers, Ethyl-Homopolymers and Cyano-Propyl-Copolymers, respectively, have been used for convenience. In all cases the transition temperatures were measured by differential scanning calorimetry (DSC) at the University of Hull using a scanning speed of 10°C min^{-1}. The transition temperature descriptions have the following form:

General Structure

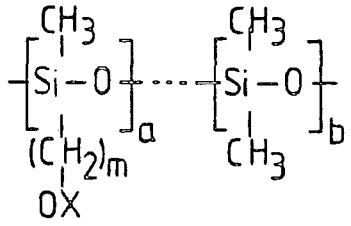

a:b=21:19
a+b= $\overline{DP}$ ~ 35

Code	m	x	Phase Transitions (C)
GN3/3	5	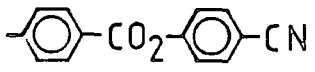	G-9 K 5 S_A 97(82,119) I
GN3/14	6	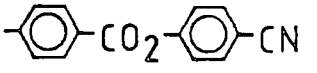	G-12 S_A 85 (78,100) I
GN3/19	5	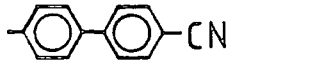	G-14 S_A 95 (87,107) I
GN3/16	8	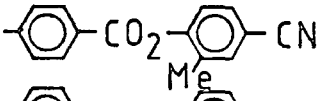	G-15 S_A 57 (51,65) I
GN3/22	6	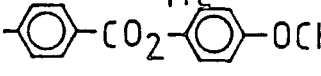	G-15 N 52 (47,57) I
GN3/18	6	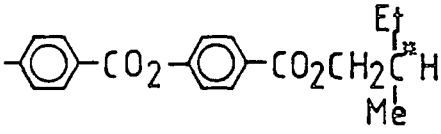	G-25 S_A 30 (22,39) I
GN4/17	5	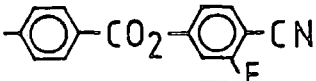	G-14 S_A 80 (73,92) I
GN4/19	6	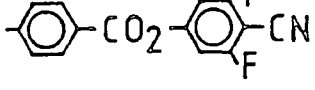	G-19 S_A 78 (72,87) I
GN4/18	5	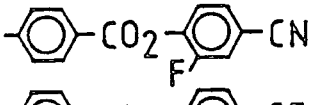	G-4 S_A 65 (58,75) I
GN4/16	6	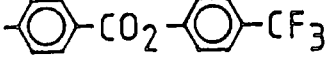	G-3 K 75 S_A 110 (90,136) I
GN4/11	6	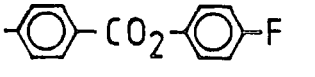	K 39 S_A 72 (58,91) I
GN4/13	5	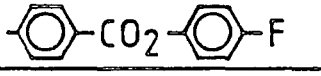	K 38 S_A 72 (59,93) I

TABLE 2.2
Structures and Transition Temperatures of Methyl-Copolymers

General Structure

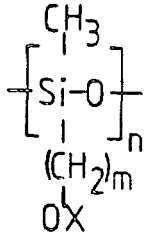

$n = \overline{DP} \sim 35$

Code	m	x	Phase Transitions (C)
GN3/15	8	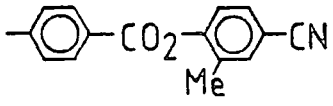	G 5 S_A 95 (91,99) I
GN3/17	6	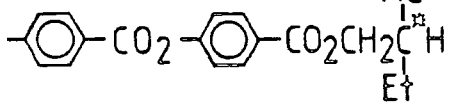	G-9 S_C 76 (63,82) I
GN4/29	5	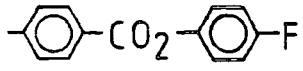	S_A 154 (138,168) I
GN4/33	5	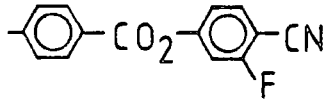	G 6 K 46 S_A 157 (146,167) I
GN2/10	5	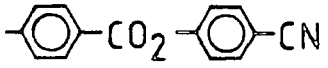	K 84 S_A 162 (149,175) I
GN2/11	6	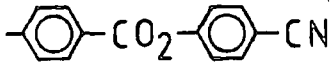	G 8 K 22 S_A 148 (136, 160) I

TABLE 2.3
Structures and Transition Temperatures of Methyl Homopolymers

General Structure

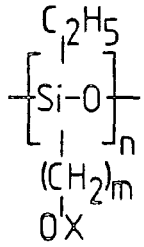

$n = \overline{DP} \sim 35$

Code	m	x	Phase Transitions (C)
GN3/25	6	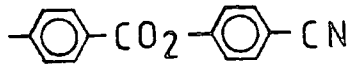	G 3 S_A 116 (106,131) I
GN3/29	5	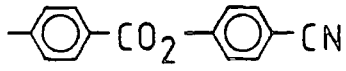	G 8 K 47 S_A 124 (114,143) I
GN3/40	8	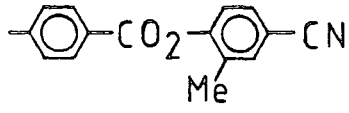	G 1 S_A 80 (74,87) I

TABLE 2.4
Structures and Transition Temperatures of Ethyl-Homopolymers

General Structure

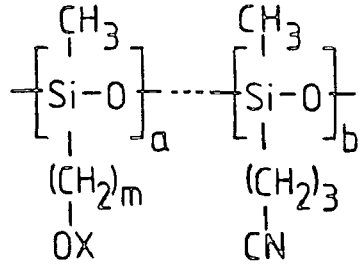

a:b=21:19
a+b= $\overline{DP}$ ~ 35

Code	m	x	Phase Transitions (C)
GN3/36	6	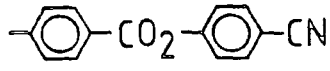	G-13 K 26 (17,38) I
GN3/37	6	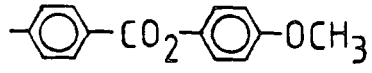	G-16 I
GN3/39	8	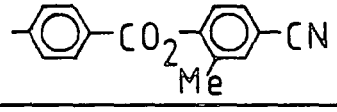	G-23 I

TABLE 2.5
Structures and Transition Temperatures of Cyano-Propyl Copolymers

G	T_g	K	T_m	$S_A/N/Ch/S_C$	$T_c(T_1,T_2)$	I
Glass Phase		Crystalline Phase (some LCPs)		Mesophase		Isotropic Phase

where T_g is the glass transition temperature, T_m is the melting transition temperature, T_c is the clearing temperature, T_1 is the start of the biphasic region and T_2 is the end of the biphasic region. The biphasic region is the temperature range over which the mesophase and the isotropic phase coexist. The clearing temperature is defined from the peak of the DSC trace.

2.4 Applications of Side Chain Liquid Crystal Polymers

A variety of technological applications have emerged in recent years for thermotropic side chain liquid crystal polymers. These materials are not direct replacements for lmmLCs, which have their major application as the active media in various types of display devices (Shanks, 1982). The high viscosities (and therefore long response times) of the LCPs prevent them competing in this market. However, LCPs may be used as electro-optical storage media, as selective optical filters and reflectors, and as dopants for monomeric liquid crystal displays to improve multiplexing capability and performance. Side chain LCPs are also being developed for use in non-linear optical devices (Mölhmann et al, 1989).

The electro-optical properties of LCPs are comparable to those of lmmLCs (see, for example, Tal'roze et al (1983), Finkelmann et al (1983), Haase (1989)). Their optical bistability has been discussed by Koide (1986) and Coles (1985). Electro-optical effects have not been observed below the

glass transition temperature (T_g) and this has resulted in the suggestion that LCPs could be used as storage media (Shibaev et al, 1983, 1985) with the information being written in the liquid crystalline phase and then frozen in as the temperature is lowered below T_g. Coles and Simon (1984) noted that the viscosity of smectic LCPs was sufficiently high that information could be stored above the glass transition without corruption.

The technology required to address liquid crystals using lasers for optical storage applications is now well understood and has been reviewed by Dewey (1984). Various types of lmmLCs have been used, in particular the smectic A cyanobiphenyls. Refinements to the medium, the writing technique, the laser absorbing dyes and the cell construction continue to be reported. Research into alternative liquid crystalline media has also been described, in particular the use of chiral smectic C liquid crystals by Nesrullaev et al (1980) and (as mentioned above) a variety of systems using side chain liquid crystal polymers. Liquid crystal polymers appear to have several advantages in this application since their smectic phases are highly viscous and extend to high temperatures. There is hence a lower risk of the corruption of stored data due to mechanical stress and the films may be exposed to higher temperatures than is typical of devices made from existing low molar mass liquid crystals.

The development of optical storage media and laser addressing techniques using a selection of the side chain polysiloxane LCPs shown in Table 2.2 has been reported by McArdle et al (1987 a,b). Writing, reading, bulk and selective erasure and grey scale have all been demonstrated using a single scanning laser system. Information in the form of optically scattering

lines was written onto homeotropically aligned films of the LCP. Blue pleochroic dyes dissolved in the liquid crystal polymer were used to absorb light at the 632.8 nm Helium-Neon laser wavelength. The mechanism by which information is written and erased using a laser is summarised in Figure 2.6 and Figure 2.7 illustrates the storage of information on a film of GN3/14. As well as this thermo-optic writing on LCPs, erasable holographic optical storage has been described using films of LCP (see for example Eich et al (1986).

The development of optical data storage systems is an important advance in information technology due to the ever increasing need for rapid and efficient data generation, retrieval, processing and storage. The density of information on an optical disk can be up to 10^8-10^{10} bit cm^{-2}, which is equivalent to about 1,200 magnetic floppy disks. The lifetime of optical disks is expected to be considerably longer than the 10 years currently provided by magnetic media. Recording media for optical storage have been compared by Clark (1985b) and by Barrett (1986). The systems which are commercially available are all based on media which are permanently changed by the writing laser, they are read-only systems. Erasable optical systems are being developed based on magneto-optic materials and materials undergoing a reversible phase change between amorphous and crystalline states: the 1mmLC and LCP memory systems described above will be in competition with these erasable systems.

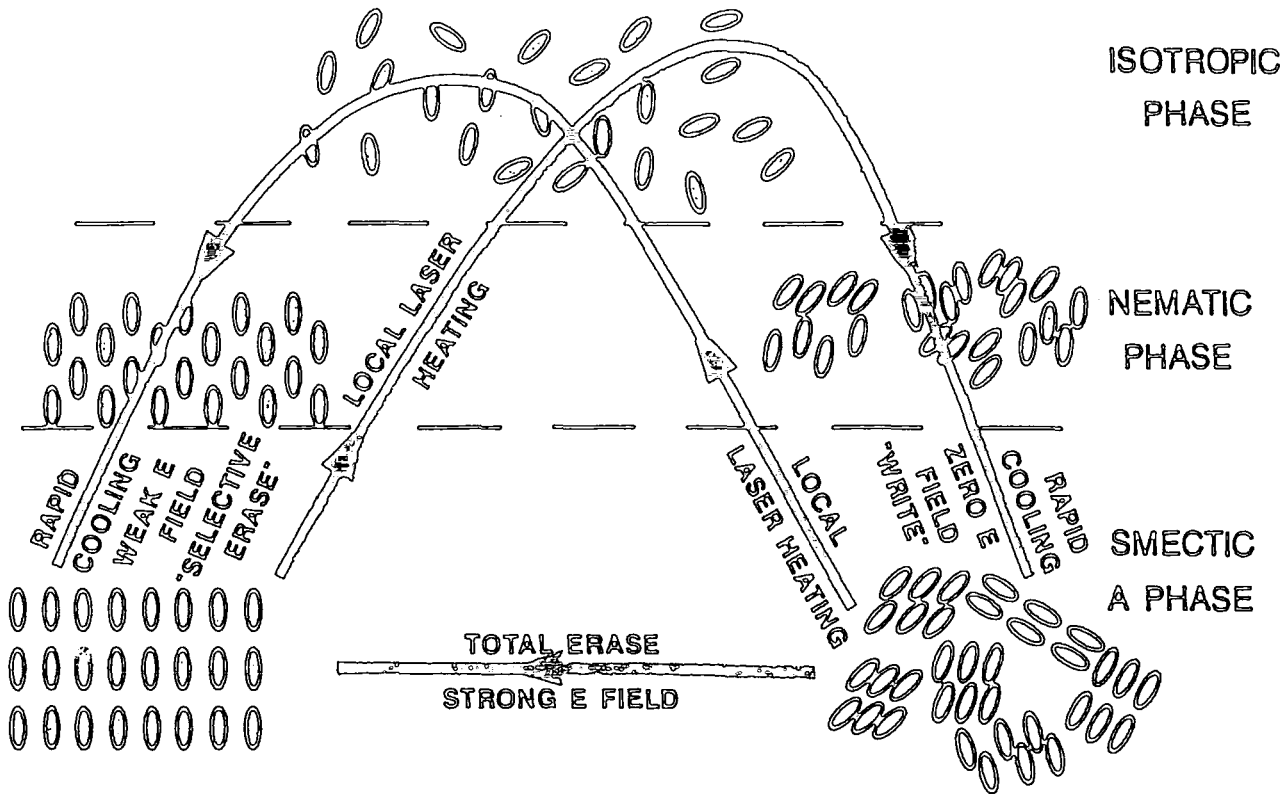

FIGURE 2.6
The mechanism by which information is written on and erased from a film of 1mmLC or LCP using an electric field and a laser

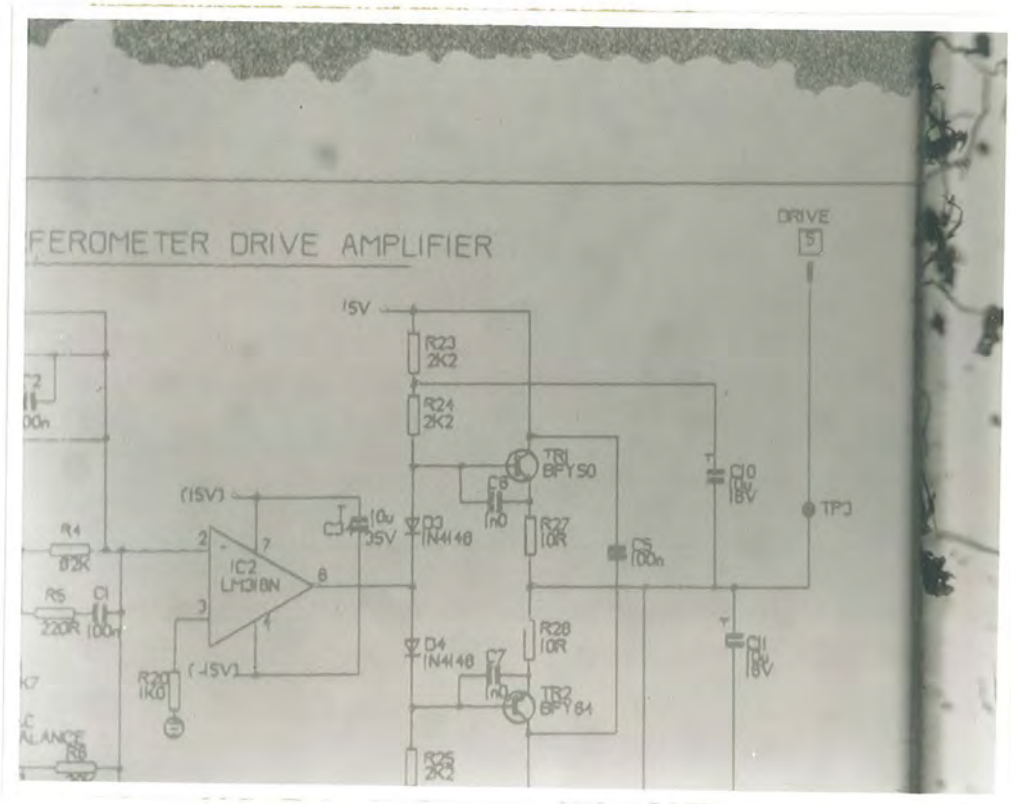

FIGURE 2.7
Part of a circuit diagram laser-written onto homeotropically aligned and dyed GN3/14. The upper part of the photograph shows the off-electrode region which is unaligned.

Chapter Three

Theoretical Background

3.1 Principles of Dielectric Spectroscopy in Mesogenic Materials

In this section, a general description of the response of dielectric media to the presence of a time-dependent electric field will be followed by a more specific discussion of the response of anisotropic materials and, in particular, of liquid crystals. Relaxation describes the irreversible processes which bring a system back to equilibrium after it has been perturbed by an external force. Dielectric relaxation is a special case of the general response of liquid crystals to any relaxation phenomenon.

3.1.1 Dielectric Polarisation

The polarisation of a dielectric material results from the relative shift of positive and negative charges. There are various mechanisms by which polarisation can occur, each of which has a characteristic frequency. The energy absorbed by the polarising species is a maximum at these frequencies; this may be measured by the quantity $\epsilon''(\omega)$, which corresponds to a conductivity

$$\sigma(\omega) = \omega\epsilon''(\omega) \qquad [3.1]$$

There is an enhancement of the permittivity $\epsilon'(\omega)$ of the material at the characteristic frequency and all lower frequencies; at higher frequencies the polarised species cannot move rapidly enough to have an effect. Figure 3.1 illustrates the predicted variations of permittivity with frequency for a simple dielectric.

If the molecules of the dielectric have a permanent moment, then dipolar polarisation may be observed. The dipole moments are randomly arranged so

that in the absence of an external electric field, the net polarisation vanishes. On application of a field, alignment of the molecular dipoles occurs as a slight adjustment of their average orientations in the presence of continued thermal agitation.

If the dielectric permittivity is measured a sufficiently long time after the field is applied, then equilibrium will be achieved and the maximum polarisation which can be observed in the presence of continued thermal agitation will be measured. This is the static dielectric permittivity, ϵ_S. In contrast, when the polarisation is measured immediately after the field is applied, allowing no time for dipolar reorientation, then the measured permittivity is low. This is the optical dielectric permittivity ϵ_∞ and is due to deformational effects alone. Between these two extremes there is a dispersion of the measured dielectric permittivity and this is used to quantify the relaxation of the molecular dipoles due to the perturbing electric field.

The permittivity and loss phenomena are described in a unified way by generalising the permittivity to become a complex function of frequency, $\omega/2\pi$:

$$\epsilon^*(\omega) = \epsilon'(\omega) - i\epsilon''(\omega) \qquad [3.2]$$

The ratio of the real part, ϵ', to the permittivity of free space, ϵ_0, is commonly referred to as the "dielectric constant".

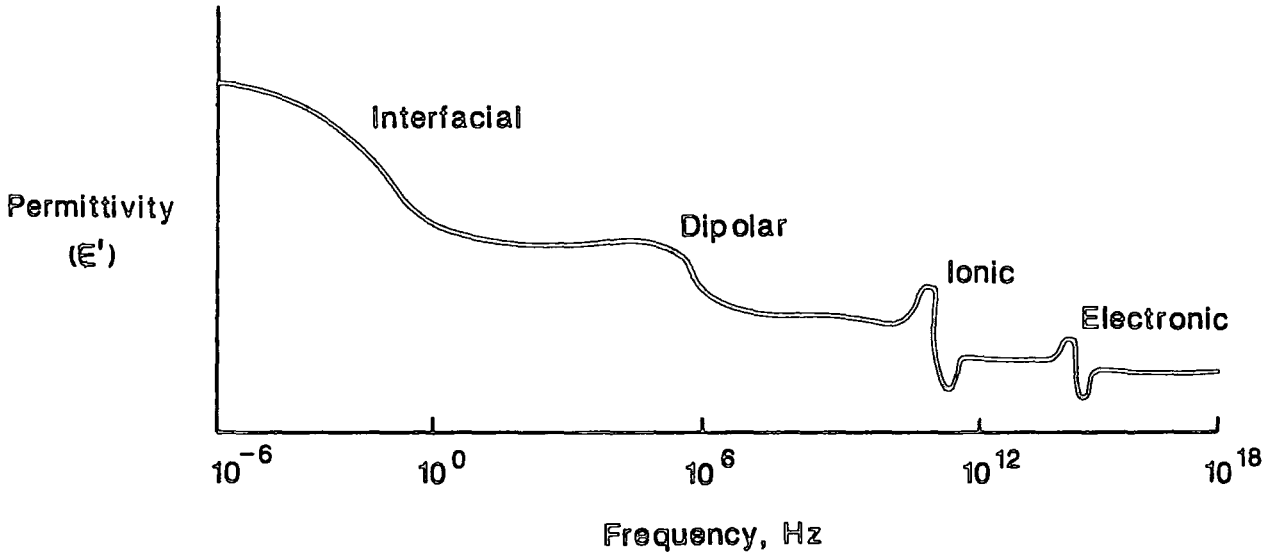

FIGURE 3.1
The predicted variation of permittivity with frequency for a simple dielectric

Dipolar polarisation was originally treated by Debye (1929). He considered polar molecules floating freely in a non-polar fluid with no restoring forces on them and subject to random thermal agitation. The frequency dependence of the complex permittivity due to a relaxation with frequency ν_R is then

$$\epsilon' = \epsilon_\infty + (\epsilon_s - \epsilon_\infty)/(1+\omega^2\tau^2) \qquad [3.3]$$

$$\epsilon'' = (\epsilon_s - \epsilon_\infty)\omega\tau/(1+\omega^2\tau^2) \qquad [3.4]$$

where

$$\nu_R = (2\pi\tau)^{-1} = \omega_R/2\pi \qquad [3.5]$$

Figure 3.2 shows ϵ' and ϵ'' plotted against ln (ω), together with a plot of the AC conductivity $\sigma = \omega\epsilon''$.

The behaviour of most dielectric materials departs to varying extents from this Debye response due to electrostatic interactions between molecules. Most systems are best described using a distribution of relaxation times rather than a single value. A variety of empirically derived descriptions of relaxation behaviour have been suggested, including those of Cole and Cole (1941), Fuoss and Kirkwood (1941), Davidson and Cole (1951), Williams and Watts (1970). These are discussed in detail by Daniel (1967) and Böttcher and Bordewijk (1978).

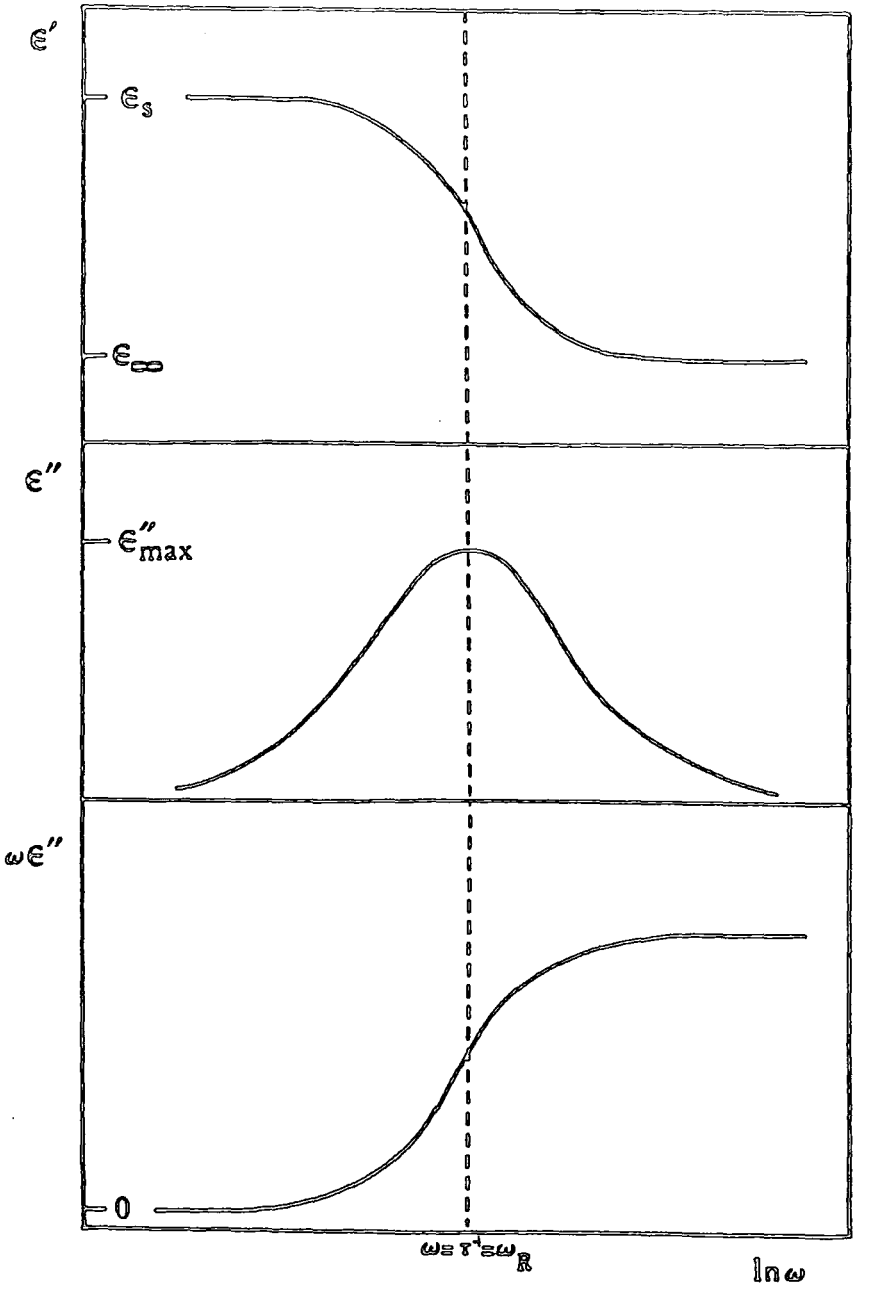

FIGURE 3.2
Schematic plots of real (ϵ') and imaginary (ϵ'') permittivity and AC conductivity, $\sigma = \omega\epsilon''$, against frequency

3.1.2 Molecular Models of Dielectric Relaxation

The molecular factors that determine the dielectric properties of liquid crystalline materials may be described using statistical mechanical theories. These model the molecular physics of anisotropic fluids and are a basis for the interpretation of data from experiments which probe the dynamics of orientational motions. Such experimental techniques include dielectric relaxation spectroscopy, nuclear magnetic resonance and electron spin resonance.

The basis of all spectroscopic measurements is the interaction between an external field and the molecules of the sample under investigation. In laboratory-fixed axes this interaction energy (H′) can be written

$$H' = \sum_{L=0}^{\infty} F^{(L)} \bar{X}^{(L)*} \qquad [3.6]$$

where $\underset{\sim}{F}^{(L)}$ is a field tensor of rank L and $\underset{\sim}{X}^{(L)}$ is the corresponding material susceptibility. The asterisk denotes complex conjugate and the overbar averaging over the molecular orientational distribution. If the orientational distribution is isotropic, all $\bar{\underset{\sim}{X}}^{(L)}$ with L>0 vanish. Molecular orientations are completely specified when the Euler angles, $(\alpha,\beta,\gamma) = \Omega$, which relate the laboratory fixed reference frame to the molecular axis system, are known. Then any orientation dependent molecular quantity can be described by the Wigner rotation matrix element $D^{L}_{m,n}(\Omega)$. The orientationally averaged material susceptibility is hence related to the molecular susceptibility $\underset{\sim}{X}^{(L)}_{mol}$ by

$$\overline{X^{(L,n)}} = \sum_{m=-L}^{L} X_{mol}^{(L,m)} \overline{D_{m,n}^{L}} \qquad [3.7]$$

where n,m describe the 2L+1 components of the tensors in a spherical basis.

Following the removal of the external field, the system will return to its initial unperturbed equilibrium state. The dissipation of the excess energy occurs via the rotational motions of the molecules, and assuming that the field is removed at, say, time t=0, the dynamics of the dissipation process are contained in the macroscopic time correlation function:

$$\overline{X^{(L,n)}(0)^{*} X^{(L,m)}(t)} \qquad [3.8]$$

Within the limits of linear response theory, this can be related to molecular properties using the angular autocorrelation functions $g_{m,n}^{L}(t)$:

$$\overline{X^{(L,n)}(0)^{*} X^{(L,n)}(t)} = \sum_{m} X_{mol}^{(L,m)*} X_{mol}^{(L,m)} g_{m,n}^{L}(t) \qquad [3.9]$$

assuming the symmetry conditions associated with a nematic fluid of rod-like molecules. This results in a definition of $g_{m,n}^{L}$ as:

$$g_{m,n}^{L}(t) = \overline{D_{m,n}^{L*}(\Omega_o) D_{m,n}^{L}(\Omega_t)} - \overline{D_{m,n}^{L*}} \; \overline{D_{m,n}^{L}} \qquad [3.10]$$

The spectral density determine the shapes, amplitudes and frequency locations of the spectral lines and is defined as the cosine Fourier transform of g(t):

$$j^L_{m,n}(\omega) = \frac{1}{2} \int_{-\infty}^{\infty} g^L_{m,n}(t) \exp(-i\omega t)dt \qquad [3.11]$$

To a first order approximation, Equation [3.10] can be factored into an amplitude part, $A^L_{m,n}$, and a temporal part, $\psi^L_{m,n}(t)$:

$$g^L_{m,n}(t) = A^L_{m,n}\psi^L_{m,n}(t) \qquad [3.12]$$

where

$$A^L_{m,n} = \{\overline{D^{L*}_{m,n}D^L_{m,n}} - \overline{D^{L*}_{m,n}}\ \overline{D^L_{m,n}}\} \qquad [3.13]$$

The $\psi^L_{m,n}(t)$ are functions of the various time constants ($\alpha^L_{m,n}$) which characterise the motions responsible for the dissipation of the perturbing energy. This factorisation follows readily when a specific model for the motion is adopted. Nordio, Rigatti and Segré (1973) modelled small-step rotational diffusion of rigid rods in a nematic potential in which the temporal function was:

$$\psi^L_{m,n}(t) = \exp\{-t\alpha^L_{m,n}\} \qquad [3.14]$$

Here the $\alpha^{L}_{m,n}$ are functions of the orientational order parameter S and this relationship allows the temperature dependence of the fundamental frequencies of the spectral absorption curves to be determined.

The general description of relaxation phenomena may be applied to dielectric relaxation when an electric field interacts with permanent dipoles in the molecules. In this case L=1 and Equation [3.6] becomes:

$$H = \sum_{m} F^{(1,m)} \overline{\mu^{(1,m)*}} \qquad [3.15]$$

where the $\mu(1,m)$ are the spherical-basis components of the mean macroscopic dipole moment. The dynamics of the permanent dipoles are therefore contained in the dipole moment autocorrelation functions:

$$\overline{\mu^{(1,m)*}(0)\mu^{(1,m)}(t)} \qquad [3.16]$$

The electric field can be parallel or perpendicular to the director, in which case $\mu_{\parallel}$ and $\mu_{\perp}$ are the electric dipole moments in these directions, respectively. The molecular electric dipole moments longitudinal and transverse to the long molecular axis are μ_l and μ_t, respectively. Then using Equation [3.9]

$$\overline{\mu_{\parallel}(0)\mu_{\parallel}(t)} = \mu_l^2 g^1_{0,0}(t) + \mu_l^2 g^1_{0,1}(t) \qquad [3.17]$$

$$\overline{\mu_{\perp}(0)\mu_{\perp}(t)} = \mu_l^2 g^1_{1,0}(t) + \mu_l^2 g^1_{1,1}(t) \qquad [3.18]$$

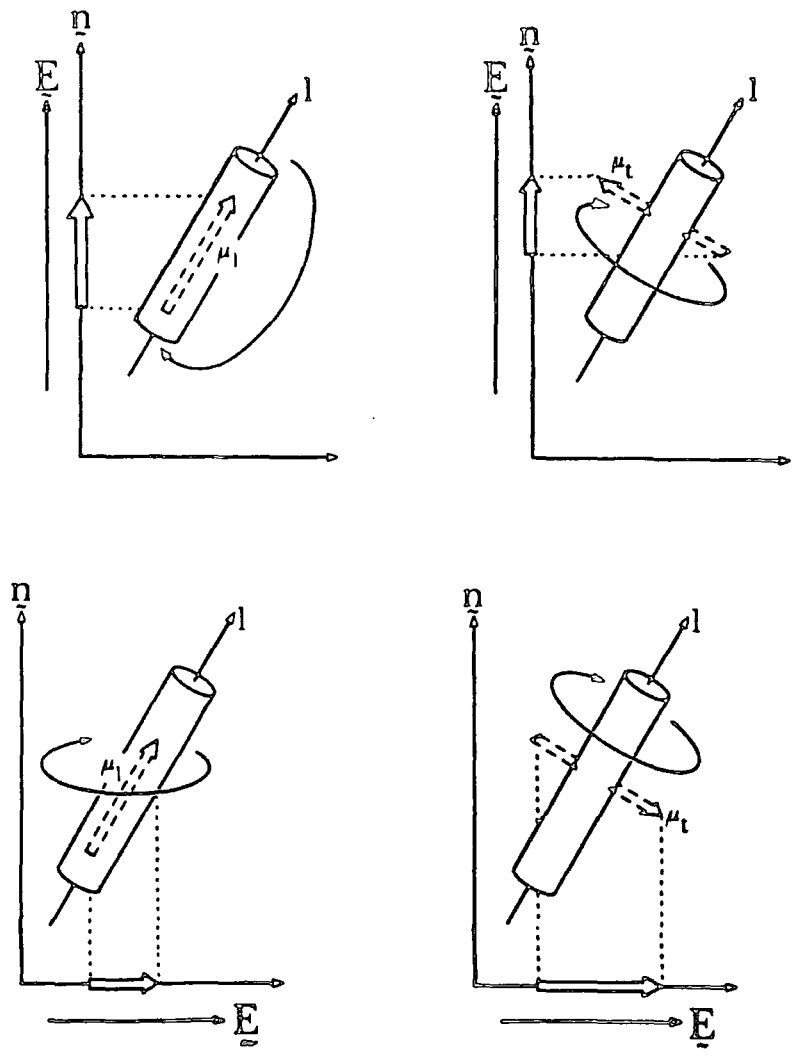

FIGURE 3.3
Rotational diffusion modes leading to dielectric relaxation in nematic liquid crystals. The molecular 'long axis' is denoted by $\underline{l}$

where the $g^1_{m,n}(t)$ are the angular autocorrelation functions. In the diffusion model, $\underline{D}$ is the molecular rotational diffusion tensor. Assuming $\underline{D}$ to be axially symmetric with principal components $D_\perp$ and $D_{||} = kD_\perp$, then Equation [3.12] can be used to express $g^1_{m,n}(t)$ as the following infinite series:

$$g^1_{m,n} = \sum_{p \neq 0} |M^p_{m,n}|^2 \exp(-\alpha^p_{m,n} D_\perp t) \qquad [3.19]$$

Where $M^p_{m,n}$ are matrix elements of the rotational diffusion eigen-functions.

Figure 3.3 illustrates the rotational motions corresponding to the modes (m,n), where

$$(0,0) = (||, l) \qquad (0,1) = (||, t)$$
$$(1,0) = (\perp, l) \qquad (1,1) = (\perp, t) \qquad [3.20]$$

Each mode is a sum over many exponential processes with characteristic relaxation times τ_p, where

$$1/\tau_p = \alpha^p_{m,n} D_\perp \qquad [3.21]$$

Equation [3.19] may be solved numerically and Figure 3.4 shows a plot of the coefficient $\alpha^p_{m,n}$ against order parameter S for an anisotropic diffusion tensor (k=11) (Clark, 1988). It can be seen that the curve for $\alpha^1_{0,0}(||, l)$ drops

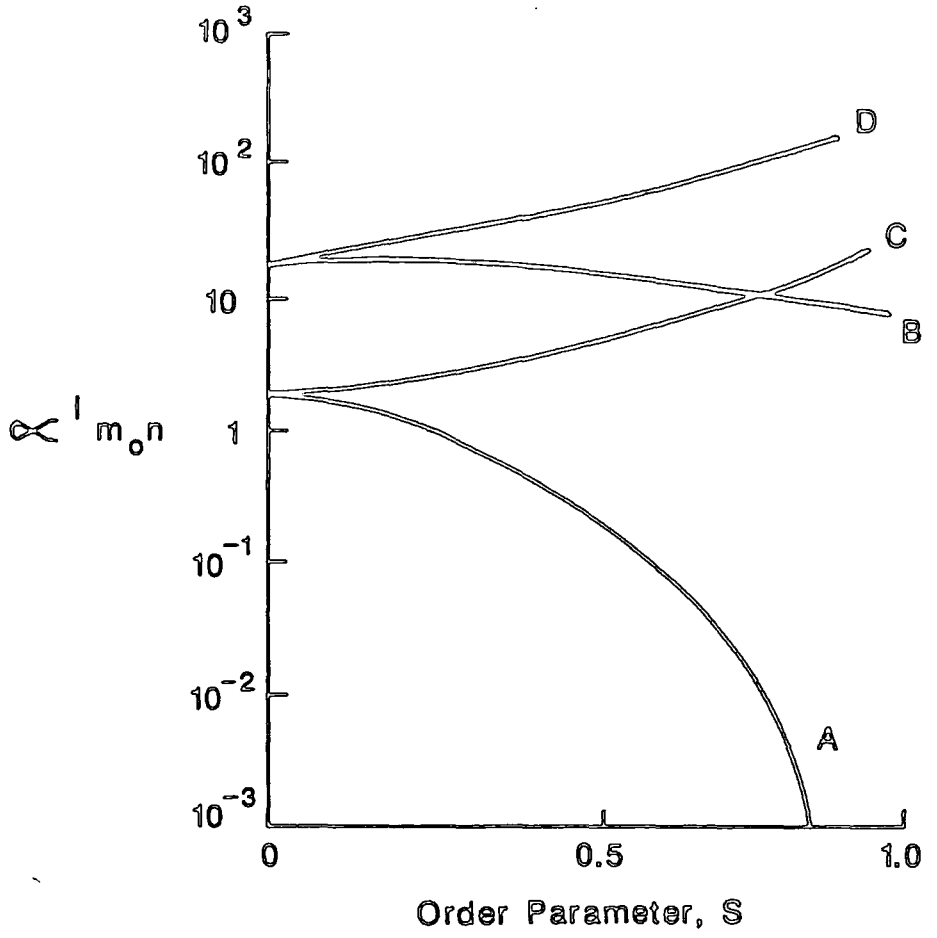

FIGURE 3.4

Plots of the coefficient $\alpha^{l}_{m,n}$ against the molecular order parameter S for an anisotropic rotational diffusion tensor $D_{\parallel}/D_{\perp} = k = 11$

A m,n = 0,0
B m,n = 1,1
C m,n = 1,0
D m,n = 0,1

rapidly with increasing S, becoming isolated from the other $\alpha^1_{m,n}$ curves. The leading term alone is a reasonable approximation for $g^1_{0,0}$, resulting in a Debye-like form for this relaxation. The low frequency of the $(||, l)$ mode for large S is in accordance with rotational diffusion against the nematic potential. The theory successfully accounts for the characteristic dielectric spectrum of nematics, namely an exceptionally low frequency relaxation in $\epsilon_{||}$ (associated with $\mu_1 \neq 0$) which has an accurately Debye-like form, despite occurring in a highly anisotropic fluid, together with a broader relaxation (being a mixture of several terms) which appears in both $\epsilon_{||}$ and $\epsilon_{\perp}$, provided both μ_1 and μ_t are non-zero.

3.1.3 Local Field Corrections

To relate these molecular processes to the macroscopic permittivity, $\underline{\epsilon}(\omega)$, the effect of the internal electric field actually experienced by the molecule has to be considered. For values of the permittivity much greater than 1, the difference between the vacuum field and the internal field has a considerable influence. There have been several approaches to describing this effect, including those by Luckhurst and Zannoni (1975) and Madden and Kivelson (1984). A frequently used description of the molecular factors determining $\underline{\epsilon}(\omega)$ is that of Maier and Meier (1961) who extended the description of the isotropic liquid phase by Onsager (1936) to the nematic phase by introducing the concept of an order parameter S to take into account the anisotropy.

Onsager treated the molecule as a polarisable point dipole at the centre of a spherical cavity. This was embedded in an isotropic continuum which exhibited the macroscopic dielectric properties. The local field was then the sum of the field produced in the empty cavity by the applied field, and the reaction field in the cavity resulting from the polarisation of the surrounding continuum by the dipole. The expression for the permittivity became:

$$\epsilon = 1 + NhF(\bar{\alpha} + F\mu^2/(3k_BT))/\epsilon_o \qquad [3.22]$$

where h is the cavity field factor, F is related to the reaction field, N is the number of molecules per unit volume, k_B is Boltzmann's constant and $\bar{\alpha} = (\alpha_l + 2\alpha_t)/3$; α_l and α_t are the polarisability components parallel and perpendicular to the long molecular axis, respectively.

Maier and Meier described the anisotropic components of polarisability and permittivity of nematic liquid crystals as follows:

$$\alpha_{\parallel} = (\bar{\alpha} + 2\Delta\alpha S/3)$$
$$\alpha_{\perp} = (\bar{\alpha} - \Delta\alpha S/3) \qquad [3.23]$$

where $\Delta\alpha = (\alpha_l - \alpha_t)$

similarly

$$\mu_{\parallel}^2 = (\mu_l^2(2S + 1) + \mu_t^2 (1 - S))/3$$
$$\mu_{\perp}^2 = (\mu_l^2 (1 - S) + \mu_t^2 (2 + S)/2)/3 \qquad [3.24]$$

Substituting Equations [3.23] and [3.24] into [3.20] gives the Maier-Meier equations.

$$\epsilon_{\parallel} = 1 + (NhF/\epsilon_o)\left\{\bar{\alpha} + \frac{2}{3}S\Delta\alpha + (F/3k_BT)[\mu_l^2(1+2S) + \mu_t^2(1-S)]\right\} \qquad [3.25]$$

$$\epsilon_{\perp} = 1 + (NhF/\epsilon_o)\left\{\bar{\alpha} - \frac{1}{3}S\Delta\alpha + (F/3k_BT)\left[\mu_l^2(1-S) + \mu_t^2\left(1+\frac{1}{2}S\right)\right]\right\} \qquad [3.26]$$

These equations correspond to [3.17] and [3.18] written in terms of the second rank order parameter S. Then $\mu_l^2(1+2S)$, $\mu_l^2(1-S)$, $\mu_t^2(1-S)$ and $\mu_t^2\left(1+\frac{1}{2}S\right)$ correspond to the modes $(\parallel, l)$, $(\parallel, t)$, $(\perp, l)$ and $(\perp, t)$ respectively. The values of μ_l, μ_t and S may be calculated from the dielectric decrements, as shown by Bone et al (1984).

The molecular field models of relaxation described in this section were developed for nematic liquid crystals. However, to a good approximation they may be applied to the smectic A phase since the long range spatial periodicity of this phase is not involved in the dipole moment relaxations, though it does influence the internal field. This means that there is continuity in passing between nematic and smectic A phases, with only slight changes in the permittivities and relaxation frequencies. The

study of such variations, together with the changes when passing from the mesophase to the isotropic phase, provides information on the anisotropic molecular environment (Bradshaw and Raynes, 1983).

There has also been a fundamental assumption in the theories described above, that the LC media are composed of rigid rod-like particles. Both real lmmLCs and LCPs are neither rigid nor rod-like. In most materials, however, the permanent dipoles are coupled to semi-rigid mesogenic moieties. The low symmetry of such moieties can be accounted for by including additional order parameters in the model. It is therefore reasonable to apply these models to interpret the dielectric relaxation spectra of polymeric side chain liquid crystals, with the assumption that a flexible spacer effectively decouples the mesogenic side groups from the polymeric backbone. Theories of dielectric relaxation in classical polymers focus on the cooperative motions of permanent dipoles associated with sites on the chain (Böttcher and Bordewijk, 1978). They also rationalise the observation of broad relaxations composed of a distribution of relaxation times, but it is very difficult to use them to interpret amplitude data. Similarities of approach do exist, however, between polymeric and mesogenic models. For example, the calculation of the permittivity of semicrystalline polymers (Boyd, 1983) is analogous to that required for an anisotropic partially ordered medium such as an LCP.

3.2 Mechanisms of Electrical Conductivity

All materials conduct electricity to a greater or lesser extent and all breakdown in a sufficiently strong electric field. For low field strengths the conduction process in many materials is ohmic, but as the

field strength is increased, the conductivity usually becomes field dependent and eventually some form of destructive, irreversible, breakdown takes place. The interpretation of low frequency or DC conductivity data for dielectrics in terms of underlying mechanisms is complicated by the fact that several processes may coexist, or even interact with each other.

3.2.1 Ionic Conductivity

Low frequency conductivity phenomena in organic materials often arise from the presence of ionic species. Polar materials tend to induce partial dissociation of these extrinsic impurities. Application of an AC electric field, whose period is long compared with the diffusion time of the ions, results in polarisation due to charge motion. The most definitive evidence for ionic conduction is the detection of electrolysis products formed on discharge of the ions as they arrive at the electrodes. However, in most materials the degree of conductivity is sufficiently low to make such measurements impractical. Charges coming into contact with the electrodes may either be removed by electrochemical reactions or, if they cannot react, they may form a space-charge layer at the interface. This means that the resistivity of the film at constant DC voltage increases with time since most of the applied voltage is dropped across the space charge regions. The true ionic conductivity is then the initial conductivity.

In the absence of space-charge layers, and for low fields, charge recombination gives rise to an ohmic relation between the applied voltage and the resulting current due to ionic charge carriers. At higher fields,

charge generation by dissociation may not keep pace with the increasing voltage and hence the I-V curve will exhibit a plateau. Generally, low field ionic conductivity can be described by the equation:

$$\sigma = \sigma_o \exp(-\phi/k_B T) \qquad [3.27]$$

where σ_0 and ϕ are experimentally determined. Ionic conduction processes under low field conditions in solid dielectrics are discussed in more detail by O'Dwyer (1973), Lamb (1967) and Blythe (1979).

A strong correlation between dielectric permittivity and conductivity may be observed in ionic materials. The reduction of Coulombic forces between ions in a high dielectric constant medium results in the dissociation energy being inversely proportional to the static dielectric constant, ϵ_S. This explains the frequently observed enhancement of conductivity by the absorption of water.

3.2.2 Schottky and Poole - Frenkel Emission

In addition to ionic conductivity, at higher fields the emission of carriers can occur. Generally the mechanism for this is either Schottky emission from the metal electrode or Poole-Frenkel emission from localised impurity states. The high fields which can be obtained across thin insulating films can result in the emission of electrons from the metal contact at negative potential into the conduction band of the insulator. This Schottky effect corresponds to thermal activation of electrons over the metal-insulator interface potential barrier, with the added effect that the applied field results in an image force lowering of

the height of this barrier, as shown in Figure 3.5 (also see Lamb, (1967)). The Poole-Frenkel effect is based on the lowering of the potential barrier against thermal excitation of trapped electrons into the conduction band of the insulator.

$$I\,(\text{Schottky}) = AT^2 \exp\left[-\left(\phi - \beta E^{\frac{1}{2}}\right)/k_B T\right] \qquad [3.28]$$

$$I\,(\text{Poole-Frenkel}) \sim E \exp\left[-\left(\phi - 2\beta E^{\frac{1}{2}}\right)/k_B T\right] \qquad [3.29]$$

where

$$\beta = (e^3/4\pi\epsilon_0\epsilon_\infty)^{\frac{1}{2}}$$

A is the effective Richardson constant, ϕ is the barrier height or work function, E is the electric field, e is the electronic charge and ϵ_∞ is the high frequency permittivity of the medium. Both processes result in non-Ohmic I-V curves with log (I) linear in $V^{1/2}$. They can be distinguished by studying the temperature response or by varying the film thickness or the electrode material.

A similar emission of charge is observed at high fields from metals in contact with semiconductors rather than insulators. The intrinsic carrier concentration (N_D) of semiconductors means that there is now a built in potential V_{bi} at zero bias at a metal junction, so in the presence of an applied potential, V, the electric field term in Equation [3.28] must be replaced by:

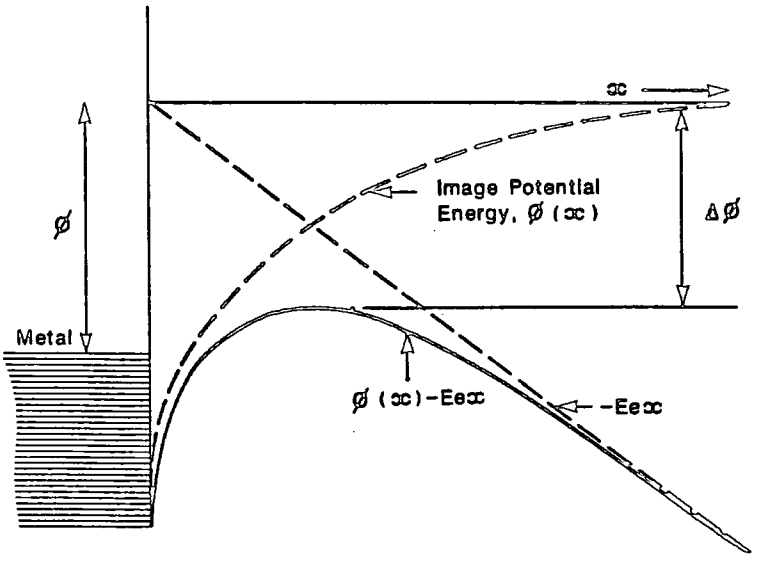

FIGURE 3.5
Image force lowering of the potential barrier in an insulator.
ϕ = metal-insulator work function, Eex = Potential = potential due to uniform electric field, $\Delta\phi$ = barrier lowering to due to the presence of an electric field.

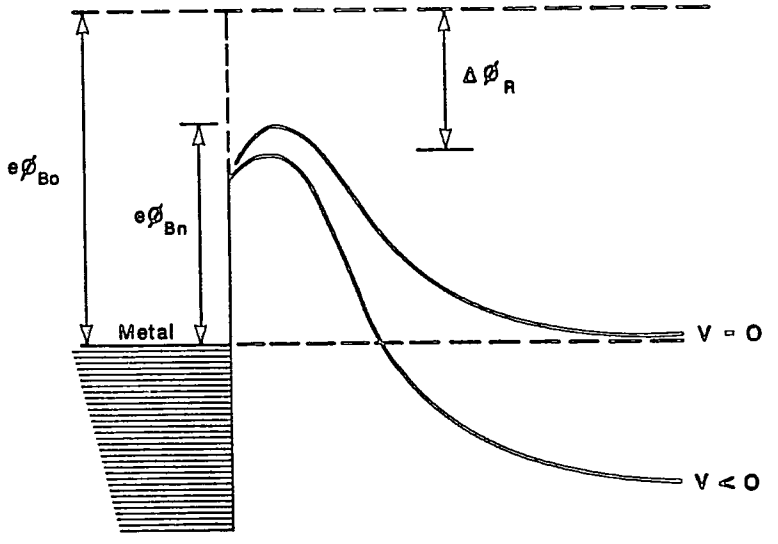

FIGURE 3.6
Image force loweriing of the potential barrier in a semiconductor.
$e\phi_{Bo}$ = intrinsic barrier height, $\Delta\phi_R$ = barrier lowering under reverse bias, $e\phi_{Bn}$ = barrier height at thermal equilibrium.

$$E = \{2eN_D(V + V_{bi} - (k_B T/e))\}^{\frac{1}{2}} \qquad [3.30]$$

and now log(I) is linear in $V^{1/4}$. The energy diagram is illustrated in Figure 3.6. The Schottky effect in semiconductors is discussed in more detail by Sze (1981) and Rhoderick (1978).

3.2.3 Interfacial and Electrode Polarisation

In the absence of surface polarisation effects, DC conductivity affects only the imaginary part of the permittivity, $\epsilon''(\omega)$, causing it to increase rapidly with decreasing frequency (Figure 3.7). This increase has been shown empirically to be proportional to ω^{-n}, where $0<n\leq 1$, and usually n~1 (see for example Jonscher (1983)). The rapid increase in $\epsilon''(\omega)$ with decreasing frequency is a significant feature of the loss spectrum of most LCPs. With increasing temperature it can even mask dielectric relaxation features. In fact, surface polarisation effects are invariably present for organic materials and this polarisation at electrodes becomes most apparent when the sample has an appreciable bulk conductivity. At low frequencies there is a characteristic increase in the apparent dielectric constant (ϵ') which arises from this high impedance layer on the electrode surface since there is sufficient time for even slight conduction through the specimen to transfer the charge carriers to these very thin electrode layers. This has the effect on the equivalent circuit of the sample of placing an electrode impedance Z_{el} in series with the actual capacitance and conduction of the sample film. The experimentally measured apparent permittivity ϵ'_{app} and conductivity $\epsilon"_{app}$ are therefore given by:

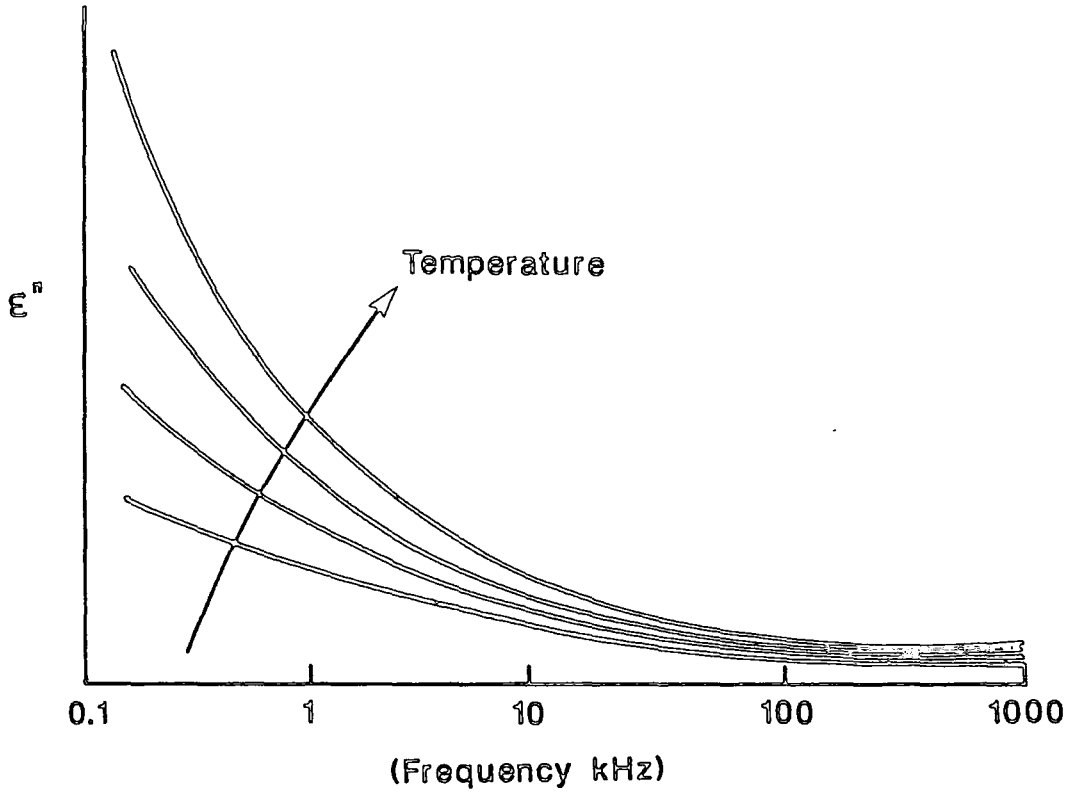

FIGURE 3.7
The influence of surface polarisation on the loss spectrum of an LCP

$$(\sigma_{app} + i\omega\epsilon'_{app})^{-1} = (\sigma + i\omega\epsilon')^{-1} + Z_{el} \qquad [3.31]$$

assuming normalisation to unit empty cell capacitance, (Johnson and Cole, 1951).

If $Z_{el} = Z_0 (i\omega)^{-n}$, $0<n\leq 1$, then Equation [3.31] can be rearranged by equating real and imaginary parts if it is assumed that $Z_0\omega^{-n}\sigma<<1$ and $\omega\epsilon'<<\sigma$ (which usually apply at low frequencies), to give:

$$\sigma_{app} = \sigma - \left(Z_o \cos\frac{1}{2}n\pi\right)\omega^{-n}\sigma^2 \qquad [3.32]$$

$$\epsilon'_{app} = \epsilon' + \left(Z_o \sin\frac{1}{2}n\pi\right)\omega^{-(n+1)}\sigma^2 \qquad [3.33]$$

The value of n is typically unity for a low viscosity liquid, decreasing to ½ for a solid or solid-like material. Both this value and the inequalities yielding the simplified forms in Equations [3.32] and [3.33] must be checked when applying this correction to $\epsilon'(\omega)$ data.

The effect of a space charge layer on a charge-injecting electrode is to enhance the local field, possibly leading to Schottky emission. This effect can be represented by replacing E in Equation [3.28] by γE, where γ is a field enhancement factor (Sessler et al, 1986).

Under conditions such as the presence of inclusions or phase separation, where the sample contains internal interfaces between regions having

different permittivities and/or conductivities, charge accumulation can result in the observation of a dielectric relaxation which is indistinguishable from that due to orientation of dipoles. This is known as a Maxwell-Wagner-Sillars (MWS) process (Böttcher and Bordewijk, 1978; Daniel, 1967). In practice, the MWS peak often occurs at very low frequencies, when it will be hidden under the DC conductivity effects. However, in these circumstances Equation [3.31] and the expression $Z_{el}=Z_0(i\omega)^{-n}$ will no longer be sufficient to describe the measured curves $\epsilon'_{app}(\omega)$ and $\epsilon''_{app}(\omega)$.

More detailed discussions of conductivity phenomena can be found in the reviews by O'Dwyer (1973), Lamb (1967) and Blythe (1979). The preceding brief introduction is generally applicable to isotropic media. It should be noted that the orientational long range order in mesogenic materials results in anisotropic conductivity. However, as will be shown in Chapter 6, studies of the DC conductivity of lmmLCs described in the literature indicate that this anisotropy is not large and the previous discussion may reasonably be used as a guide to the conductivity of lmmLCs and LCPs. There has been no description of electronic transport mechanisms through the bulk of the films since mesogenic structures are generally not inherently conducting. Electronic conduction in molecular solids is discussed in detail by Movaghar (1987).

3.3 Viscosity of Liquid Crystals

Viscosity is the measure of the internal friction of a fluid. This friction becomes apparent when a layer of fluid is made to move in

relation to another layer; that is, to shear. In laminar flow, each layer of fluid moves at a velocity (v) proportional to its distance from the lower plate (see Figure 3.8), hence

$$\frac{\text{Force}}{\text{Area}} = \eta \frac{dv}{dy} \qquad [3.34]$$

where the viscosity, η, is the constant of proportionality. If the viscosity is independent of the velocity gradient, then the flow is described as Newtonian. If the viscosity depends on the velocity gradient, then there is non-Newtonian flow. One of the most common types of non-Newtonian flow is pseudoplastic behaviour (also called shear thinning) in which the viscosity decreases with increasing shear rate (see Figure 3.9).

In a nematic liquid crystal the flow depends on the angles that the director makes with the flow direction and with the velocity gradient. Translational motions are also coupled to inner orientational motions of the molecules, so flow disturbs the alignment and causes the director to rotate. These factors make it difficult to conduct experiments which produce meaningful quantitative results. If it is assumed that the orientation of the director is fixed (for example by a strong magnetic field), then, using the axes defined in Figure 3.10, three limiting cases define the viscosity coefficients (η_1, η_2 and η_3) illustrated in Figure 3.11. These are often called the Miesowicz coefficients (Miesowicz, 1936). The effective viscosity for a fixed director at arbitrary angles θ' and ϕ' is therefore

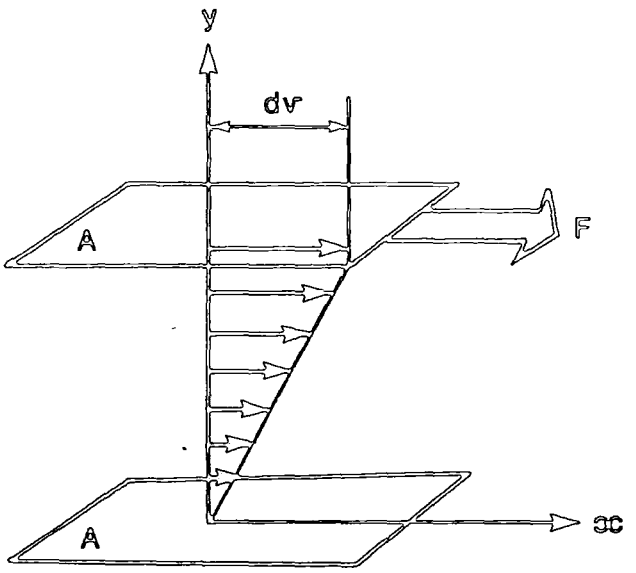

FIGURE 3.8
Schematic diagram showing the principle of laminar flow

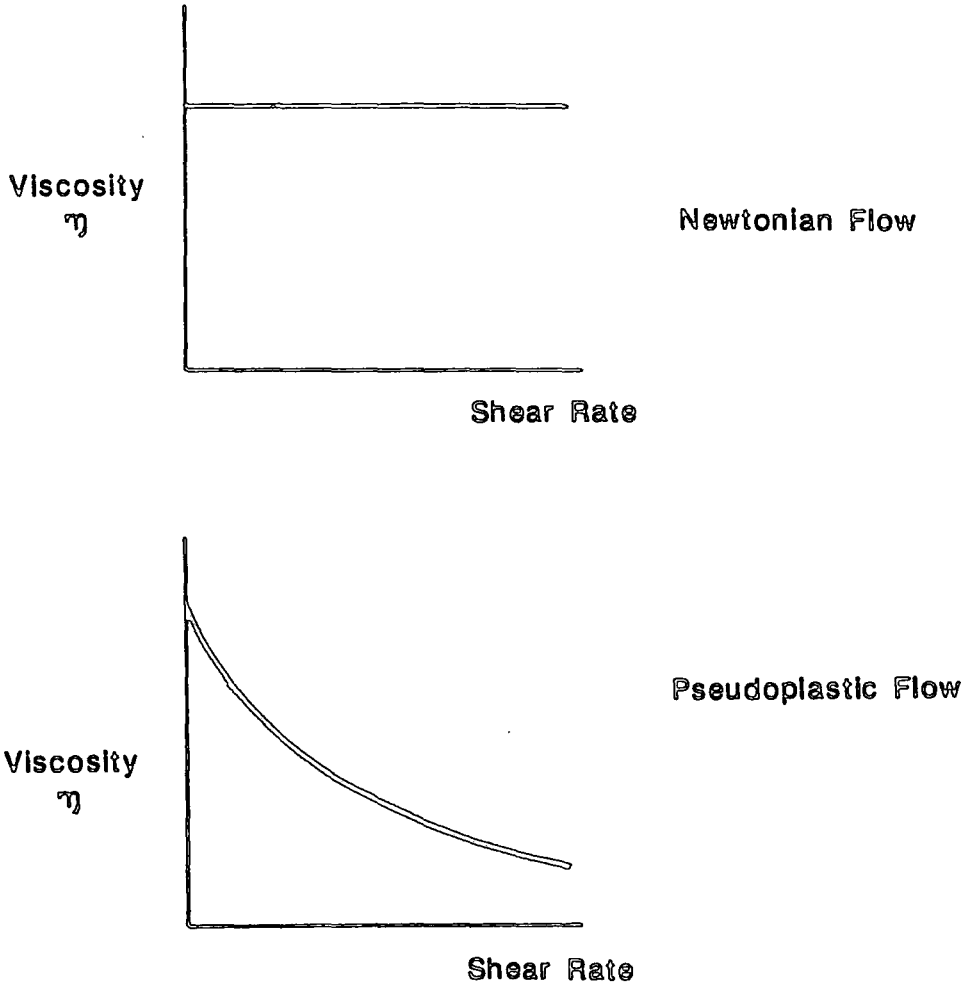

FIGURE 3.9
A comparison of Newtonian and non-Newtonian flow characteristics

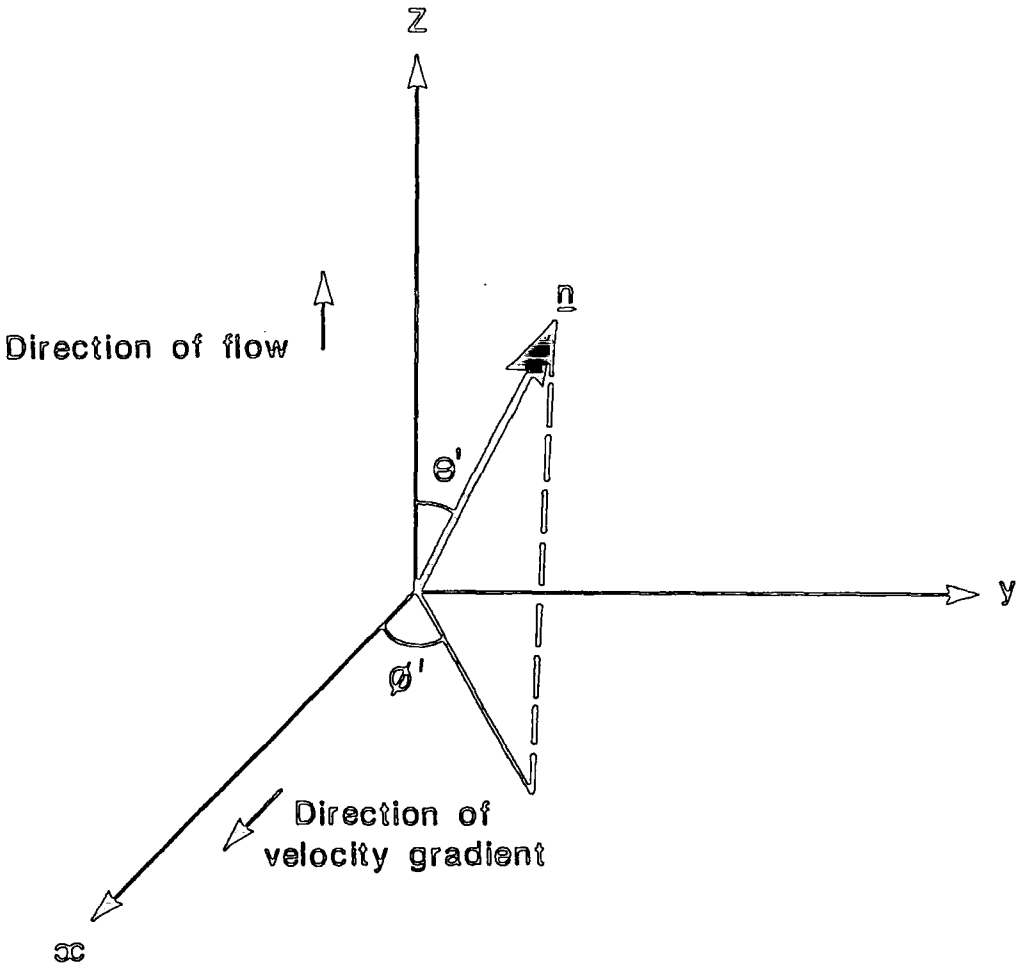

FIGURE 3.10
Definition of the orientation of the liquid crystal director $\underline{n}$ with respect to the shear plane

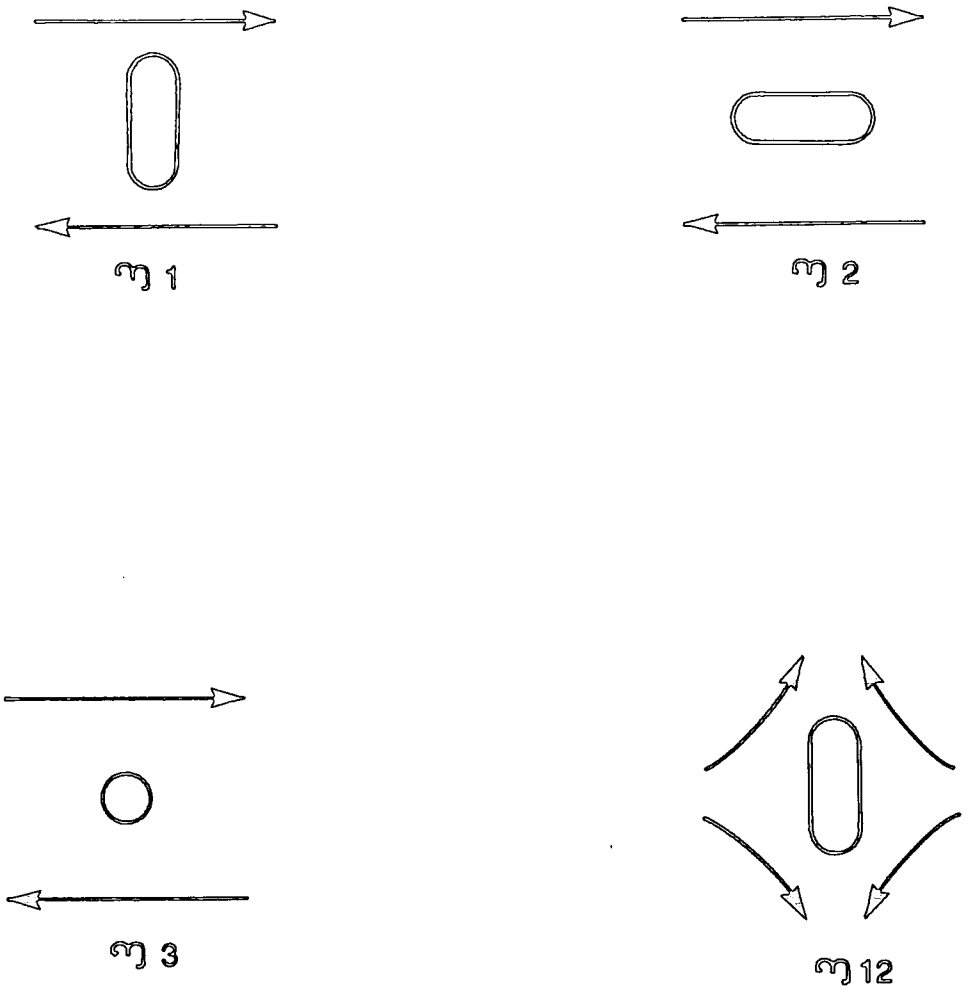

FIGURE 3.11
The Miesowicz viscosity coefficients of a nematic liquid crystal

$$\eta = (\eta_1 + \eta_2 \cos^2\theta')\sin^2\theta'\cos^2\phi' + \eta_2\cos^2\theta' + \eta_3\sin^2\theta'\sin^2\phi' \quad [3.35]$$

Removing the restriction of fixed director orientation, then two shear torque coefficients (γ_1 and γ_2) can also be defined relating the viscous torque to the elastic and frictional forces.

In isotropic liquids, the ionic mobility is generally directly related to the macroscopic viscosity. However, in the liquid crystal it is not known which viscosity coefficient, or which linear combination, has to be considered in the viscous force on a moving ion. The existence of several independent coefficients of viscosity means that it is not possible to apply Stoke's law relating mobility to viscosity directly to nematic liquid crystals.

Methods of measuring these viscosity coefficients have been described by de Jeu (1980), who also noted that the relationship described in [Equation 3.35] only applies to nematic liquid crystals. The apparent viscosities of smectic liquid crystals are high due to the mechanisms limiting movement between layers and to the presence of defects. As a nematic-smetic A transition is approached, pretransitional smectic order causes the divergence of η_2, γ_1 and γ_2.

Casagrande et al (1984) and Fabre and Veyssie (1987) have studied the viscoelastic behaviour of LCPs and shown that it is dominated by the

flexible polymeric nature of the backbone. This is in contrast to the static properties, such as permittivity, which are governed by the mesogenic side group and which are similar to those of lmmLCs.

3.4 Optical Properties of Liquid Crystals

Many crystalline solids are optically anisotropic, or birefringent. In the case of a uniaxial crystal, there are two principal refractive indices, n_o and n_e. The refractive index n_o is observed for an "ordinary" ray associated with a light wave where the electric vector vibrates perpendicular to the optical axis. The 'extraordinary' index n_e is observed for a linearly polarised light wave where the electric vector is parallel to the optical axis (Hecht and Zajac, 1974).

Nematic or uniaxial smectic liquid crystals are birefringent due to the anisotropic electrical polarisability and the optical axis is that of the director. Hence,

$$n_o = n_\perp$$

$$n_e = n_{||}$$

$$\Delta n = n_e - n_o = n_{||} - n_\perp \qquad [3.36]$$

The birefringence Δn is usually positive.

Generally molecules in liquid crystalline compounds do not contain chromophores and are colourless, or only slightly coloured. Rod shaped dye molecules dissolved in the liquid crystals are ordered by the liquid crystal matrix (Blinov, 1983) and the observed dichroism determines the

degree of order of the dye molecules: in general this order parameter is not the same as that of the liquid crystal. If $D_{//}$ and $D_{\perp}$ are the optical densities for light polarised parallel and perpendicular to the absorption dipole of the dye (assumed to form an angle β with the long axis), then the orientational order parameter of the liquid crystal may be written:

$$S = \frac{D_{||} - D_{\perp}}{D_{||} + 2D_{\perp}}(1-(3/2)\sin^2\beta)^{-1} = \frac{N-1}{N+2}(1-(3/2)\sin^2\beta)^{-1} \qquad [3.37]$$

where N = $D_{//}/D_{\perp}$ and S_d = (N-1)/(N+2) is the order parameter describing the orientational ordering of the transition moment of the dye.

The characteristics of a dye are defined using either the molar extinction coefficient (e) or the absorption coefficient (k). If I_0 and I are the intensities of light falling on and passing through the sample, respectively, c is the concentration of dye and l is the layer thickness, then:

$$I = I_0 10^{-ecl} \qquad [3.38]$$

or I/I_0 = exp (-kl) (Beer Lambert Law). [3.39]

k is related to the general description of the refractive index at wavelength λ by the following:

$$k = 4\pi\kappa/\lambda \qquad [3.40]$$

where $n^* = n - i\kappa$

The optical density:

$$OD = \log (I_0/I) = ecl = kl \qquad [3.41]$$

is often measured for convenience in comparative studies of the effect of, for example, temperature on liquid crystalline order.

Chapter Four

Experimental Techniques

4.1 Dielectric Relaxation Spectroscopy

The dielectric response of a sample is completely characterised by mapping its behaviour, at thermal equilibrium, throughout the range of frequency and temperature over which the component systems are dielectrically active. The experimental data describe a surface in (ϵ'',$\log_{10}\nu$,T) space or (ϵ', $\log_{10}\nu$,T) space,as illustrated in Figure 4.1.

The permittivity and dielectric loss of a material are measured by introducing a sample into a capacitor, waveguide or other container which forms part of an electric circuit. This circuit is then subjected to an alternating voltage or a voltage step and the subsequent response is detected. However, care is needed to ensure that effects due to the external circuit are not attributed to the material under test.

4.1.1 Equipment

There are two fundamental methods of measurement, each of which is appropriate for a different frequency regime. For measurements at frequencies less than about 10^7 Hz, a direct relationship is assumed between the sample response and that of an equivalent circuit. At higher frequencies it is unreasonable to describe the circuits using discrete elements; it is more appropriate to use distributed impedances. Surveys of dielectric measurement techniques are readily available in the literature (Daniel 1967, Harrop 1972).

All the dielectric results described in this work have been obtained using a Hewlett Packard HP4192A Impedance Analyser. Measurements were typically made over a frequency range between 100 Hz and 1 MHz assuming

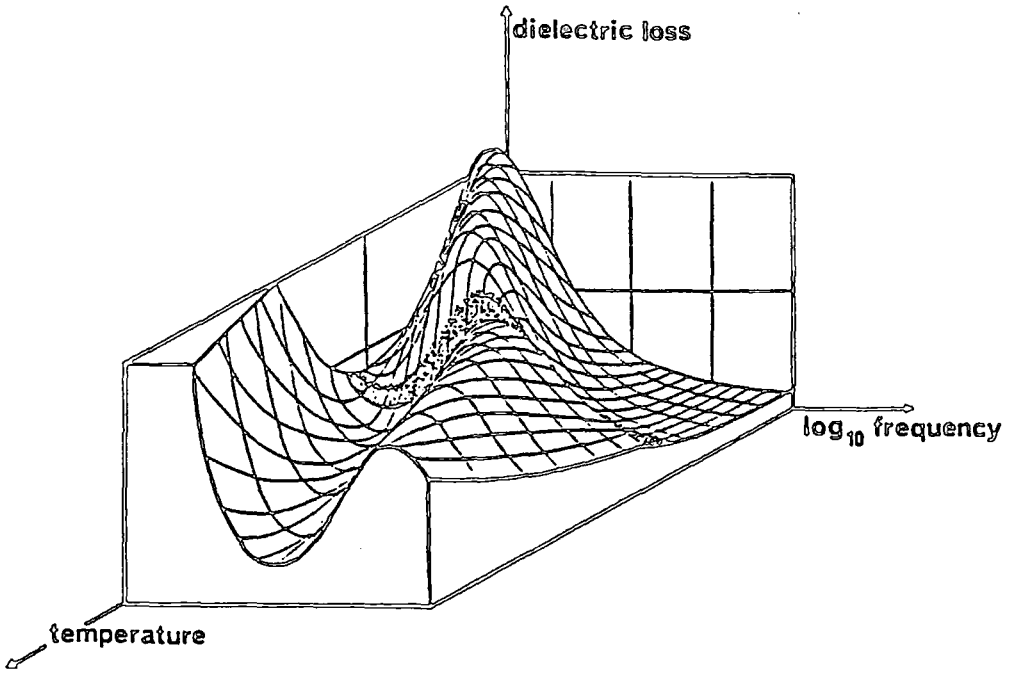

FIGURE 4.1
Dielectric response surface (ϵ'', $\log_{10}$v,T) for the LC polymer II (see Appendix IV for structure)

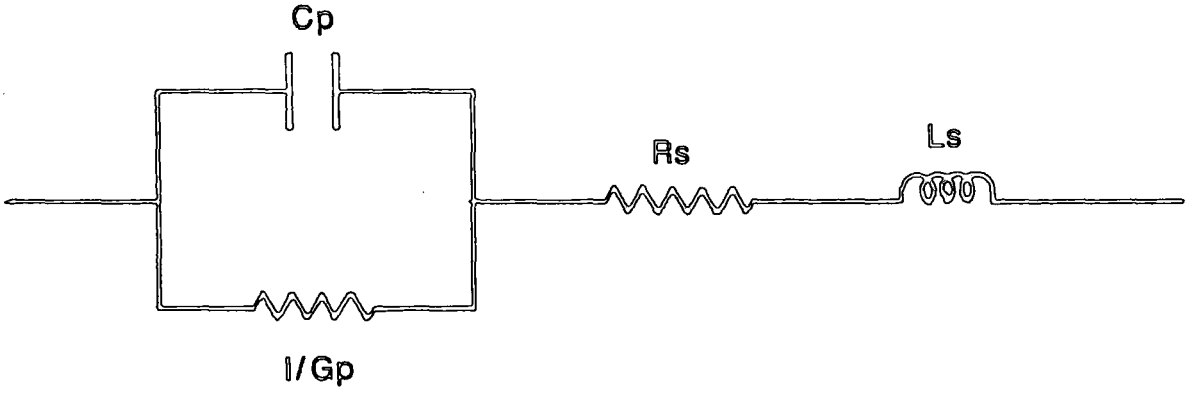

FIGURE 4.2
Equivalent electric circuit used for correcting dielectric and conductivity measurements of liquid crystalline materials in glass sandwich cells

the principle of equivalent circuits. The Impedance Analyser measured the vector ratio between an applied test signal voltage and the current flowing through the sample. A test voltage of 100 mV was used to avoid any possibility of dielectric reorientation of the director. A Hewlett Packard 9816 microcomputer was used to control the impedance analyser using a modification of a programme originally supplied by the Marconi Research Centre, Chelmsford. The frequency was scanned automatically between programmed limits, with 20 data points being collected per decade in a logarithmic distribution. These were stored directly on disk to allow data manipulation. Measurements were made in the "average" mode of the impedance analyser which allows about 1.05 seconds per reading.

4.1.2 Equivalent Circuit

The sample was treated as a capacitor C_p with conductance G_p in parallel. A resistance R_s and inductance L_s were introduced in series to model electrode and lead effects (O'Konski, 1968), see Figure 4.2. The capacitance C and conductance G measured by the impedance analyser in parallel mode are related to the equivalent circuit parameters by:

$$G/(G^2+\omega^2C^2) = G_p/(G_p^2+\omega^2C_p^2) + R_s \qquad [4.1]$$

$$C/(G^2+\omega^2C^2) = C_p/(G_p^2+\omega^2C_p^2) - L_s \qquad [4.2]$$

Plots of the left-hand sides of Equations [4.1] and [4.2] for an empty cell (G_p=0) against ω and $1/\omega^2$, respectively, yield straight lines whose intercepts on the y-axis gives R_s and L_s, respectively, with the slope of Equation [4.2] giving $1/C_p$ for the empty cell. Data points at low

frequency were avoided when fitting the straight lines since for an empty cell the impedance was too high. On filling the cell, the sample specific quantitites C_p and G_p can be found from the measured quantitites C and G by rearranging Equations [4.1] and [4.2] to give the following:

$$G_p = [(G/(G^2+\omega^2C^2))+R_s]/\left[(G/(G^2+\omega^2C^2)-R_s)^2+((\omega C/(G^2+\omega^2C^2))+\omega L_s)^2\right] \qquad [4.3]$$

$$C_p = [(G/(G^2+\omega^2C^2))+L_s]/\left[(G/(G^2+\omega^2C^2)-R_s)^2+((\omega C/(G^2+\omega^2C^2))+\omega L_s)^2\right] \qquad [4.4]$$

These quantities are related to the complex dielectric permittivity ($\epsilon^* = \epsilon' - i\epsilon''$) by:

$$\epsilon''(\omega) = \frac{G_p}{\omega}.\frac{1}{C_o} \qquad [4.5]$$

$$\epsilon'(\omega) = C_p.\frac{1}{C_o} \qquad [4.6]$$

Where C_0 is the capacitance of the empty cell, assuming negligible fringing fields.

The accuracy of these corrections was tested by measuring the permittivity of the standard liquid 1,2-dichloromethane and of the liquid crystal K24.

The error in the measured permittivities was between 1% and 5% depending on the quality of the containing cell construction. This demonstrated that the technique could reasonably be used to illustrate qualitative trends and that reliable quantitative results could be produced with care.

4.1.3 Temperature Control

All measurements were made with the sample in a Linkam TH600 hot stage having a TMS90 controller. This allowed up to ten stages of programmed temperature control together with up to 99 hours stability at a given temperature. The manufacturers claimed an accuracy of ±0.1°C. The Linkam hot stage allowed optical access to the cell being measured. Controlled cooling between room temperature and about 10°C was achieved by directing nitrogen which had been cooled in iced water through the stage. Before measuring at any given temperature, the impedance analyser reading was allowed to become steady. This temperature stabilisation took between 5 and 20 minutes for high and low temperatures of the LCP, respectively.

4.1.4 Sample Containment

Two principal methods of containing LCPs for dielectric measurements have been described in the literature. The first uses a dismantlable cell in which the LCP is prepared from the melt directly onto the lower electrode surface (see, for example, Zentel et al (1985)). It is restrained by a barrier, for example made from PTFE, which also acts as a spacer to maintain the upper electrode at a fixed distance. The upper electrode is usually held in position by springs. The second method uses a pre-formed

cell to contain the LCP, which is introduced by capillary action from the melt (see, for example, Parneix et al (1987)). The latter technique has been used in this work for several reasons:

(i) The cell can be readily made of glass with transparent indium tin oxide (ITO) electrodes. Optical access is an important part of liquid crystal studies since their appearances can be directly related to the director configuration.

(ii) A fixed cell arrangement allows the empty cell capacitance, resistance and inductance values to be determined under the same conditions as when the sample is measured. Though this does assume that the thickness does not change on filling, measurements of thickness in empty and partially filled cells have shown negligible variation.

(iii) The sample and cell can be stored for future measurements. This was considered to be important since only small quantities of sample were available.

(iv) The viscosity of the polysiloxane backbone LCPs under investigation was generally sufficiently low to allow reasonably rapid capillary filling of the cells (20 minutes to about 2 hours). The viscosity of many LCPs having polyacrylate backbones is too high for this to be an appropriate technique.

The cell geometry used for measurement is illustrated in Figure 4.3. The construction of the cell is standard to liquid crystal display manufacture. A flow diagram of the process is given in Appendix I. Important features for reliable dielectric measurements were found to be the following:

(i) Spacers were excluded from the active electrode area by using a mask at the deposition stage.

(ii) The glass was cleaned twice after etching the electrode and then the cell was assembled immediately to prevent contamination.

(iii) Twenty-five micron diameter chopped glass fibres were used as spacers (compared with 6-10 μm spacers used for liquid crystal displays). This reduced the time for the cells to fill by capillarity.

(iv) The resistivity of the indium tin oxide coated glass was 5 Ω/square.

This last feature was particularly important when measurements were being made at elevated temperatures and frequencies higher than about 50 kHz. It was found that the LCPs were sufficiently conducting, particularly in the isotropic phase, for the electrode resistance to dominate the equivalent circuit of Figure 4.2 at high frequencies. Excessive losses were observed for values of R_S greater than about 20 Ω.

Top View

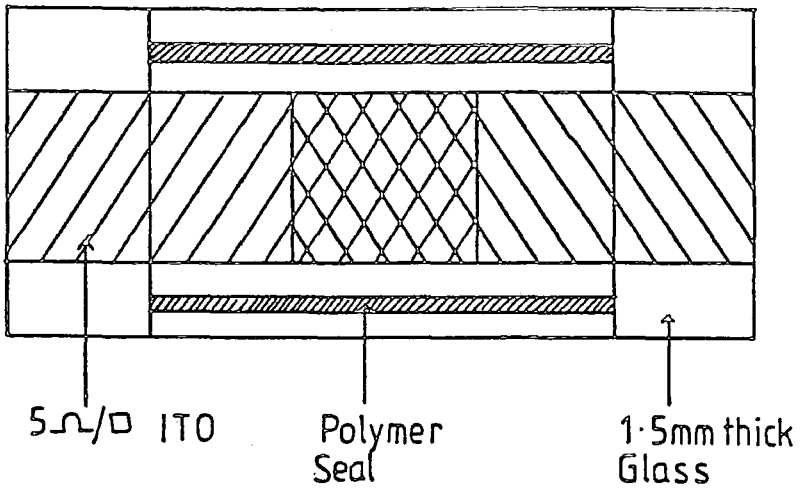

Side View

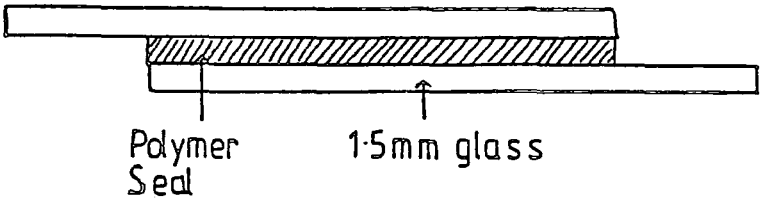

Side Elevation

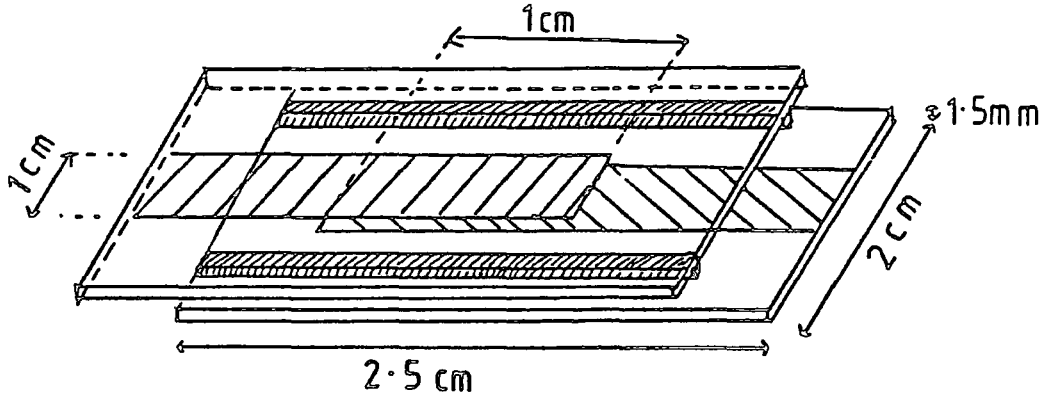

FIGURE 4.3
Schematic diagram of the cell used for dielectric and conductivity measurements

A very simple two terminal electrode arrangement was used in these cells. In this configuration, fringing electric fields can result in inaccurate values of permittivity. More accurate results are achieved by introducing an earthed guard ring separated from the active electrode by a distance rather less than the cell thickness. An attempt was made to manufacture such cells following the design of Bradshaw (1984). However, the pre-requisite of a low resistivity (therefore relatively thick) ITO coating made it difficult to etch the fine 10 μm gap between the electrode and guard ring. It was also difficult to align the top and bottom electrode patterns precisely during cell assembly. A simple overlapping two terminal cell was found to produce sufficiently accurate results, as shown in Section 4.1.2 with reference to measuring the permittivity of standard materials. The electrode area was only 1 cm^2 since it was difficult to ensure that larger area electrodes were defect free and parallel throughout.

The LCPs were introduced into the pre-formed cells by capillarity. The cells were heated under vacuum at a temperature greater than 100°C for about 30 minutes to drive off any surface moisture. A Gallenkamp vacuum oven was used with dried silica gel pellets to absorb moisture in the oven. A liquid nitrogen cold trap prevented backflow of oil or fumes from the vacuum pump to the oven. The LCP was then placed on the edge of the cell and heated under vacuum to a temperature about 15-20°C higher than its clearing temperature. Bubbling of the sample was often observed as it degassed. It was found that thorough degassing reduced the probability of dielectric breakdown. The samples generally flowed slowly into the cells. The polysiloxane copolymer LCPs predominantly used in this work

took between 20 minutes and 3 hours to fill a 4 cm^2 x 25 μm cell. Polysiloxane homopolymer or polyacrylate LCPs tended to take many more hours to fill similar cells.

In all cases where organic polymers are subjected to high temperatures, sample degradation and crosslinking are cause for concern. The use of a vacuum oven and the lowest possible filling temperatures provided some safeguard against these problems.

4.1.5 Alignment

Although considerable information can be obtained about molecular dynamics in LCPs by studying unoriented samples, alignment can provide additional information. In particular, the origin of the relaxation peaks can be confirmed and the dielectric anisotropy and order parameter quantified. For lmmLCs alignment of the director in a desired orientation is a relatively straightforward procedure. Electric and magnetic fields and various surfactants coated onto the cell walls can be used. The higher viscosity of LCPs makes such alignment more difficult.

(i) Homeotropic Alignment

To produce homeotropic alignment (that is, the director perpendicular to the cell walls) of LCPs having positive dielectric anisotropy ($\epsilon_{\parallel} > \epsilon_{\perp}$), an electric field was applied across the sample whilst cooling slowly from the isotropic phase. Voltages of between about 50V and 150V (3 kHz, sinewave) were applied to achieve varying degrees of alignment (Attard and Williams, 1986a). Dielectric breakdown frequently occurred in fields of this magnitude (see Chapter 6) but most success was found by heating the

LCP to about 10°C above the isotropic transition temperature, applying the electric field and then slowly cooling at about 2°C min^{-1} to around 5°C below the biphasic region. The temperature was maintained for about 10-15 minutes and then further more rapid cooling occurred, after which the field was removed. The effect of cooling rate on the alignment of LCPs has been described by Attard and Williams (1986b). Alignment was retained after the field was removed due to the high viscosity of the LCPs. Not all LCPs described in this work were aligned homeotropically.

(ii) Homogenous/Planar Alignment

To produce homogenous or planar alignment of LCPs (that is, the director parallel to the electrode, unidirectional for homogeneous) several methods are described in the literature. These include magnetic field alignment (see, for example, Parneix et al (1987)), two frequency switching (Araki et al, 1986) and the use of surfactants and annealing (Ringsdorf et al, 1982). Attempts have been made here to produce alignment by all of these methods, with varying degrees of success. Samples were not routinely aligned homogeneously.

A sample of LCP having the same structure as GN3/14 but with contamination by an unknown amount of side chain precursor, was subjected to magnetic fields of 1.5T and 8T. The former was obtained from a superconducting magnet used by the Picker Research Laboratories, Wembley. The latter was obtained using a research magnet at the Clarendon Laboratory, Oxford University. Reasonable alignment was achieved when viewed by polarising microscopy, however the impracticality of applying this technique to other

samples meant that it was not pursued. A qualitative observation was that temperature, time and field strength were all critical parameters in producing magnetic field alignment.

Planar alignment can be produced in an LCP having positive dielectric anisotropy by using an electric field at a frequency at which the longitudinal dipole moment is unable to respond. The field therefore reorients the transverse dipole moment. For most LCPs under investigation this frequency was about 50 kHz at room temperature and, at the high temperatures needed to allow reorientation to occur, the frequency shifted to about 3 MHz. Unfortunately it was difficult to maintain a sufficiently high field strength at this frequency, so this method was not pursued either.

Liquid crystals are routinely aligned homogeneously using surfactants such as buffed polyimide or obliquely evaporated silicon monoxide. It was found that LCPs could be induced to exhibit a degree of homogeneous alignment by using a buffed polyimide surfactant together with prolonged annealing a few degrees below the biphasic transition temperature. Often this could only be observed optically as an increase in the size of smectic focal conics, though it could be detected dielectrically by the increase in the amplitude of the α peak and decrease in the amplitude of the δ peak. Care was needed to ensure that sample degradation did not occur during the annealing process.

4.1.6 Curve fitting

The dielectric loss spectra of liquid crystal polymers are composed of overlapping peaks since the relaxation modes illustrated in Figure 3.2 are closely spaced in the frequency domain. In fact, the higher frequency modes coalesce into broad bands. The experimental loss spectra often appear to lack clearly resolvable features, so to identify the constituent loss peaks a theoretical lineshape must be fitted to the experimental data.

The choice of line-shape function is arbitrary and several functional forms have been suggested (Böttcher and Bordewijk, 1978). The most commonly used form is that suggested by Fuoss and Kirkwood (1941).

$$L(\nu) = L^{\circ}\,\mathrm{sech}[\beta \ln(\nu/\nu^{\circ})] \qquad [4.7]$$

where L° is the amplitude of maximum loss, ν° is the frequency of maximum loss and β $(0<\beta\leq 1)$ defines the width of the absorption curve. When $\beta=1$ the Debye formalism is regained (see Section 3.1). The half height peak width on a logarithmic frequency scale is approximately $1.14/\beta$. The amplitude of a spectrum composed of n loss curves is

$$L_{tot}(\nu) = \sum_{i=1}^{n} L_i^{\circ}\ \mathrm{sech}\ [\beta_i ln(\nu/\nu_i^{\circ})] \qquad [4.8]$$

The experimental spectra are fitted using Equation [4.8]. Previous workers have shown that an efficient method of performing this fitting process is to use an interactive computer programme which allows the amplitude, width and position of individual loss curves to be modified

separately. An estimate must be made of the number of loss curves contained in a given experimental spectrum since the minimum number of component curves should be used. The experience gained from studies of 1mmLCs (Buka et al, 1979), together with that of Attard (1986) in his studies of polysiloxane LCPs, suggested that most spectra could be adequately fitted by two overlapping Fuoss-Kirkwood curves, together with a conductivity curve of the form $G(\nu) = \lambda\nu^{-\epsilon}$ where λ is the strength factor, ν is the frequency and ϵ is typically 1. A computer programme written at the Department of Chemistry, University College Wales, Aberystwyth, was used to perform the fitting process. It was modified to run on an HP9816 computer as well as to allow a graphical illustration of the variation between experimental data and the theoretical line shape.

4.2 Electrical Conductivity

The electrical conductivity of a wide selection of LCPs has been measured to provide information about the mechanisms of conduction. Methods of influencing and reducing the apparent conductivity were also investigated. Both the low field AC conductivity and the high field DC conductivity have been measured. The former measurements were relatively quick and simple and therefore have been used to study the influences on the observed conductivity of LCPs. The longer DC conductivity experiments revealed information about the mechanism of conduction in LCPs and the selection of experimental variables was largely governed by the AC conductivity experimental results. The build up of space charge in the vicinity of the electrodes was studied by measuring the real component of permittivity as a function of frequency. A study of the surface roughness of a selection

of surfactants was also undertaken and related to the apparent conductivity of the LCPs and the formation of space charge at the electrodes.

4.2.1 Alternating Current Conductivity

The low field alternating current conductivity was measured using the same equipment, technique and cell design as described in Section 4.1. The impedance analyser was used to measure the conductance G as a function of frequency at each temperature and then this was corrected using the equivalent circuit shown in Figure 4.2 and Equation [4.3]. The conductivity (σ) was then calculated to allow for slight differences in the measuring cell geometries using:

$$\sigma = G\frac{d}{A} = G\frac{\epsilon_o}{C_o} \qquad [4.9]$$

where d and A are the cell thickness and electrode area respectively, ϵ_0 is the permittivity of free space and C_0 is the empty cell capacitance.

4.2.2 Direct Current Conductivity

The circuit used to measure the high field direct current conductivity is shown in Figure 4.4. The Keithley 230 Programmable Voltage Source provided a constant voltage, irrespective of the current drawn. The current varied over several orders of magnitude depending on the temperature and voltage applied. The smallest currents measured were about 10^{-9}A and hence shielding was necessary to reduce noise. The

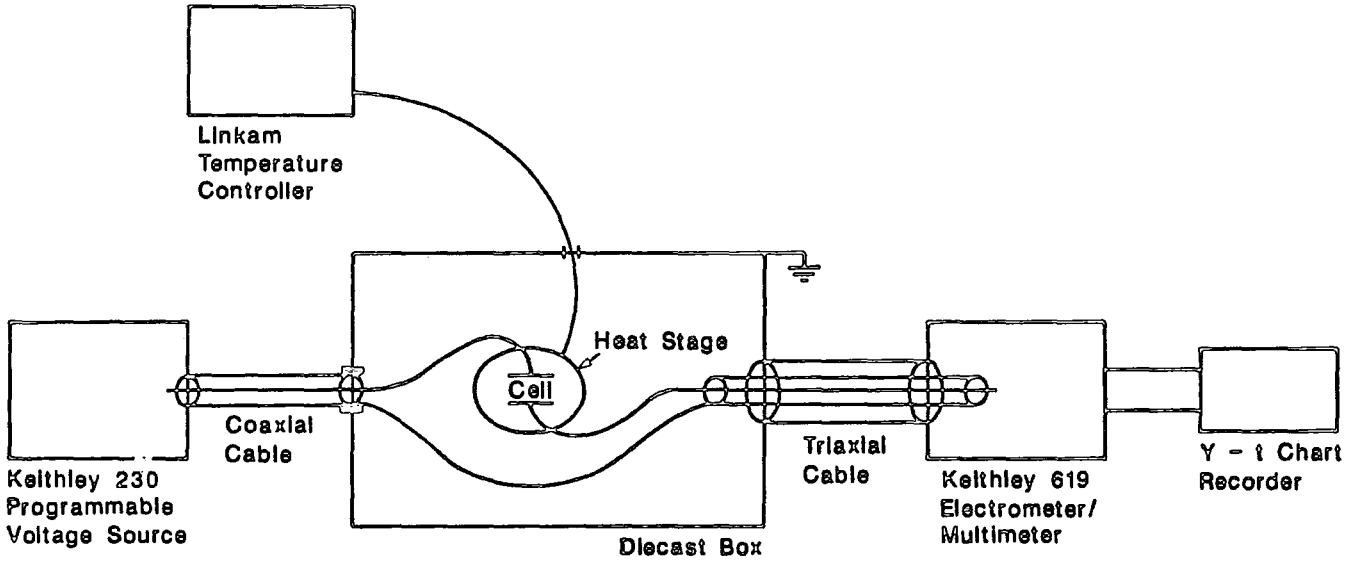

FIGURE 4.4
Schematic diagram of equipment used to measure the DC conductivity of liquid crystals and LCPs under high field conditions

current was monitored as a function of time using the chart recorder. An approximately constant value was achieved after 30-90 minutes. This static value of the current was used in all calculations.

In these high field measurements, the voltages were sufficiently large to induce director realignment. To avoid incorporating the anisotropic conductivity properties of the lmmLCs and LCPs into the results, the materials under investigation were always homeotropically aligned initially (see Section 4.1.5 for technique). Since they all had positive dielectric anisotropy ($\epsilon_{\parallel} > \epsilon_{\perp}$) the measuring field did not then affect the alignment significantly.

4.2.3 Surface Layers

The effect of various surfactants and electrode materials was studied, primarily by observing the AC conductivity and permittivity. In some cases the surfactants were commercial products for which details of the composition were not available. The methods for depositing silicon monoxide, organosilane barrier layer, UV curable epoxy and buffed and unbuffed polyimide onto the ITO electrode are described briefly in Appendix II. The coated plates were assembled into cells following the usual procedure outlined in Appendix I.

The surface roughness of the electrode materials and surfactants was assessed qualitatively by electron microscopy. A thin layer of gold was evaporated onto a plate of each sample and then photographed from an angle of 45° using a Cambridge 250 Scanning Electron Microscope.

4.3 Bulk Viscosity

4.3.1 Measurement of the Bulk Viscosity of GN3/14

The relatively high viscosity of the LCP was difficult to measure reliably with the equipment available. It was therefore extrapolated from measurements on mixtures of GN3/14 with the 1mmLC S2 (as supplied by BDH Chemicals Ltd). All the mixtures were dyed in solution with 3% wt/wt of the BDH dye D102 in order to relate the results to device conditions. The solvent was thoroughly removed using a low pressure vacuum pump. The transition temperatures of the materials are summarised in Appendix IV.

4.3.2 Equipment

The Brookfield HBTDV II Cone and Plate Viscometer was used to measure the viscosity of each mixture. The cone is driven at discrete rotational speeds and the resistance to rotation, caused by the sample between the cone and a stationary flat plate, is detected by a calibrated beryllium-copper spring. The torque in the spring is proportional to the shear stress in the fluid. This shear stress, together with the known geometric constants of the cone and the rate of rotation, allows the viscosity to be calculated (see Figure 4.5).

The CP40 cone was used, which has a 0.8° cone angle. This allowed measurements on small sample volumes. However, the manufacturer's claim that 0.5 cm^3 was sufficient was found to be rather unrealistic and a volume of about 1 cm^3 produced more reliable results.

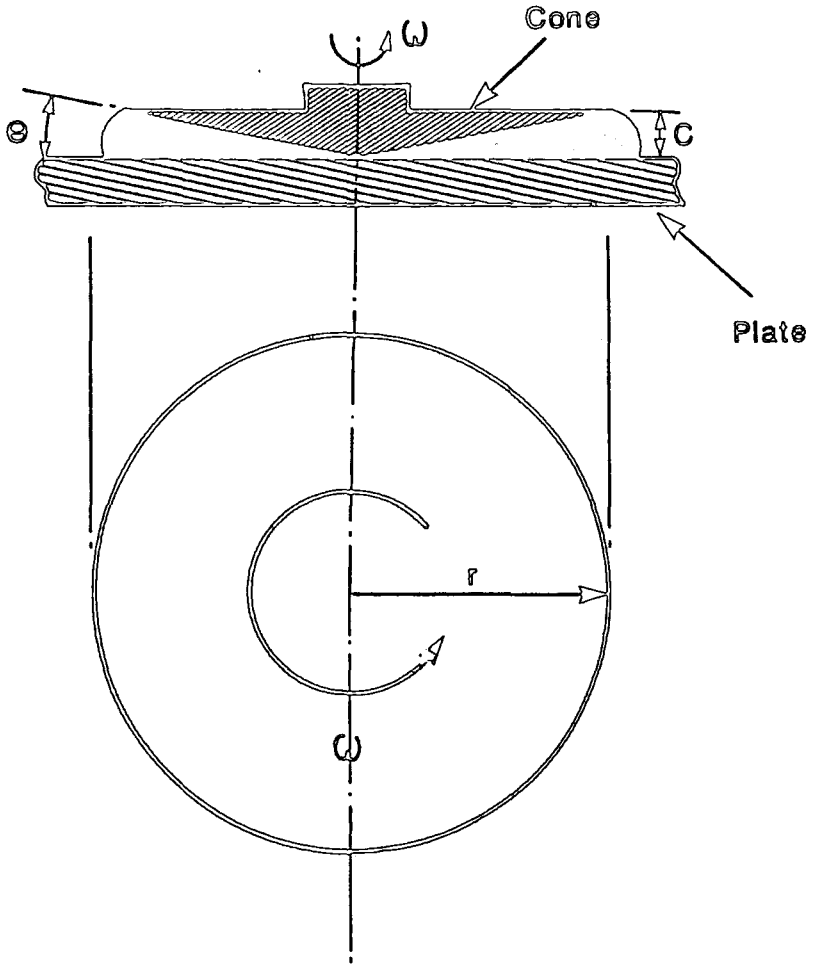

FIGURE 4.5
The measurement of viscosity using a cone and plate viscometer

Shear stress = $T/(2/3)\pi r^3$

Shear rate = $\omega/\sin\theta$

Viscosity = 100 x shear stress/shear rate

where T = % full scale torque, r = cone radius,
ω = cone speed, θ = cone angle

The temperature of the sample was varied by circulating water through a jacket around the sample cup. A Julabo model HC5 water bath was used. A thermocouple was inserted through the connecting hose near to the sample cup to improve the temperature control.

The accuracy of the measurement technique was tested by measuring the viscosity of castor oil, olive oil and the 1mmLCs E43, E7 and E9 and comparing the results with literature values. The error was found to be ±10%. Sources of error included impure samples, a temperature difference between the thermocouple and the sample holder and the difficulties associated with setting the cone-plate gap correctly.

4.4 Measurement of Optical Characteristics

The extinction coefficient (e) of blue pleochroic dyes has been measured in well aligned low molar mass liquid crystals. Optical studies of two LCPs have also been carried out with the aim of observing the change in alignment with temperature and time. Stability of alignment is an important criterion when assessing the suitability of LCPs as optical storage media. Samples were aligned homogeneously and then the optical path length measured parallel and perpendicular to the director as a function of temperature. Measurements were also made on homeotropically aligned samples. The samples were photographed using a Nikon polarising microscope at the start and end of a three month period.

4.4.1 Equipment

A diagram of the equipment is shown in Figure 4.6.

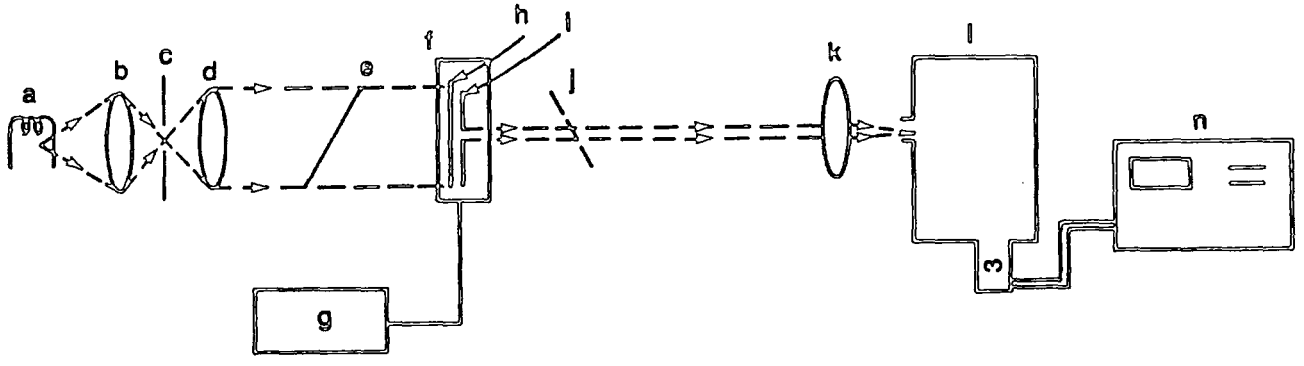

FIGURE 4.6
Optical equipment used to measure the extinction coefficients of pleochroic dyes and the optical density of LCPs

Key to Figure 4.6

a Xenon arc lamp

b lens

c pinhole } collimator

d lens

e linear polariser (under motorised control)

f Linkam TH600 heat stage

g Linkam TMS90 controller

h sample cell

i pinhole (100 μm)

j analyser (motorised)

k focussing lens

l SPEX 1870C spectrograph with 300 grooves/mm grating

m detector -EG&G 1412-1024-element silicon diode array

n EG&G OMA III

4.4.2 Sample Containment and Alignment

Homogeneous alignment was achieved following the method described by Meredith (1982). A pattern of interdigitated electrodes was designed which allowed the field to be applied in the plane of the cell. The pattern was etched into aluminium and cells produced of the form shown in Figure 4.7. The cells were manufactured in a similar way to the dielectric measurement cells - see Appendix I. Key features for successful optical measurements were found to be the following:

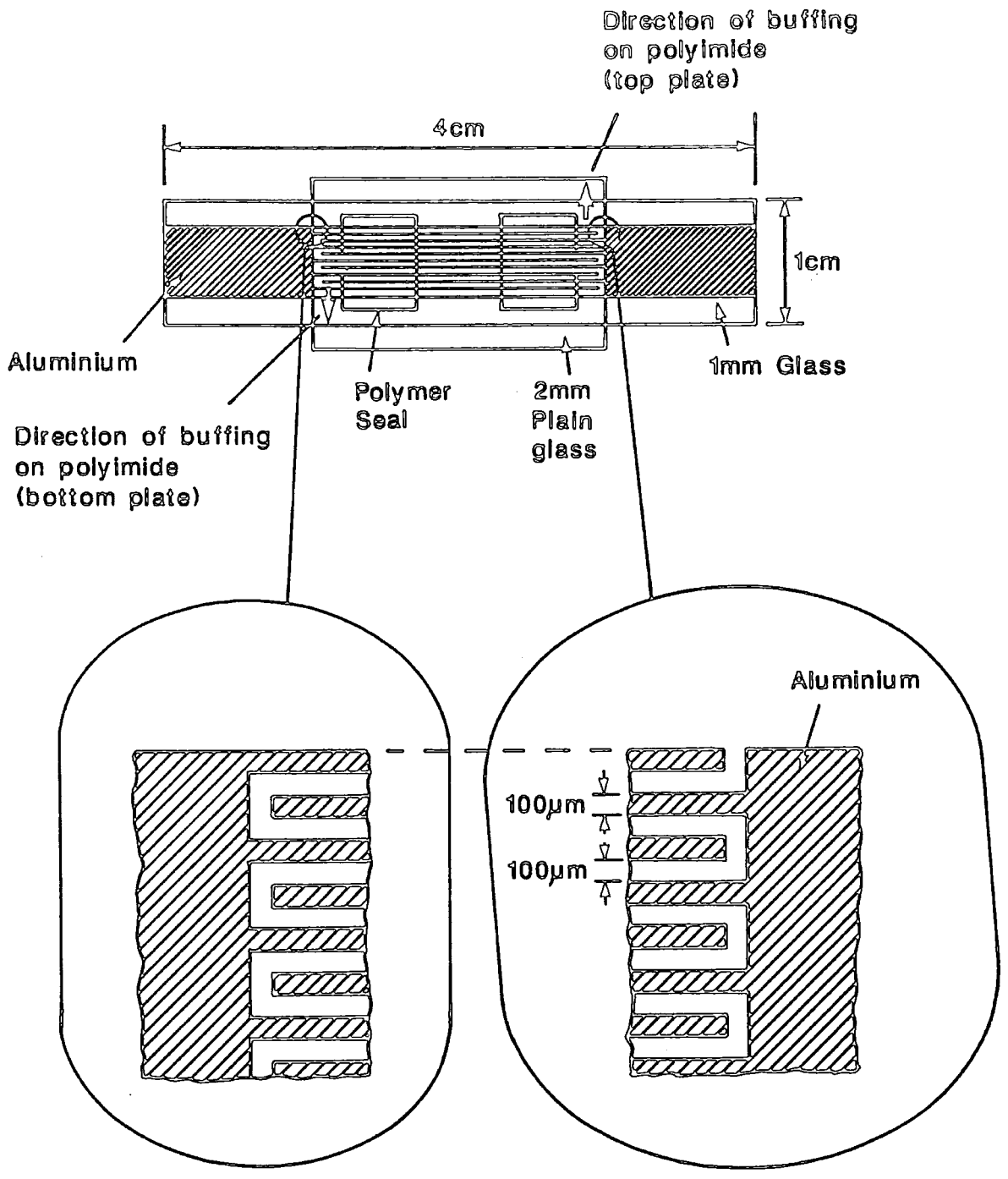

FIGURE 4.7
Schematic diagram of interdigitated electrode measuring cells

(i) Six micron diameter chopped glass fibre spacers were used. These were not deposited in the measuring area.

(ii) Polyimide was spun onto both inner cell surfaces and then buffed perpendicular to the electrode bars.

(iii) The upper plate was made from plain glass with no ITO on it.

The cells were filled by capillary action from the melt and then aligned by applying the field in the isotropic phase and slowly cooling in the presence of the field - as described in Section 4.1.5. Areas of good alignment were identified using a polarising microscope and measurements were made through a 100 μm pinhole.

Homeotropic alignment was achieved using cells having simple overlap electrode patterns. These were the same as the dielectric cells discussed earlier, except that high resistivity (200 Ω/square) ITO was used (since it was more transparent) and 9 micron spacers were deposited.

4.4.3 Measurement of extinction coefficient and optical density

The orientation of the polariser with respect to the director of the LCP is critical in these experiments. The director and polariser were aligned as follows:

(i) The polariser and analyser were crossed by jogging the motorised analyser until there was minimum light transmission (no sample cell

in beam). This was best performed in the "YT" mode of the OMA in which the light intensity over a wavelength range of about 400 nm was integrated and plotted as a function of time.

(ii) The cell was replaced in the beam and the polariser and analyser rotated together until there was minimum light transmission. Again the "YT" mode was used and the polariser and analyser were always rotated clockwise to take into account the different backlash characteristics of the motors. Four positions of minimum transmission were identified - two when the polariser was parallel to the director and two when it was perpendicular.

(iii) The analyser was removed from the beam.

The transmission through the cell (I) was measured with the polariser parallel and then perpendicular to the director. The lamp spectrum (I_0) was measured with no cell present for both orientations of the polariser, as well as the dark current of the photodetectors for the exposure time used.

The optical density in each orientation was calculated from:

$$\text{Optical Density} = \log_{10}\left(\frac{I_o - \text{Dark}}{I - \text{Dark}}\right) \qquad [4.10]$$

For dyed samples, the extinction coefficient of the dye was calculated from:

$$\text{Extinction Coefficient} = \frac{1}{cl} \times \ln\left(\frac{I_o - \text{Dark}}{I - \text{Dark}}\right) \qquad [4.11]$$

where c = concentration of dye (in g molecules^{-1})

and l = thickness of measurement cell

The dye concentration may be found using

$$c = \frac{\text{mass of dye}}{\text{molecular weight of dye}} \times \frac{1000}{\text{Volume of LC in cell}} \qquad [4.12a]$$

or

$$c = \frac{\text{wt\% of dye}}{\text{molecular weight of dye}} \times 1000 \times \text{density of LC} \qquad [4.12b]$$

Chapter Five

Results and Discussion – Dielectric Relaxation Spectroscopy

5.1 Introduction

The molecular dynamics of a wide range of liquid crystal polymers have been studied using dielectric relaxation spectroscopy and the results are described in this Chapter. The tendency of LCPs to exhibit polymer-type dielectric behaviour is compared with their tendency to show mesogenic properties. The influence of structure on their ability to reorient in an electric field is also discussed. LCPs are well suited to study by dielectric relaxation spectroscopy. This is due to the dipolar nature of the mesogenic moieties and, in general, the absence of coexistent amorphous and liquid crystalline phases. Their anisotropic permittivity and permeability facilitate alignment by electric and magnetic fields. Measurements of aligned LCPs, together with the ease of substitution of functional groups at various molecular sites, allows interpretation of the relaxation mechanics.

The relaxation frequencies are related to molecular motions and are therefore strongly influenced by changes in temperature (Hill and Dissado, 1982). Below the glass transition of the LCP the chain configuration is frozen into a fixed arrangement. Dielectric relaxation then arises from local dipolar reorientation of small numbers of atoms. At higher temperatures, many monomer units are cooperatively involved in the reorientation process. When dielectric loss is plotted as a function of temperature there are two or more peaks, conventionally labelled in polymer studies as α,β,γ with decreasing temperature (Boyer, 1978). The α peak is associated with the glass transition. This sequence corresponds to increasing frequency at fixed temperature. All the results described here have been produced by scanning frequency at fixed temperature. A

characteristic of both lmmLCs and side chain LCPs is a further relaxation at a lower frequency than the α relaxation. This is conventionally labelled δ. β and γ relaxations have been observed below the glass transition temperature as internal reorientations.

5.2 Nomenclature and Real Spectra

An example of a dielectric loss spectrum is shown in Figure 5.1. This refers to GN4/19 at 30°C and has been fitted using the Fuoss Kirkwood lineshapes described in Section 4.1.6. The lower frequency curve is relatively narrow with a half-height width approaching the Debye curve value of 1.14 units of $\log_{10}\nu$. This corresponds to a process having a single relaxation time and is identified as the δ peak. The higher frequency peak is very broad in comparison (around 2 decades in the frequency spectrum) and is therefore a combination of several relaxation processes. This is the α peak. By reference to Equations [3.17] and [3.18], the δ peak can be seen to be the result of the $g'_{0,0}(t) \equiv (||, l)$ reorientation mode. The α peak is a combination of the $g'_{1,0} \equiv (\perp, l)$, $g'_{1,1} \equiv (\perp, t)$, and $g'_{0,1} \equiv (||, t)$ modes which depend on the director orientation in the sample.

The rate of change of peak frequency with temperature is an indication of the ease of reorientation of the molecular dipoles. The loss spectrum of GN3/19 is plotted at several temperatures in Figure 5.2. The frequency locations of the maximum of each of the loss peaks are plotted on an Arrhenius activation energy diagram in Figure 5.3. The Arrhenius equation

$$\nu = \nu^{\circ}\exp(-E_a/kT) \qquad [5.1]$$

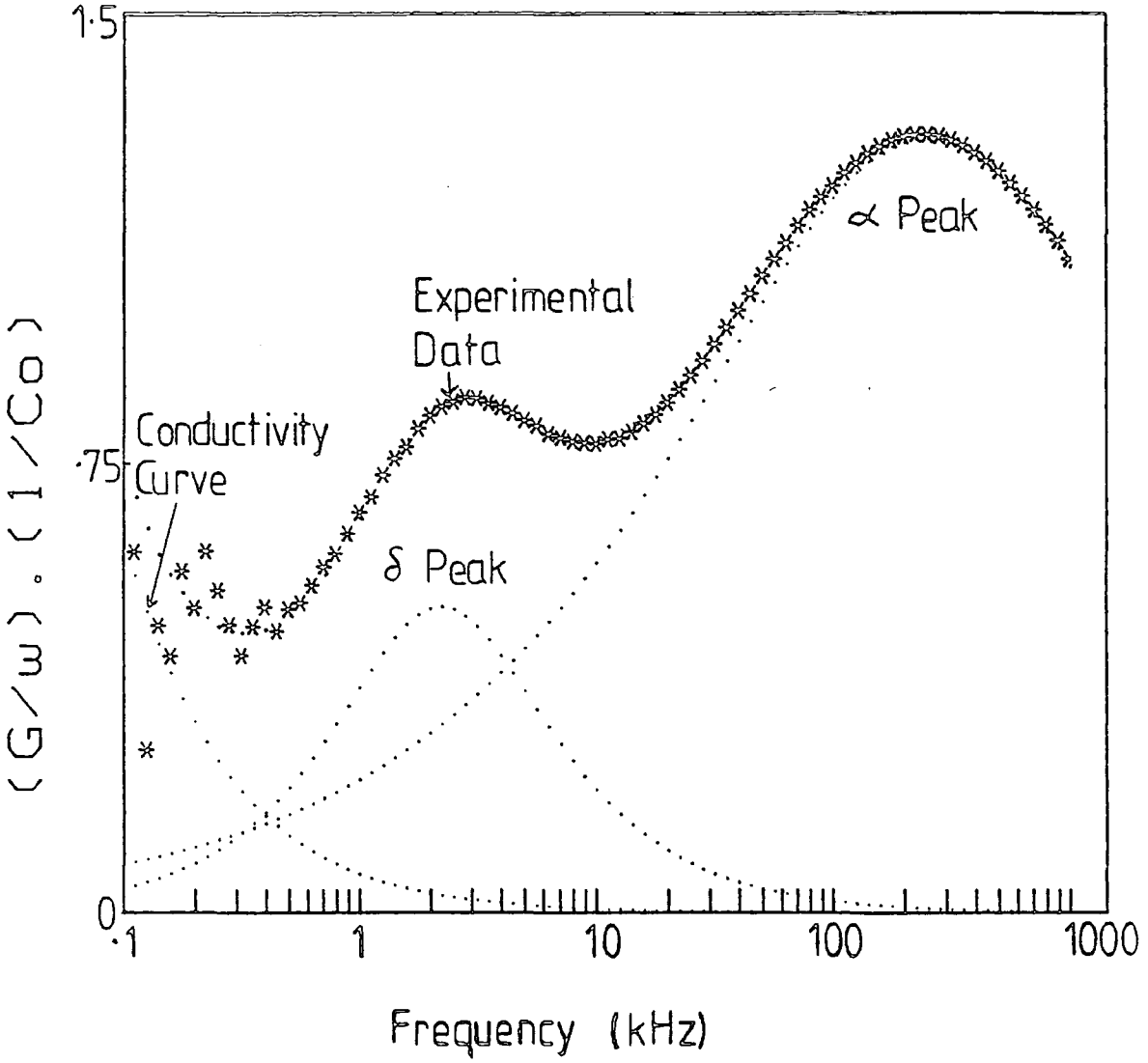

FIGURE 5.1
The loss spectrum of GN4/19 at 30°C fitted with a conductivity curve and two overlapping Fuoss Kirkwood curves.

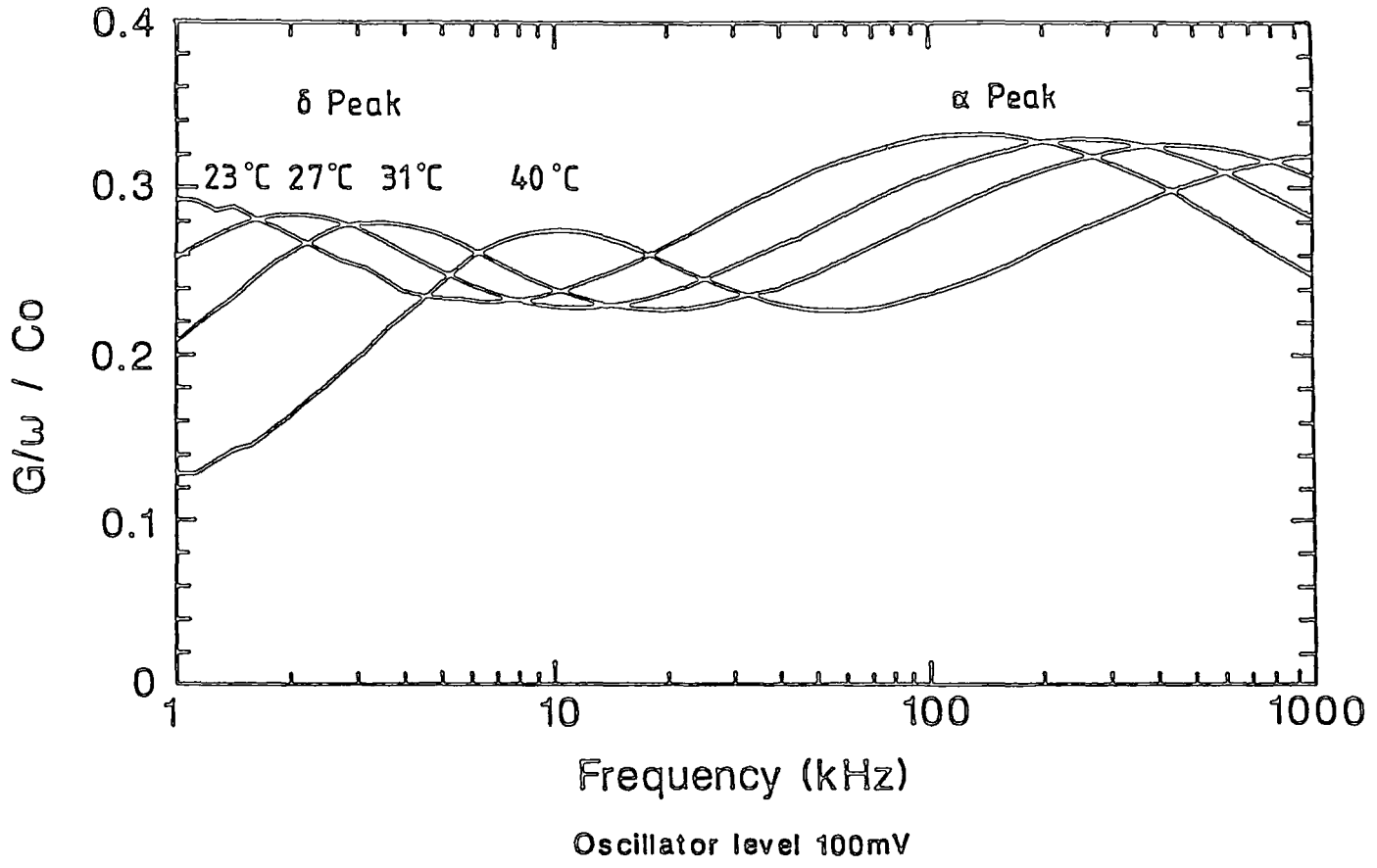

FIGURE 5.2
The loss spectrum of unaligned GN3/19 at 23°C, 27°C, 31°C and 40°C.

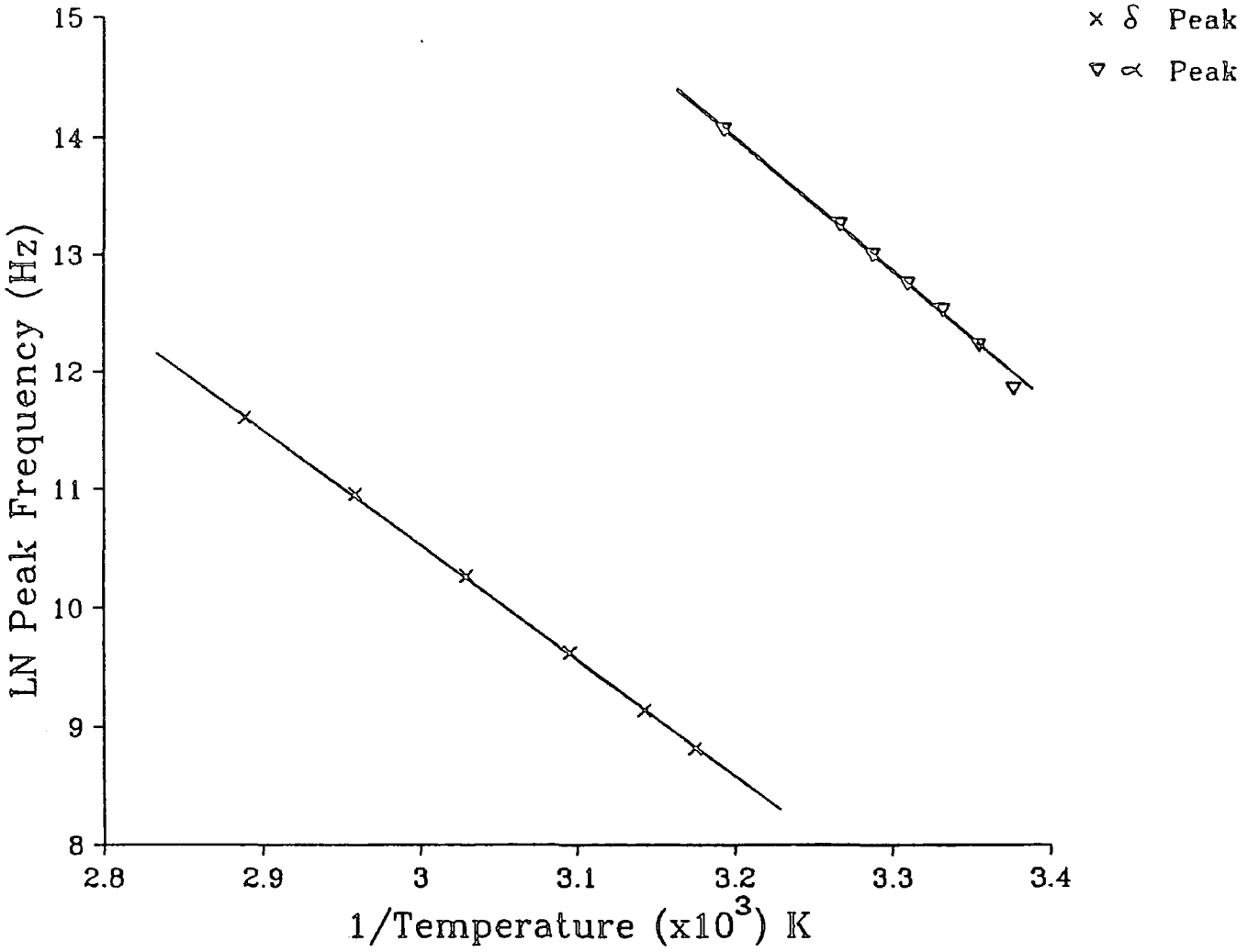

FIGURE 5.3
Arrhenius activation energy plot for unaligned GN3/19.

where ν° is the frequency of maximum loss, is commonly used to calculate the activation energy (E_a) of LCPs, but it should be noted that it becomes increasingly unsuitable as the glass transition temperature is approached. As discussed in Section 5.5.1, the Vogel-Fulcher formalism is then more suitable. From Figure 5.3, the δ and α relaxation energies are 80 $kJmol^{-1}$ and 98 $kJmol^{-1}$ respectively.

5.3 The Influence of Alignment on the Dielectric Loss Spectra of LCPs

Since the amplitudes of the δ and α loss peaks depend on the orientation of the mesogenic director, they can be used to monitor the alignment of a liquid crystalline sample. The δ peak is associated solely with the component of permittivity parallel to the director ($\epsilon_{||}$) so its amplitude is enhanced by an increase in the degree of homeotropic alignment. The δ peak is absent in the case of perfect homogenous alignment. The α peak amplitude is conversely enhanced by homogenous alignment and decreased by homeotropic alignment, though it is present in both orientations provided that the mesogenic moiety dipole has a transverse component. Attard and Williams (1986a) have described the use of dielectric relaxation spectroscopy as a "non-optical" method of monitoring director alignment.

The loss spectra of GN3/14 have been compared at 30°C in three states of alignment. A degree of homeotropic alignment was produced by applying a 60 V_{rms}, 3 kHz sine wave, across the sample while cooling from the isotropic phase and a degree of homogeneous alignment was produced by applying an 8T magnetic field in the plane of the containing cell while cooling from the isotropic phase (see Section 4.1.5. for a description of alignment methods). The final measurements were made on an unaligned

(approximately random) sample. Figure 5.4 shows that the δ peak is almost completely suppressed by the magnetic field alignment, while its amplitude is considerably enhanced by the electric field alignment. The converse applies in the case of the α-peak. The positions of the loss peaks are the same in all states of alignment, in agreement with the observation of Attard (1986) that the degree of director alignment only affects the intensities of the various processes and not their relaxation times.

In Figure 5.5 the dielectric spectra of GN3/3 are summarised after alignment by applying progressively larger electric fields. The δ peak increases in amplitude with increasing homeotropic alignment. Ideally this method can be used to indicate dielectrically whether complete alignment has been achieved. However, care needs to be taken over the actual aligning technique. It was found that if the sample was allowed to cool too rapidly in the field, the peak amplitude appeared to reach a maximum, though the sample was not perfectly aligned when viewed using a polarising microscope. Attard et al (1986b) have demonstrated that the rate of cooling in the field is a critical factor in achieving good alignment with LCPs.

It is difficult to produce a quantitative interpretation of the dielectric behaviour of samples with incomplete alignment. The spatial variation of the director $\underline{n}(\underline{r})$ results in a dielectrically non-uniform sample because of the anisotropy of the permittivity. In general, it is only possible to calculate bounds for the sample permittivity. The simplest approach,

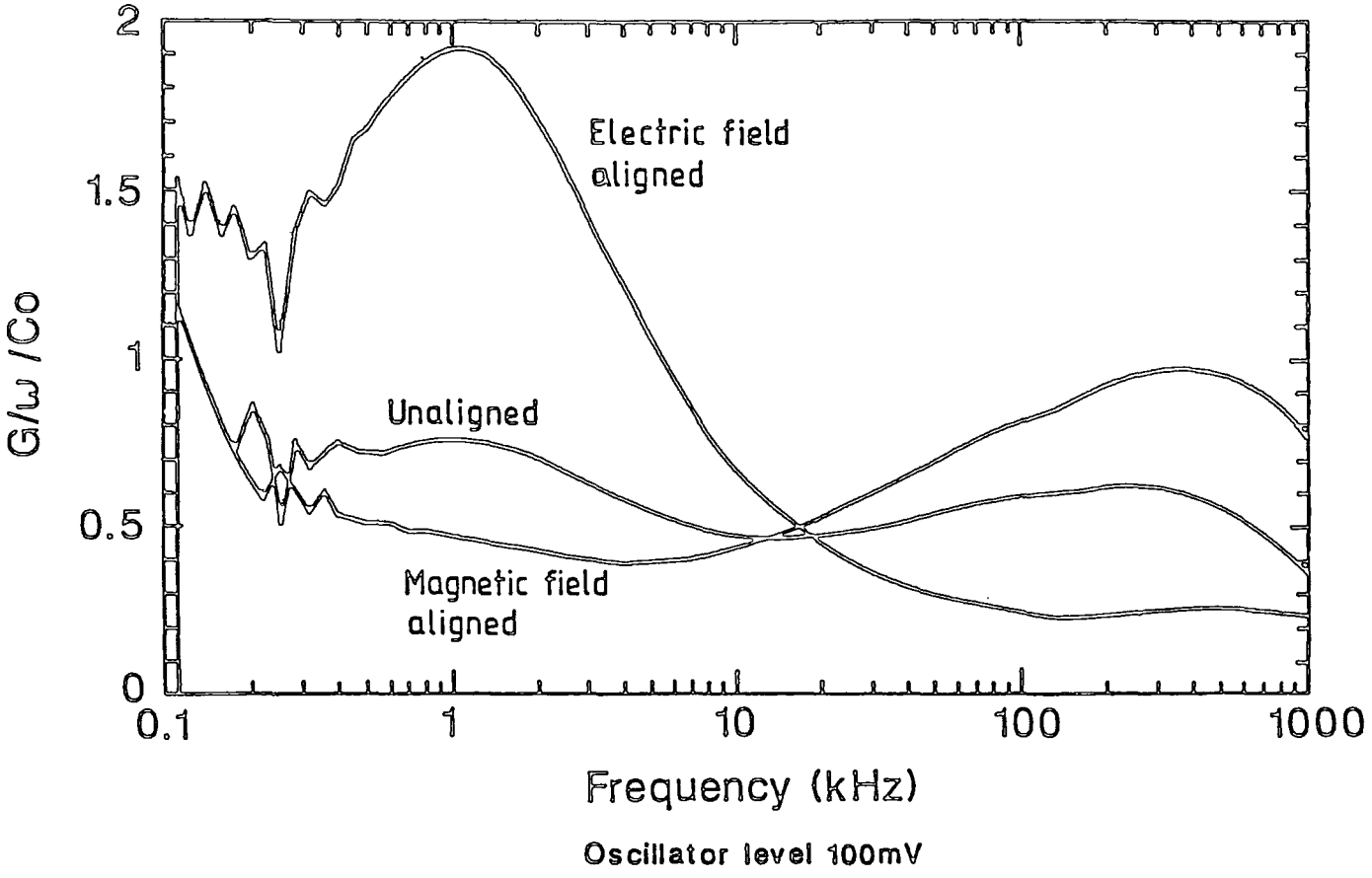

FIGURE 5.4
The affect of alignment on the loss spectrum of GN3/14 at 30°C.

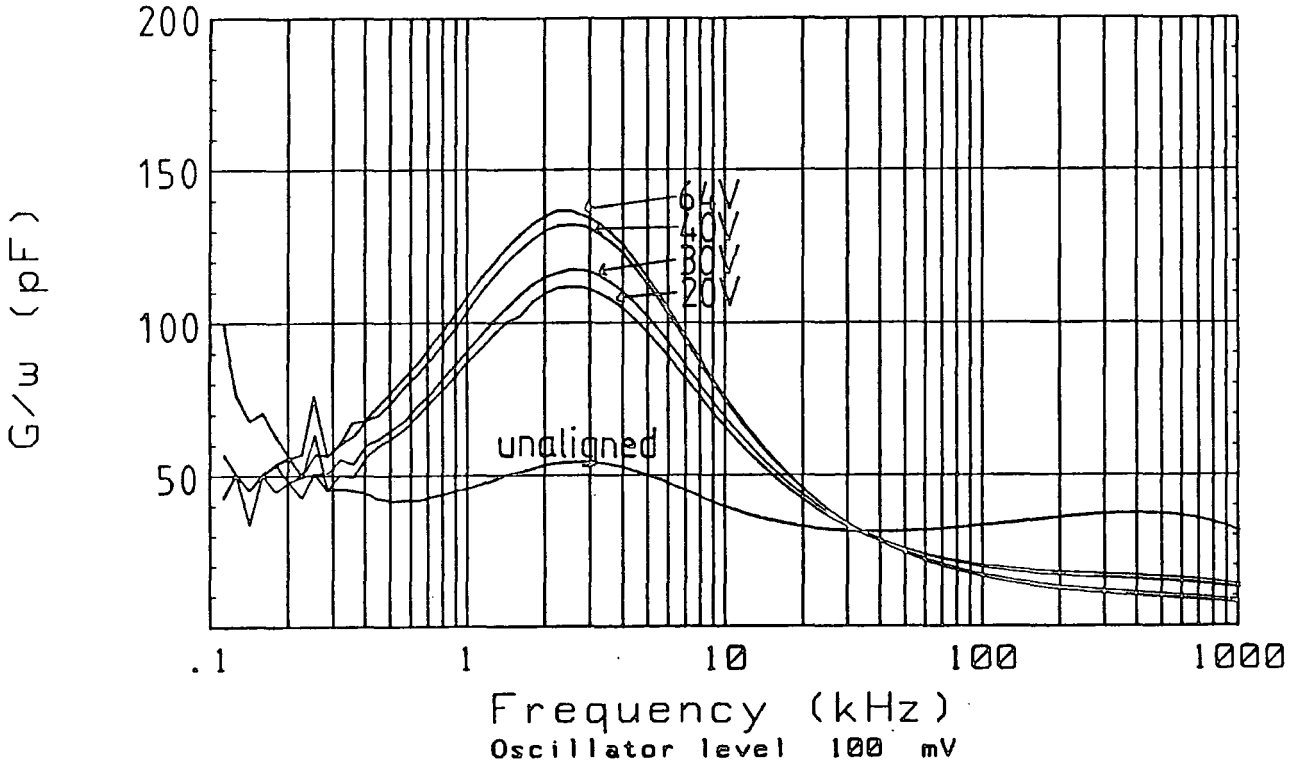

FIGURE 5.5
The loss spectra of GN3/3 at 40°C after alignment in progressively increasing electric fields.

giving widest bounds, is to assume a uniform electric field $\underline{E}$ and uniform displacement $\underline{D}$, both taken to be normal to the sample film, to give, respectively:

$$\epsilon_U = (1/d)\int \epsilon(\underline{r})d^3\underline{r} \qquad [5.2]$$

and

$$(1/\epsilon_L) = (1/d)\int [1/\epsilon(\underline{r})]d^3\underline{r} \qquad [5.3]$$

where the integrals are taken over a unit area of sample film of thickness d, U = upper, L = lower, and

$$\epsilon(\underline{r}) = \epsilon_{||} \cos 2\theta + \epsilon_{\perp} \sin 2\theta \qquad [5.4]$$

for a nematic, where θ is the angle between the director and $\underline{E}$ or $\underline{D}$.

Misalignment may be described by an ordering tensor, q_{zz}, (De Gennes, 1974) so Equation [5.4] becomes

$$\epsilon(\underline{r}) = 1/3\ \epsilon_{||}(1+2q_{zz}) + 2/3\ \epsilon_{\perp}(1-q_{zz}) \qquad [5.5]$$

Attard has described the use of an order parameter S_d ($-0.5 \leq S_d \leq 1$) to quantify the director misalignment. This is a macroscopic quantity, in comparison with the (microscopic) molecular order parameter S which describes the distribution of the molecular long axes about the director. Two approaches to the calculation of S_d have been proposed. In the first

(Attard, 1986), the loss peaks are resolved using a Fuoss-Kirkwood fitting process, then the intensities are compared at a temperature in the mesophase and one in the isotropic phase. In the second method (Attard et al, 1987b), the value of S_d for a partially aligned sample is found from its permittivity and that of completely aligned samples of the material at the same frequency and temperature.

Neither model has proven to be directly useful in this work since relaxation peaks which could be fitted were rarely observed in the isotropic phase, and perfectly aligned samples could not be produced reliably.

5.4 Stability of Alignment

The stability of the alignment is of great importance when considering the application of these side chain LCPs as optical storage media. Information is stored and read out using the optical contrast between aligned and unaligned regions. If the states of alignment vary, then the contrast is degraded and eventually the information is lost. Since the state of alignment can be measured by dielectric relaxation spectroscopy, this technique may be used to quantify any variation.

Figure 5.6 shows the change in δ peak amplitude with temperature for several LCPs. There is a significant difference between the rate of change of peak height with temperature for different materials. However, there is a similar rate of change with temperature for unaligned and aligned samples of the same LCP and for homopolymers and copolymers having the same mesogenic side group (e.g. GN2/10 and GN3/3, or GN2/11 and

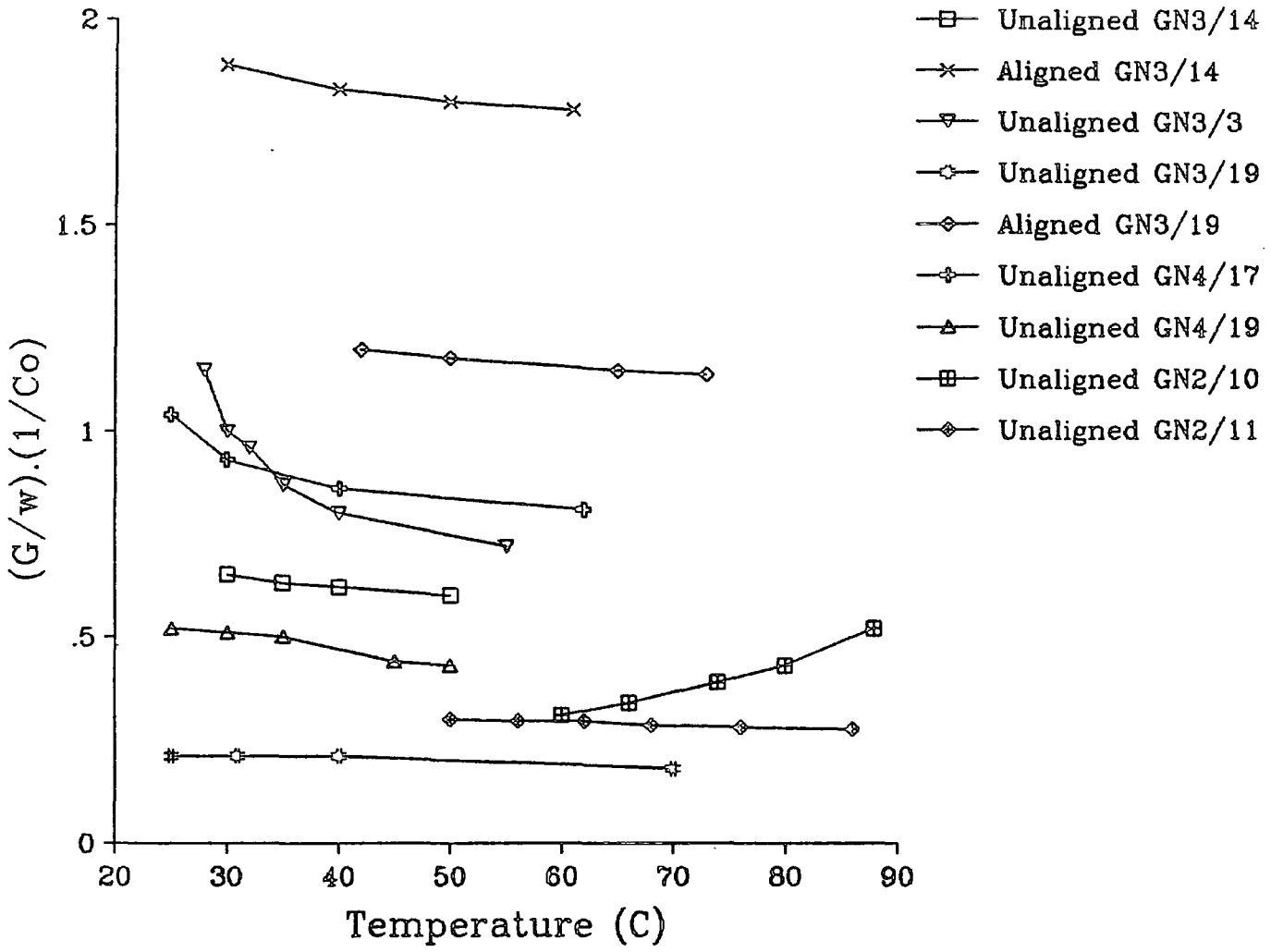

FIGURE 5.6
The change in the δ peak amplitude with temperature of a variety of homopolymer and copolymer LCPs.

GN3/14). An explanation for the difference between materials is proposed in Section 5.5 discussing the influence of structure on dielectric properties. However, it does appear that GN3/19 and GN3/14 are particularly stable against the variation of alignment with temperature.

The practical importance of the measured variations in these materials has been investigated. The peak height ϵ''_{max} can be related to the relaxation strength (or dielectric decrement) by

$$\Delta\epsilon_i = 2\epsilon''_{max}/\beta \qquad [5.6]$$

where β is the Fuoss-Kirkwood linewidth parameter (see Equation [4.7]) and "i" is the δ or α loss peak. In Table 5.1 the values of $\Delta\epsilon_\delta$ for GN3/3 are compared with similar values for the polymer I, as measured by Attard et al (1986c) (see Appendix IV for structure and transition data). The results for I are for both an unaligned sample and for an electric field aligned sample which is considered to have good homeotropic alignment. It can be seen that the variation of alignment with temperature is less than the variation between unaligned and aligned samples at the same temperature. The change in the alignment of GN3/3 is greater than that of polymer I, probably due to the higher viscosity of the latter.

Temperature (°C)	27	30	32	35	40	55	70
$\Delta\epsilon_\delta$	3.5	2.54	2.42	2.30	1.96	1.72	1.72

TABLE 5.1(a)
Variation of the dielectric decrement (or relaxation strength) with temperature of an unaligned sample of GN3/3.

Temperature (°C)	32	36	38	43	47	51	55	60	70
$\Delta\epsilon_\delta$ (unaligned)	2.62	2.57	2.53	2.37	2.38	2.28	2.23	2.18	2.06
$\Delta\epsilon_\delta$ (aligned)	8.61	8.37	8.57	8.03	7.77	7.55	7.42	7.26	6.82

TABLE 5.1 (b)
Variation of the dielectric decrement (or relaxation strength) with temperature of unaligned and aligned samples of the polymer I, as measured by Attard et al (1986a).

This technique is therefore useful to identify the best materials in terms of director stability with temperature. The results also indicate that the difference between unaligned and aligned states is likely to be sufficiently great that stored information should not be significantly degraded over this temperature range.

5.5 The Influence of Structure on Dielectric Relaxation in LCPs

5.5.1 Reference Temperatures

In order to compare the physical properties of different materials, it is necessary to identify conditions for normalising the results. With LCPs there are three temperatures which apparently could be used as references

in this normalisation process. These are the absolute clearing temperature T_C, the absolute glass transition temperature T_g and the absolute temperature T_o.

For the static dielectric behaviour ($\epsilon_{\parallel}'$ and $\epsilon_{\perp}'$ as functions of frequency), Equations [3.25] and [3.26] suggest that $T\epsilon_{\parallel}$ or $T\epsilon_{\perp}$ should be compared at equal values of the order parameter S. The mean field theory of Meier and Saupe (1959) leads to the conclusion that equal T/T_C corresponds adequately to equal S.

For the relaxation frequency ν_R, which is a dynamic dielectric quantity, there are other considerations to be included. From the discussion by Meier and Saupe (1966) of the δ relaxation frequency, ν_R may be written:

$$\nu_R = \nu_D / g \qquad [5.7]$$

where ν_D is the Debye relaxation frequency and g is a retardation factor arising from the nematic potential. It is thus reasonable to assume that g is a function of T/T_C. There is empirical evidence (Attard et al, 1987d) that for all mesogenic materials, the underlying relaxation frequency ν_D has a Vogel-Fulcher form:

$$\nu_D = \nu_D^o \exp[-A/(T - T_o)] \qquad [5.8]$$

where T_0 is a temperature related to the glass transition temperature. The relaxation frequency would therefore be expected to take the form:

$$\nu_R \sim \frac{\nu_D(T-T_o)}{g(T/T_c)} \qquad [5.9]$$

It is difficult to envisage using this relationship in practice since it would be exceedingly complicated to perform comparisons in such a two-dimensional way (that is, as a function of both $T-T_0$ and T/T_c). It should be noted that T_g is generally used for comparisons rather than T_0 to avoid attempting to determine the latter. In the following comparison of the dielectric behaviour of a variety of LCPs, T_c and T_g have been used separately as reference temperatures. This has led to the conclusion that properties of side chain LCPs which are mainly determined by the orientationally anisotropic molecular interactions should be scaled to T_c, whereas properties mainly related to cooperative motions which freeze at the glass transition should be scaled to T_g. The LCPs show hybrid properties of mesogenic and polymeric materials.

5.5.2 The Mesogenic Group

(a) Dynamic Behaviour - The Relaxation Frequency

Both the chain dynamics of the backbone and the dynamics of the mesogenic side groups are important considerations in describing the dielectric spectra of LCPs. In Table 5.2 the frequency locations ν_R of the δ and α relaxation peaks are summarised at 0.92 T_c and 1.18 T_g for a wide selection of LCPs having different core structures, lateral and terminal substituents and spacer groups; both homopolymers and copolymers are included. The mean and standard deviation values given for each relaxation loss peak and scaling temperature indicate that there is a significant correlation in response when scaling to T_g. This suggests

that these dynamics are determined by transitions between different conformations of the polymer backbone and these motions freeze at T_g. Returning to Equations [5.7] and [5.8], it would appear that the parameter A is therefore related to T_g, and that more than 20°C below T_c the corresponding retardation factor g has approximately the same value for all the materials considered.

		$0.92T_c$			$1.18T_g$	
Code	Temp/°C	$\log_{10}(\nu_R^{\delta}/Hz)$	$\log_{10}(\nu_R^{\alpha}/Hz)$	Temp/°C	$\log_{10}(\nu_R^{\delta}/Hz)$	$\log_{10}(\nu_R\alpha/Hz)$
GN3/3	67	4.75	-	38	3.39	5.68
GN3/14	56	4.33	6.93	35	3.29	5.96
GN3/15	65	3.90	5.05	55	3.23	4.63
GN3/16	30	3.3	4.92	31	3.3	4.92
GN3/19	65	4.76	-	31	3.42	5.65
GN3/22	26	2.95	-	31	-	-
GN4/17	51	4.17	6.03	30	3.02	5.11
GN4/18	40	3.06	5.36	45	3.31	5.63
GN4/19	50	4.32	6.34	25	3.08	5.14
GN3/40	50	2.85	4.27	50	2.85	4.27
Mean Relaxation Frequency		3.84 ±0.74	5.56 ±0.92		3.21 ±0.19	5.22 ±0.56

TABLE 5.2
Dielectric data illustrating the influence of the mesogenic side-chain group on relaxation frequencies.

(b) Static Behaviour - Calculation of Dipole Moments

The variations in the relaxation strengths (or dielectric decrement, see Equation [5.6]) and the permittivity of these LCPs arise from the range of dipole moments in the side groups. The theoretical effective dipole moment can be calculated for each LCP from the resolved component moments of each dipolar group (Klingbiel et al, 1974). This can be compared with

the experimental value calculated from the dielectric decrements. Any differences between the theoretical and experimental values may be related to the degree of correlation and interaction between side groups of the polymer. Dunmur et al (1980) have discussed the effects of such correlations in nematic lmmLCs.

The group dipole moments used to calculate the theoretical effective dipole moments are summarised in Appendix III, together with an example of the method of calculation. Only the side group dipole moments have been included.

The dipole moments may be found experimentally from the sum total of the dielectric decrements of the observed mesogenic relaxation processes. Using Equations [3.25] and [3.26] and also the derivation of $\Delta\epsilon_{\parallel}^{\delta}, \Delta\epsilon_{\parallel}^{\alpha}, \Delta\epsilon_{\perp}^{\delta}, \Delta\epsilon_{\perp}^{\alpha}$ described by Bone et al (1984) then:

$$T\Delta\epsilon_{\delta} + T\Delta\epsilon_{\alpha} = \frac{\rho h F^2}{3\epsilon_o k_B}\left[\frac{1}{3}\mu_l^2(1+2S) + \frac{2}{3}\mu_l^2(1-S) + \mu_l^2\right]$$

$$= \frac{\rho h F^2}{3\epsilon_o k_B}\mu_{eff}^2 \qquad [5.10]$$

where

$$hF^2 = \frac{\bar{\epsilon}(2\bar{\epsilon}+1)(\bar{\epsilon}_{\infty}+2)^2}{3(2\bar{\epsilon}+\bar{\epsilon}_{\infty})^2} \qquad [5.11]$$

$\bar{\epsilon}_{\infty}$ is the high frequency dielectric permittivity (the square of the refractive index measured at the same frequency) and $\bar{\epsilon}$ is the mean permittivity.

Tables 5.3 and 5.4 summarise the experimental values of the effective dipole moment at 0.92 T_c and 1.18 T_g respectively for several LCPs, as well as the theoretical values of the side group dipole moment. Since the data in these tables refer to temperatures significantly below T_c, S will vary only weakly with temperature and hence the quantities $T\Delta\epsilon_\delta$ and $T\Delta\epsilon_\alpha$ should do the same. This is seen from the table to be the case. The correlation of the experimental values of the effective dipole moment with molecular structure is excellent. The impact of the bridging ester group in GN3/3 and GN3/14 is evident when compared with GN3/19, and the effect of changing the fluorine position in GN4/18 can be seen compared with GN4/17 and GN4/19. The somewhat larger effective dipole of GN3/40, relative to GN3/3 and GN3/14, could be taken as an indication that antiparallel correlation is more hindered in the homopolymer. The absolute value of the moment obtained for GN3/19 is a little smaller than the value of $\sim 10 \times 10^{-30}$ Cm made for monomeric alkyl cyanobiphenyls, which in turn is smaller than the $\sim 15 \times 10^{-30}$ Cm of a "free" molecule without antiparallel correlation (Dunmur et al, 1978). The values of GN3/3 and GN3/14 are distinctly smaller than the estimate of 25×10^{-30} Cm made for monomeric cyanophenyl benzoates by Klingbiel et al (1974).

The experimental values of μ_{eff} are all considerably smaller than the theoretical values. Inter-and intra-molecular correlations may account for the differences. In the following three sections the influence on these interactions of the mesogenic core, the terminating functional group and the spacer, respectively, are studied in detail. It is interesting to note that Bormuth and Haase (1988) in their study of the relaxation spectra of LCPs having laterally fixed mesogenic side groups, found that

the relaxation strengths were more similar to those of 1mmLCs than to end fixed LCPs such as those discussed above. Together with the fact that the relaxation loss peaks were also narrower, this suggests that the inter- and intra-molecular correlations found in conventional side chain LCPs are reduced by fixing the mesogens laterally.

Code	$T\Delta\epsilon_\delta$	$T\Delta\epsilon_\alpha$	$T\Delta\epsilon_\delta + T\Delta\epsilon_\alpha$	$\mu \times 10^{30}$ (Cm) (Experimental)	$\mu \times 10^{30}$ (Cm) (Theoretical)
GN3/40	337	1870	2206	15	20.1
GN3/15	450	2493	2943	17.1	20.1
GN3/16	319	1104	1423	12.9	20.1
GN4/17	684	1478	2161	15.3	23.8
GN4/18	556	1085	1642	13.3	17.3
GN4/19	310	2003	2313	16	23.8
GN4/16	100.8	401	502	7.7	12.6

TABLE 5.3
Comparison of the experimental and theoretical dipole moments of LCPs at 0.92 T_C.

Code	$T\Delta\epsilon_\delta$	$T\Delta\epsilon_\alpha$	$T\Delta\epsilon_\delta + T\Delta\epsilon_\alpha$	$\mu \times 10^{30}$ (Cm) (Experimental)	$\mu \times 10^{30}$ (Cm) (Theoretical)
GN3/19	152	442	595	7.4	15.8
GN3/3	613	837	1451	12.2	19.5
GN3/14	142	1343	1484	12.6	19.5
GN3/29	379	1466	1845	12.8	19.5
GN3/25	452	1423	1875	13.2	19.5
GN3/40	337	1870	2206	15	20.1
GN3/15	519	2194	2714	16.4	20.1
GN3/16	319	1104	1423	12.9	20.1
GN4/17	612	1723	2335	15.9	23.8
GN4/18	571	1140	1712	13.6	17.3
GN4/19	310	1747	2057	15.1	23.8

TABLE 5.4
Comparison of the experimental and theoretical dipole moments of LCPs at 1.18 T_g.

(c) The Core Group

The influence of the core group can be studied by comparing GN3/3, GN3/19, GN4/17 and GN4/18. These are all copolymers having -$(CH_2)_5O$-alkoxy spacer groups and cyano terminated mesogenic groups. Data from these LCPs are summarised in Table 5.5.

	GN3/3	GN3/19	GN4/17	GN4/18
Core structure	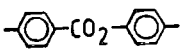	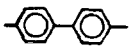	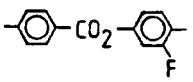	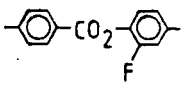
1.18 T_g	38.5	31	30	45
δ position peak $\log_{10}\nu_R$	3.39	3.42	3.02	3.31
δ peak width* (decades)	1.39	1.37	1.24	1.37
α peak position ($\log_{10}\nu_R$)	5.68	5.65	5.11	5.63
α peak width* (decades)	2.53	2.59	2.74	3.93
δ peak activation energy** ($kJmol^{-1}$)	106	80	98	98

* half-height peak width = $1.14/\beta$ ** Arrhenius activation energy

TABLE 5.5
A comparison of the dielectric properties of LCPs having different mesogenic core structures

The loss spectra at 1.18 T_g are shown in Figure 5.7. The peak width is directly related to the anisotropic molecular interactions between mesogenic side groups. In the case of an ideal Debye relaxation loss peak, the half-height width is about 1.14 decades. Interactions between the relaxing dipoles modify the local field and the loss peaks are broadened. It can be seen from Table 5.5 that the δ peak width of GN4/17 is particularly narrow and the α peak width of GN4/18 is particularly broad. These effects probably arise from the substitution of a lateral

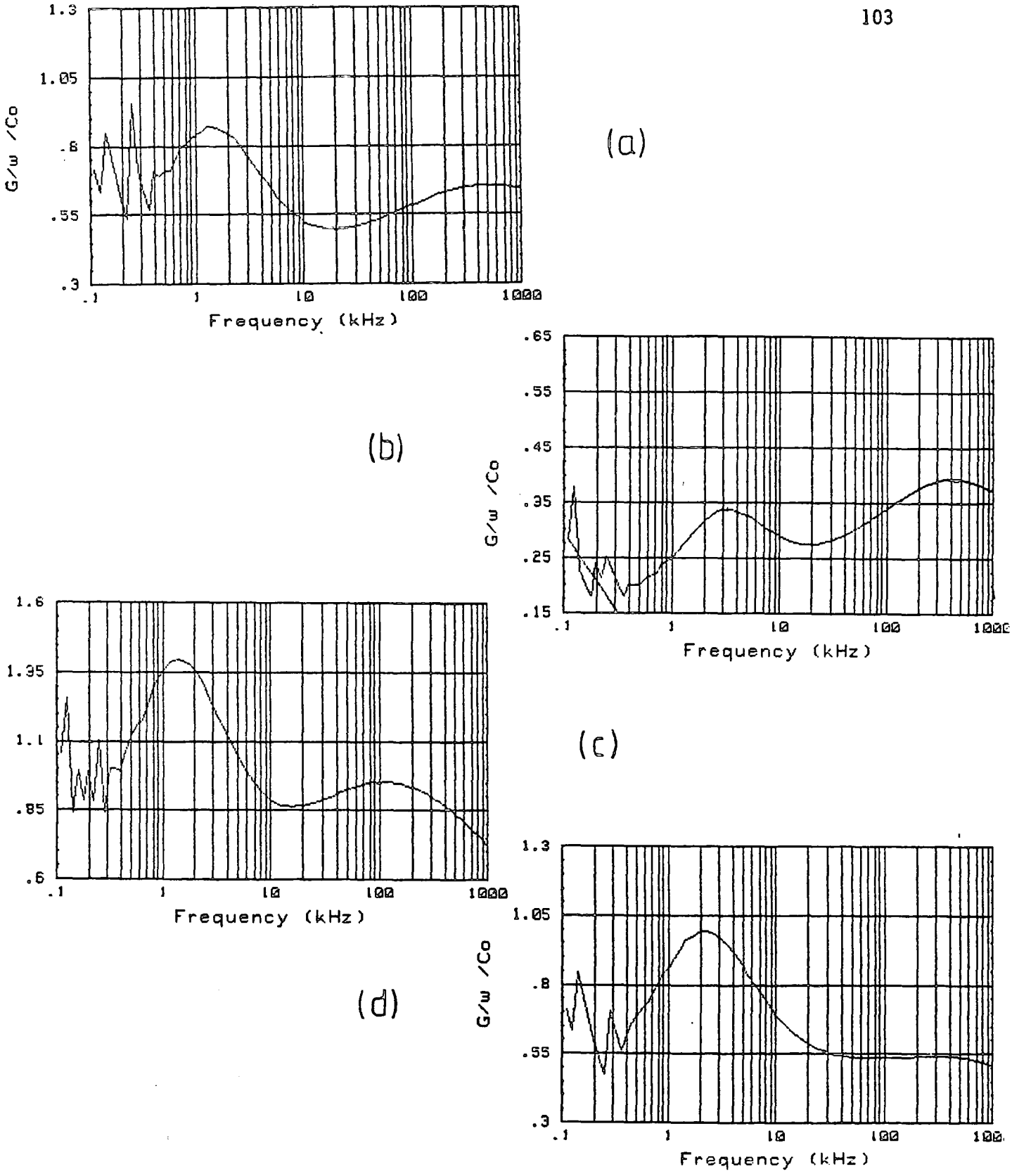

FIGURE 5.7
The loss spectra of (a) GN3/3 at 35°C, (b) GN3/19 at 31°C, (c) GN4.17 at 30°C and (d) GN4/18 at 45°C.

fluorine group in the meta and ortho position respectively. In the meta position, the dipole arising from the highly electronegative fluorine predominantly reinforces the longitudinal dipole moment of the mesogenic moiety. This enhanced dipole moment is therefore likely to be subject to less hindrance from other side groups, so reducing the range of relaxation frequencies and narrowing the δ peak. In the ortho position (GN4/18) the fluorine group contributes mainly to the transverse dipole moment of the mesogenic moiety. The α relaxation peak is composed of at least 3 separate relaxation processes (see Section 3.1.2) with similar relaxation frequencies. An increase in the transverse dipole moment particularly affects the relaxation frequencies of the (1,0) and (1,1) modes. The spectrum of relaxation frequencies encompassed by the α peak might therefore be expected to increase and the α peak to broaden. The ortho substitution also increases the steric hindrances of rotational motions of the side group.

The effect of a biphenyl core, as opposed to a phenyl benzoate core is most apparent in the low δ peak activation energy of 80 $kJmol^{-1}$ of GN3/19 and in the very stable peak amplitude with changing temperature as shown in Figure 5.6. Antiparallel correlation frequently occurs in 1mm cyanobiphenyl liquid crystals (Dunmur et al, 1978). Similar correlations occur between cyanobiphenyl side groups of LCPs, either as inter- or intra-chain interactions (Parneix et al, 1987). This correlation results in cooperative motion of side groups over a relatively long range. The activation energy for relaxation of the longitudinal dipole moment (δ

relaxation) is therefore reduced, but the relative orientation of the side groups with respect to each other stays fairly constant: hence there is a very small change in alignment with temperature.

(d) The Terminal Group

The most significant role of the terminal group is in determining the sign of the anisotropy of the dielectric permittivity ($\Delta\epsilon$) of a mesogenic moiety. Strongly dipolar species such as cyano and fluoro groups tend to result in liquid crystals having positive dielectric anisotropy ($\epsilon_{\parallel} > \epsilon_{\perp}$), whereas alkoxy groups tend to lead to negative dielectric anisotropy. The terminal group also influences the correlation between mesogens. Relaxation of the end group alone can only be observed at temperatures well below the glass transition when cooperative motions have been frozen out. Zentel et al (1985) have compared the behaviour of n-butoxy and methoxy end groups and observed a relaxation present only in the case of the LCP having the n-butoxy end group. They termed this the γ_2 loss process and measured an apparent activation energy of 24 ± 4 $kJmol^{-1}$. Such internal reorientations are not normally observed for LCPs having the more flexible polysiloxane backbone. Five LCPs were available to compare the effects of different end groups: GN3/14, GN3/22, GN4/11, GN4/16 and GN3/18. All these LCPs were copolymers having a $-(CH_2)_6O-$ alkoxy spacer group and a phenyl benzoate core. Some of the LCPs showed anomalous dielectric relaxation spectra and possible interpretations will be suggested.

i) GN3/14

GN3/14 may be considered as a "standard" in this set of LCPs in that its dielectric spectra are easily measured and readily interpreted using the formalism described in Section 5.2. Figure 5.8 shows the loss spectra of an unaligned sample of GN3/14 at several temperatures. The Arrhenius activation energies for the δ and α processes are 94 and 91 $kJmol^{-1}$ respectively, and the half-height peak widths for these loss processes are 1.25 and 2.78 decades, respectively, at a reduced temperature of 0.92 T_c.

ii) GN3/22

GN3/22 has weakly negative dielectric anisotropy (i.e. $\Delta\epsilon$~-2) due to the methoxy terminating species. This LCP has a relatively low macroscopic viscosity, being a "tacky" solid at room temperature. This allowed surface alignment techniques to influence the bulk alignment of the LCP. Reasonable degrees of homeotropic and homogeneous alignment were produced using lecithin and rubbed polyimide, respectively. Figure 5.9 compares the spectra of unaligned and partially homeotropically aligned samples at 45°C, while Figure 5.10 shows the loss spectra as a function of temperature for the partially homeotropically aligned sample.

The δ relaxation of GN3/22 has a relatively high activation energy of 128 $kJmol^{-1}$ and a broad half-height peak width of 1.54 decades. These values indicate that the longitudinal dipole moment is subject to considerable steric hindrance. In contrast, the α relaxation is evidently a relatively unhindered process. The α loss peak occurs approximately four decades higher in frequency than the δ relaxation peak, making it difficult to produce a reliable estimate of the activation energy or peak

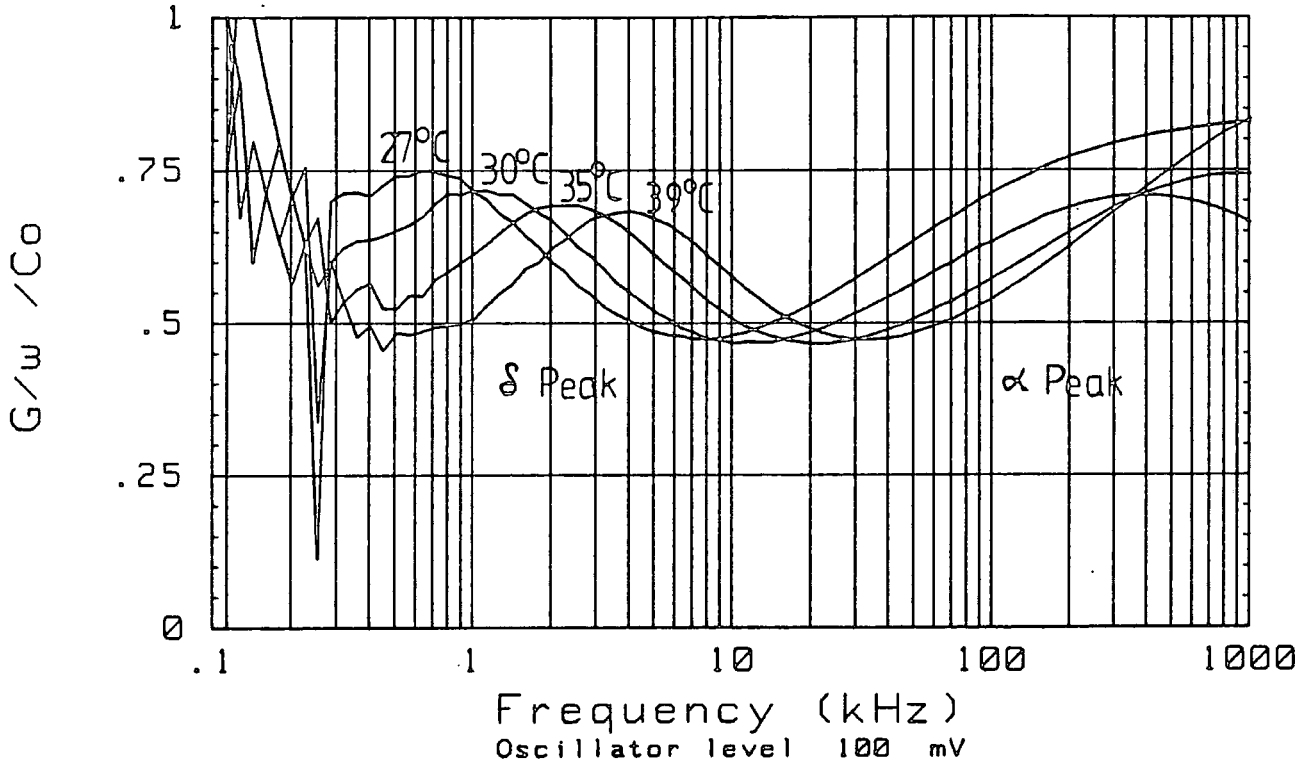

FIGURE 5.8
The loss spectra of unaligned GN3/14 at 27°C, 30°C, 35°C and 39°C.

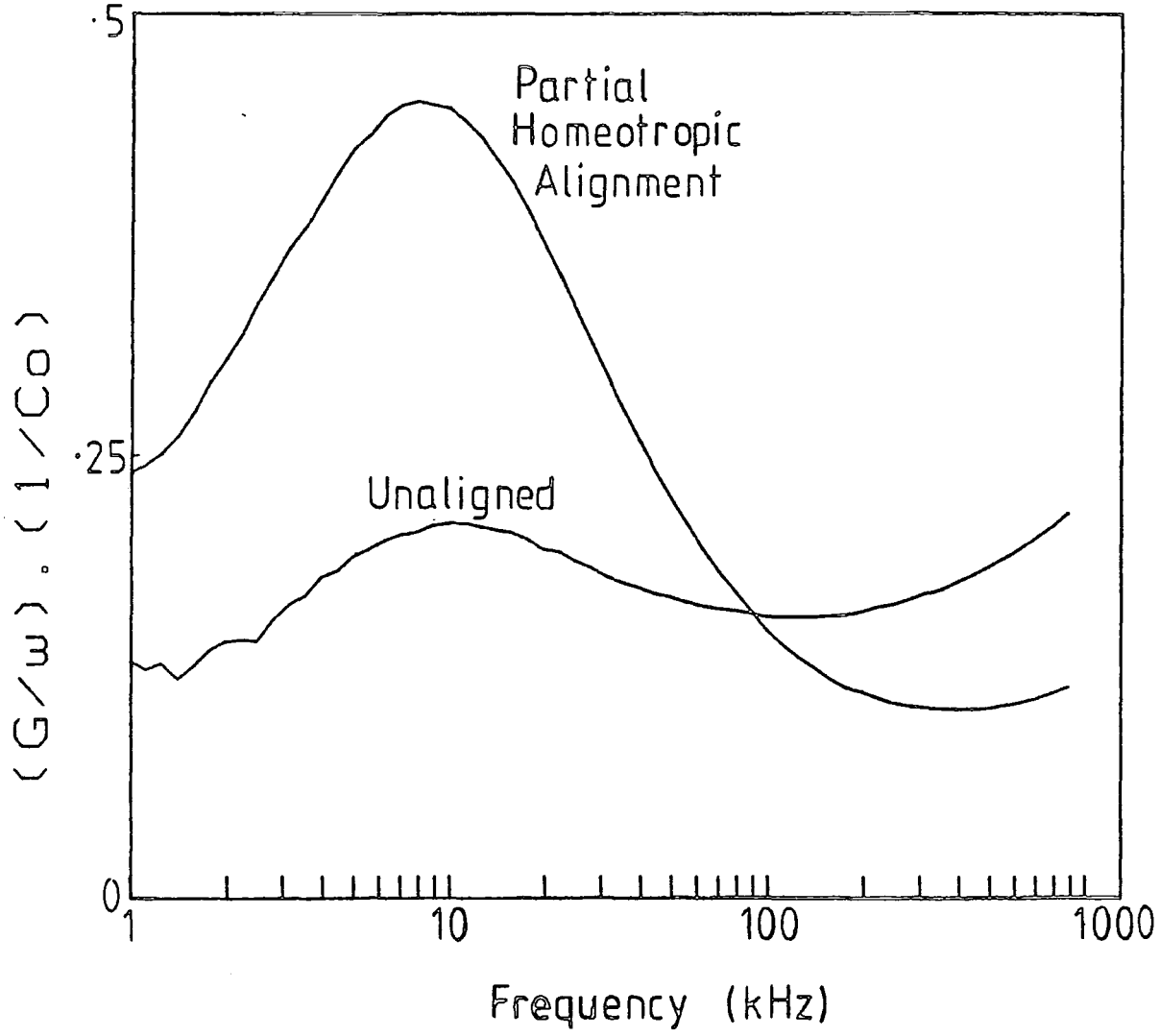

FIGURE 5.9
The loss spectra of an unaligned sample and a partially homeotropic aligned sample of GN3/22 at 40°C.

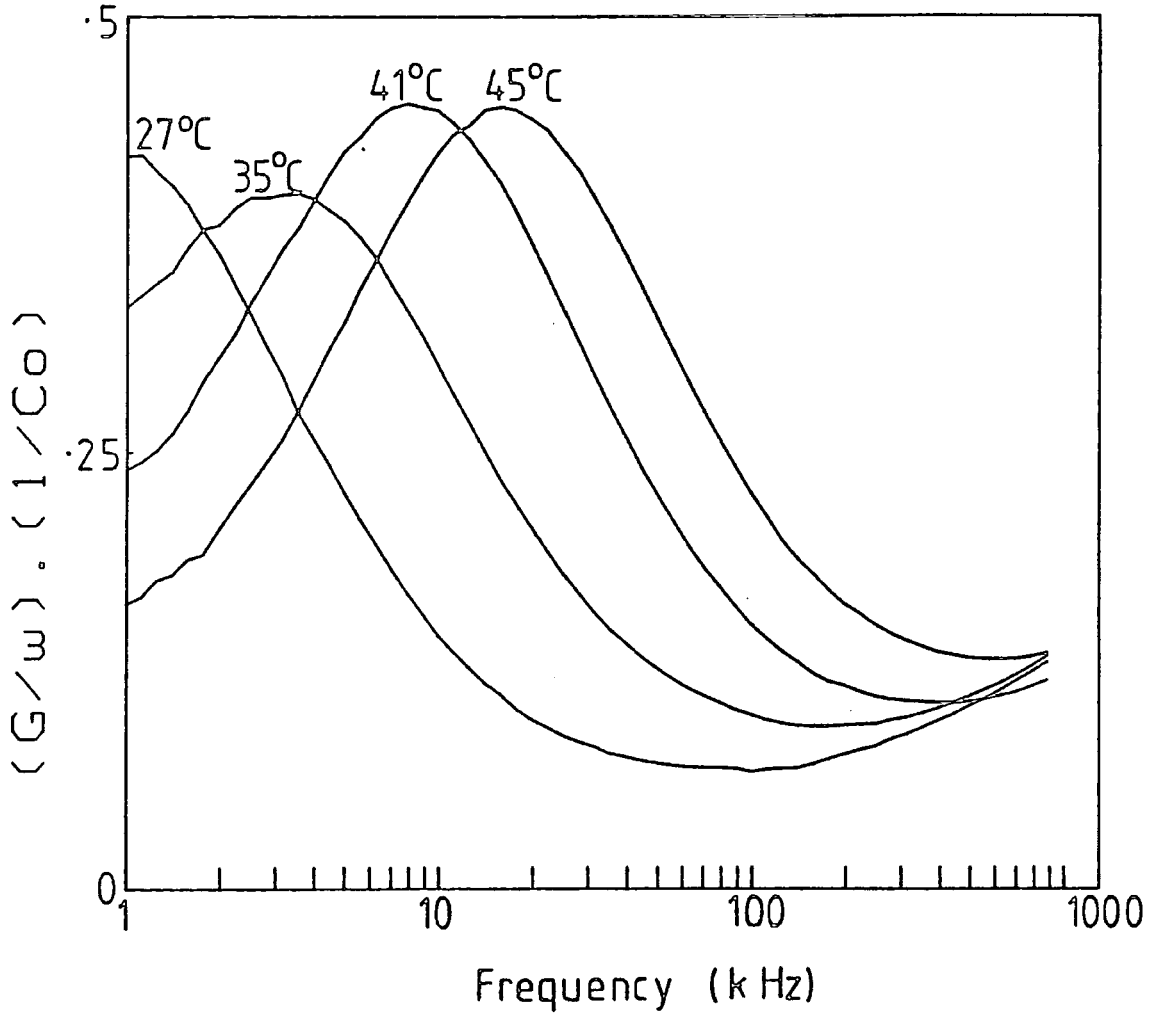

FIGURE 5.10
The variation of the loss spectrum of partially homeotropically aligned GN3/22 with temperature.

width. The high α relaxation frequency, together with the low viscosity exhibited by this LCP shows that the absence of a smectic layer structure results in a lower micro viscosity. The reorientation of transverse dipole moments appears considerably easier in this nematic phase than in the more ordered smectic phase.

iii) GN4/11 and GN4/16

These LCPs have -F and $-CF_3$ terminating species respectively. They show a positive dielectric anisotropy. The dielectric spectra of the LCPs have several features which are unusual when comparing them with the "standard" GN3/14. Figures 5.11 and 5.12 show the loss spectra of GN4/11 and GN4/16 respectively, as a function of temperature. Relaxation processes only become active at temperatures above the melting transition of each LCP. The reason for this transition is not clear since all the LCPs were subject to extensive purification procedures, but it does imply that these polymers have a tendency to form crystalline structures.

Figure 5.13 shows the loss spectra of GN4/11 at 50°C in an unaligned state and after applying an electric field to induce partial homeotropic alignment. The lower frequency relaxation peak is increased in amplitude by electric field alignment, consistent with δ-type relaxation behaviour. This broad loss peak can be fitted using two narrow (about 1.6 decades half-height width) Fuoss-Kirkwood loss curves separated by about one decade (see Figure 5.14). They have similar activation energies of about 95 $kJmol^{-1}$. This splitting could be a consequence of the crystalline tendency of GN4/11. Mixtures of chemically different mesogenic compounds are known to show distinct low frequency relaxations associated with each

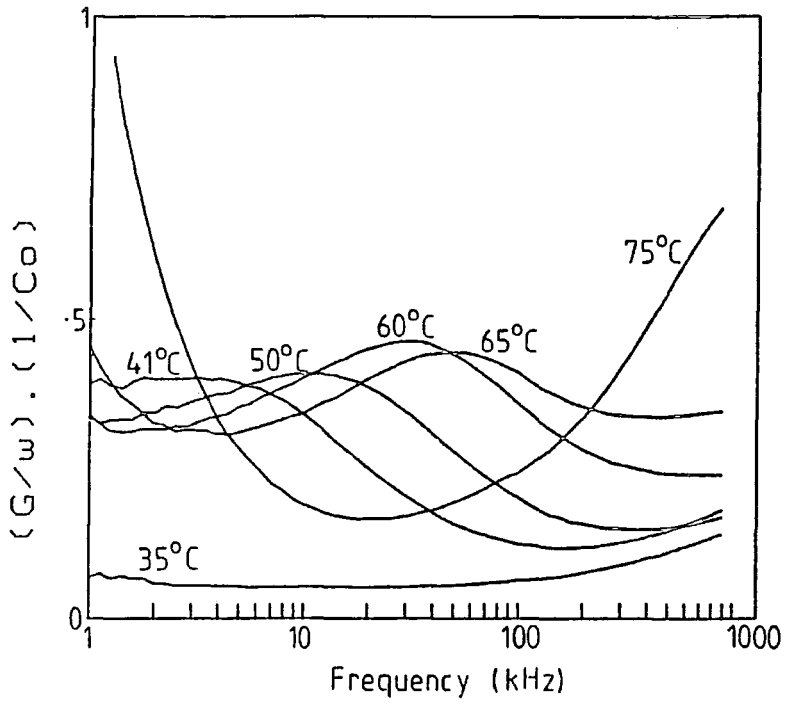

FIGURE 5.11
The variation of the loss spectrum of GN4/11 with temperature.

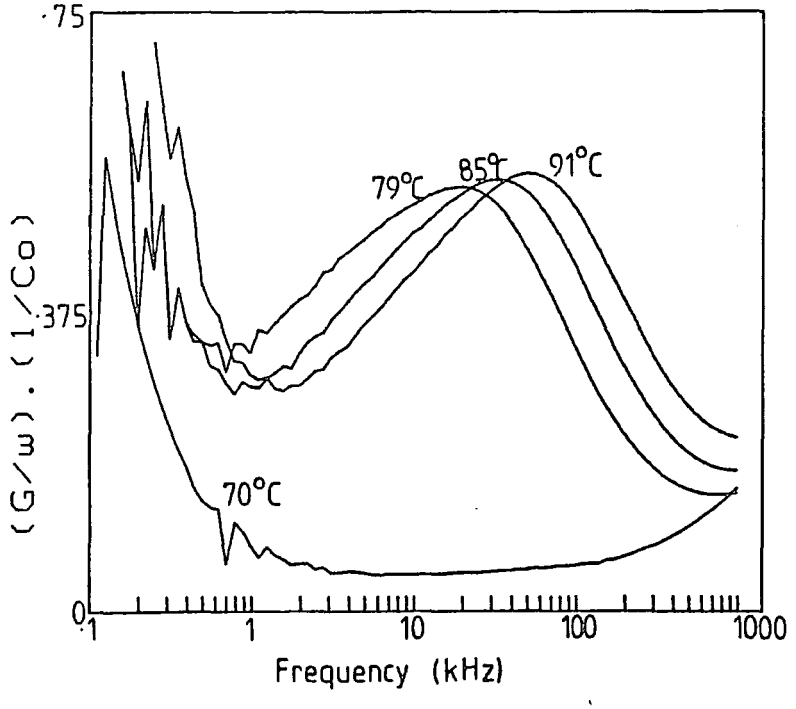

FIGURE 5.12
The variation of the loss spectrum of GN4/16 with temperature.

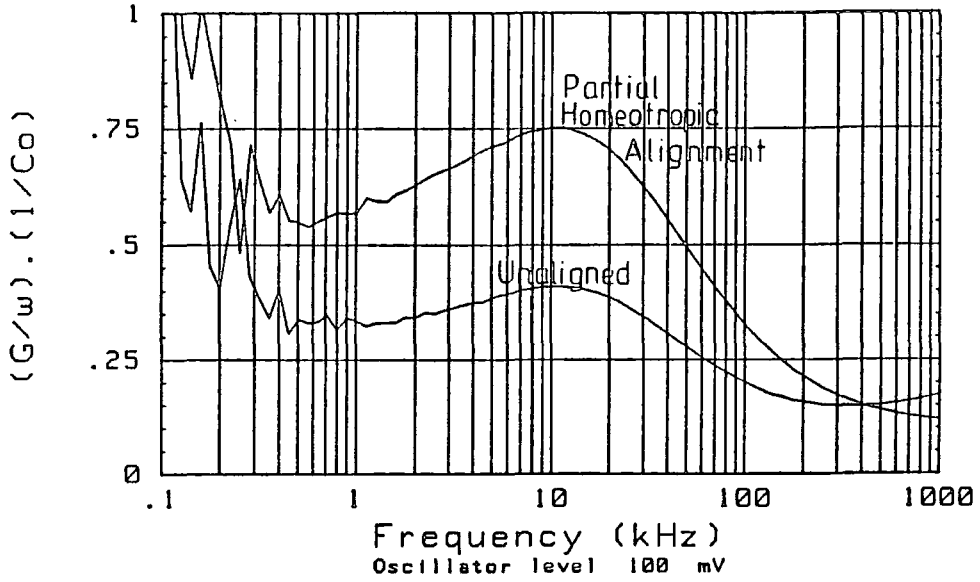

FIGURE 5.13
The loss spectra of GN4/11 at 50°C in an aligned state and after application of 75V (3 kHz sine) electric field to produce partial homeotropic alignment.

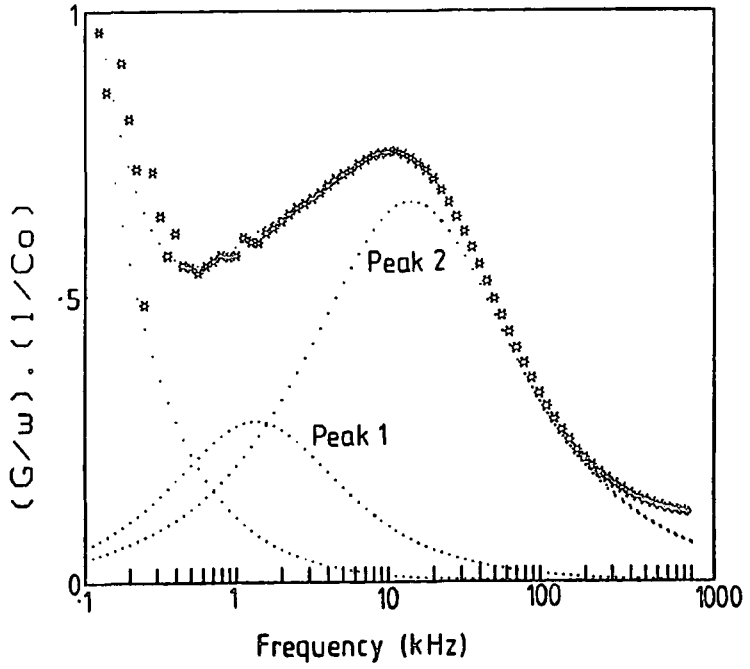

FIGURE 5.14
The loss spectrum of GN4/11 at 50°C fitted with two Fuoss Kirkwood curves.

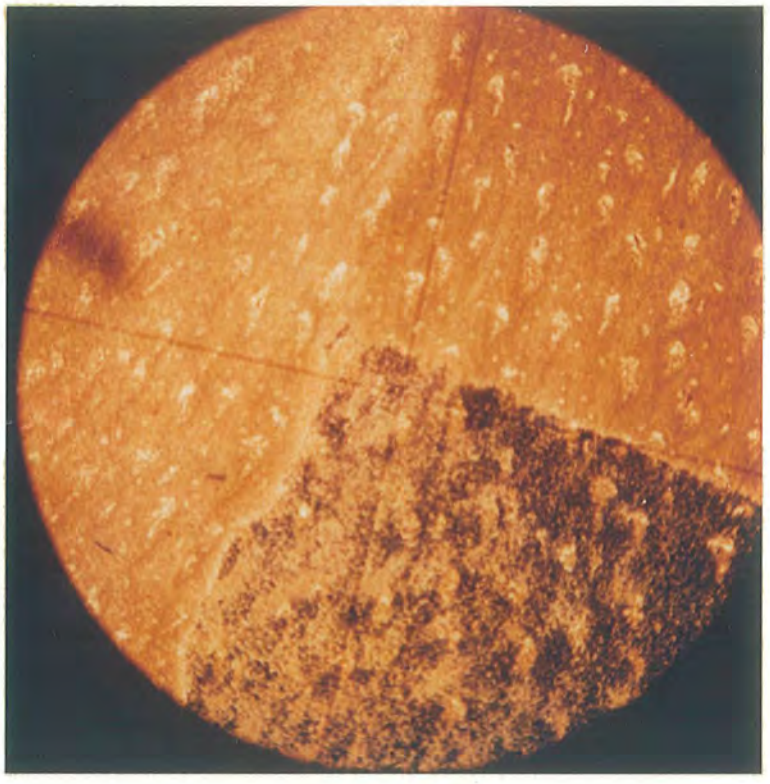

FIGURE 5.15
A photograph of the texture of GN4/11 at room temperature, taken between crossed polarisers (65x magnification) after alignment in an electric field of 75 V_{rms} (3 kHz sine).

component (Clark, 1985a), whereas chemically similar compounds exhibit a single dielectric spectrum: Pranoto et al (1986) reported that a siloxane liquid crystalline copolymer consisting of a mixture of cyano-terminated and methoxy-terminated phenyl benzoate side groups showed a single unsplit δ peak. If the local field environment in GN4/11 varies between crystalline type and mesomorphic, distinctly different δ relaxation frequencies would be expected. Figure 5.15 is a photomicrograph taken between crossed polarisers of the texture of GN4/11 at room temperature after alignment at elevated temperatures using 75V rms. Bright regions are apparent, these appear to be crystallites. Only the low frequency tail of the α relaxation could be observed at about 1 MHz in these experiments. There is evidently a large separation between the α and δ relaxations in GN4/11.

GN4/16 behaves in a similar way to GN4/11. The δ peak Arrhenius activation energies were both about 83 $kJmol^{-1}$ and the half-height peak widths about 1.4 decades, while the peak separation remained at about one decade.

These LCPs are clearly unsuitable as room temperature information storage media. However, these results do show that dielectric relaxation spectroscopy is a sensitive probe of molecular dynamics and the local field environment and they also emphasise that fitting is an important part of the process of interpreting the results.

iv) GN3/18

GN3/18 has a chiral terminating group; in low molar mass LCs this structure would be expected to produce a smectic C mesophase. The homopolymer does indeed form the S_C phase, but the copolymer GN3/18

exhibits the less ordered smectic A phase. It is biphasic at room temperature. X-ray studies by Sutherland (1987) have indicated that GN3/18 has an interdigitated smectic A structure with almost total overlap of the side groups, in contrast to the rather less complete overlap in LCPs such as GN3/14 and GN3/3.

The dielectric loss spectrum of GN3/18 shows different properties in the mesophase, biphasic region and isotropic phase; the loss spectrum is shown at several temperatures in Figure 5.16. At 9°C the large peak is well fitted by two broad Fuoss Kirkwood loss curves (see Figure 5.17) having half-height widths of 2.45 and 2.19 decades, respectively, and separated by 0.5 decades. At higher temperatures in the mesophase, the spectra appear to be fitted by two loss curves separated by 2-3 decades (see Figure 5.18). The shallow maximum of the lower curve is difficult to identify accurately, however, due to the low frequency conductivity tail. In the biphasic region there continues to be two well separated loss curves which can be fitted by broad peaks (half height width 2.19 decades), see Figure 5.19. In the isotropic phase there is apparently a single loss peak. This is resolved by the fitting process into two narrow peaks (1.15 and 1.63 decades width) 0.6 decades apart, see Figure 5.20.

An interpretation of these spectra in terms of relaxation mechanisms is not obvious. A likely explanation is that in the plots from 15°C to 35°C the lower frequency peak corresponds to the δ relaxation and the higher frequency peak corresponds to the α relaxation. The α relaxation can probably be fitted by two Fuoss-Kirkwood curves (as shown at 9°C) because the $-CO_2CH_2C^*(H)(Et)(Me)$ terminal group contributes mainly to the

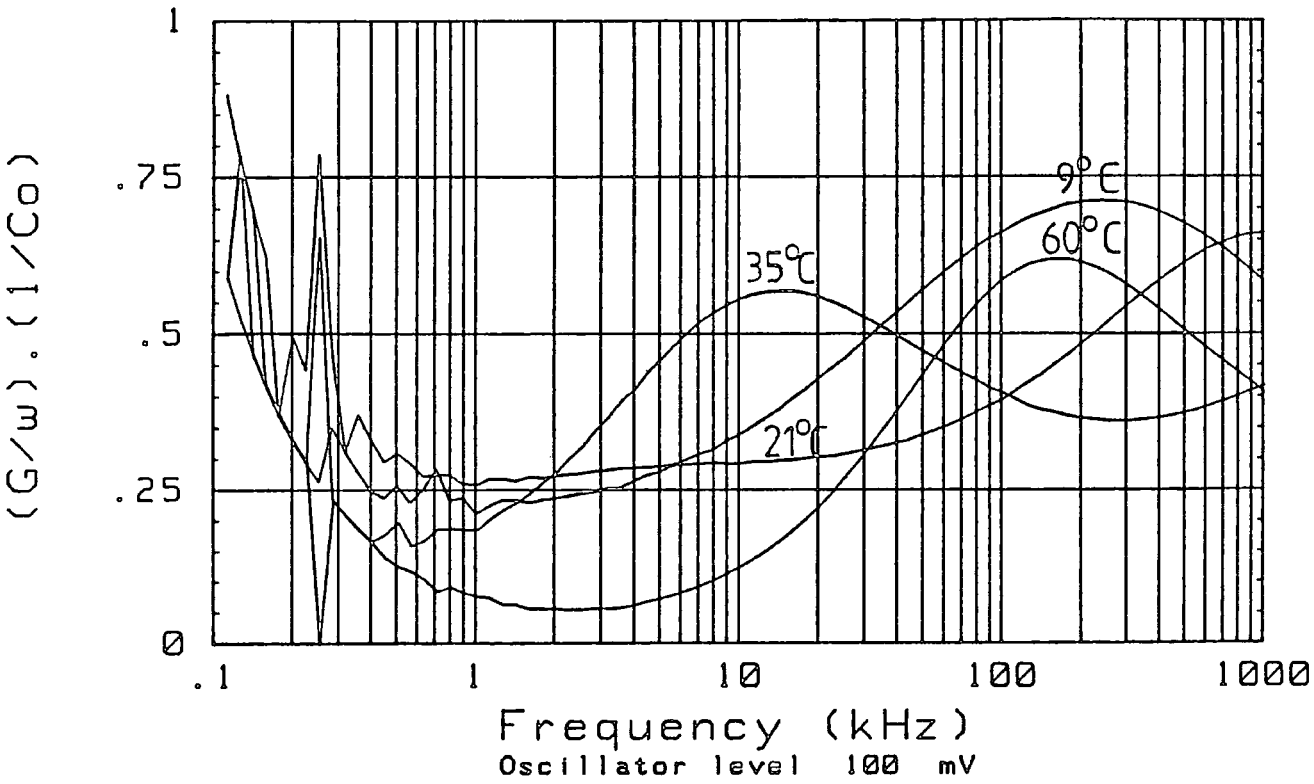

FIGURE 5.16
The variation of the loss spectrum of GN3/18 with temperature.

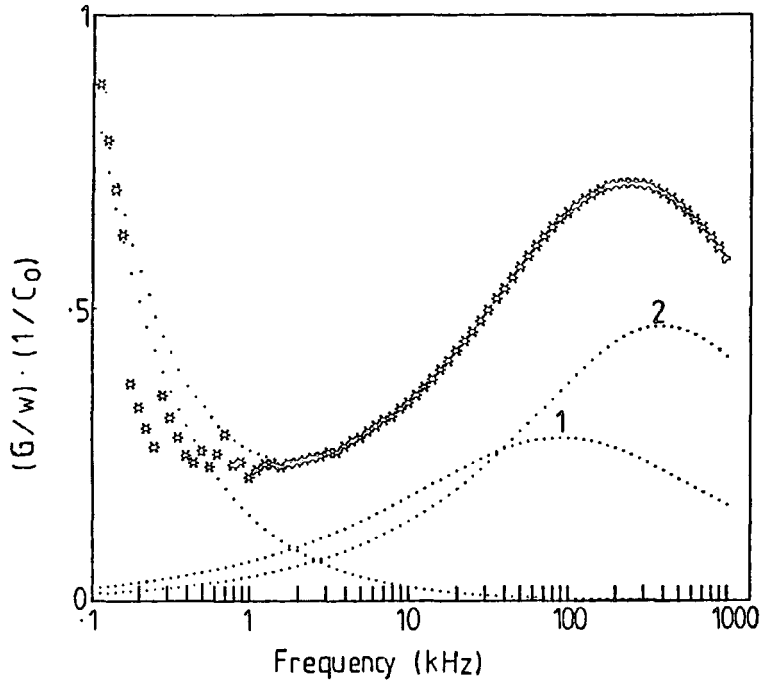

FIGURE 5.17
The loss spectrum of unaligned GN3/18 at 9°C fitted with two Fuoss Kirkwood curves.

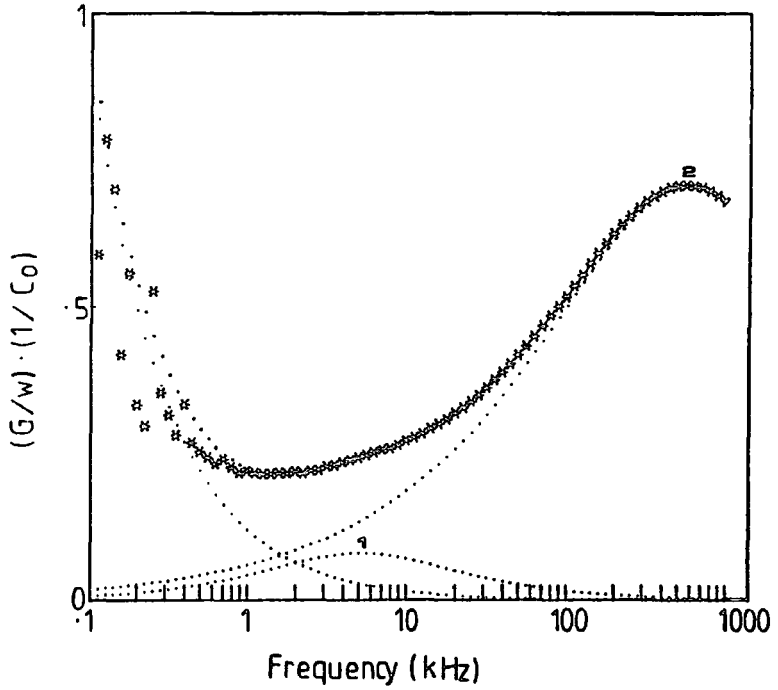

FIGURE 5.18
The loss spectrum of unaligned GN3/18 at 15°C fitted with two Fuoss Kirkwood curves.

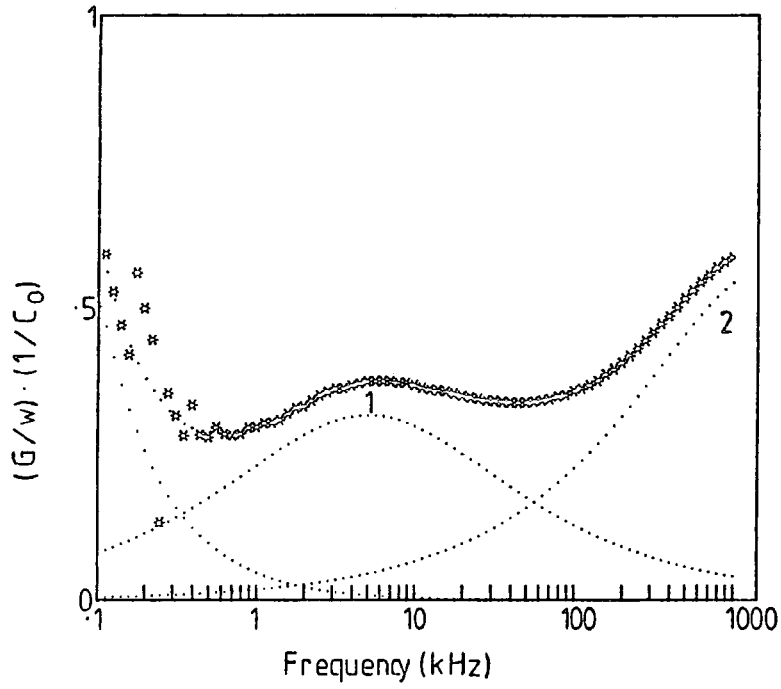

FIGURE 5.19
The loss spectrum of unaligned GN3/18 at 25°C fitted with two Fuoss Kirkwood curves.

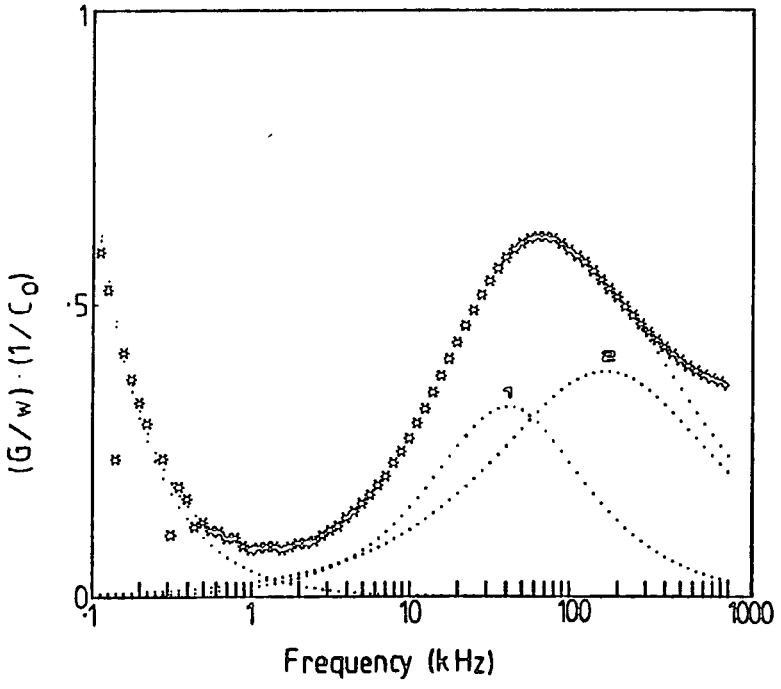

FIGURE 5.20
The loss spectrum of GN3/18 at 50°C fitted with two Fuoss Kirkwood curves.

transverse dipole moment of the side group. Either there is a separation of the three modes which lead to the α relaxation, or relaxations of the two ester groups (one from the middle and one from the end of the side group) can be observed separately due to different local fields for the two regions. The complete interdigitisation observed in the X-ray studies would be expected to lead to different degrees of constraint on the reorientation of the two areas of the side group. A similar explanation has been proposed by Endres et al (1987) to explain their observation of two loss peaks in a combined main-chain/side-chain LCP. The complete interdigitisation and consequent steric hindrance probably causes the unusually broad δ peak observed for this LCP.

In the isotropic phase, the two clearly resolved relaxations may be understood if it is assumed that the rotational diffusion tensor is sufficiently anisotropic for distinct relaxation times to be associated with the longitudinal and transverse components. A similar effect was observed by Bone et al (1984) in their study of dialkyl phenyl benzoate esters. Using their equation for the anisotropy in the rotational diffusion tensor:

$$\frac{D_{\parallel}^{rot}}{D_{\perp}^{rot}} = 2\left(\frac{\epsilon_o'^{l}}{\epsilon_o'^{l}}\right)\left(\frac{2\epsilon_o'^{l} + \epsilon_\infty'^{l}}{2\epsilon_o'^{t} + \epsilon_\infty'^{t}}\right)\left(\frac{\omega^{t}}{\omega^{l}}\right) - 1 \qquad [5.12]$$

it can be shown that $D_{\parallel}^{rot}/D_{\perp}^{rot}$ for GN3/18 is about 7.5. This suggests that a degree of local ordering remains in the isotropic phase.

These five examples have shown that the terminating group plays a crucial role in determining the dielectric response of side chain LCPs. The cyano terminating group encourages antiparallel correlation between side groups and as a result the α and δ relaxations are considerably closer in frequency than for the other structures. The nematic phase of GN3/22 results in a considerable reduction in the hindrance to reorientation of transverse dipole moment components. Local ordering is apparent even in the isotropic phase of GN3/18 due to the highly interdigitated structure. Finally, different types of molecular interactions and local field environments were detected in GN4/11 and GN4/16, apparently due to the coexistence of mesogenic and non-mesogenic phases.

(e) The Spacer

The spacer is a flexible link, usually an alkyl or alkoxy chain, which joins the mesogenic side group to the polymer backbone. The length of this spacer is influential in determining the mesophase behaviour (Finkelmann et al, 1978; Gemmel et al, 1985). At temperatures sufficiently far below the glass transition to reduce the activity of most dipolar species to a minimum, a relaxation peak has been observed in polyacrylate LCPs which is attributed to the flexible spacer allowing internal reorientations between the relatively stiff acrylate chain and the pendant mesogens. Zentel et al (1985) called it the γ_1 relaxation and measured an Arrhenius activation energy of 35±10 $kJmol^{-1}$, Parneix et al (1987) called it the β relaxation. Above the glass

transition temperature, the spacer length influences the microviscosity - by lengthening the spacer the loss peaks are shifted to higher frequencies and the activation energies are reduced (Parneix et al, 1987).

In the LCPs available, it was possible to detect this behaviour, though the effect was slight since comparisons could only be made between C_5 and C_6 spacer lengths. Table 5.6 compares the δ peak Arrhenius activation energies of two pairs of LCPs.

n†	5	6	5	6
Code	GN3/3	GN3/14	GN4/17	GN4/19
δ peak Activation energy ($kJmol^{-1}$)	106	94	98	92

† n is defined as the spacer length $-(CH_2)_n-O-$

TABLE 5.6
Comparison of the activation energies of LCPs having odd and even spacer lengths.

The spacer also appears to play a role in determining the stability of alignment (see Section 5.4). Figure 5.6 contains information on the rate of change of δ peak alignment with temperature for several LCPs, including 3 pairs of LCPs having the same structures except for $-(CH_2)_5O-$ and $-(CH_2)_6O-$ spacer lengths respectively, i.e. GN4/17 and GN4/19, GN3/3 and GN3/14, GN2/10 and GN2/11. The even alkoxy spacer length ($-(CH_2)_5O$) appears to consistently result in less stable alignment than the odd spacer ($-(CH_2)_6O-$). This is perhaps unexpected since the longer $-(CH_2)_6O-$ spacer increases the decoupling of the mesogenic moiety from the backbone

and should therefore decrease the rigidity and stability of the system. A possible explanation is that the equilibrium condition of the even spacer length is a linear all-trans arrangement, whereas the odd spacer length results is a less symmetric coupling of the backbone and mesogen. This would therefore increase the steric hindrance of the mesogens and result in a more stable molecular configuration with respect to temperature changes.

5.5.3 The Polymer Backbone

The backbone has a distinctive influence on the phase behaviour of LCPs. The more mobile the backbone, the easier it is to induce a smectic layered structure in which the backbone is constrained between the layers. Polyacrylate and polymethacrylate backbones tend to induce nematic mesophases, whereas the more flexible polysiloxane backbone favours smectics (Pranoto et al, 1986). This arises because rotation about the siloxane bond increases the conformational freedom, allowing it to stabilise the increased order of a smectic phase. The impact of chain flexibility on relaxation frequencies could be quantified by studying the scaling relative to the glass transition temperature (see Section 5.5.2(a)).

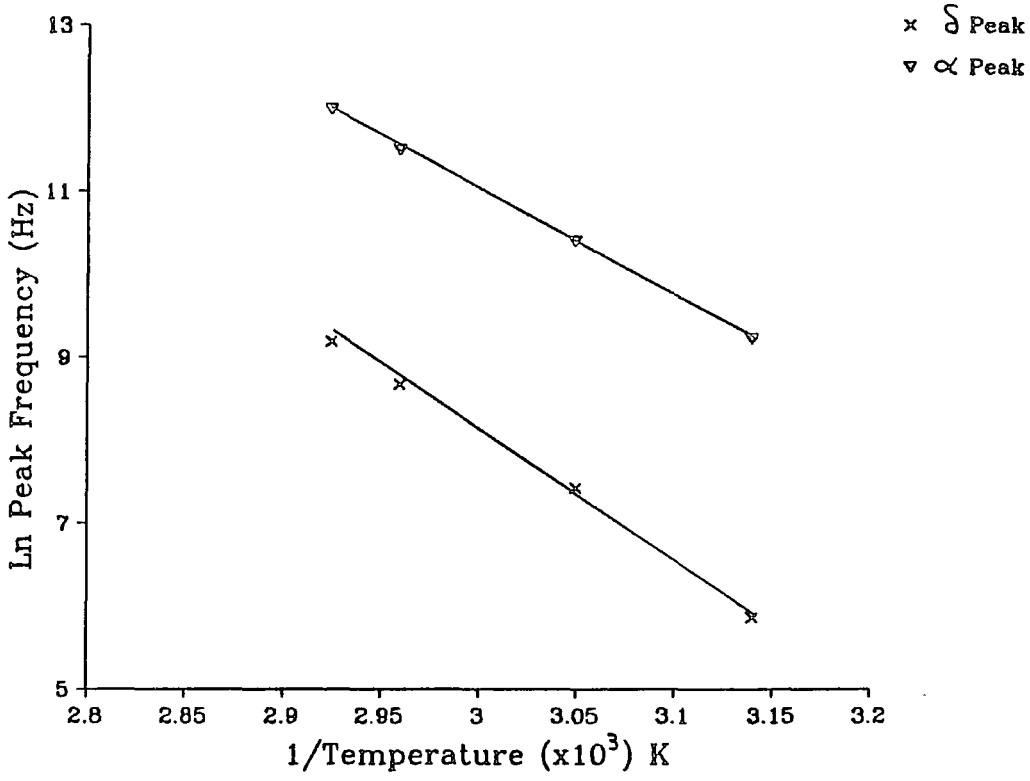

(a)

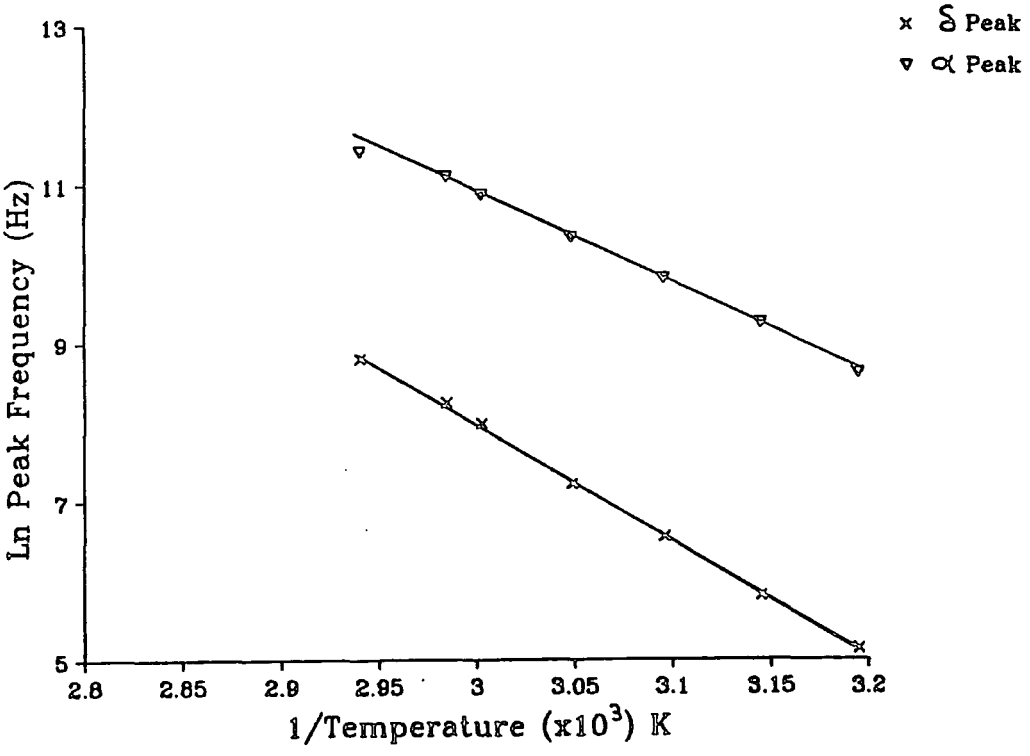

(b)

FIGURE 5.21
Arrhenius activation energy graphs for (a) GN3/15 and (b) GN3/40.

The backbone frequently carries polar species and hence may be dielectrically active in its own right. This may lead to multiple peak relaxation spectra. Alternatively, the dipoles can simply contribute to the α and δ relaxation processes of the side group. Bormuth et al (1987a,b) compared nematic polyacrylate LCPs in which the dipole strengths of the side groups were the same while those of the backbone varied. In a comparison of -Cl and -H substitution on the backbone, an enhancement of the δ-relaxation strength was observed in the former case due to the additional longitudinal dipole. A reduction in the α-relaxation strength was attributed to antiparallel ordering of the chloro- and ester groups in the backbone structure.

Substitution of a species having a large free volume onto the backbone disrupts the packing of side groups and influences the phase transition behaviour as well as the dielectric relaxation response. Zentel et al (1985) observed this behaviour in polyacrylate and polymethacrylate LCPs. A similar comparison can be made between the homopolymers GN3/15 and GN3/40 in which the only difference is the methyl and ethyl substitution respectively onto the backbone. The dielectric characteristics of these LCPs are summarised in Table 5.7. The Arrhenius activation energy graphs for each material are shown in Figure 5.21.

Code	GN3/15	GN3/40
δ peak Activation Energy ($kJmol^{-1}$)	130	125
α peak Activation Energy ($kJmol^{-1}$)	105	95
1.18 T_g	55°C	50°C
δ peak position (log_{10} Hz)	3.23	2.85
α peak position (log_{10} Hz)	4.52	4.27
δ peak half-height width (decades)	1.20	1.15
α peak half-height width (decades)	3.68	3.35
Effective dipole moment, μ_{eff}*	16.4×10^{-30} Cm	15×10^{-30} Cm

* Experimental results, see Table 5.4

TABLE 5.7
Comparison of the dielectric responses of methyl and ethyl substituted liquid crystal homopolymers.

The isotropic phase transition temperature of GN3/40 is lower then GN3/15, which is indicative of a less ordered structure. The more bulky and less flexible backbone of GN3/40 results in lower relaxation peak frequencies when comparing at temperatures normalised to T_g. The reduced tendency to smectic ordering would also account for the slightly lower activation energy values and the narrower relaxation peaks.

Substitution of large molar volume groups onto the backbone dilutes the mesogenic content of the LCP. In the case of GN3/15, the methyl groups on the backbone account for about 6.7% of the total molecular mass, whereas in the case of GN3/40 the ethyl groups account for more than 12% of the total molecular mass. The effective dipole moment values reflects these

dipole concentrations; μ_{eff} for GN3/40 is about 90% of that of GN3/15.

5.5.4 Copolymers

Many of the LCPs used as examples in the previous sections have been copolymers. In this section a more systematic survey of the relative behaviour of copolymers and equivalent homopolymers is presented. There are many types of liquid crystal copolymers. Mesogenic, non-mesogenic, polar and non-polar groups may be substituted onto the backbone in addition to the desired mesogenic side group. The substitution may be alternate, in blocks or random; all the copolymers described here are randomly substituted. The motivation for the synthesis of LC copolymers is strongly based on the benefits they should provide when using the materials for technological applications. The viscosity of the LCP may be varied considerably by the judicious choice of substituents and the substitution of non-mesogenic electro-active groups can confer properties such as dichroism and optical nonlinearity without the problems of phase separation and immiscibility which often arise in guest-host systems. However, the non-mesogenic substituents not only dilute the mesogenic groups, but may hinder oriented packing of the mesogens.

(a) Mesogenic Substitution

Further evidence for the interpretation of dielectric relaxation as a cooperative process was produced by Pranoto et al (1986) and Haase et al (1985) when they observed the relaxations of polysiloxane liquid crystal copolymers having methoxy terminated mesogenic side groups together with either cyano or chloro terminated mesogenic substituents. A single δ relaxation process was observed, the activation energy of which was higher

in the smectic than the nematic phase. Liquid crystal copolymers with this type of structure are particularly appropriate for use in dual frequency devices.

(b) Non-dipolar substitution

A variety of liquid crystal copolymers having mesogenic and methyl groups substituted randomly onto a polymethylsiloxane backbone have been studied. This structure has been shown to confer benefits in applications such as thermo-optic optical storage (McArdle et al, 1987 a,b). The dielectric behaviour of such copolymers differs from the corresponding homopolymers because of the reduced microviscosity. The dielectric responses of two such pairs of materials are compared in Table 5.8. The loss spectra of GN4/17 and GN4/33 are shown as a function of temperature in Figures 5.22 and 5.23 respectively. In general the copolymers have lower Arrhenius activation energies and more widely separated loss peaks than the homopolymers. The α peak width of the copolymers is considerably narrower than the homopolymers, probably due to reduced steric hindrance. The effect on the δ peak width is slight.

As noted earlier, this type of copolymer does result in a dilution of the mesogenic dipoles. The sum of the α and δ peak dielectric decrements is related to the total relaxation strength and, in both pairs, the copolymer relaxation strength is about half that of the homopolymer. This is reflected in the effective dipole moment values; μ_{eff} of the copolymers is only 75% of that of the homopolymers. These examples clearly indicate the

balance between microviscosity and high dipolar strength (and therefore permittivity) which must be considered when choosing LCPs for practical applications.

Mesogenic Side Group	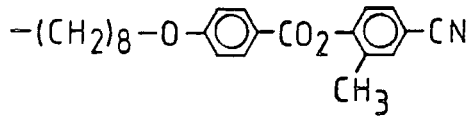		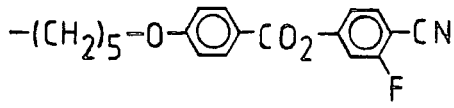	
Code	GN3/15 Homopolymer	GN3/16 Copolymer	GN4/33 Homopolymer	GN4/17 Copolymer
δ Peak Arrhenius Activation Energy ($kJmol^{-1}$)	130	102	107	98
α Peak Arrhenius Activation Energy ($kJmol^{-1}$)	105	80	160	75
Reduced temperature	1.18 Tg	1.18 Tg	1.194 Tg	1.194 Tg
Temperature	55°C	30°C	60°C	35°C
δ peak position (log_{10}(Hz))	3.23	3.3	3.31	3.34
α peak position (log_{10} (Hz))	4.63	4.92	5.135	5.43
δ half-height peak width (decades)	1.32	1.24	1.18	1.22
α peak half-height width (decades)	3.17	2.71	4.65	2.75
$T(\Delta\epsilon_\delta + \Delta\epsilon_\alpha)$*	2714	1423	4953	2357
Experimentally determined effective dipole moment, μ_{eff}	16.4	12.9	20.8	15.9

* $\Delta\epsilon_i = 2\epsilon''max(i)/\beta(i)$ where $i=\delta,\alpha$.

TABLE 5.8
Comparison of the dielectric responses of comparable pairs of copolymer and homopolymer LCPs.

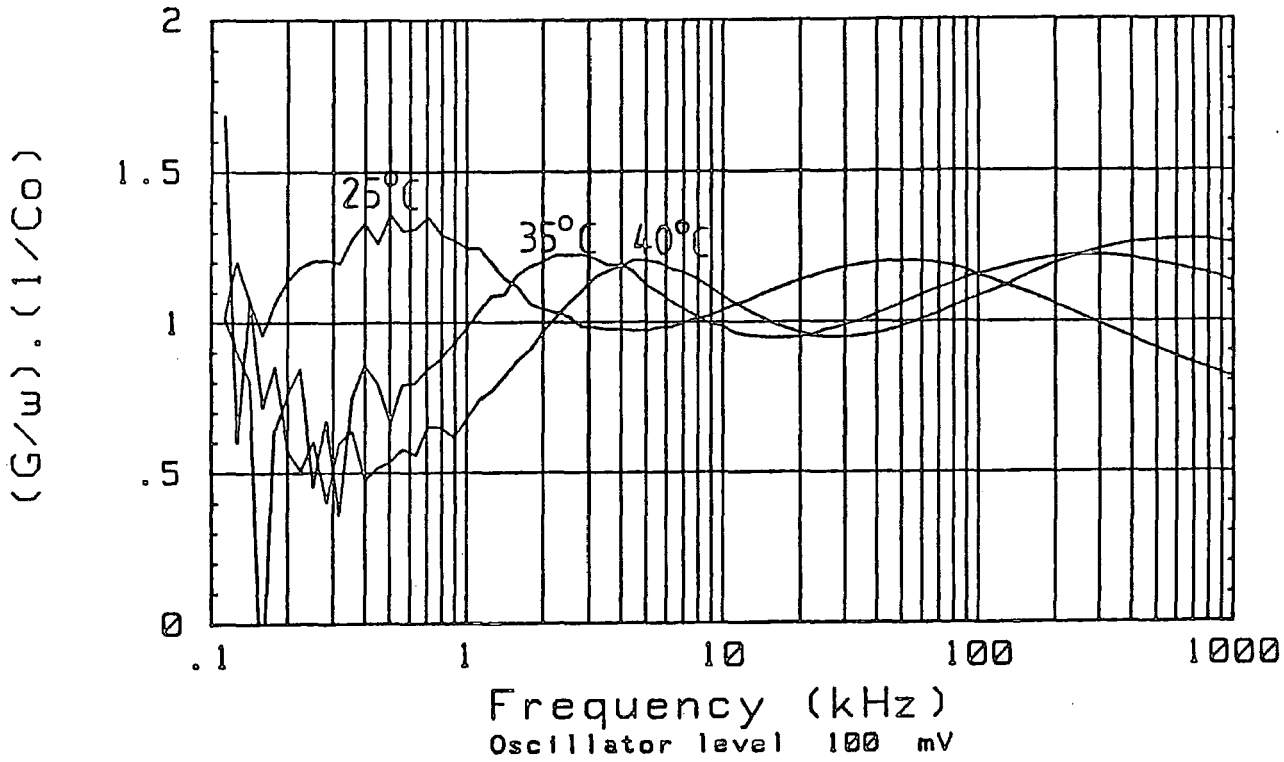

FIGURE 5.22
The variation of the loss spectrum of unaligned GN3/17 with temperature.

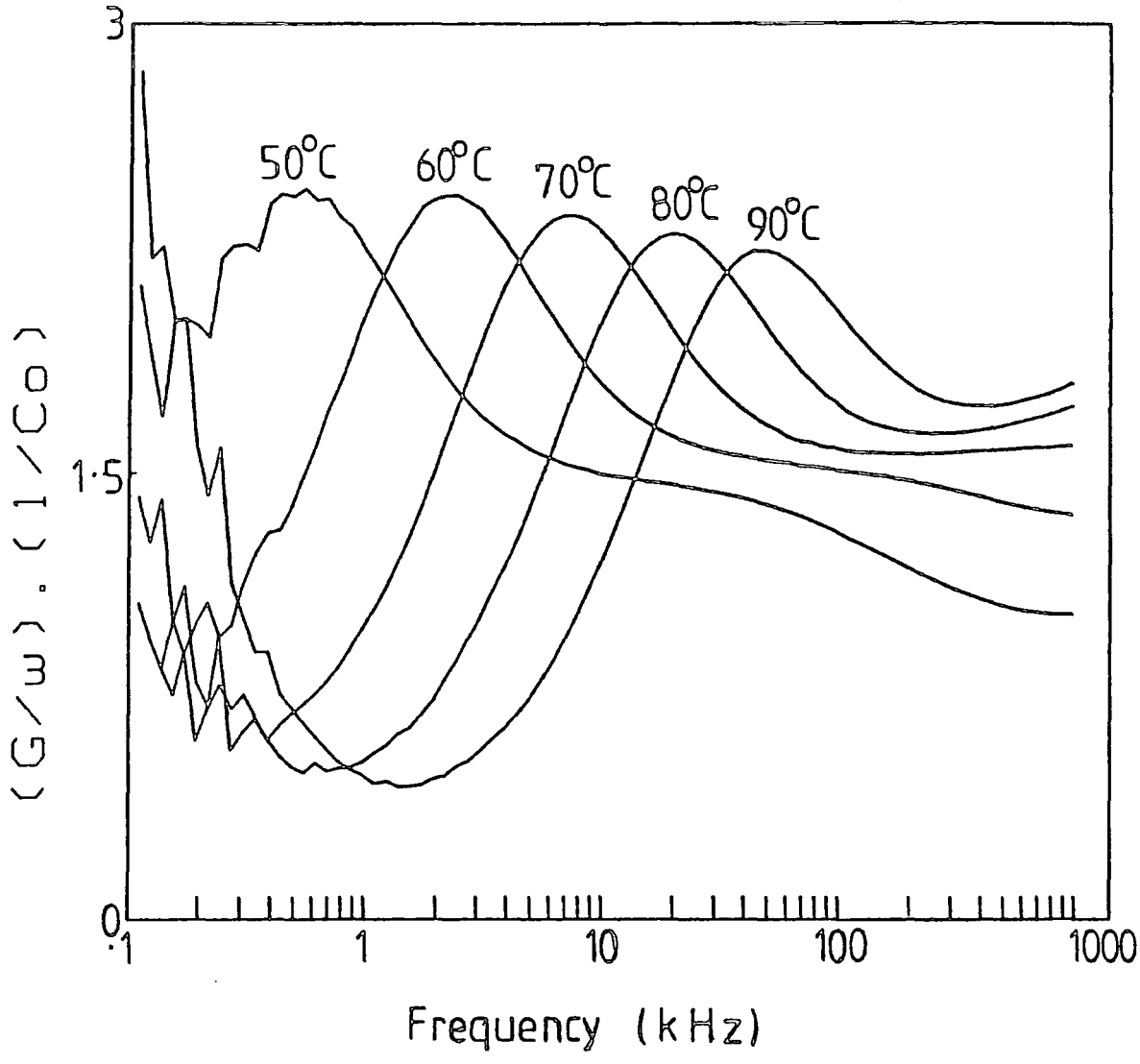

FIGURE 5.23
The loss spectrum of unaligned GN4/33 shown at 50°C, 60°C, 70°C, 80°C and 90°C.

(c) Dipolar (Non-Mesogenic) Substitution

The LCPs shown in Table 2.5 were synthesised in the hope of overcoming the problem of low dipole concentration identified in the LCPs described in Section 5.5.4(b) above, while retaining their low viscosity and consequent ease of handling. However, it was found that the cyano-propyl substituent (a dipolar non-mesogenic side group) suppressed the tendency to form a mesophase, lowering the clearing point by over 100°C relative to comparable homopolymers and causing it to lie below an also depressed T_g of about -20°C. Only very symmetric mesogenic groups such as the cyano phenyl-benzoate group of GN3/36 were able to induce a weak biphasic region at room temperature.

The dielectric responses of the homopolymer GN3/15 and the copolymer GN3/39, which has a cyano-propyl group substituted in addition to the mesogenic moiety, are compared in Table 5.9. The loss spectra of GN3/15 and GN3/39 are plotted as a function of temperature in Figures 5.24 and 5.25 respectively.

In the case of GN3/15, peak 1 refers to the δ peak and peak 2 to the α peak. Since GN3/39 is in the isotropic phase at 21°C, the two well separated loss peaks may not necessarily be associated with δ and α type reorientations. However, the locations of the peaks are consistent with those of GN3/15 at the same reference temperature of 1.14 T_g, while the Fuoss-Kirkwood fitted peak widths are ordered as for δ and α processes, though they are slightly broader than usual.

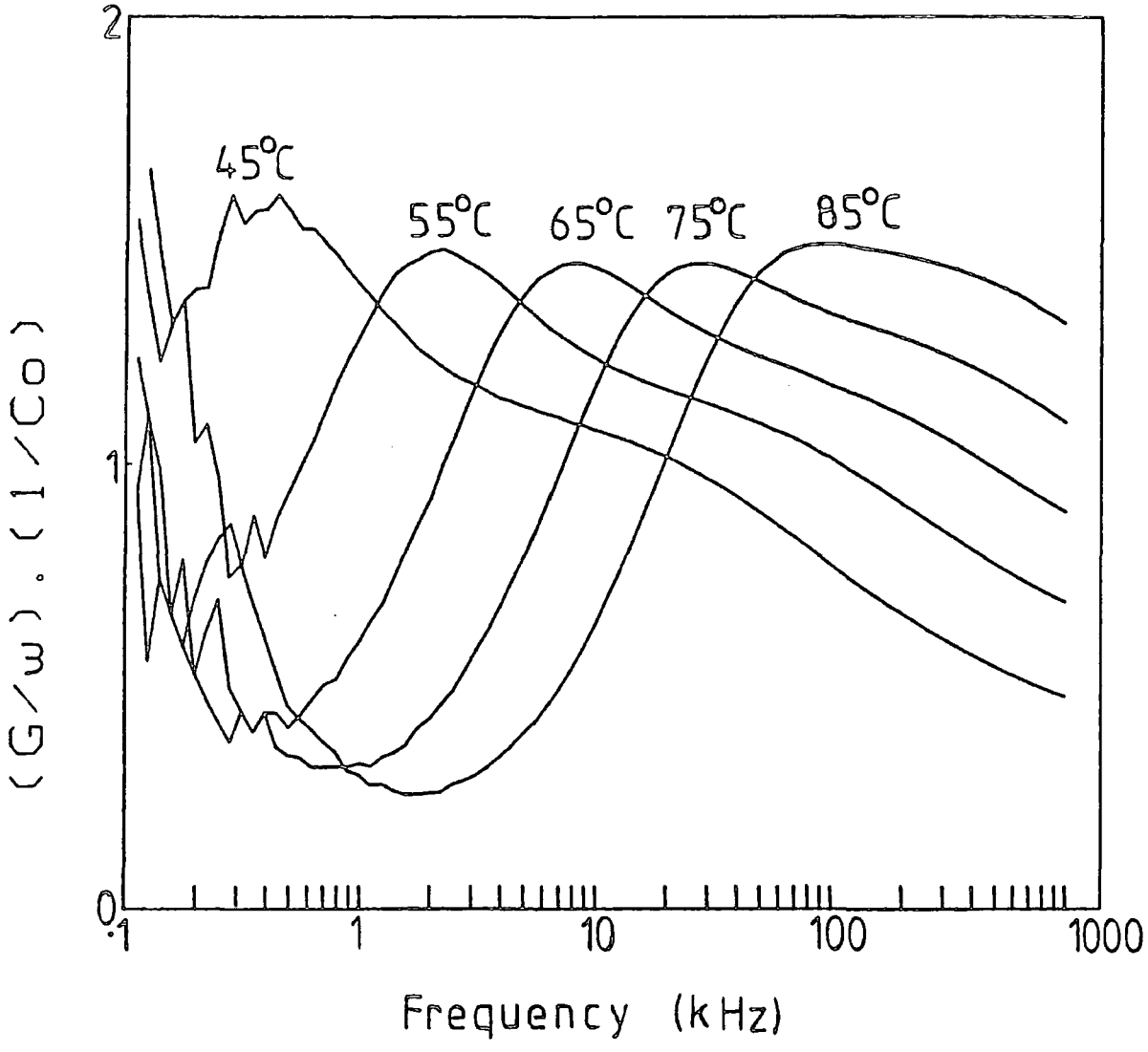

FIGURE 5.24
The dielectric loss spectra of unaligned GN3/15 at 45°C, 55°C, 65°C, 75°C and 85°C.

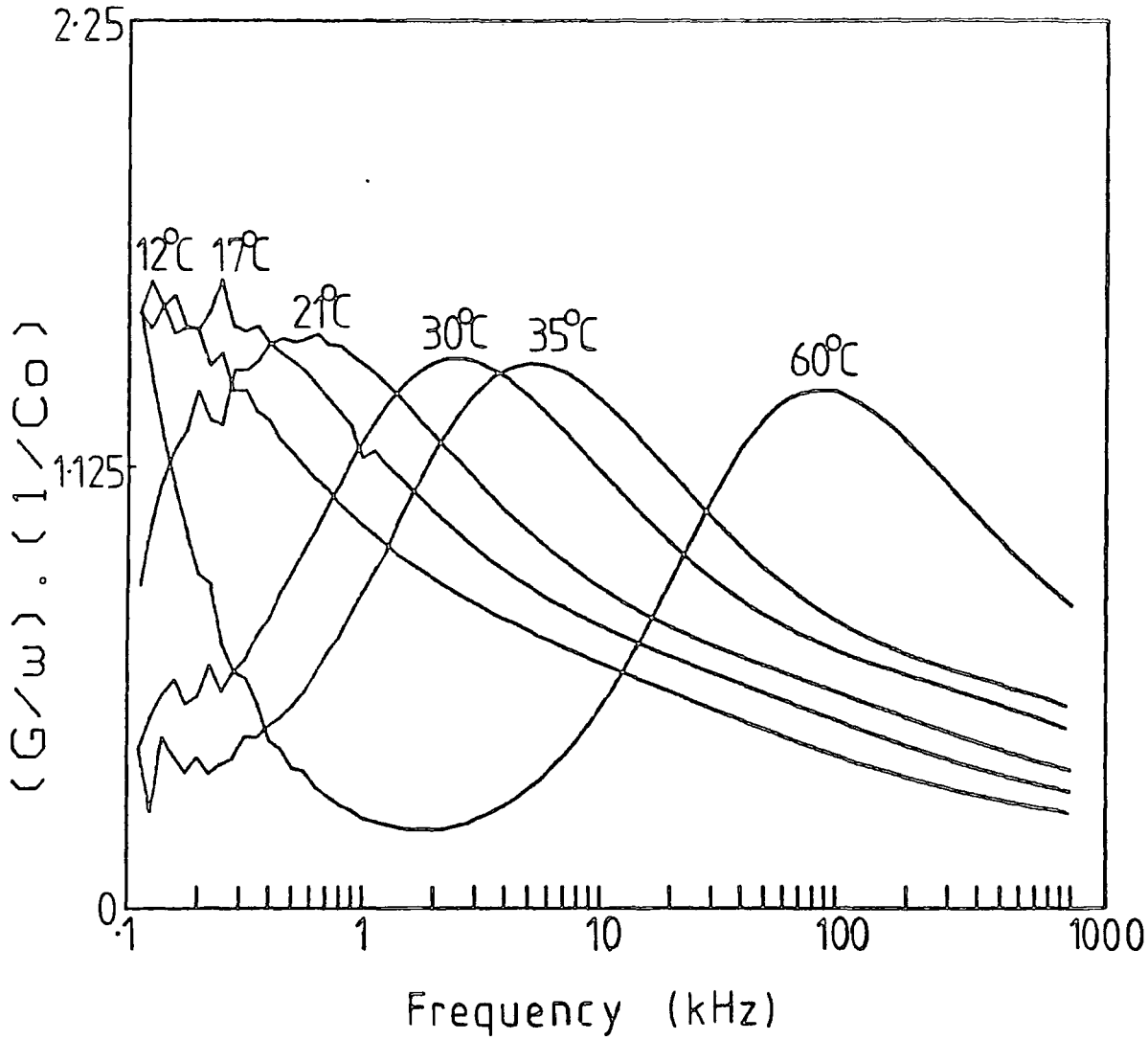

FIGURE 5.25
The variation of the loss spectrum of GN3/39 with temperature.

Code	GN3/15 Homopolymer	GN3/39 Copolymer
Peak 1 Arrhenius Activation Energy ($kJmol^{-1}$)	130	133
Peak 2 Arrhenius Activation Energy ($kJmol^{-1}$)	105	184
Reference Temp. 1.14 T_g	45°C	21°C
Peak 1 position ($\log_{10}$(Hz))	2.56	2.72
Peak 2 position ($\log_{10}$(Hz))	4.00	4.42
Peak 1 half-height width (decades)	1.21	1.78
Peak 2 half-height width (decades)	3.45	4.22
Dielectric Decrement $^*\Delta\epsilon_1$	2.1	6.05
Dielectric Decrement $^*\Delta\epsilon_2$	6.03	6.67

* $$\Delta\epsilon_i = \frac{2\epsilon_{i,\max}}{\beta_i} \qquad i = 1, 2$$

TABLE 5.9
Comparison of the dielectric responses of a liquid crystal homopolymer and a cyano-propyl copolymer having the same mesogenic side group.

The comparability of relaxation frequencies at a temperature referenced to T_g in isotropic and liquid crystalline materials appears to be further evidence that the relaxation frequencies are determined by the dynamics, which are ultimately responsible for glass formation. However, two explanation are possible for the observation of two distinct loss peaks in isotropic GN3/39:

i) Since it is known that mixtures of sufficiently dissimilar molecules show distinct relaxations associated with each molecule,

the peaks may be assigned to relaxations of the mesogenic group and the cyanopropyl group (probably with the latter at higher frequency). On this basis, the dielectric decrements of 6.05 and 6.67, respectively, would give estimates of 14×10^{-30} Cm and 15×10^{-3} Cm for the dipole moments of the mesogenic and cyanopropyl groups, respectively. This is consistent with the values calculated for a variety of LCPs (see Section 5.5.2(b)).

ii) Alternatively, as discussed in Section 5.5.2.4 with reference to GN3/18, if the anisotropy of the rotational diffusion tensor is sufficiently great, two relaxations will be seen in the isotropic phase even if the two dipole-bearing side-groups are behaving as a single "average" moiety. Using Equation [5.12] yields an estimate of 105 for $D_{\parallel}/D_{\perp}$ for GN3/39 at 1.14 T_g. This is considerably higher than the value calculated for GN3/18, but is still similar to the values calculated by Bone et al (1984).

It is not possible to judge which interpretation is correct from the information available. This ambiguity is a limiting feature of dielectric relaxation spectroscopy.

5.6 Dielectric Permittivity

5.6.1 Measurement of the Anisotropic Permittivity Components

The dielectric permittivity ($\epsilon'(\omega)$) provides valuable information for the development of electrically driven devices using LCPs and a change in sign of the permittivity from positive to negative with increasing frequency may be exploited by two-frequency switching techniques (see, for example,

Haase and Pranoto, 1984; Attard et al, 1987). However, the difficulty in achieving complete alignment of LCPs caused problems when attempting to measure the anisotropic components of permittivity, $\epsilon'_{\parallel}$ and $\epsilon'_{\perp}$. Low molar mass liquid crystals can be completely aligned using surface treatments or an external field and Clark et al (1980) have described a technique for extrapolating the change in permittivity with field to infinite field conditions and hence complete alignment. The dependence of permittivity on field strength for LCPs cannot be extrapolated in a similar way due to their high viscosity, thus it is difficult to identify an impartial technique for validating apparently complete alignment. As discussed in Section 5.3, the δ relaxation peak disappears in the case of perfect homogenous/planar alignment (i.e. $\epsilon'_{\perp}$ is measured) but there is no similar characteristic of complete homeotropic alignment (i.e. in which $\epsilon'_{\parallel}$ is measured).

An estimate of the parallel permittivity component $\epsilon'_{\parallel}$ can be produced by monitoring the δ peak amplitude until a maximum is reached as progressively larger aligning fields are applied. This technique was used without great success in this work, since even on very slow cooling in the presence of the fields optical examination of the cells showed that complete alignment had not been achieved. It was hence not possible to produce values of $\epsilon'_{\parallel}$ with reasonable accuracy. The perpendicular permittivity component ($\epsilon'_{\perp}$) of several LCPs was calculated with more success using the method described by Haws et al (1987). This uses the fact that the δ relaxation is not present in perfect planar/homogenous alignment. There is therefore no variation in the permittivity with

frequency over that frequency range where, for other states of alignment, the δ relaxation is apparent as a decrease in the permittivity (see Figure 3.2). It is hence unnecessary to achieve complete planar/homogeneous alignment (which is a difficult task with LCPs) in order to calculate $\epsilon_{\perp}$. A cross-over frequency, ν_c, exists within the δ relaxation through which the permittivity curves for all states of alignment pass. This point can be identified by measuring the frequency spectrum of permittivity in any two states of alignment. Then $\epsilon_{\perp}$ is the permittivity at the cross-over frequency since the unvarying planar/homogeneous permittivity spectrum must also pass through this point.

If the spherical mean value of permittivity $\bar{\epsilon} = 1/3(\epsilon_{\parallel} + 2\epsilon_{\perp})$ can be determined from either completely randomised samples or by extrapolation from the isotropic phase and $\epsilon_{\perp}$ calculated as above, then both principal permittivities can be found without necessarily using aligned samples. This ideal case relies on there being no discontinuities at the isotropic phase transition due to the presence of antiparallel correlation effects (Bradshaw, 1984). In the following sections, values of the perpendicular component of permittivity and the isotropic permittivity are tabulated for several LCPs. However, extrapolation and calculation of $\epsilon_{\parallel}$ are not shown due to the unacceptable approximations required when extrapolating over the large temperature intervals involved.

5.6.2 The Calculation of the perpendicular component of permittivity($\epsilon_\perp$)

Values of $\epsilon_\perp$ obtained from permittivity measurements at the cross-over frequency (ν_c) are summarised in Table 5.10.

Code	Temperature	ν_c (kHz)	$\epsilon_\perp$
GN3/3	38.5 (1.18 T_g)	1.023	7.3
GN3/14	40 (0.87 T_c)	1.8	7.3
GN3/19	40 (0.85 T_c)	7.6	4.7
GN4/19	50 (0.92 T_c)	3.98	9.6
GN4/33	56.2 (1.18 T_g)	0.63	13.5
GN3/29	104 (0.95 T_c)	90	7.2

TABLE 5.10
Values of $\epsilon_\perp$ calculated by observing the cross over frequency in the permittivity spectra of each LCP in different states of alignment.

Figures 5.26 and 5.27 show how these values were achieved for GN3/3 and GN4/33 respectively at 1.18 T_g.

As expected, GN3/29, GN3/3 and GN3/14 show similar values of $\epsilon_\perp$ since the major contributor to the transverse dipole moment is the central ester group in each case. The permittivity of the 1mmLC equivalent to the side group of GN3/14 (called C6CN - structure and transition data shown in

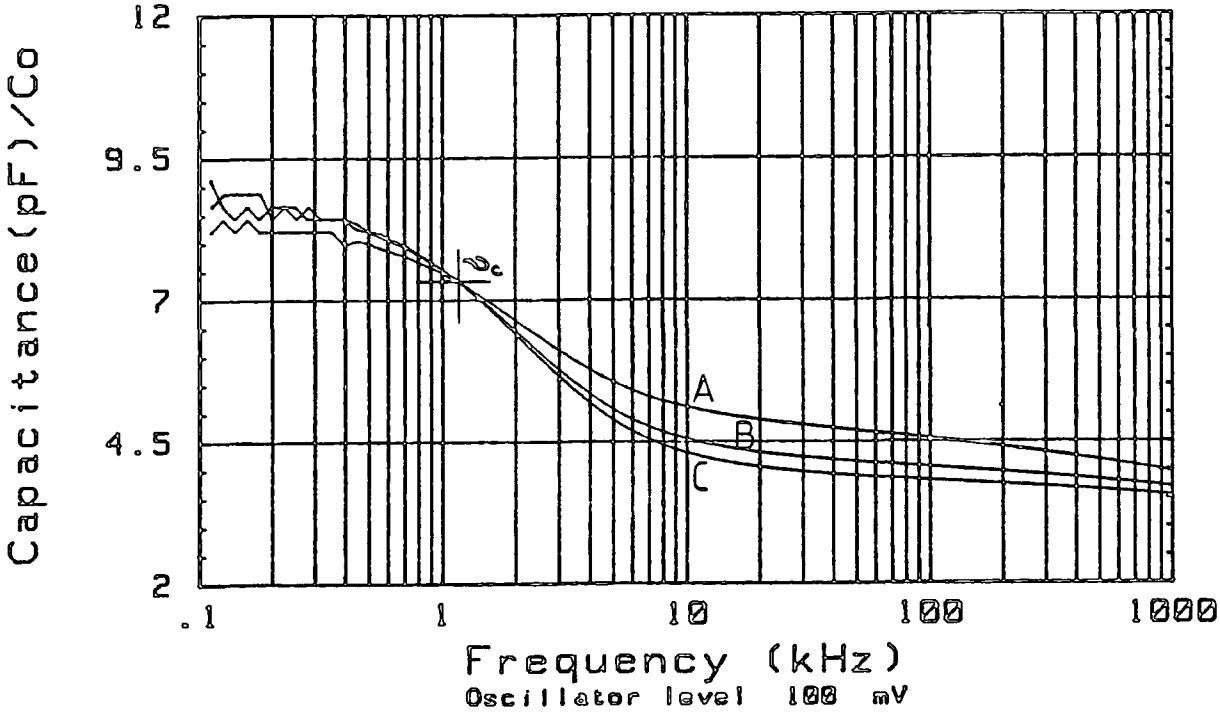

FIGURE 5.26
The calculation of $\epsilon_{\perp}'$ for GN3/3 at 38.5°C. The cross-over frequency, ν_c, is found from the intersection of the permittivity plots after alignment with (A) 26V, (B) 50V and (C) 85V.

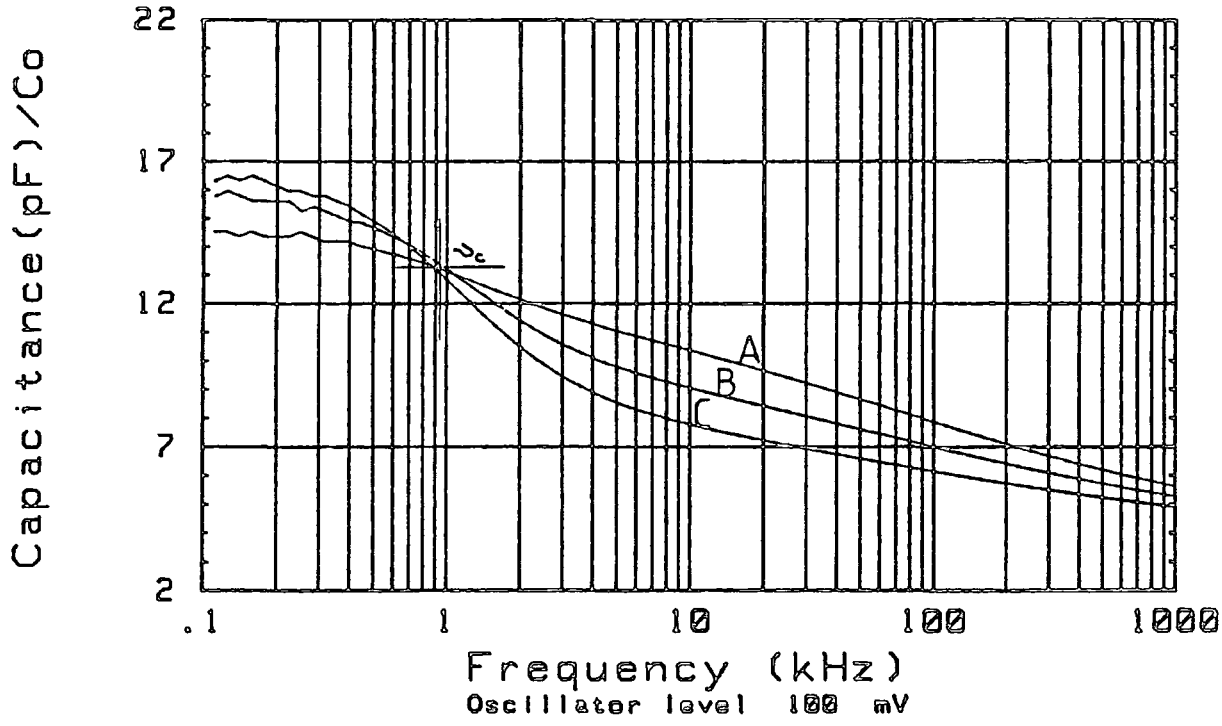

FIGURE 5.27
The calculation of ϵ_1' for GN4.33 at 56.2°C. The cross-over frequency, ν_C, is found from the intersection of the permittivity plots after alignment with (A) 45V, (B) 75V and (C) 140V.

Appendix IV) was measured as a function of temperature both parallel and perpendicular to the director by using measuring cells coated with rubbed polyimide and lecithin surface alignment agents respectively. If the measurements are extrapolated to a comparable reduced temperature of 0.92 T_C, then $\epsilon_\perp$ is approximately 8 in good agreement with the values calculated for the LCPs. It must be noted, however, that Klingbiel et al (1974) reported measurements of the permittivities of the 1mmLC equivalent to the side group of GN3/3. Their values for $\epsilon_\perp$ and $\epsilon_{||}$ of 11.66 and 27.9 respectively at 0.985 T_C appear to be higher than the values reported above even taking into account the higher reduced temperatures. A possible explanation could be that the LCs were subjected to different purification procedures.

The value of $\epsilon_\perp$ for GN3/19 is lower than for the other LCPs since the central ester group is not present. Parneix et al (1987) have measured the permittivity components of an homologous series of cyano biphenyl side chain LC homopolymers having polyacrylate backbones. At a comparable reduced temperature of 0.85 T_C, $\epsilon_\perp$ was about 7.3. This higher value could be attributed to a contribution to the transverse dipole moment from the acrylate backbone, or alternatively to less antiparallel ordering than in the copolymer, or to the higher density of dipoles.

The values of $\epsilon_\perp$ for GN4/19 and GN4/33 would be expected to be similar at the same reduced temperature of 0.92 T_C. The values are actually 9.6 and 11.5 respectively. The difference could again arise from a higher degree of antiparallel ordering in the copolymer GN4/19 due to reduced steric

hindrance or to the lower density of dipoles in the copolymer. X-ray studies of the two structures would provide more information on the packing.

This method of calculating $\epsilon_\perp$ is useful in certain cases, but it is limited by the fact that a cross-over frequency must be apparent in the frequency range under inspection at the required temperature. The values of $\epsilon_\perp$ that are calculated appear to be reasonable, as shown by comparisons with values reported in the literature and measurements in 1mmLC equivalent materials.

5.6.3 Permittivity Measurements in the Isotropic Phase

The static permittivity ϵ' of these LCPs is modified at high temperatures (particularly in the isotropic phase) by a contribution from a charged double layer formed on the electrode surfaces. This electrode polarisation is discussed in detail in Chapter 6. Corrections can be applied to find the "true" static permittivity of the sample. These corrected values will be used in this section.

The values of permittivity in the isotropic phase (ϵ_0) have been compared at 1.1 T_2 for convenience (where T_2 is the transition temperature between the biphasic region and the isotropic phase) and they are summarised in Table 5.11. The static permittivities of groups of LCPs having the same mesogenic moiety are plotted as a function of temperature in Figures 5.28 and 5.29. The biphasic region is marked in each case. The alignment is assumed to be random in the smectic phase. These figures shown that the cyano-propyl substituted copolymers (GN3/39 and GN3/36) have the highest

values of ϵ_o while the copolymers having non-dipolar main chain substituents tend to have slightly lower values of ϵ_o compared with the corresponding homopolymer. These effects arise from the variation in dipole concentration and are consistent with the calculation of dipole moments in Section 5.5.2(b).

Category of LCP	Code	Temperature	ϵ_o
Methyl-Copolymer	GN3/3	158	8.8
	GN3/19	140	7.1
	GN3/14	137	9.3
	GN3/16	99	9.2
	GN3/22	90	4.9
	GN3/18	70	5.9
	GN4/17	128	13.1
	GN4/16	177	6.2
	GN4/18	109	9.0
	GN4/19	123	12.2
	GN4/13	130	5.9
	GN4/11	128	5.7
Methyl-Homopolymer	GN4/33	211	13
Ethyl-Homopolymer	GN3/40	114	10.3
	GN3/25	171	9.1
	GN3/29	184	9.4
Cyano-Propyl Copolymer	GN3/36	80*	14.0
	GN3/37	55*	8.9
	GN3/39	80*	13.3

TABLE 5.11
The measured permittivity of LCPs in the isotropic phase at 1.1 T_2 (except for those LCPs marked with an asterisk (*) which did not exhibit a mesophase-isotropic phase transition).

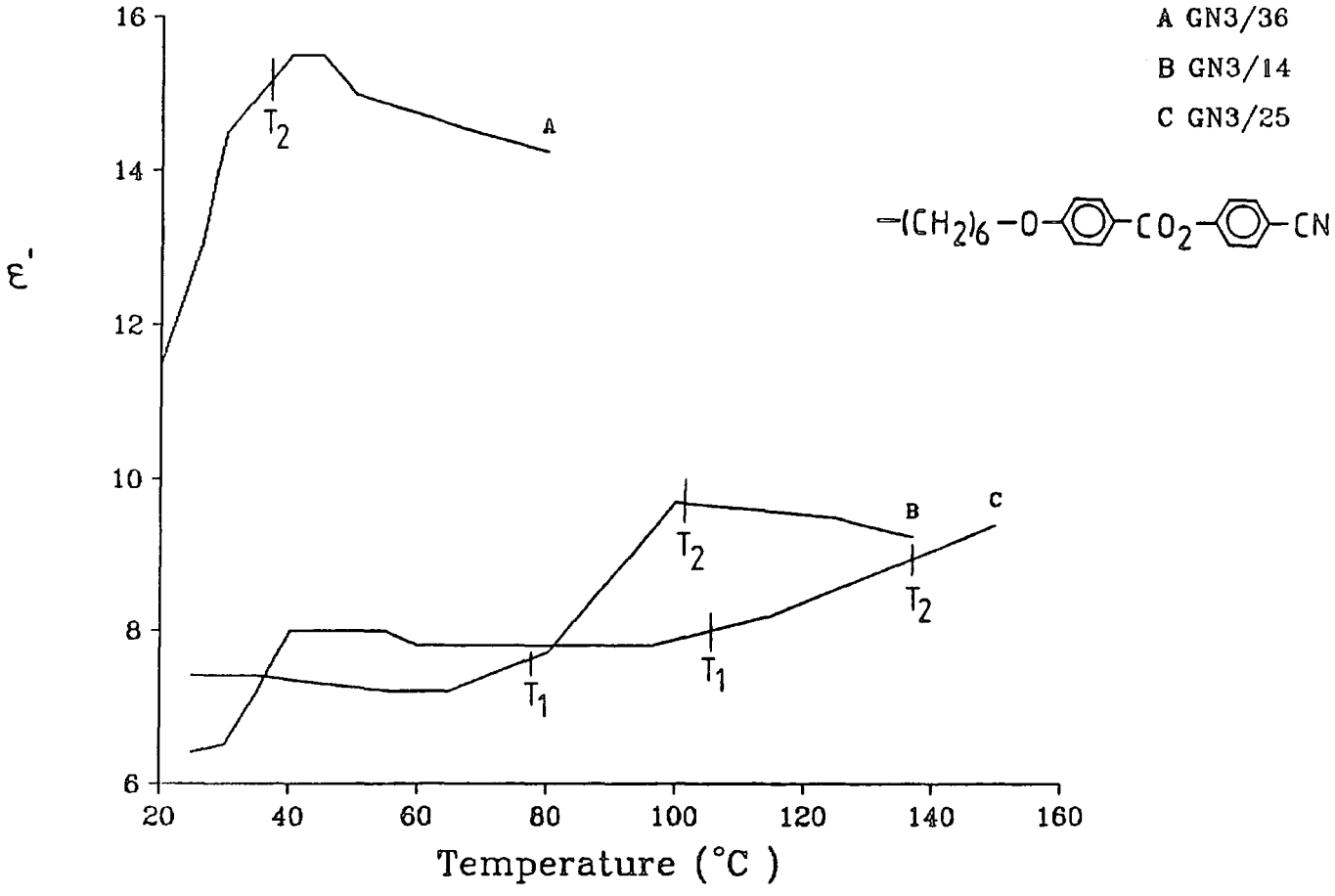

FIGURE 5.28
The static permittivity of LCPs (measured at about 100 Hz) having the same mesogenic side group. T_1 and T_2 indicate the start and end of the biphasic region, respectively.

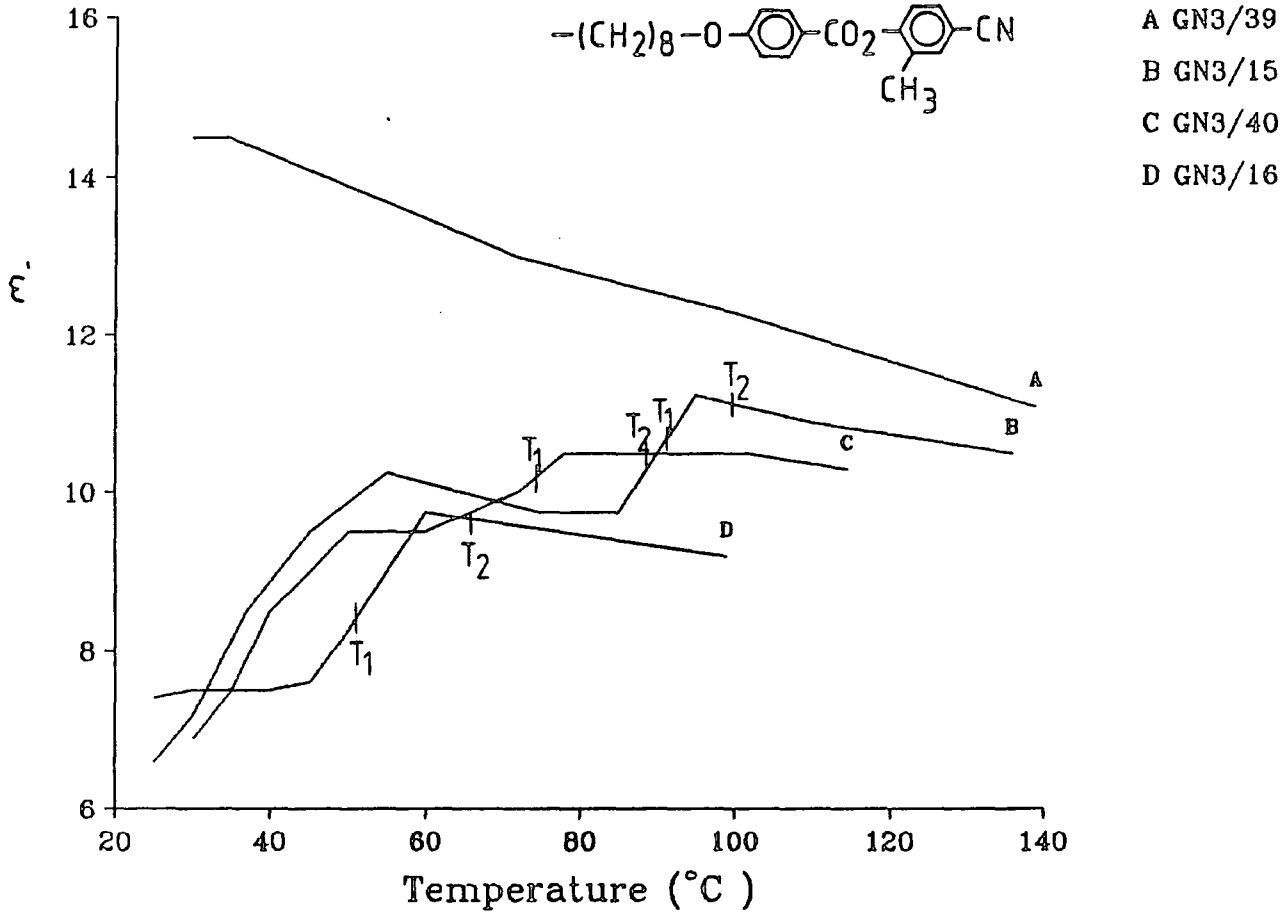

FIGURE 5.29
The static permittivity of LCPs (measured at about 100 Hz) having the same mesogenic side group. T_1 and T_2 indicate the start and end of the biphasic region, respectively.

5.7 Summary

Dielectric relaxation spectroscopy has been used to study the molecular dynamics of a wide variety of LCPs having polysiloxane backbones. The LCPs were shown to behave in a broadly similar way to lmmLCs, though the loss peaks were observed to be shifted about 3 decades lower in frequency. This is consistent with the theory that LCPs may be treated as mesogens loosely strung together by a polymeric backbone. Cooperative reorientation processes in the mesophase, observed as δ and α relaxations, were studied for many LCPs over a broad temperature range. The loss spectra were fitted using overlapping Fuoss-Kirkwood lineshapes and the peak amplitudes, frequency locations and half-height widths were used to calculate quantities such as peak intensity, activation energy and apparent dipole strength.

The LCPs were compared directly at temperatures referenced to the clearing temperature (T_c) and the glass transition temperature (T_g). It has been shown that a significant correlation exists between the loss peak frequency locations of LCPs with considerably different structures when these are referenced to T_g. This suggests that the molecular dynamics are determined by transitions between different conformations of the backbone which freeze at T_g.

The sensitivity of the loss peak amplitude to the state of alignment of an LCP has been used to show that some structures are inherently more stable than others due to steric hindrance. However, the variations in alignment

with temperature up to about 50°C were shown to be smaller than the difference between aligned and unaligned samples so the effect on the performance of an optical memory device is likely to be slight.

The variety of LCP structures which were available allowed the influence of the various structural components of an LCP on the relaxation behaviour to be studied in some detail. The effect of variations in the mesogenic core, the terminal and spacer groups and the backbone were observed independently. A selection of homopolymers and copolymers were also available. Many of the features dependent on structure, such as anti-parallel correlation and odd-even effects, correspond exactly with those observed in lmmLCs. As with lmmLCs, local ordering was shown to be retained in the isotropic phase of some LCPs.

Finally, a method has been described which allows the perpendicular component of permittivity, $\epsilon_{\perp}$ to be calculated without recourse to planar or homogeneously aligned samples. The values of $\epsilon_{\perp}$ for a selection of LCPs have been tabulated, as have the values of permittivity in the isotropic phase.

Chapter Six

Results and Discussion– Electrical Conductivity

6.1 Introduction

This Chapter describes the results of a broadly based investigation into topics such as the magnitude of the conductivity of LCPs as compared to that of commercial 1mmLCs, the influence of handling and contamination, the methods of quantifying the apparent electrical conductivity and whether the mechanisms of conduction in LCPs are similar to those observed in classical organic polymers and 1mmLCs. A review of the electrical conduction behaviour of low molar mass liquid crystals and classical polymers will be followed by a study of low field, AC conductivity phenomena in a wide range of LCPs. The second half of the Chapter concentrates on the behaviour of GN3/3 and the 1mmLC S2 under high DC field conditions. The use of electrode surfactants as a possible solution to the problems caused by conductivity in devices made from these LCPs is also described. There are undoubtedly many questions which remain unanswered at the end of this study, but the intention has been to indicate areas which would profit from further investigation.

Well purified samples of non-ionising low molar mass liquid crystals would theoretically have very low intrinsic electrical conductivity (less than 10^{-19} $(\Omega cm)^{-1}$). However, in practice a residual concentration of ionic impurities remains even after careful purification, resulting in a typical value for the conductivity of 10^{-10} to 10^{-12} $(\Omega cm)^{-1}$. Blinov (1983) has noted that even after perfect purification procedures have been carried out, ions may still appear in a liquid crystal due to the injection of electrons from the cathode and their subsequent capture by neutral molecules. Ionic currents may result from extrinsic charge carriers or may

result from ions formed near the electrodes. Under normal conditions, electron transport mechanisms may be neglected in LCs since their electronic conductivity is extremely low.

In low frequency electric fields, the drift of ions may result in the formation of space-charge layers at the electrode surfaces. The intense electric field in such an electrical double-layer can lead to Schottky-type emission of charge. This has been discussed in detail by Blinov (1983). Mada et al (1986,1988) observed that space-charge forms at the electrodes even for very pure liquid crystals. They found that in a DC field, the capacitance of nematic LCs increases for the first tens of milliseconds and then decreases with a long relaxation time of about one second as the electrical double layers at the surface reach equilibrium. Significant effects were observed even with 99.99% pure liquid crystals. Schottky emission has also been reported by Lesniak et al (1980) in a variety of cholesteric liquid crystals.

Sprokel (1973,1974) studied the properties of the double layers using doped liquid crystals. He used the Gouy Chapman theory to calculate surface charge density and the Johnson-Cole formalism of electrode impedance (see Section 3.2.3) to calculate the actual permittivity of the sample, as well as that of the space-charge layer. For the liquid crystal MBBA doped with 0.76 mol/mol choline chloride and contained in a cell about 250 μm thick, Sprokel showed that under an applied low frequency potential difference of 1V, the field in the surface double layer was about 10^4 Vcm^{-1}. A field of this magnitude could be expected to result in charge emission effects.

The electrical conductivity of liquid crystals is anisotropic, but to a lesser extent than the dielectric permittivity or refractive index. Usually for nematic lmmLCs there is positive anisotropy ($\sigma_{\parallel} > \sigma_{\perp}$), however Jadzyn et al (1987) observed strong pretransitional effects with the anisotropy changing sign in some cases. Mircea-Roussel et al (1975) made an extensive study of the anisotropy of the conductivity of smectic liquid crystals and identified two categories. In the first, $\sigma_{\parallel}$ was on average 5 times less than $\sigma_{\perp}$; it was easier for the charge to flow within the smectic layers than perpendicular to them. In these liquid crystals the smectic layer thickness was found to equal the molecular length. The second group of smectic lmmLCs exhibited no preferential direction for the flow of charge. The layer spacing in these liquid crystals was greater than the molecular length and the layers contained pairs of associated molecules.

The electrical conductivity of non-mesogenic polymers varies between that of, for example, polydiacetylene (which has a conductivity similar to that of doped semiconductors) to polyethylene and polystyrene which are amongst the best insulators known. Electrical conduction in polymers may be either electronic or ionic, though in most polymeric materials it is very difficult to measure any electronic conductivity at all. There is considerable commercial interest in developing both better insulating polymers (e.g. for cable shielding or electronic circuit insulation) and highly conducting polymers, with the organic superconductor envisaged by some researchers. The electrical conductivity of polymers is discussed by Blythe (1979) and Block (1979).

In most polymers there is predominantly impurity conduction at low field strengths, with the build up of space charge at the electrodes contributing to Schottky emission at higher fields. Szymanski and Bak (1986) found the nature of the electrodes to be important in determining the carrier injection into organic molecular solids such as p-terphenyl and described the influence of injected carriers on their electrical properties as "crucial". Suzuoki et al (1985 and 1987) studied polyethylene and ethylene-vinyl acetate copolymer and showed that the cathode field was enhanced by space charge and that the conduction could be explained by Schottky-type electron injection under this enhanced field. Sessler et al (1986) came to the same conclusions in their study of polyimide; they also identified the importance of separating interface and bulk phenomena in the study of polymer conduction processes. The injection of charge by the electrodes may account for polymeric conductivity even when there is no evidence of bulk conduction (Ko and Hirsch, 1981).

The transfer of charge at metal-polymer contacts has probably been most thoroughly studied by Akande and Lowell (1987) and Lowell (1988). These workers showed that change transfer is an intrinsic property of polymers and not a function of preparation, as well as being only weakly affected by the relative work function of the electrode.

6.2 Low Frequency, Low Field Phenomena

6.2.1 A Comparison of the Conductivity of LCPs and Commercial 1mmLCs

The techniques for purifying commercial 1mmLCs for display applications are well developed and result in room temperature values for the

resistivity of typically about 10^{10} Ωcm. In contrast, purification procedures are still being developed for these polysiloxane LCPs (Nestor et al, 1987). To compare the conductivity of commercial 1mmLCs and the LCPs, the low field AC conductivity of a range of mixtures of the LCP GN3/14 with the BDH 1mmLC S2 has been measured and the results are described in this section. Details of the mixtures are summarised in Appendix IV. The mixtures were dyed with 3% wt/wt of the dye D102 (known to be highly stable) to allow comparison under the conditions in operation in optical storage devices. A test voltage of 100 mV was used to avoid reorientation of the director and to reduce the probability of electrical double layers forming at the electrode surfaces.

The conductivity of S2, GN3/14 and 3:1, 1:1 and 1:3 wt/wt mixtures were compared in the mesophase and isotropic phase at constant reduced temperatures of 0.92 T_c and 1.1T_2, respectively. Ionic conductivity was expected to be the prime conduction mechanism and this depends on the mobility of the free charge carriers. It is therefore related to the thermal energy of the system and the viscosity. The samples were hence compared at a temperature referenced to the clearing temperature. Figure 6.1 shows the conductivity as a function of inverse temperature at 0.92 T_c and 1.1T_2 for each mixture. In the smectic phase (0.92 T_c) there is a good linear relationship between the samples, while in the isotropic phase the pure LCP is slightly less conducting than predicted. The thermal activation energy of conductivity of S2 and the 3:1 mixture of GN3/14 to S2 was calculated in the isotropic phase and was found to be 37.9 $kJmol^{-1}$ in each case.

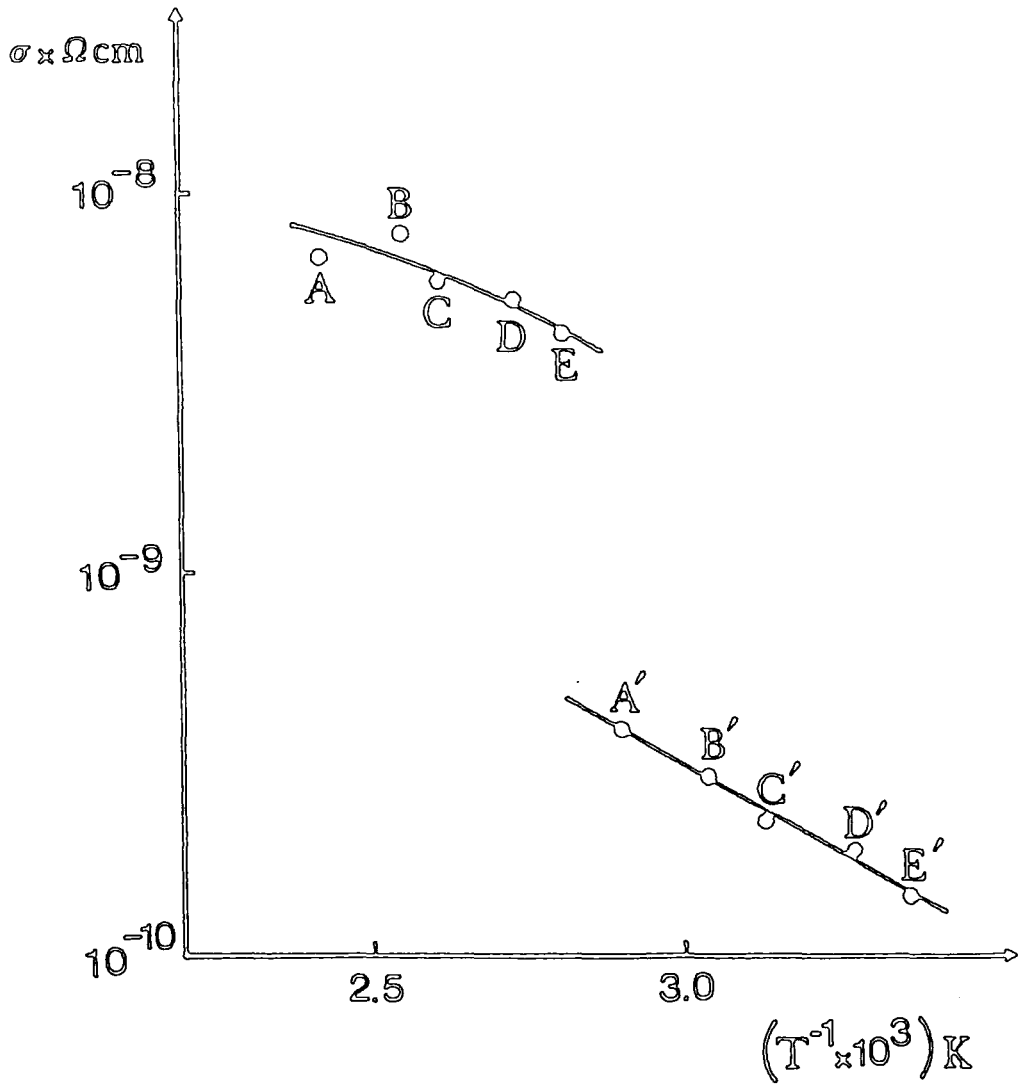

FIGURE 6.1
Low field AC conductivity against inverse temperature at $1.1T_2$ (A to E) and $0.92T_c$ (A′ to E′) for a series of mixtures of the LCP GN3/14 with the commercial 1mmLC smectic mixture S2.

A,A′	=	100% GN3/14		-
B,B′	=	75% GN3/14	:	25% S2
C,C′	=	50% GN3/14	:	50% S2
D,D′	=	25% GN3/14	:	75% S2
E,E′	=	-		100% S2

These results clearly suggest that the steady state transport processes in the bulk of the commercial 1mmLC S2 and the LCP GN3/14 are essentially identical. There is no indication of an excess of conducting impurities in the LCPs. An analysis of the nature and levels of the impurities in the LCPs GN3/3 and GN3/14 and the commercial 1mmLC S5 (BDH Chemicals Ltd) using mass spectrometry provided quantitative information to support this observation. The results are summarised in Table 6.1.

Element	GN3/3	GN3/14	S5
Lithium	70	70	70
Boron	50	50	N.D.
Sodium	N.D.	230	N.D.
Aluminium	70	70	70
Sulphur	300	60	300
Chlorine	200	200	200
Potassium	20	80	900
Platinum	10	10	N.D.

TABLE 6.1
Impurity concentration as determined by mass spectrometry. Concentrations are gives in parts per million (ppm). The detection limit was 3ppm, N.D. indicates none detected.

The platinum present in the LCPs is due to the chloroplatinic acid used to catalyse the addition of side groups to the backbone during synthesis. The largest variation between the samples is the presence of more than 200 times as much sodium in GN3/14 as in the other samples. Although these results do not indicate whether the sodium is ionised, it must be noted

that the ionisation potential of sodium is relatively low. In the following section, GN3/14 is shown to be more conducting than many of the other LCPs under investigation, and this high level of sodium contamination may provide an explanation.

In summary, despite the fact that one of the more conducting LCPs was used for the comparison, there is evidence that this LCP is no more conducting, and therefore does not have a higher level of conducting impurities, than the ImmLC S2, currently used in commercial laser written storage displays.

6.2.2 AC Conductivity of LCPs

A method has been developed to compare the conductivities of the wide variety of LCPs described in Tables 2.2 to 2.6. In the low field regime, ionic conduction may be assumed to predominate (Blinov, 1983) and hence the conductivity can be related to the concentration of charged impurities. Variations between LCPs were expected because of the variety of mesogenic side groups (including those with highly electro-negative fluorine substituents which tend to encourage ionic dissociation) and the variety of backbones which required slightly different synthetic routes.

The LCPs were used as supplied and the AC conductivity of unaligned samples in dielectric cells (having uncoated low resistivity ITO electrodes) was measured. A plot of the conductivity of GN3/25 as a function of inverse temperature at 3.5 KHz is shown in Figure 6.2. This frequency was routinely used when aligning LCP films for use in optical storage devices. The conductivity of 17 LCPs has been compared in the isotropic phase at the reduced temperature of 1.1 T_2, the results are

summarised in Figure 6.3. There appears to be a significant correlation between the data points of 12 of the LCPs. A straight line has been calculated from these values using linear regression (correlation coefficient of 0.96) to act as a guide to the eye.

As discussed in Section 6.2.1, the high sodium content of GN3/14 possibly accounts for its high conductance and deviation from the line. A common characteristic of the remaining LCPs which deviate from the line is the fact that they exhibit a melting transition; GN4/16 and GN3/29 which fall below the line also exhibit a glass transition. The LCPs lying on the line exhibit a glass transition alone. The melting transition could be a sign of a higher impurity concentration, or of differences in the microstructure which would affect the viscosity and therefore mobility of charge carriers. The LCPs GN3/3 and GN4/33 have melting transitions and yet do not show anomalous conduction behaviour. For these LCPs, the measuring temperature was considerably further from the melting transition temperature and it seems likely that any crystalline-type microstructure would have been completely destroyed by thermal motion. It is likely that both a higher level of ionic contamination and differences in mobility contribute to the observed conductivity behaviour. X-ray diffraction studies would provide more information on the microstructure of these LCP.

Having discussed the "anomalous" LCPs, it is now necessary to consider the physical mechanism whereby 12 LCPs having considerable structural variations can produce a straight line of this form. One possible explanation will be discussed.

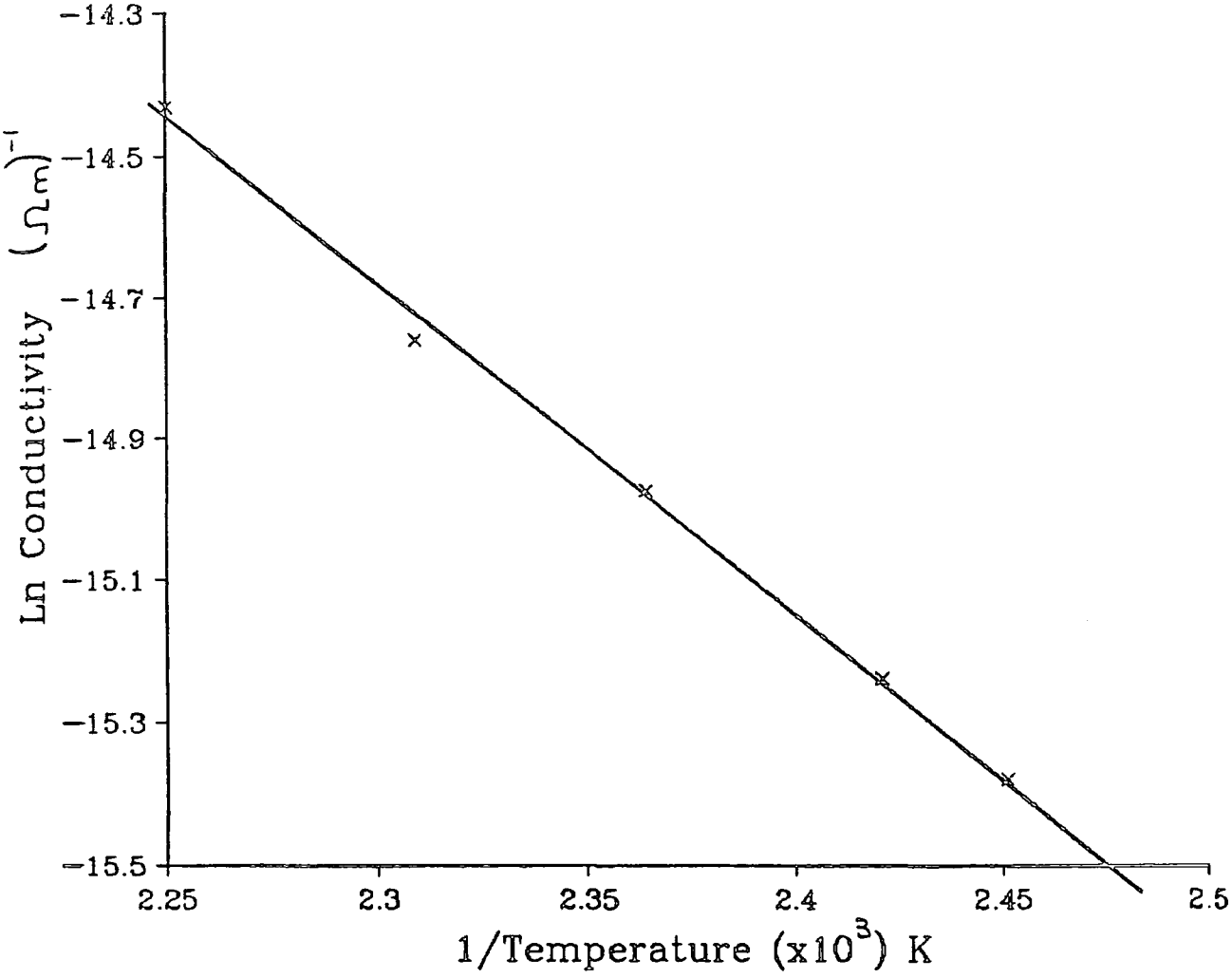

FIGURE 6.2
The variation of the AC conductivity (at 3.5 kHz) of GN3/25 with temperature.

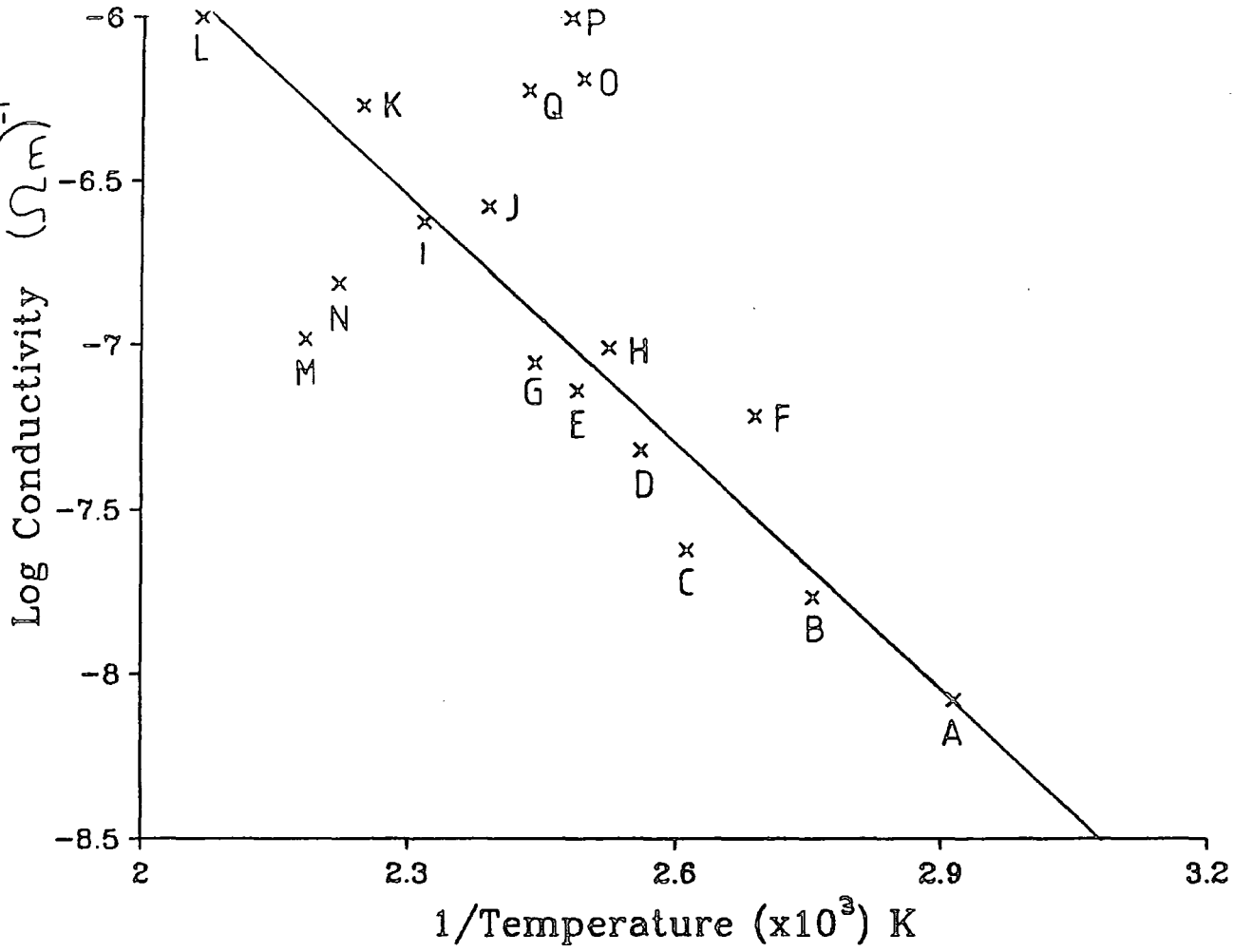

FIGURE 6.3
A comparison of the AC conductivity (at 3.5 kHz) of 17 LCPs measured at the reduced temperature of $1.1T_2$. A straight line fit using LCPs A to L has been shown as a guide to the eye.

A	GN3/18	B	GN3/22	C	GN4/18
D	GN3/17	E	GN4/17	F	GN3/16
G	GN3/15	H	GN4/19	I	GN3/3
J	GN3/19	K	GN3/25	L	GN4/33
M	GN3/29	N	GN4/16	O	GN4/11
P	GN4/13	Q	GN3/14		

When calculating the Arrhenius activation energy of conduction of a material in which the conduction arises from ionic species, the logarithmic conductivity is plotted against inverse temperature. This form of graph was used in Figure 6.3 when comparing different LCPs. A straight line relationship between different materials might suggest that they all have the same concentration of conducting species and the same thermal activation energy of conductivity (see Equation [3.27]). Data were available to calculate the activation energy and pre-exponential factor (related to the concentration of conduction species) for GN3/25, GN3/17 and the anomalous LCP GN4/11 in the isotropic phase. The results are summarised in Table 6.2.

LCP	Arrhenius Activation Energy, E_a ($kJmol^{-1}$)	Pre-exponential factor, σ_o ($\Omega\ m)^{-1}$
GN3/25	37.9	0.015
GN3/17	45.0	0.04
GN4/11	44.5	1.25

TABLE 6.2
Characterisation of LCPs using the ionic equation $\sigma=\sigma_o \exp(-E_a/k_BT)$ (see Equation [3.27]).

The LCPs all have similar values of E_a, but the pre-exponential factors of GN3/25 and GN3/17 are about 100 times less than that of GN4/11. This would suggest that all the LCPs have similar thermal activation energies of conduction, but the LCPs lying on the line have a lower concentration of conducting species. However, the results from three LCPs alone are insufficient to provide conclusive evidence to support this theory and the isotropic conductivity of several more LCPs must be studied in detail.

There is practical significance in the empirical observation of a linear relationship between the conductivity and inverse temperature of these LCPs. By making a single measurement of AC conductivity at a reduced temperature of 1.1 T_2, the conductivity of a newly synthesised LCP can be compared with the large number that have already been studied. If the conductivity falls in the straight line region indicated in Figure 6.3, then it is reasonable to suggest that its behaviour will be comparable with the other LCPs on the line. It is very difficult to compare the conductivity of different materials and a graph of the form shown in Figure 6.3 could be the means of defining a standard for the conduction behaviour of LCPs.

6.2.3 Electrode Polarisation

The build up of space charge at electrodes usually results from imperfect contact between the metal electrode and the sample and may be aggravated by the products of electrolysis. It can be quantified using the concept of an impedance in parallel with the sample as described in Section 3.2.3. Figure 6.4 shows the success of correcting for the electrode polarisation of GN3/19 at 155°C when n is taken to equal ½ in Equation [3.33], which can then be rewritten in the form:

$$\epsilon_{app} = \epsilon + \frac{Z_o G^2}{\sqrt{2}\omega^{3/2} C_o} \qquad [6.1]$$

where C_0 is the empty cell capacitance.

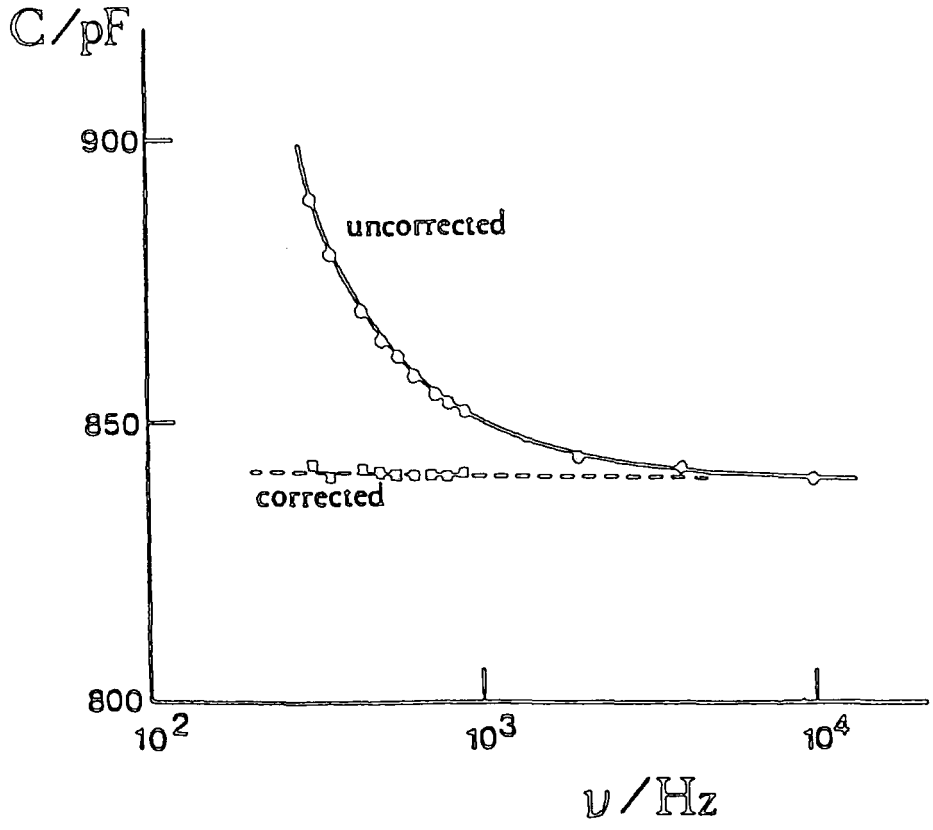

FIGURE 6.4
Uncorrected and corrected values of the measured cell capacitance for polymer GN3/19 at 155°C.

The values of Z_0 for the LCPs used in the previous section have been calculated at 1.1 T_2 and are summarised in Table 6.3. It was not possible to calculate Z_0 for approximately half of the LCPs since there was no apparent increase in the low frequency permittivity at this reduced temperature. This suggests that these LCPs are not sufficiently conducting to allow the build up of charge in the vicinity of the electrodes. Indeed Figure 6.3 shows all of these LCPs have a bulk conductivity of less than 10^{-7} $(\Omega m)^{-1}$. The magnitude of the electrode impedance calculated for each of the remaining LCPs is related approximately to the relative magnitude of its bulk conductivity at the reduced temperature of 1.1 T_2.

This result indicates that there is a limiting conductivity of 10^{-7} $(\Omega m)^{-1}$ for the formation of space charge in these LCPs. The ionic mobility varies as a function of temperature according to Equation [3.27] and the reduced temperature of 1.1 T_2 leads to approximately half of the LCPs studied being in a sufficiently conducting state to allow the observation of a charged double layer at the electrode. Although electrode polarisation was not observed in the other half of the LCPs, it is likely that it would be apparent at a sufficiently high temperature for the bulk conductivity to be greater than 10^{-7} $(\Omega m)^{-1}$.

LCP Code	Temperature (°C)	$Z_o \times 10^6$ (Ω)
GN4/17	128	-
GN4/19	123	-
GN3/15	136	-
GN4/18	110	-
GN3/40	123	-
GN3/22	90	-
GN3/16	99	-
GN3/17	117	-
GN3/18	70	-
GN3/29	185	slight
GN4/16	177	1.77
GN3/19	140	2.4
GN3/3	158	2.6
GN4/33	212	2.62
GN4/11	128	4.14
GN3/25	171	6.79
GN3/14	137	9.76
GN4/13	130	12.5
GN4/29	211	50.3

TABLE 6.3
Calculation of electrode impedance using $Z_{el} = Z_o\ (i\ \omega)^{-\frac{1}{2}}$ and Equation [6.1]

6.2.4 A Comparative Study of the Conductivity of GN3/15

Reference has already been made to the difficulty in comparing the values of conductivity measured for these polysiloxane side chain LCPs and those reported in the literature. In addition to the need to compare materials, the methods of measurement should be compared directly to identify the influence of factors such as cell construction. To this end the

conductivity of the homopolymer GN3/15 has been studied and compared with measurements made on samples from the same batch of the LCP by G.S. Attard (University College Wales, UCW) and C.P. Legrand (University of Lille). Their experimental techniques for studying mesogenic dielectric properties are described by Attard et al (1986a) and Legrand et al (1985), respectively. The conductance was measured as a function of temperature into the isotropic phase, except at UCW where only the biphasic region could be readily achieved.

The low frequency loss behaviour at 400 Hz as a function of temperature is shown under each set of measuring conditions in Figure 6.5. The losses observed in the smectic phase are almost identical in each case, any slight differences are readily attributable to differing states of alignment in the samples. As the biphasic region is approached, the results obtained by Attard and Legrand diverge significantly from those measured using the method described here. The AC conductivity is plotted as a function of inverse temperature in Figure 6.6 and compared with the results of Legrand. The conductivity in the isotropic phase measured by the latter is an order of magnitude larger.

The main difference between each of the experimental techniques is the electrode composition; brass and steel were used by Legrand and Attard, respectively and low resistivity indium tin oxide (ITO) was used in this work. These results suggest that the electrode plays an important role in determining the build up of space charge and the apparent AC conductivity. The influence of a variety of electrodes and surfactants is discussed in detail in the next section, however this study of GN3/15 alone indicates

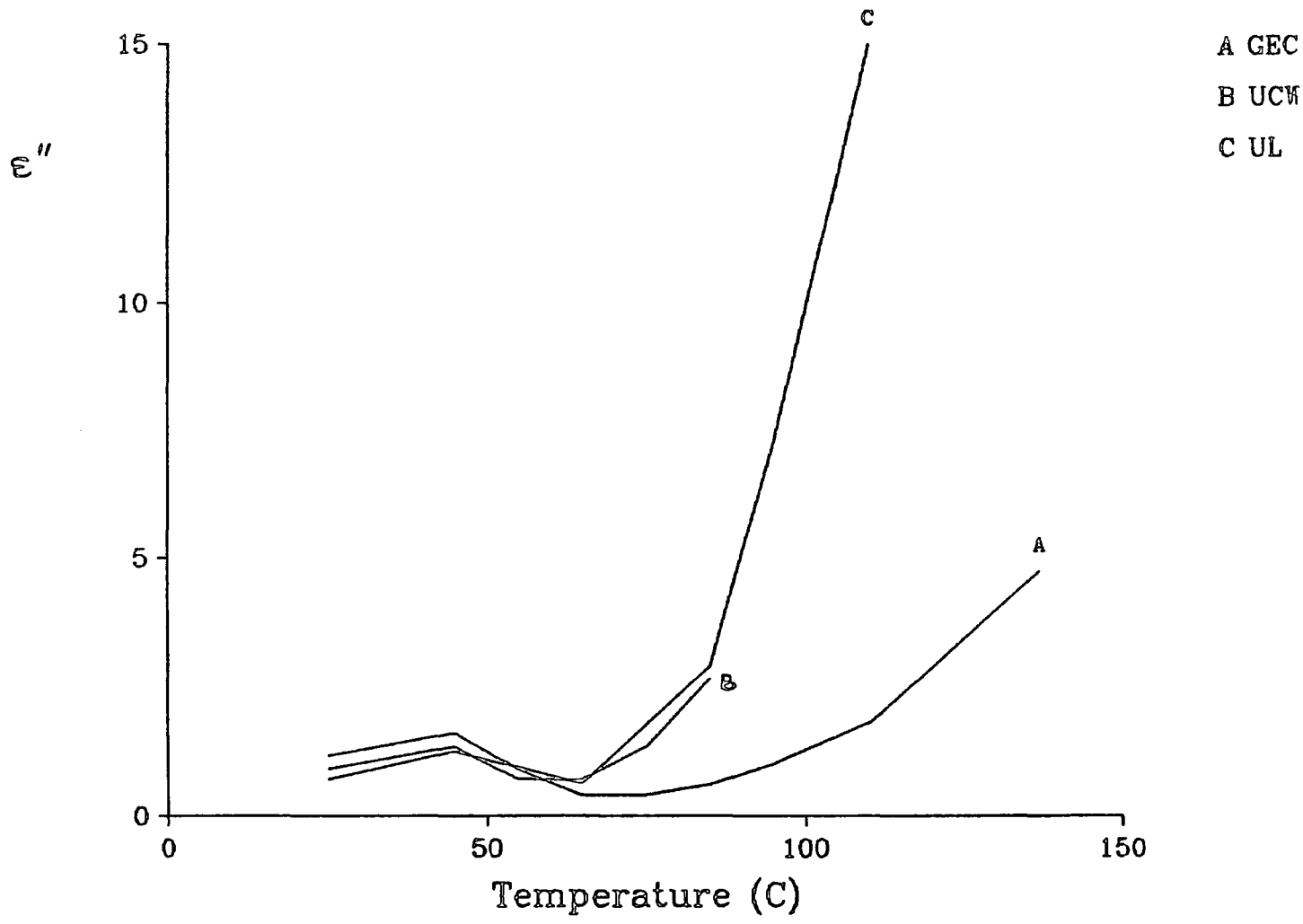

FIGURE 6.5
The variation of the imaginary component of the permittivity of GN3/15 (at 400 Hz) with temperature: A - measured at GEC, B - measured at the University College Wales, C - measured at the University of Lille.

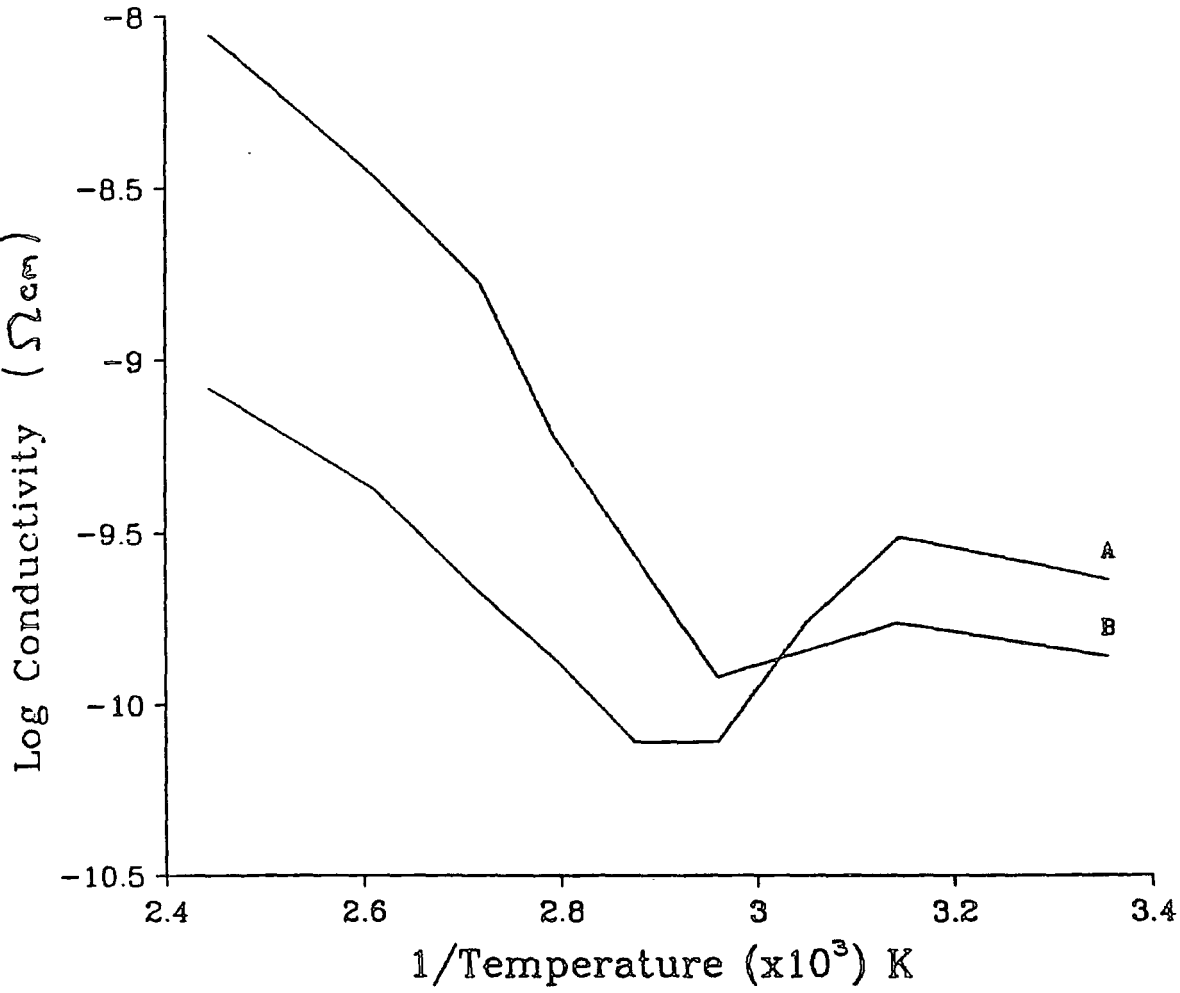

FIGURE 6.6
A comparison of the variation of the conductivity of GN3/15 with temperature as measured at A-GEC, B-University of Lille.

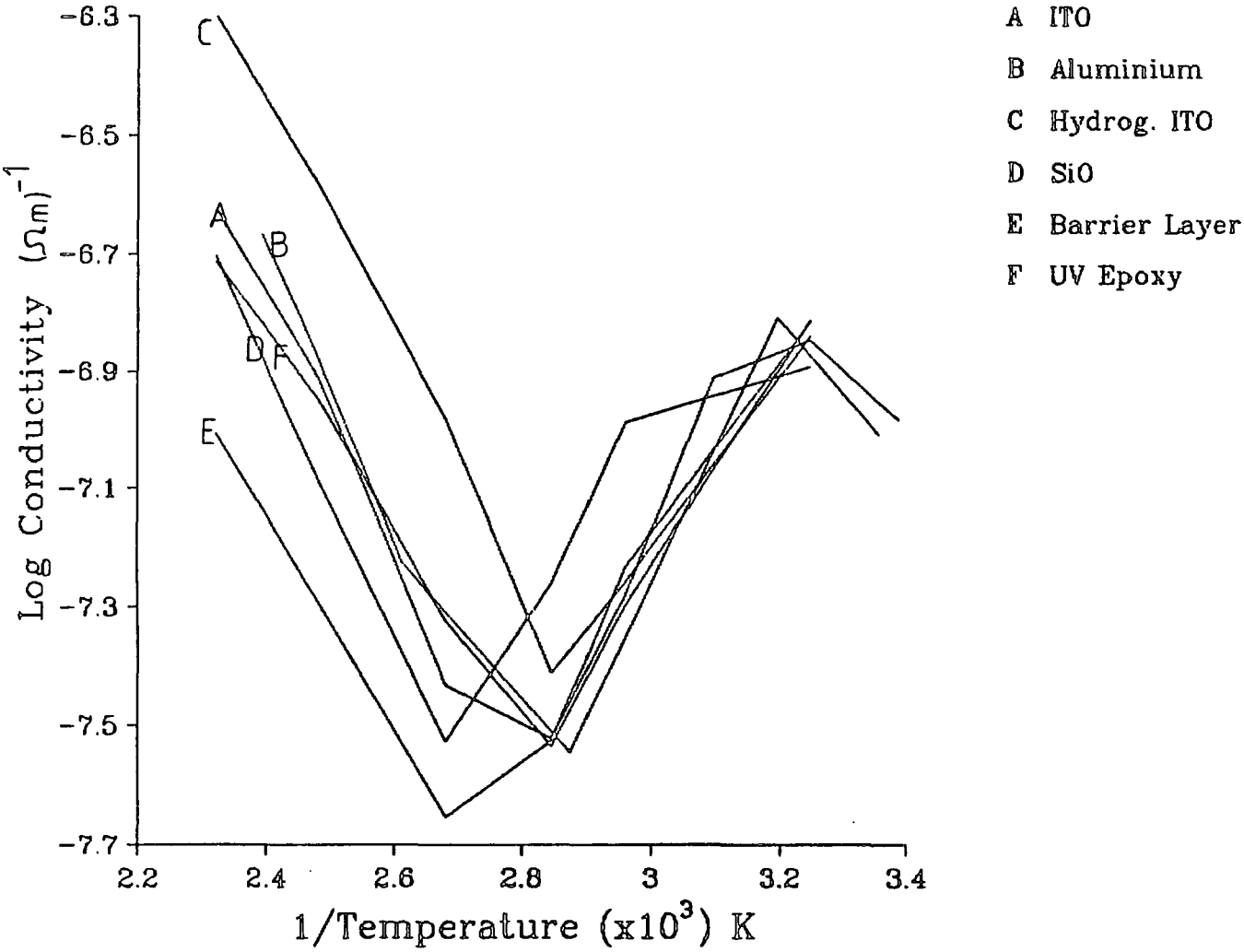

FIGURE 6.7
The conductivity of GN3/3 (at 3.5 kHz) as a function of inverse temperature measured in a variety of cells having different electrodes and electrode surfactants.

that care should be taken when comparing results from different measuring techniques. It is useful to note that the permittivity in the isotropic phase at 136°C and at 50 kHz was measured as about 10.0 at the University of Lille and 10.2 by the author, so these differences due to electrode composition primarily affect the low frequency responses (less than about 1 KHz). The observations also have technological significance for the development of aligned films of LCPs since the presence of space charge at electrodes and high apparent conductivity are known to contribute to dielectric breakdown (O'Dwyer, 1973).

6.2.5 The Influence of the Electrode Surface

The results of the previous section suggest that the LCP-electrode interface and the chemical nature of the electrode play an important role in the formation of space charge and in determining the magnitude of the apparent conductivity. This behaviour has been studied in more detail by measuring the conductivity of the LCP GN3/3 in cells with electrodes of low resistivity ITO, aluminium and hydrogenated ITO. The latter were produced by reacting ITO electrodes in a hydrogen plasma to reduce the oxide. The result is a more conducting surface of indium and tin. The effect of evaporated silicon monoxide, an organosilane barrier layer, polyimide and UV curable epoxy as surfactants on ITO electrodes were also investigated. Figure 6.7 summarises the conductivity as a function of inverse temperature under each of these experimental conditions. The values of electrode impedance, Z_0, in each type of cell at 158°C have been calculated using Equation [6.1] and are summarised in Table 6.4.

Surface Layer	$Z_0 \times 10^6$ (Ω)
Barrier Layer	-
UV Curable	-
Polyimide	0.8
SiO (perpendicular evaporation)	1.2
SiO (60° evaporation)	1.4
Aluminium	1.6
5 Ω/square ITO	3.9
Hydrogenated ITO	4.3

TABLE 6.4
The electrode impedance measured in cells with a variety of electrodes and electrode surfactants containing GN3/3 at 158°C.

There is reasonable correlation between the magnitude of the electrode impedance and that of the bulk conductivity. The lowest conductivity in the isotropic phase was measured with the organosilane barrier layer and no electrode polarisation could be detected. The ITO and hydrogenated ITO had high values of bulk conductivity and the largest electrode polarisation values. The formation of a high impedance layer at the electrode surface in the case of polymers in general may be due to imperfect contact between the metal electrode and the specimen (Blythe, 1979). Since the polymeric organosilane barrier layer, the UV curable epoxy and the polyimide showed little or no electrode polarisation, it seems reasonable to assume that they form a good match with the LCP at the surface. This match could be partially chemical in nature, however the

actual physical texture of the surface appears to be significant. Even though the aluminium and the ITO electrodes were both deposited by sputtering, the values of Z_0 are significantly different.

To assess the surface characteristics in more detail, plates which had been coated with the surfactants and different electrodes from unassembled cells were studied by electron microscopy. Photographs of the surfaces of the organosilane barrier layer, the UV curable epoxy, buffed and unbuffed polyimide, aluminium and 5 Ω/square ITO are shown in Figure 6.8. There is an excellent correlation between the roughness of the surface and the magnitudes of Z_0 from Table 6.4. The ITO and the aluminium surfaces are extremely uneven, while the organosilane barrier layer surface is virtually featureless. The UV curable epoxy surface is not smooth as would be predicted, however it has an "undulating" lattice type structure, rather than being based on "bumps" as are the aluminium and the ITO. It appears that this more open structure does not encourage the formation of space charge. Although the hydrogenated ITO surface was not photographed, Major et al (1988) have reported a roughening of the surface of ITO after hydrogenation. This would be consistent with the measurement of a large value of Z_0.

These results suggest that the apparent conductivity and electrode polarisation of an LCP can be reduced by coating the electrode with a smooth polymer based surfactant. This has practical benefits since there should be a reduction in the tendency to dielectric breakdown in the film of LCP when there is less space charge and a lower apparent conductivity.

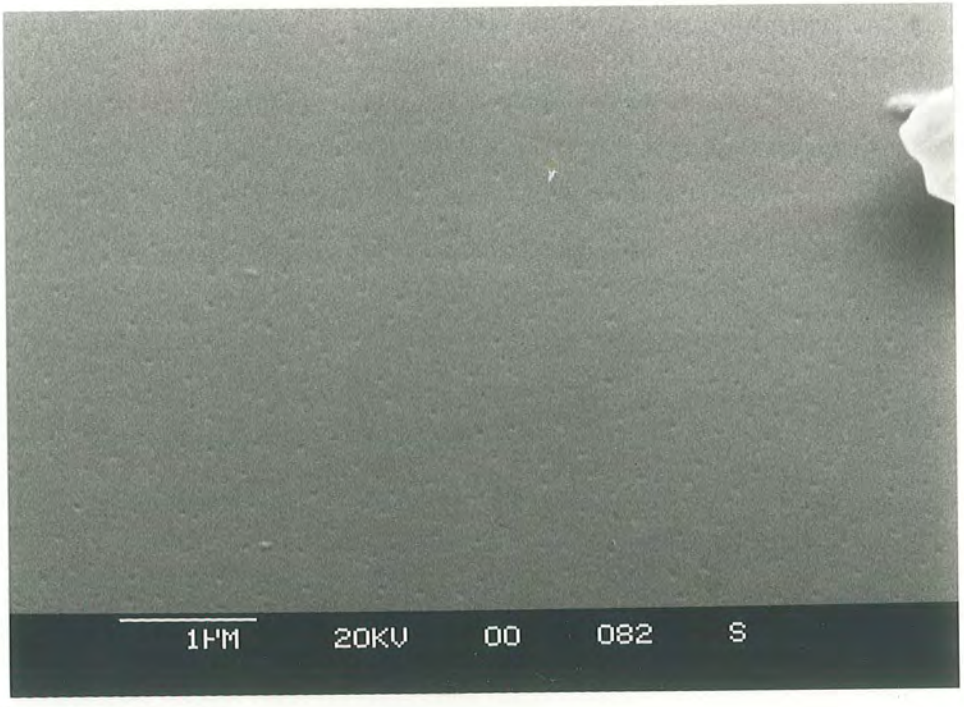

FIGURE 6.8(a)
Scanning electron microscope photograph of the surface of an organosilane barrier layer spun onto ITO coated glass.

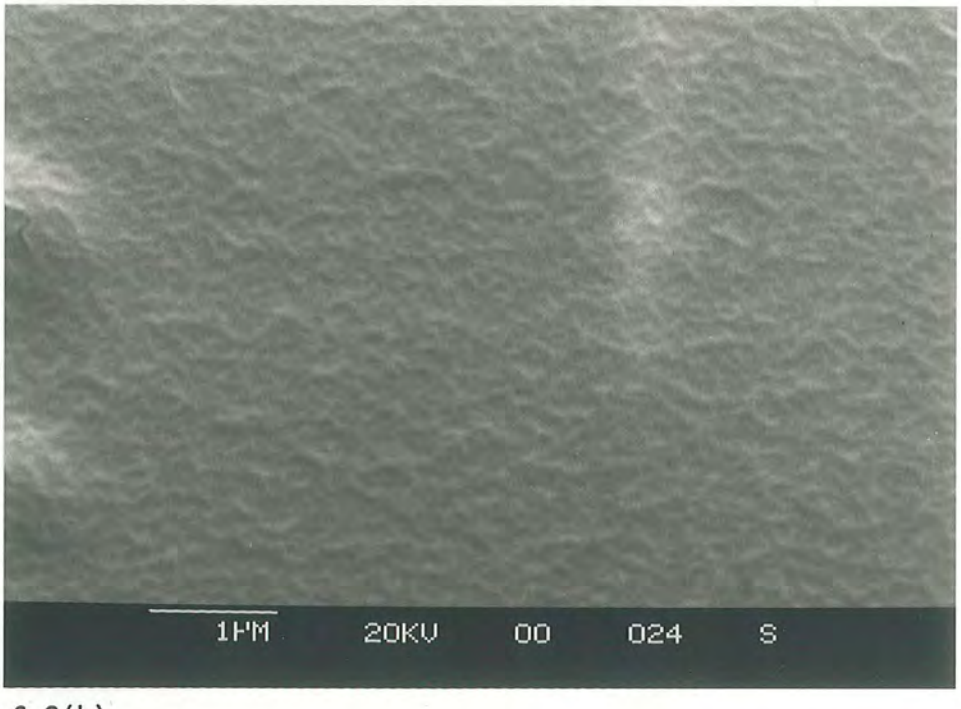

FIGURE 6.8(b)
Scanning electron microscope photograph of the surface of UV curable epoxy spun onto ITO coated glass.

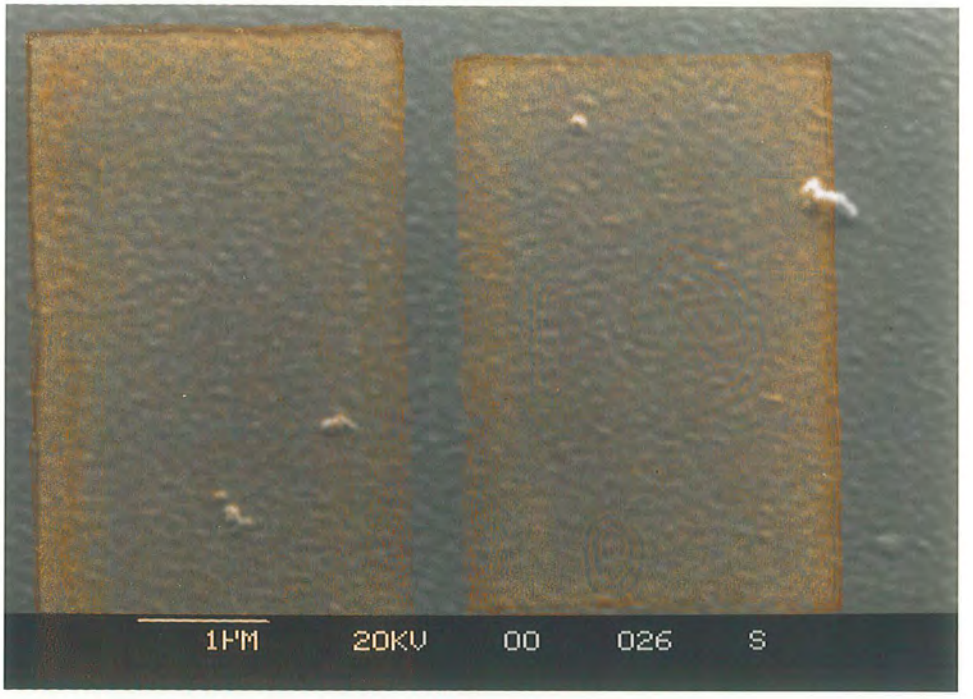

FIGURE 6.8(c)
Scanning electron microscope photograph of the surface of unbuffed polyimide spun onto ITO coated glass.

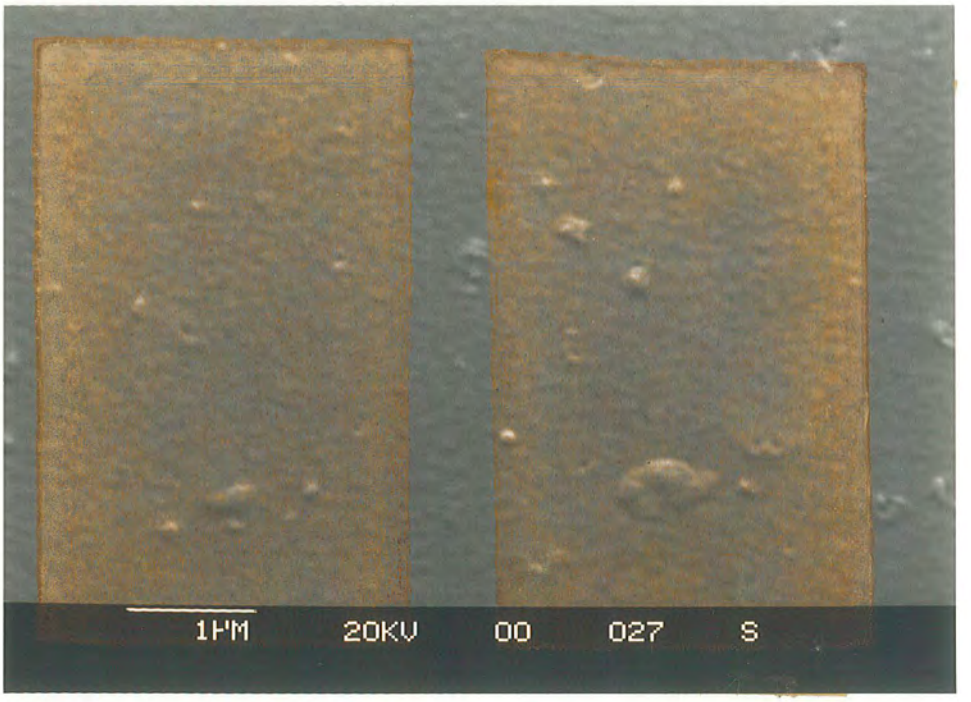

FIGURE 6.8(d)
Scanning electron microscope photograph of the surface of buffed polyimide spun onto ITO coated glass.

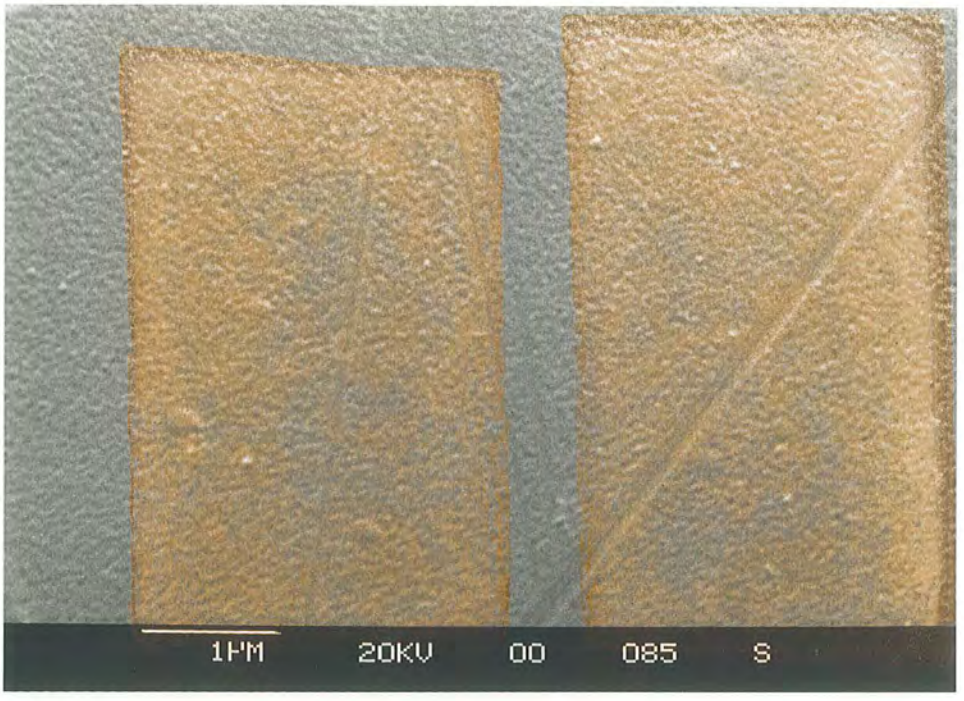

FIGURE 6.8(e)
Scanning electron microscope photograph of the surface of aluminium sputtered onto glass.

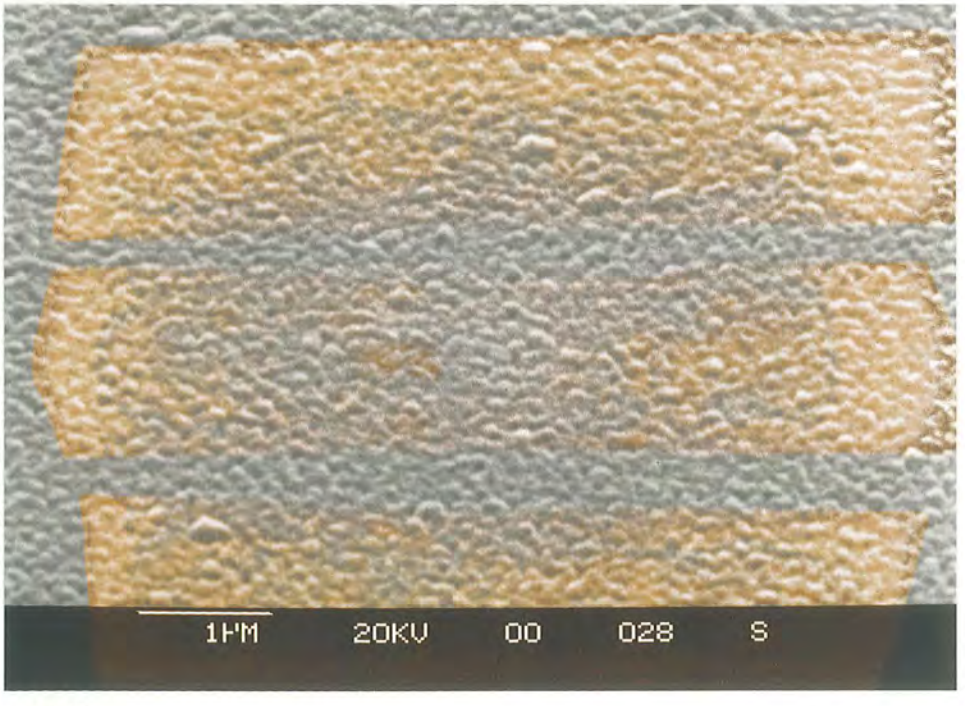

FIGURE 6.8(f)
Scanning electron microscope photograph of the surface of 5 Ω/square ITO sputtered onto glass.

6.3 High Field Conductivity

The behaviour of LCPs in large electric fields is particularly relevant to the development of practical devices requiring electric field aligned films of material. Information about the mechanisms of conduction and methods of controlling it has been obtained from a study of the behaviour of GN3/3 in large DC electric fields, as compared with the 1mmLC S2. The influence of the electrode composition and surface have also been investigated.

6.3.1 GN3/3

The current-voltage characteristic of GN3/3 has been measured at 40°C and 70°C. In each case there was distinctly different conductivity behaviour. On application of each voltage, a large displacement current was observed with the time to steady state taking between fifteen minutes and an hour depending on the voltage and temperature. Figure 6.9 shows the I-V plot at 40°C in a 25 μm cell having low resistivity ITO electrodes. The linear relationship at higher voltages between current and voltage probably indicates that ionic conduction is the predominant mechanism for current flow at this temperature. The low values of current measured below 30V are possibly due to residual reorientation effects of the side groups in the electric field.

Measurements at 70°C were made in a cell having one low resistivity ITO electrode and one aluminium electrode. The forward and reverse bias I-V characteristic is shown in Figure 6.10 and Figure 6.11 shows that above a threshold of about 4V, plots of log I against $V^{\frac{1}{2}}$ are very accurately linear, although the two lines have different slopes. The obvious

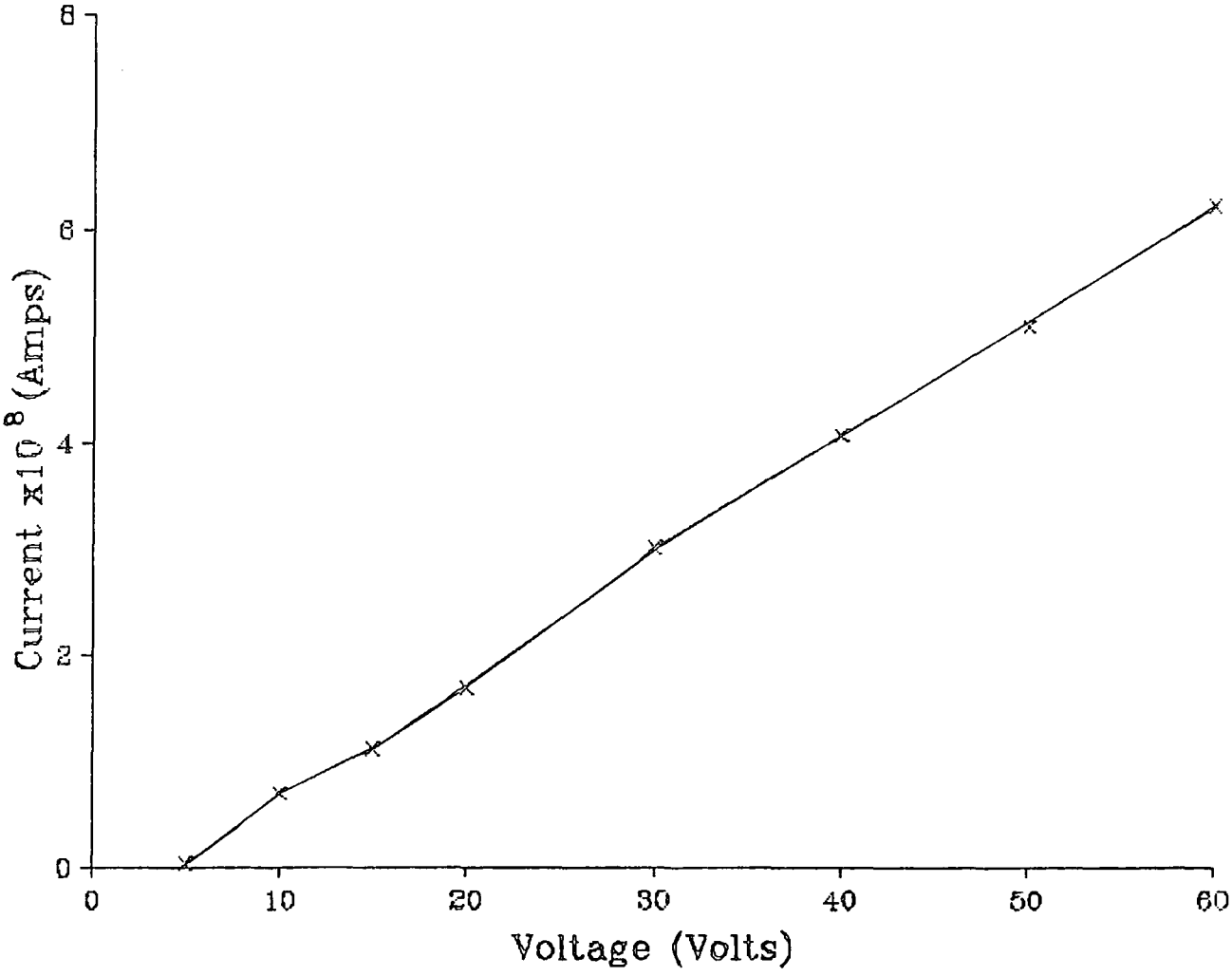

FIGURE 6.9
The current-voltage characteristic of GN3/3 at 40°C (measured using low resistivity ITO electrodes).

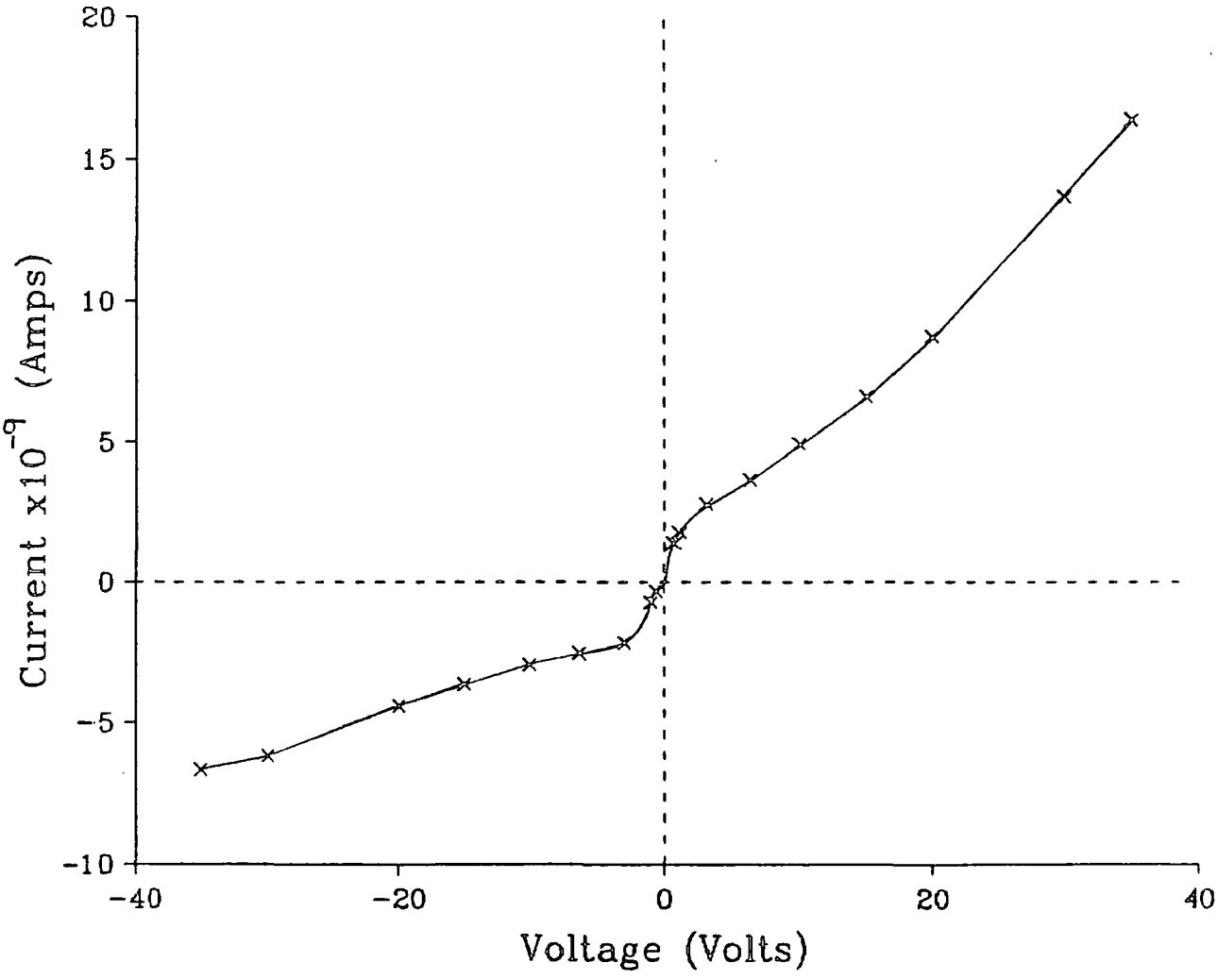

FIGURE 6.10
The current-voltage characteristic of GN3/3 at 70°C (measured in a cell having one ITO electrode and one aluminium electrode).

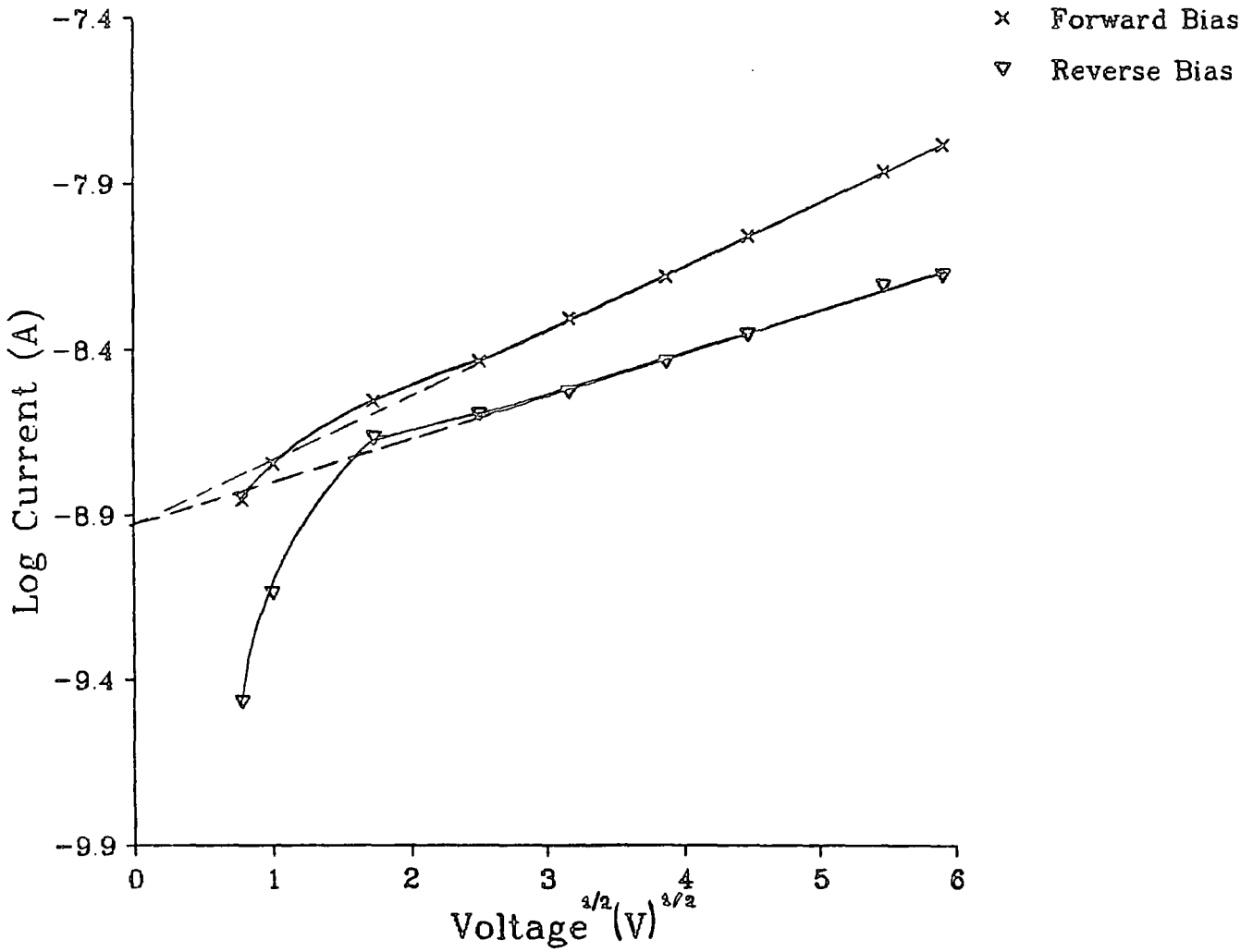

FIGURE 6.11
The relationship between the logarithmic current and (voltage)$^{1/2}$ for GN3/3 at 70°C (measured in a cell having one electrode of ITO and the other of aluminium).

dependence on electrode composition confirms that it is probably a Schottky (i.e. surface controlled) rather than a Poole-Frenkel (i.e. bulk controlled) process, see Equation [3.28].

The relatively low threshold voltage for Schottky emission may be understood by noting that the effect of a space charge layer on a charge-injecting electrode is to enhance the local field (Sessler et al, 1986). This effect can be represented by replacing E in Equation [3.28] by γE, where γ is a field enhancement factor. Then:

$$I = AT^2 \exp\{-[\phi - \beta(\gamma E)^{1/2}]/k_B T\} \qquad [6.2]$$

Estimates of γ may be obtained from the observed slopes by assuming a value for ϵ_∞ in the definition:

$$\beta = (e^3/4\pi\epsilon_o\epsilon_\infty)^{1/2}$$

Taking ϵ_∞ = 2.8 (an estimate of the refractive index squared), then γ is equal to 7.8 and 3.4 for the forward and reverse characteristics respectively. These values of γ are slightly higher than the value calculated for Kapton polyimide by Sessler. To assess the validity of the results, a Debye-Hückel approximation may be applied to describe the electrode polarisation (Clark, 1988). Assuming a cell of thickness d, with identical electrodes and filled with an insulating medium containing as an impurity a 1:1 electrolyte yielding monovalent ions, then:

$$\gamma \approx 1/2 \ \lambda d \qquad [6.3]$$

where

$$\lambda = (2e^2 n_o / \epsilon_o \epsilon k_B T)^{1/2} \qquad [6.4]$$

n_0 being the number concentration of ionised impurities and ϵ the permittivity of the medium. Using d = 25 μm, T = 343K, ϵ = 10 and n_0 = (1.3 x 10^{27}) C_0 m^{-3}, where C_0 is the number fraction of ionic carrier pairs relative to the number concentration of mesogenic groups, then to obtain a value of γ=5 it is necessary to assume a value for C_0 of 10^{-9}. This would be typical of the intrinsic carrier concentration at room temperature of a semiconducting material such as germanium and hence confirms that these results for the field enhancement factors do not require unreasonable levels of carrier concentration.

6.3.2 S2

DC conductivity measurements have been made using dyed and undyed samples of the 1mmLC S2. The electrodes of the measuring cells were low resistivity ITO and a measuring temperature of 35°C was used in each case. The current-voltage characteristic is shown in Figure 6.12, and Figure 6.13 shows that for each sample plots of log I against $V^{1/4}$ were linear, in contrast to the case of the LCP GN3/3 discussed above in which log I against $V^{1/2}$ was linear. The former relationship is consistent with the form predicted by Equation [3.30] for a typical semiconductor in contact with an injecting metal electrode. The observation of a semiconductor response for S2, rather than the insulator response of the LCP GN3/3 is probably due to the increased mobility of the charge in S2. It should be noted that measurements were made at a higher reduced temperature and also the viscosity of S2 is considerably less than that of the LCPs (see

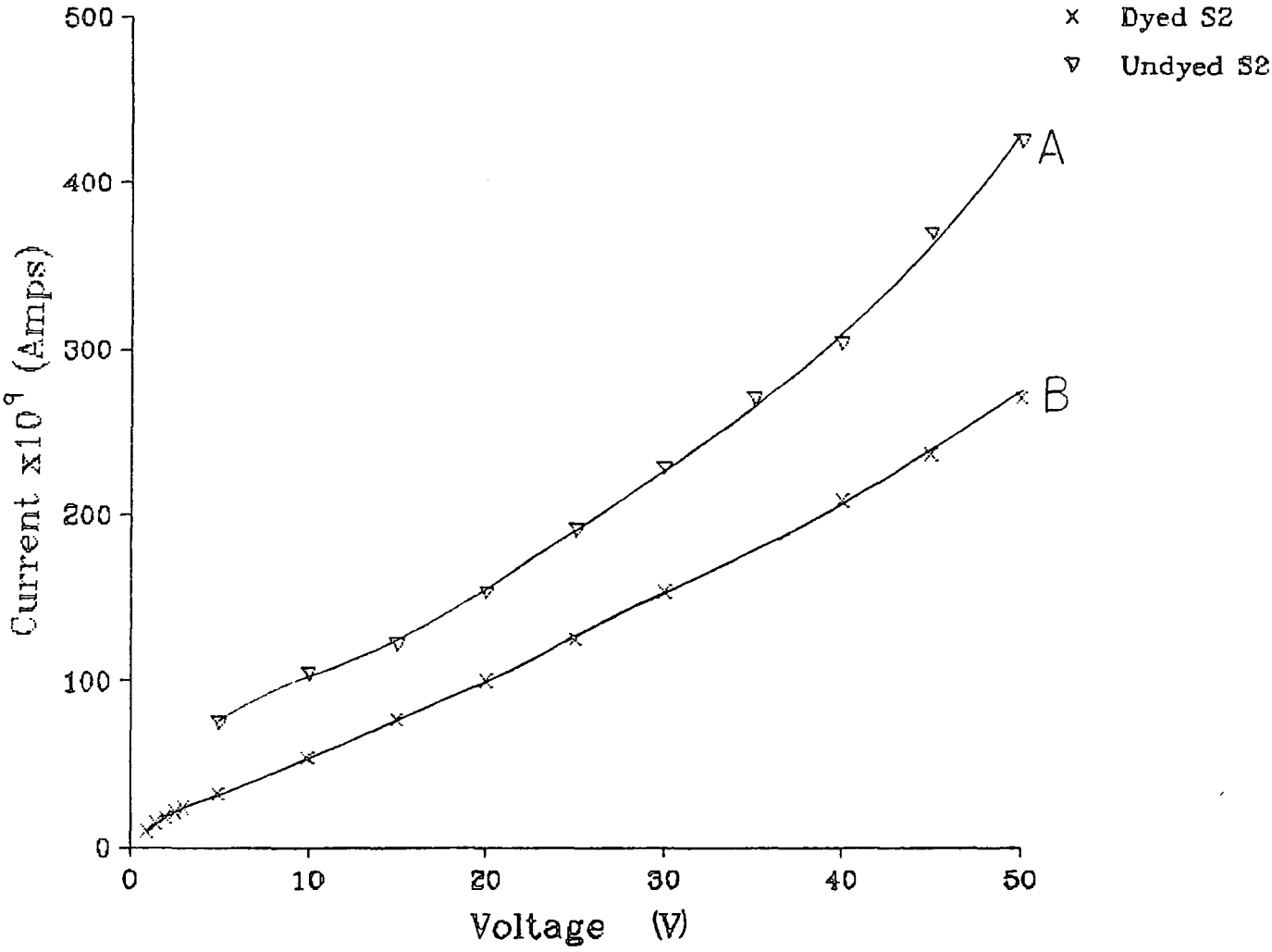

FIGURE 6.12
The current-voltage characteristic of the 1mmLC smectic mixture S2 at 35°C (A) as supplied, (B) dyed with 3% wt/wt D102. The measuring cells had low resistivity ITO electrodes.

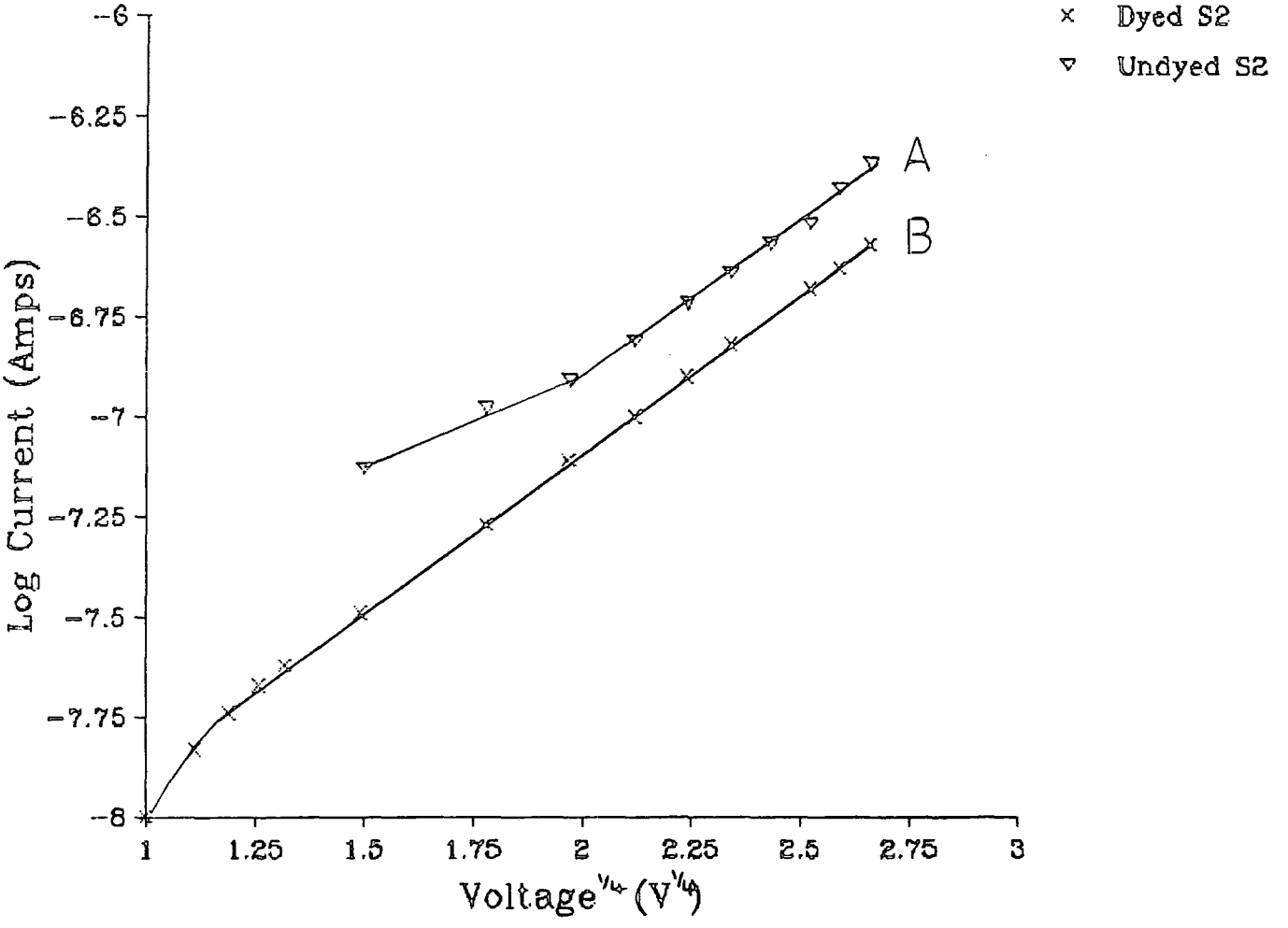

FIGURE 6.13
Plots of the logarithmic current versus (voltage)$^{1/4}$ for the 1mmLC smectic mixture S2 at 35°C (A) as supplied, (B) dyed with 3% wt/wt D102.

Section 7.1). It is also possible that S2 has a higher intrinsic carrier concentration than GN3/3 since it was shown in Section 6.2.1 that S2 is comparable with GN3/14, one of the more conducting LCPs. Ginnai et al (1980) in their studies of Langmuir Blodgett films, showed that the measured I-V response during tunnelling conduction may be linear on a log $I\text{-}V^{1/4}$ plot, as well as obeying the usual Statton's model. However, it is unlikely that tunnelling conduction plays a major role in the S2 due to the thickness of the films and the relatively high measurement temperature. The dyed and undyed samples of S2 produced virtually identical results, within the accuracy of this experiment, suggesting that the effect of the dye on the conduction behaviour is slight.

Although the charge transport mechanism in the bulk of both LCPs and 1mmLCs is usually ionic, it was noted in Section 6.1 that charge emission at the electrodes can result in the ionisation of neutral molecules and hence an increase in the current flow. No evidence is presented here to confirm the mechanism of charge transport through the samples.

6.3.3 The Influence of an Insulating Barrier

The DC conductivity of undyed samples of the LCP GN3/3 and the 1mmLC S2 was measured at 70°C and 40°C, respectively, using cells in which the electrode had been coated with UV epoxy. The results of Section 6.2.5 indicated that this reduced the build up of space charge in the vicinity of the electrodes under low field AC conditions. The I-V characteristics for GN3/3 and S2 are shown in Figure 6.14. It was not possible to fit these data to any of the standard forms related to conduction mechanism. The best fit was obtained for GN3/3 by plotting log I versus log V. This

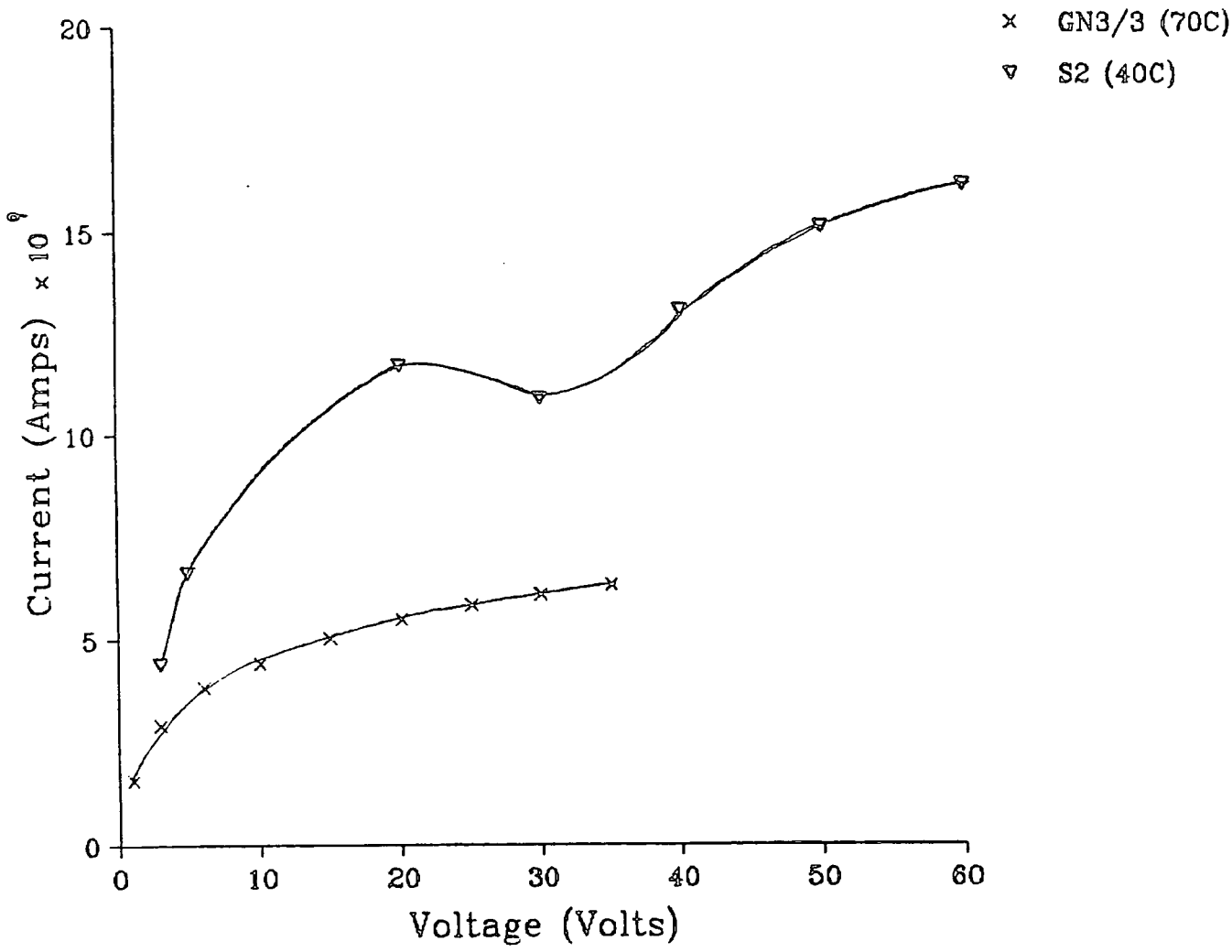

FIGURE 6.14
The current-voltage characteristics of GN3/3 at 70°C and S2 at 40°C (measured in cells having UV coated electrodes).

relationship applies to space-charge-limited conduction (Lamb, 1967), the character and magnitude of which is mainly determined by the presence of localised states which can trap and store charge in equilibrium with the free charge. It is mainly observed in insulators at room temperature and below and hence it is unlikely to be be the predominant mechanism here.

It is most likely that in the complicated electrical environment of these metal/insulator/semiconductor junctions, several conduction mechanism will be occurring. It would be necessary to study a wider voltage range and a range of film thicknesses and temperatures to produce a reliable model for the electrical response. However, since the standard Schottky model is no longer applicable, it appears that the UV curable epoxy layer could have reduced the emission of charge into the LCP from the ITO electrode. This may be due to a higher threshold voltage being required for Schottky emission since the field will be partly dropped across the insulating layer. This could also result in incomplete alignment of the LCP layer. Information concerning the dielectric permittivity and thickness of the UV curable epoxy layer would be needed to calculate the magnitude of this effect. Alternatively, as mentioned above, there is less space charge at the LCP-UV curable epoxy interface than at an LCP-ITO interface, possibly due to better physical or chemical matching. This will result in less field enhancement in the vicinity of the electrode, which was shown in Section 6.3.1 to be the major cause of the low threshold voltage for Schottky emission into LCPs from metal electrodes. This explanation suggests that Schottky emission would be observed at higher voltages in cells with UV epoxy coated electrodes and also implies that it should be

possible to align films of the LCP with a reduced probability of dielectric breakdown due to a reduction in the build up of charge at the surfaces.

6.4 Summary

In this Chapter, the electrical conduction behaviour of LCPs has been investigated. Low field AC conductivity measurements were used to study a wide range of LCPs. It was shown that the magnitude of the conductivity of commercial low molar mass LCs and these custom synthesised LCPs is comparable and a method was identified whereby the conductivity of different LCPs could be compared. A threshold conductivity of 10^{-7} $(\Omega m)^{-1}$ was identified for LCPs, beyond which electrical double layers could be observed to form at the surface of ITO electrodes. The electrode surface was shown to play an important role in determining the magnitude of both the apparent conductivity of the LCP and the impedance of electrical double layers near the surface of the sample. The microscopic surface texture was varied using different surfactants on the electrodes and an organosilane barrier layer and UV curable epoxy significantly reduced the measured space charge, probably because of the good physical match with the LCP.

High field DC conductivity measurements of the LCP GN3/3 and the 1mmLC S2 showed that Schottky type charge emission occurred at the electrodes at a sufficiently high temperature. It again appeared that an appropriate electrode surfactant (UV curable epoxy) could reduce the emission of charge, possibly due to the reduction in the formation of electrical

double layers at the electrode surface and hence a reduction in the intensity of the local field to below the minimum for observable Schottky emission.

Chapter Seven

Results and Discussion – Viscosity and Optical Properties

7.1 Viscosity Studies

7.1.1 Introduction

The viscosity of a material is an important parameter when developing methods of manufacturing commercial products. There have been many studies of the viscosity of main chain liquid crystal polymers (see, for example, the reviews by Wissbrun (1981) and Baird (1985)) because of their widespread use as high tensile strength fibres (for example, the LC polyimide sold commercially by DuPont as "kevlar"). There have been fewer reports of measurements of the viscosity of side chain liquid crystal polymers.

The LCPs studied here appeared to have widely different viscosities. This was most evident from the variation in the time required for glass sandwich cells to fill with the LCPs by capillary action. Some LCPs (such as GN3/36) were viscous liquids, some (such as GN3/14) were soft tacky solids, and others (such as GN2/10) were hard brittle solids at room temperatures.

Since GN3/14 was routinely used for optical storage studies (McArdle et al, 1987a,b), a series of experiments have been performed using this LCP to provide preliminary viscosity data for a device specification. Quantitative results have been produced and several areas were identified in which further work could lead to useful information about these materials.

7.1.2 Shear Viscosity of Mixtures

Mixtures of GN3/14 with the 1mmLC S2 were found to be non-Newtonian fluids in which the viscosity decreased with increasing shear rate. Measurements were made starting with the highest shear rate of 100 rpm. This pseudoplastic response was also observed by Hardouin et al (1982) in their study of main chain LCPs. However, a constant viscosity was approached at high shear rates for all the samples and this was assumed to correspond to the bulk viscosity of the sample at that temperature. The variation of viscosity with shear rate for the mixture 50% S2: 50% GN3/14 over a range of temperatures is shown in Figure 7.1.

The values of bulk viscosity as a function of temperature are summarised in Figure 7.2 for each sample. In the cases of the mixtures with 50% and 75% GN3/14 respectively, a decrease is the viscosity occurs in the mesophase about 10°C below the start of the biphasic region. Measurements were made starting with the highest temperature. This decrease in viscosity is probably due to shear alignment in these samples. It is known that flow alignment in 1mm nematic LCs usually leads to the director orientating almost parallel to the flow direction (Bock et al, 1986). In the vicinity of the isotropic transition, the director orientation varies from the flow direction by an angle θ_s. According to the Leslie-Ericksen Theory the shear viscosity under flow alignment is given by:

$$\eta_s = \eta_2 + (\eta_1-\eta_2)\sin^2\theta_s \qquad [7.1]$$

where η_1 and η_2 are the components of the viscosity perpendicular and parallel to the director respectively (de Jeu, 1980). For these smectic

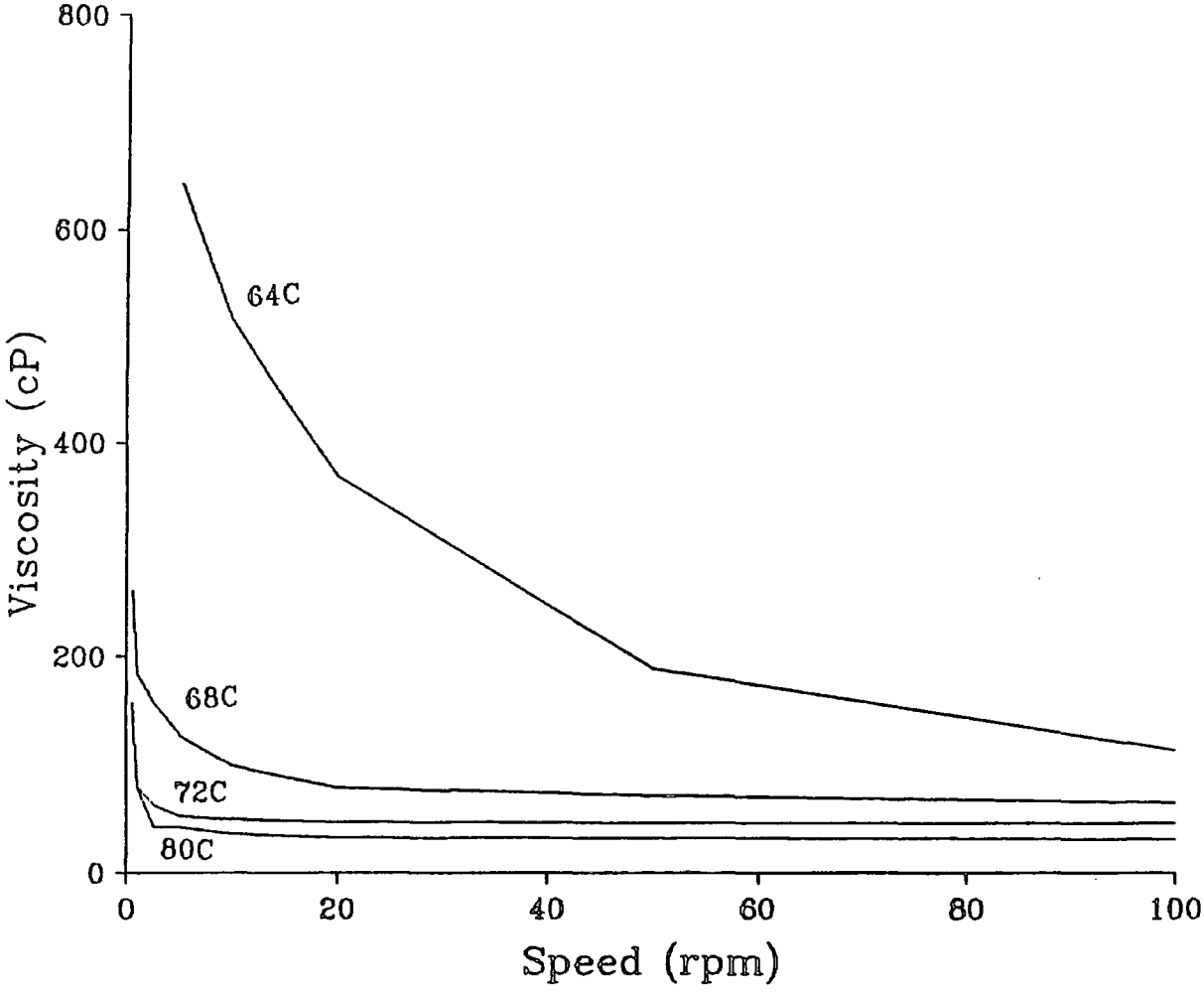

FIGURE 7.1
The variation of the viscosity with shear rate of the mixture 50% GN3/14: 50% S2 over a range of temperatures.

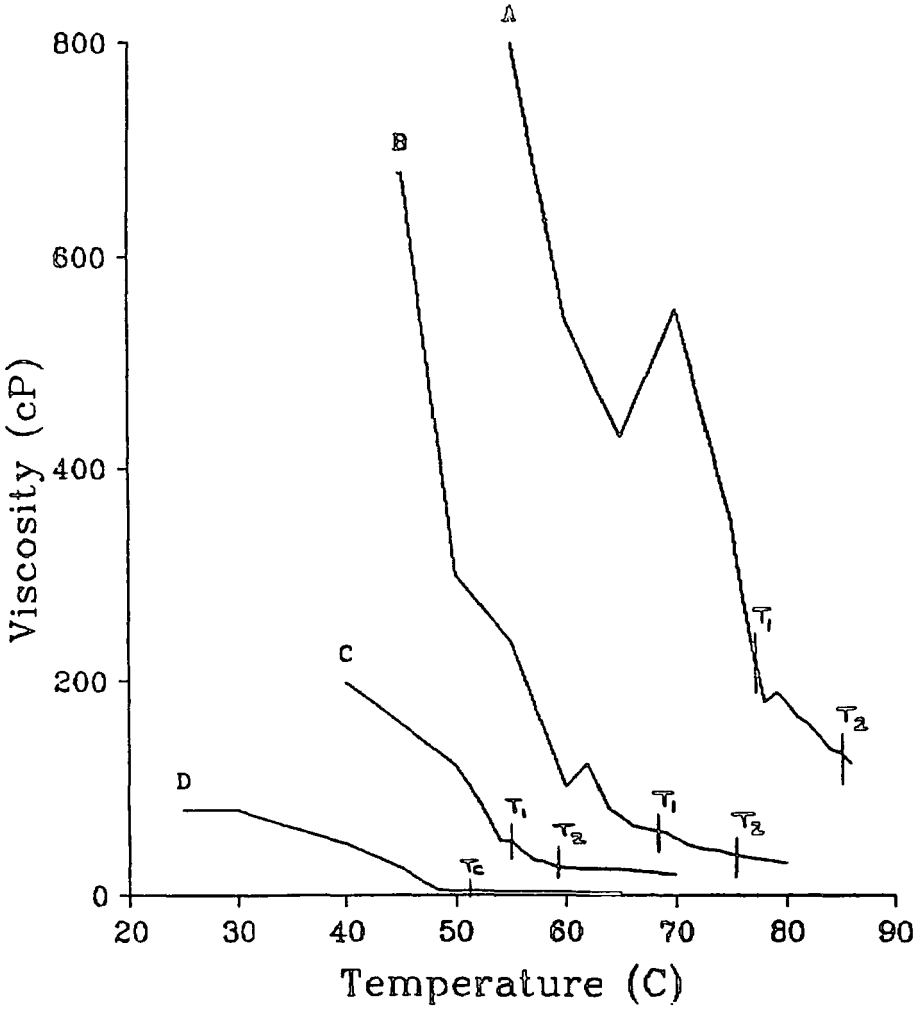

FIGURE 7.2
The viscosity is a function of temperature of S2 and mixtures of S2 and the LCP GN3/14. T_1 and T_2 indicate the start and end of the biphasic region, respectively. T_c is the clearing temperature of S2.

polymer/LC mixtures there is a distinct temperature range over which shear alignment appears to occur, in which case η_2 would be predominant. At higher and lower temperatures the mean value of η_1 and η_2 is measured.

Similar behaviour is not apparent in the mixture 25% GN3/14: 75% S2 or in S2 alone. Bock et al (1986) observed that shear alignment is not seen in smectic lmmLCs because the director rotates in the shear plane, so the mean value of η_1 and η_2 is measured. This would account for the smooth transition from the isotropic phase to the mesophase in the viscosity - temperature plot for S2. Evidently the mixture 25% GN3/14: 75% S2 behaves in a similar way. The mixtures with a higher concentration of LCP possibly shear align over part of the temperature range because the polymer backbone disrupts the smectic layers, resulting in a tendency to nematic - like viscosity behaviour.

7.1.3 Shear Viscosity of GN3/14

A set of reference temperatures needs to be defined in order to use these data to predict the viscosity of GN3/14. Three values have been chosen; 1.02 T_2, $(T_1+T_2)/2$ and 0.93 T_2. These represent the isotropic phase, biphasic region and smectic phase respectively. It is worth mentioning at this stage that there would have been value in referencing to the glass transition too, had that data been available. There is evidence that dynamic responses of LCPs are governed by the characteristics of the polymer backbone, in contrast to the static responses which are governed by the mesogenic components (see Section 5.5.2(a)).

The viscosity of each sample at the three reduced temperatures is shown in Table 7.1 and plotted in Figure 7.3. The viscosity of pure GN3/14 at each reduced temperature has been calculated by extrapolation of these graphs and the results are summarised in Table 7.2. The viscosity increases by a factor of about four as the phase of the material changes from the isotropic to the smectic phase.

Reduced Temperature	Composition	Temperature (°C)	Viscosity η (cP)
1.02 T_2	S2	55.4	3.44
	75% S2: 25% GN3/14	74.8	18
	50% S2: 50% GN3/14	81.5	29
	25% S2: 75% GN3/14	91.2	80
$(T_1+T_2)/2$	S2:	48.5	4
	75% S2: 25% GN3/14	62.5	25
	50% S2: 50% GN3/14	71.3	45
	25% S2: 75% GN3/14	80.4	80
0.93 T_2	S2	26.4	80
	75% S2: 25% GN3/14	44.1	222
	50% S2: 50% GN3/14	50.2	300
	25% S2: 75% GN3/14	59.1	540

TABLE 7.1
Summary of the viscosity of S2 and mixtures with GN3/14 at reduced temperatures in the mesophase, biphasic region and isotropic phase.

Reduced Temperature	Temperature (°C)	Extrapolated Viscosity (cP)
1.02 T_2	109.5	317
$(T_1+T_2)/2$	92	539
0.93T_2	75.8	1270

TABLE 7.2
Extrapolated values of the viscosity of GN3/14.

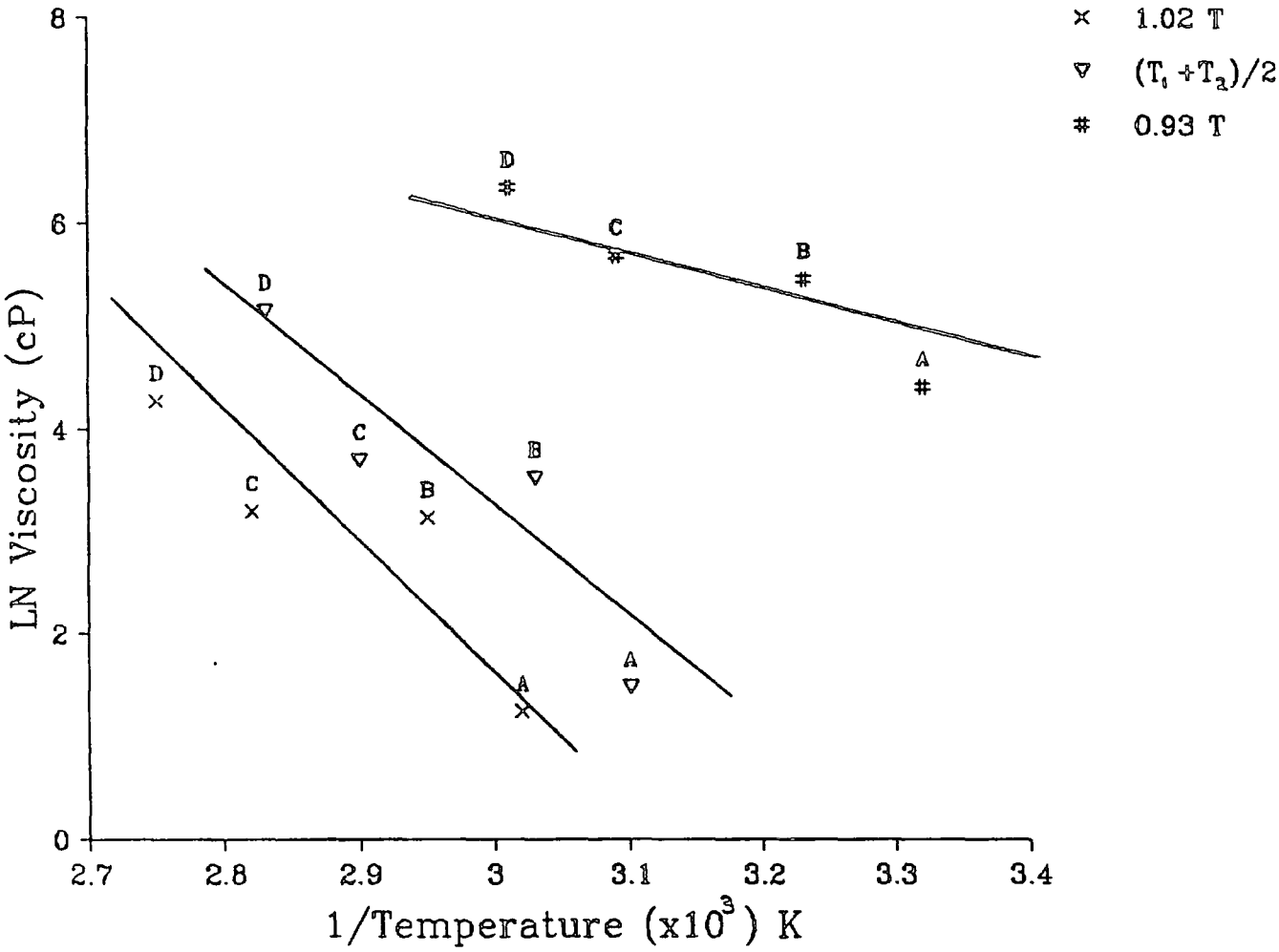

FIGURE 7.3
A comparison of the viscosity of (A) S2, (B) 75% S2 : 25% GN3/14, (C) 50% S2: 50% GN3/14, (D) 25% S2 : 75% GN3/14, at three reduced temperatures.

There are few reports of measurements on liquid crystals or LCPs which would allow direct comparison with these results. Fabre et al (1987) found the shear viscosity of the homopolymer P^{6}_{So} (structure and transition data in Appendix IV) to be about 2400 cP in the isotropic phase. This is about ten times more than the copolymer GN3/14. Bock et al (1986) measured the viscosity of the 1mmLC 4-n-Butyloxyphenyl 4-n-pentylbenzoate as about 3cP in the isotropic phase, which is about one hundred times less than the copolymer GN3/14. The results described here are largely consistent with values of viscosity measured by Humphreys et al (1988) using nematic-polymer liquid crystal mixtures.

A direct comparison between the shear viscosity of GN3/14, the equivalent homopolymer and the 1mmLC equivalent to the side group would help to quantify the effect of structure. The dielectric relaxation spectroscopy studies described in Chapter 5 have indicated the effect of structure on micro-viscosity. It would be interesting to relate these results to the effect of structure on bulk viscosity by studying a wider range of LCPs.

There could also be additional practical benefits in measuring the bulk viscosity of LCPs. Fabre et al (1987) identified a similarity between the bulk viscosity η and the twist viscosity γ_1 of side chain LCPs. Bock et al (1986) had already shown that γ_1 could be calculated from η to an accuracy of about 20% for a wide variety of nematic 1mmLCs. This observation led to the conclusion that shear viscosity measurements could possibly be used as a replacement for the complex Freedericksz transition experiments which are usually used to measure γ_1.

7.1.4 Walden's Rule

According to Stoke's law, the ionic mobility is directly related to the viscosity of a solution. However, their anisotropic properties mean that the ionic mobility of liquid crystals cannot be calculated directly from the viscosity. In the Stokes-Einstein viscous model, the product of the limiting equivalent conductance (λ_0) and the viscosity of the solvent (η) is a constant, assuming the ionic radius is not modified by solvation phenomena. This is expressed by Walden's Rule:

$$\mu \eta = \text{constant} = R \qquad [7.2]$$

where μ is the ionic mobility and η is the viscosity. Hérino (1981) and Szwajczak and Szymanski (1986) showed that Walden's Rule is obeyed for several nematic 1mmLCs. Hérino also concluded that viscous friction, rather than dielectric friction, plays the leading part in the mechanisms limiting ionic mobility.

In Chapter 6, it was noted that ionic conduction is likely to be the major contributor to the conductivity of the 1mmLCs and LCPs under investigation. The constant R in Equation [7.2] has been evaluated for S2 at three temperatures in the isotropic phase and the results summarised in Table 7.3 show that Walden's Rule does indeed appear to be obeyed.

The behaviour of the mixture 25% S2: 75% GN3/14 was also investigated, but in this case the value of R varied between 5×10^{-6} Cm^{-1} at 81°C to $7.6 \times 10^{-6} Cm^{-1}$ at 85°C. Following Szwajczak and Szymanski (1986), Equation [7.2] may be rewritten in the form:

$$\mu\eta^{H} = \text{constant} = R \qquad [7.3]$$

where H is the ratio E_μ/E_η, E_η and E_μ being the thermal activation energies of viscosity and ionic mobility respectively. The values of E_η and E_μ were calculated for this mixture from the Arrhenius plots shown in Figures 7.4 and 7.5, respectively, resulting in a value of 0.7 for the ratio H. In contrast, values of these activation energies were calculated for S2 and were found to be identical within experimental error, see Table 7.4, confirming the previous conclusion.

Temperature (°C)	Conductivity $(\Omega m)^{-1}$	Viscosity (cP)	R (Cm^{-1})
55	$7x10^{-7}$	3.8	$2.7x10^{-6}$
60	$8x10^{-7}$	3.3	$2.8x10^{-6}$
65	$1x10^{-6}$	2.5	$2.6x10^{-6}$

TABLE 7.3
Data to confirm the validity of Walden's Rule for S2.

Thermal Activation Energy $(kJmol^{-1})$	S2	25% S2: 75% GN3/14
Viscosity E_η	36.4	57.7
Conduction E_σ	37.9	37.9

TABLE 7.4
Comparison of the Arrhenius activation energies of electrical conductivity and viscosity in the isotropic phase.

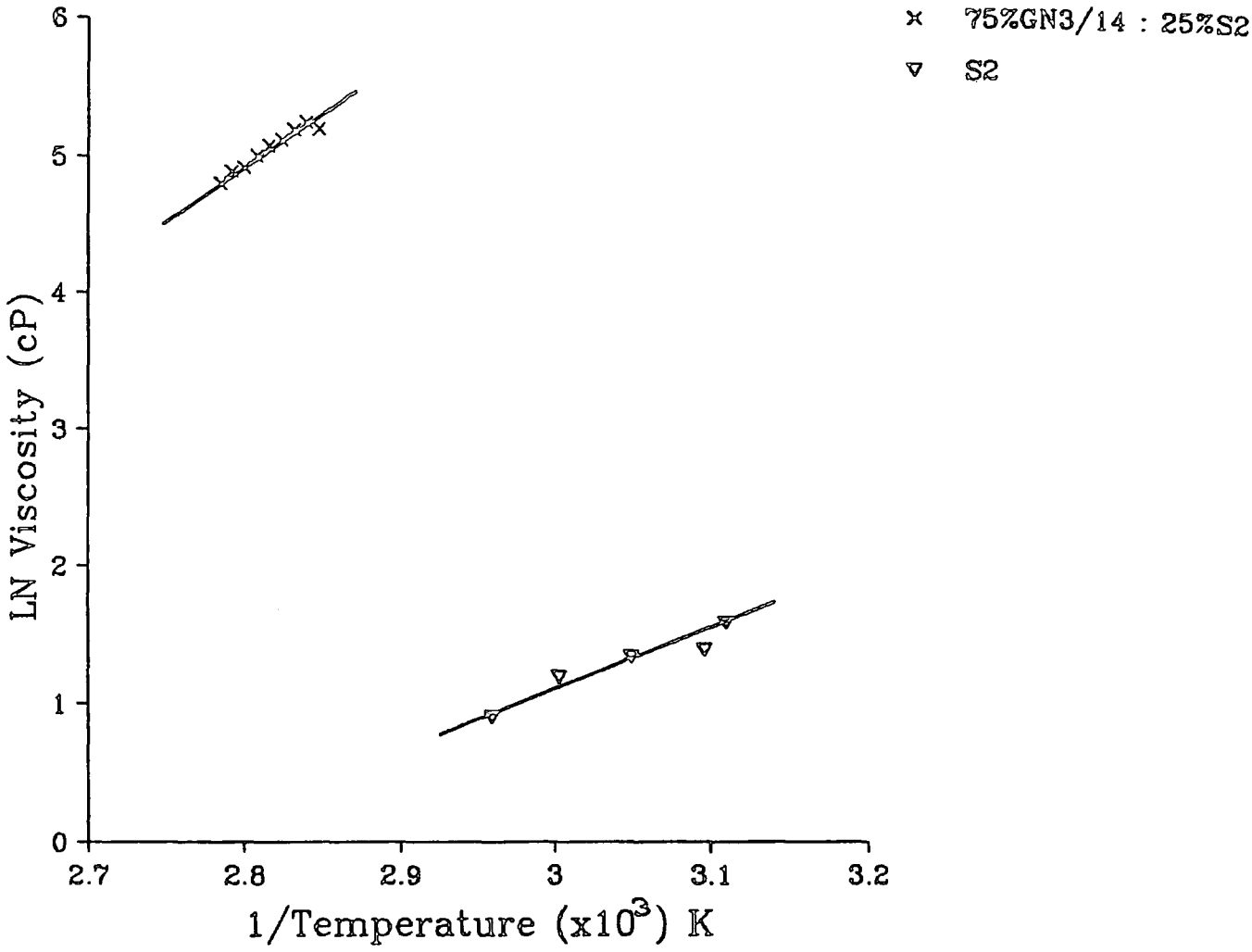

FIGURE 7.4
Arrhenius plot used to calculate the activation energy for viscosity of S2 and the mixture of 25% S2 : 75% GN3/14.

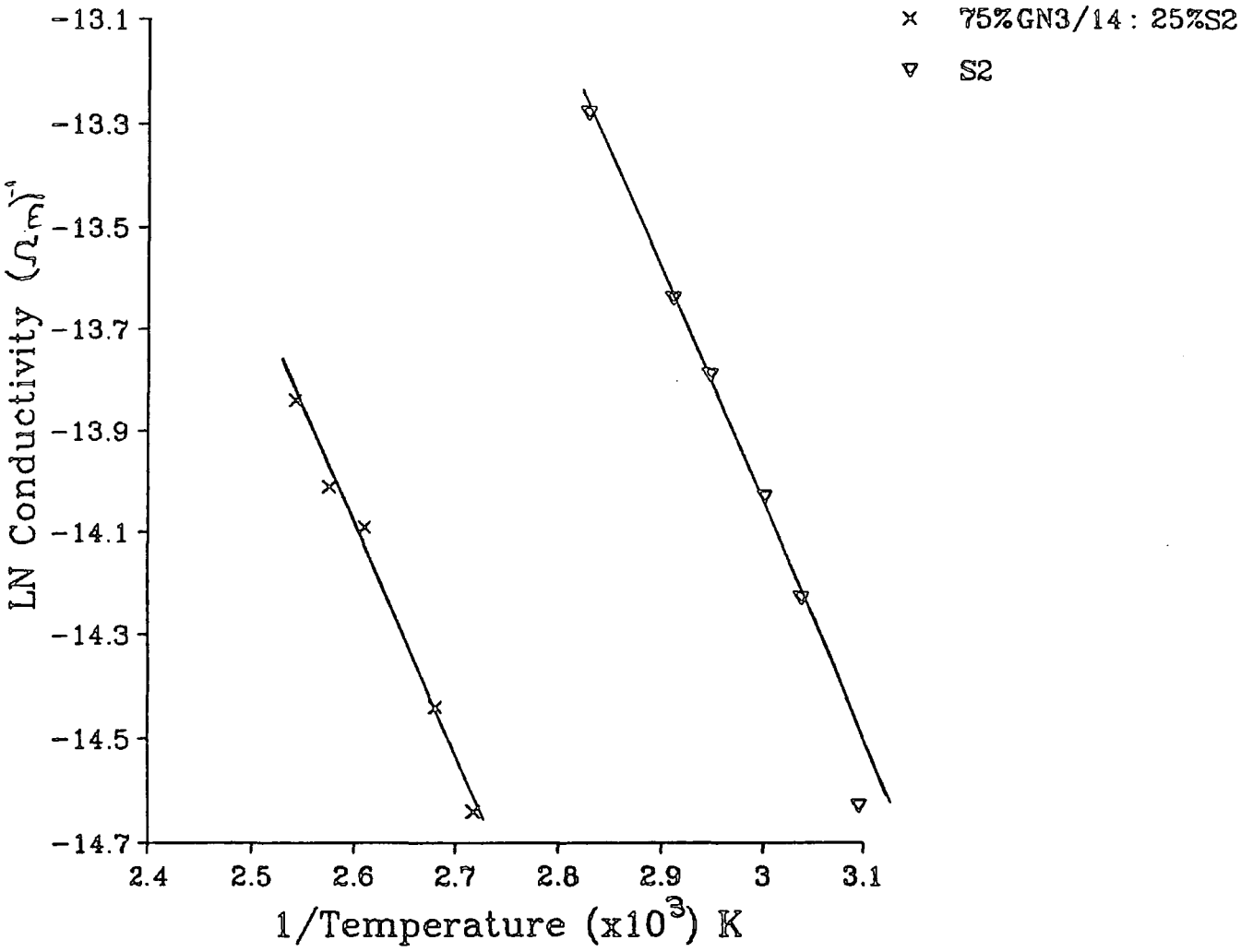

FIGURE 7.5
Arrhenius plot used to calculate the activation energy of ionic mobility for S2 and the mixture of 25% S2 : 75% GN3/14.

There are several possible reasons for the failure of the S2:GN3/14 mixture to obey Walden's Rule:

(i) It is likely that the errors associated with measuring the higher viscosity of this mixture will be larger since it is more difficult to produce a uniform sample without air gaps.

(ii) Slightly different temperature regimes were used to calculate the thermal activation energies of viscosity and conductivity respectively, whereas in the case of S2 they were identical. The value of E_η was calculated from results close to the biphasic region and it is possible that transitional effects were still in evidence.

iii) When applying the Walden's Rule to nematic liquid crystalline phases, Szwajczak and Szymanski (1986) noted that the anisotropy means that the microscopic viscosities rather than the bulk viscosity should be used. They also noted the product of the perpendicular components of viscosity and mobility ($\mu_\perp \eta_\perp$) were not constant, whereas the parallel components ($\mu_{||} \eta_{||}$) were constant, as were the viscosity and mobility of unoriented samples.

In the isotropic phase, liquid crystals would not be expected to exhibit orientational effects, and indeed the results of S2 confirm that this is the case. However some liquid crystal polymers have already been shown to retain considerable anisotropy into the isotropic phase (in Section 5.5.4(c) the anisotropy of the

diffusion tensor was calculated in the isotropic phase). During the measurement of viscosity the shearing action would also be expected to encourage alignment. If alignment was retained in the mixture of 25% S2: 75% GN3/14, then Walden's Rule would not be obeyed.

7.1.5 Summary

A brief preliminary study of the bulk viscosity of the LCP GN3/14 has been carried out. Mixtures of the LCP with the 1mmLC S2 were shown to have non-Newtonian (pseudoplastic) viscosity behaviour. When the concentration of LCP was greater than 50%, a decrease in viscosity was observed at about 10°C below the start of the biphasic region, possibly due to shear alignment effects. This is in contrast to the behaviour of 1mm smectic LCs in which shear aligning is not observed. The bulk viscosity of GN3/14 was calculated by extrapolation from the results of the mixtures and was found to be about four times larger in the mesophase than in the isotropic phase.

A direct (linear) relationship between the viscosity and electrical conductivity of S2 in the isotropic phase was also observed showing that Walden's Rule is obeyed. This was not the case in an S2:GN3/14 mixture, the most likely reason being the retention of anisotropic behaviour above the clearing temperature.

7.2 Optical Characterisation Studies

7.2.1 Introduction

In this section, the optical characterisation of dyes for use in the development of LCP optical memory devices is described, together with an optical investigation of the stability of aligned films of LCP with respect to time and temperature. Imperfectly aligned films and consequent problems of reproducibility were the main obstacles to producing satisfactory quantitative results. However, the relative merits of a number of dyes and LCPs were assessed and the production and measurement of homogeneous samples of polysiloxane LCPs have been demonstrated using the technique described by Meredith et al (1982) (previously this had only been applied to poly-methacrylate based LCPs).

7.2.2 Pleochroic Dyes for use in Optical Storage Devices

If the structure of a dopant dye molecule is chemically similar to the mesogenic unit in a liquid crystalline material, the dye will tend to adopt the same anisotropic orientation as the liquid crystalline phase. Heilmeier (1968) first described a liquid crystal display based on such a guest-host system and Eidenshink (1984) has reviewed the properties of dyes for display applications. Blue pleochroic dyes have been dissolved in these LCPs to absorb the Helium-Neon laser energy during the writing process. The dyes were dissolved in the polymers using solvents such as methylene dichloride and acetone. These solvents were then thoroughly removed by prolonged heating in a vacuum oven. The characteristics of the dye are important in determining both the sensitivity of the film and the resolution of the written features. Urabe et al (1983) showed that the

resolution can be improved by using dyes with a high dichroic ratio (that is, the absorption parallel to the director is high compared to that perpendicular to the director).

Three blue dyes have been studied; D16, D102 and F512. D16 and D102 are sold commercially by BDH Chemicals Ltd and the structures are shown in Appendix IV. F512 is sold by E Merck, the structure is not available. The isotropic extinction coefficients of each dye in the 1mmLCs K24, S2 and E7, respectively, are shown in Figure 7.6. Both D102 and F512 are strongly absorbing at the Helium-Neon laser wavelength of 632.8 nm. However, the amplitude of the absorption peak of D16 is considerably lower and occurs at about 570 nm; both factors result in this being a less appropriate dye for use in optical storage devices.

The dichroic ratios of D102 and F512 were measured, again using 1mmLCs as the host materials. Well aligned dyed and undyed samples are required and this is most readily achieved using 1mmLCs in cells coated with surfactants to produce the appropriate alignment. The results are summarised in Table 7.5. Clearly, the dichroic ratio of F512 is highest. It should be noted, however, that the manufacturers claim a dichroic ratio of 10 for D102 in E63 at room temperature. The reason for this discrepancy is likely to be that a better state of alignment was achieved in the nematic E63 as compared with the smectic S2.

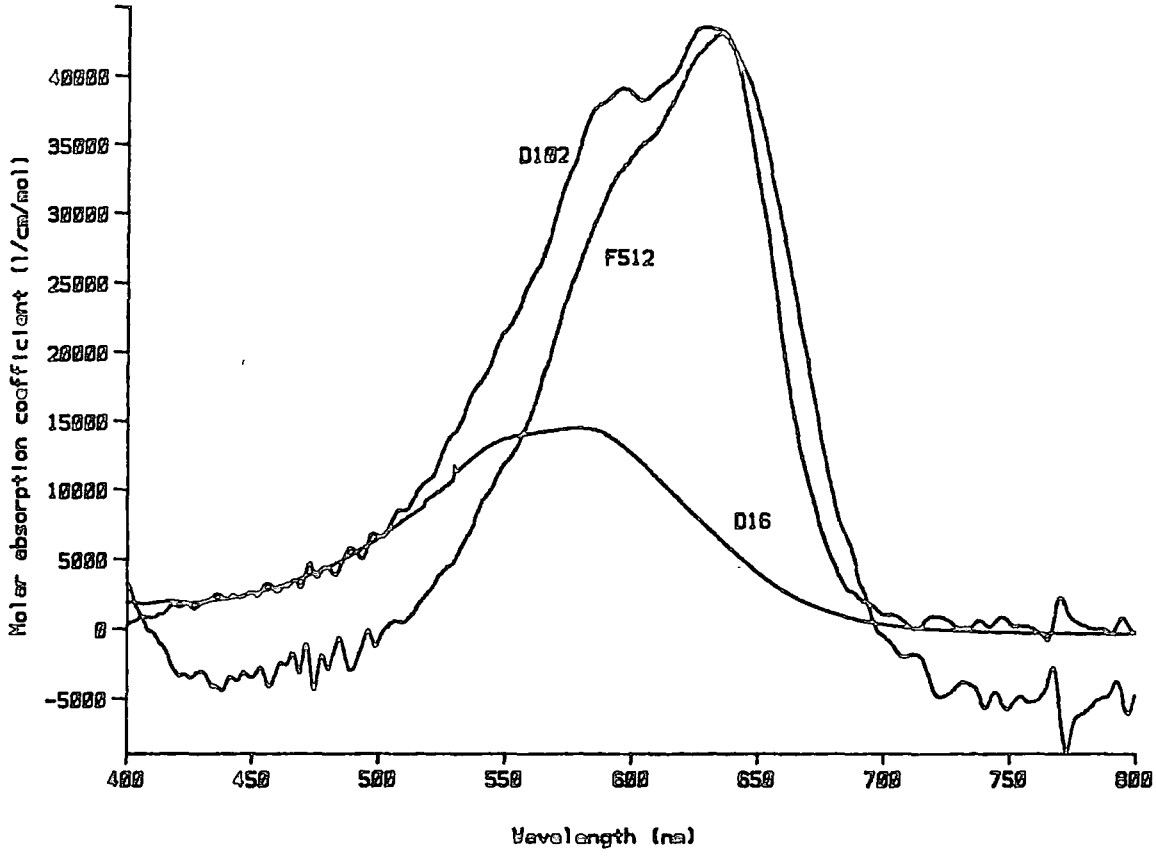

FIGURE 7.6
The isotropic extinction coefficient of (A) D16 in k24, (B) D102 in S2 and (C) F516 in E7, measured at room temperature.

Dye and Host	Temperature	$\epsilon_{\parallel} \times 10^{-4}$ ($l cm^{-1} mol^{-1}$)	$\epsilon_{\perp} \times 10^{-4}$ ($l cm^{-1} mol^{-1}$)	Dichroic Ratio	Order Parameter
F512 in E7	30	10.5	0.7	15	0.82
	35	10.4	0.8	13	0.80
	55	9.4	1.2	7.8	0.69
D102 in S2	30	7.5	1.3	5.8	0.61
	35	7.5	1.4	5.4	0.59
	45	7.4	1.7	4.4	0.53

TABLE 7.5
A comparison of the extinction coefficients of FS12 and D102 at 632.8 nm.

7.2.3 The Temperature Stability of Alignment in Dyed LCPs

A high degree of homogeneous alignment was achieved in GN3/14 dyed with 3% D102 and GN4/19 dyed with 3% F512 using an electric field applied between interdigitated electrodes. Figures 7.7 and 7.8 are photomicrographs of the textures of GN3/14 and GN4/19 after alignment with 140V and 160V, 3 kHz sine wave, respectively, as viewed by polarising microscopy. These show that both samples exhibited homogeneous alignment; a well aligned sample would be seen as a monodomain of a single colour. The optical densities at 633 nm (see Equation [3.41]) of each LCP at several temperatures are summarised in Figure 7.9. The extinction coefficients were not measured as a sufficiently similar state of alignment could not be achieved in different cells containing dyed and undyed samples. The dye order parameter, S_d, (see Equation [3.37]) at 30°C was 0.36 in the case of D102 in GN3/14 and 0.6 for F512 in GN4/19.

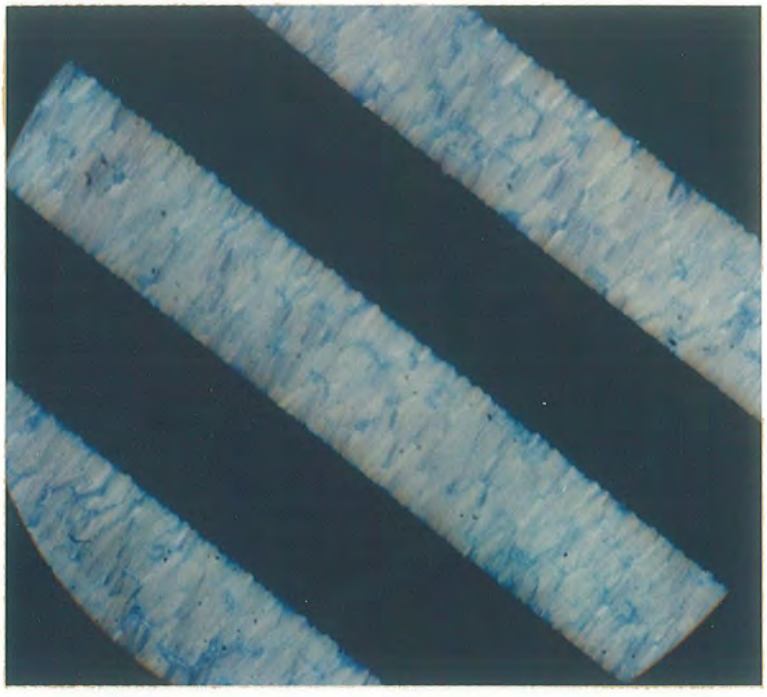

FIGURE 7.7
The texture of GN3/14 dyed with 3% D102 after alignment with 140V, 3 kHz sine wave, applied between interdigitated electrodes (190x magnification).

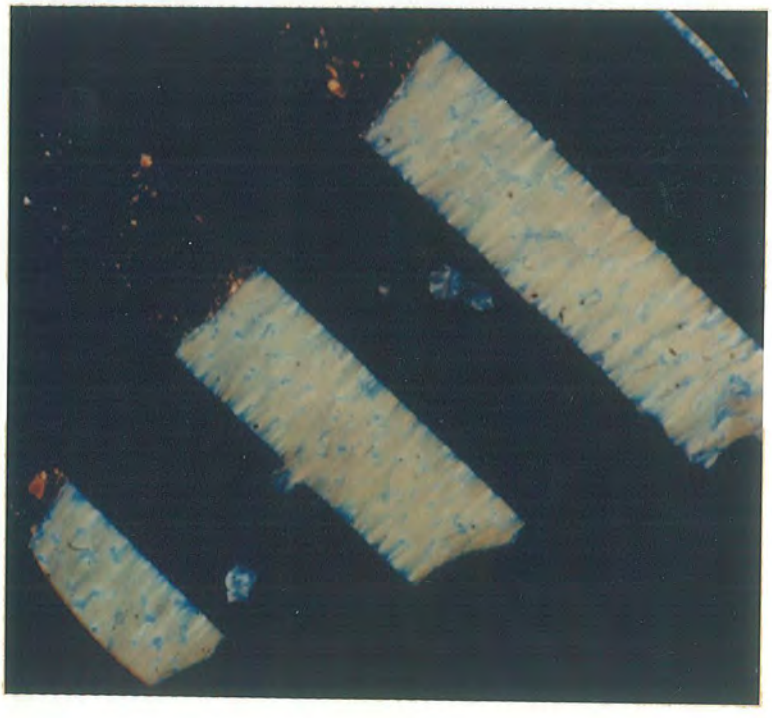

FIGURE 7.8
The texture of GN4/19 dyed with 3% F512 after alignment with 160V, 3 kHz sine wave, applied between interdigitated electrodes (190x magnification).

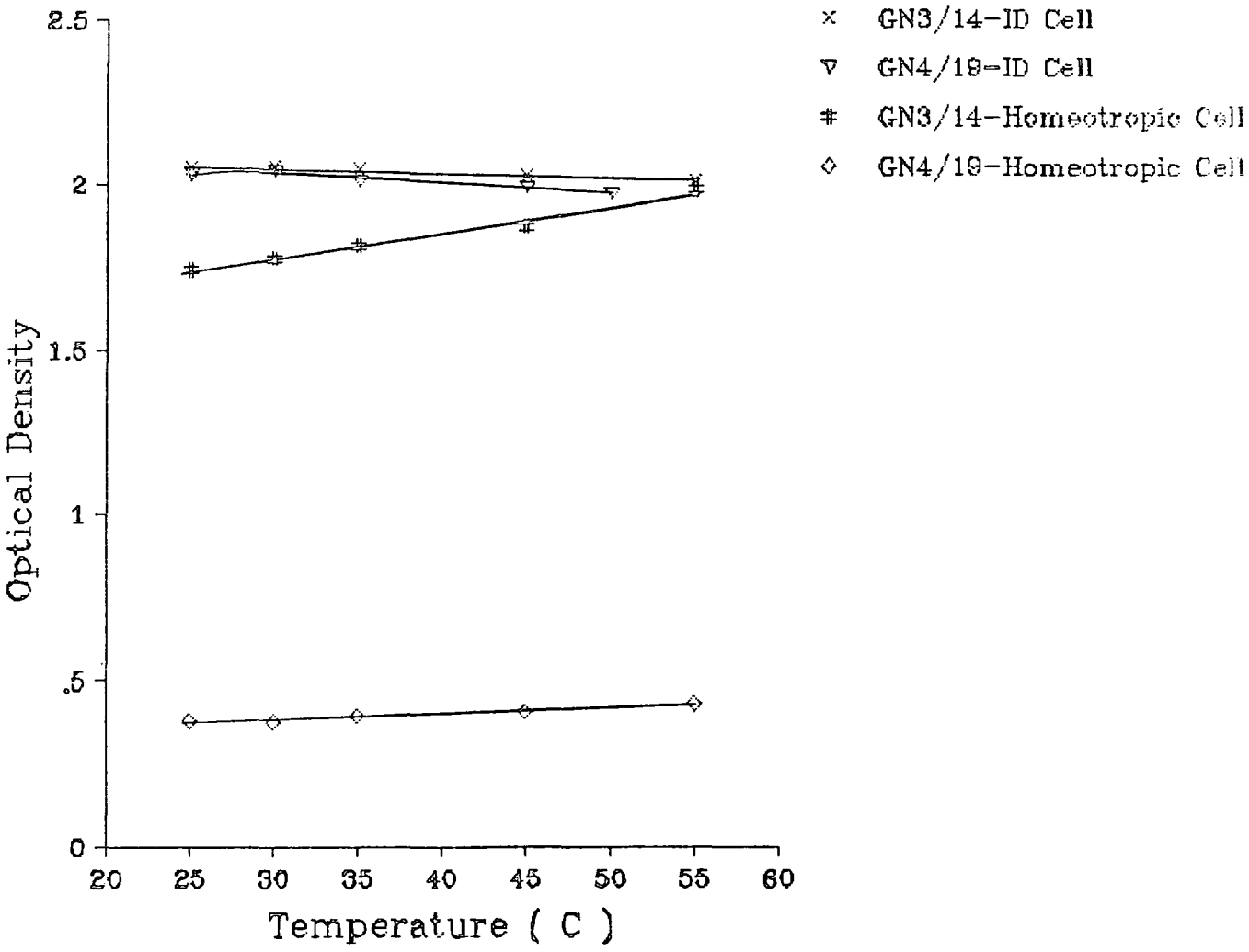

FIGURE 7.9
The optical densities of GN3/14 dyed with 3% D102 and GN4/19 dyed with 3% F512, measured at 633 nm and shown as a function of temperature.

The alignment of GN3/14 and GN4/19 appears to be very stable up to 55°C. This provides optical confirmation of the dielectric loss measurements discussed in Section 5.4.

7.2.4 The Stability of Alignment in Dyed LCPs Over Time

The sequence of photographs in Figures 7.10 and 7.11 showing GN3/14 dyed with D102 and GN4/19 dyed with F512, respectively, compare the alignment of each 24 hours and three months after alignment in an electric field. There is little apparent change in the state of GN4/19, however there is considerably disruption to the alignment of GN3/14 even after 24 hours, and after 3 months it is almost unrecognisable. Figure 7.12 shows the same sequence of photographs for an undyed sample of GN3/14 and a similar trend can be observed. This suggests that the dye is not responsible for the changes. The structure of GN3/3 is similar to that of GN3/14, differing only in the length of the methylene spacer. The state of alignment of undyed GN3/3 is compared before and after a three month period in Figure 7.13. There is again very little change over time, indicating that GN3/14 is probably anomalous and in general LCPs can retain homogeneous alignment for long periods of time.

Homeotropically aligned samples of LCPs on which information had been written using a laser exhibited a tendency to similar behaviour. The clarity of information written on GN3/14 appeared to deteriorate over time as a focal conic texture developed in the previously dark background (viewed between crossed polarisers). The information on films of other LCPs remained sharp a year after the initial writing took place.

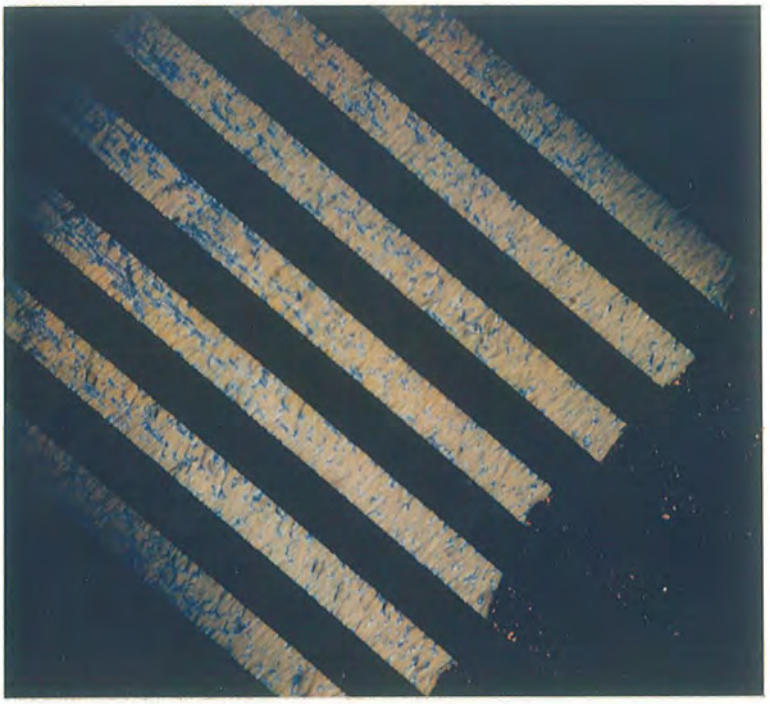

FIGURE 7.10(a)
The texture of GN3/14 dyed with 3% D102 is shown here after alignment with 140V, 3 kHz sine wave, applied between interdigitated electrodes (60x magnification).

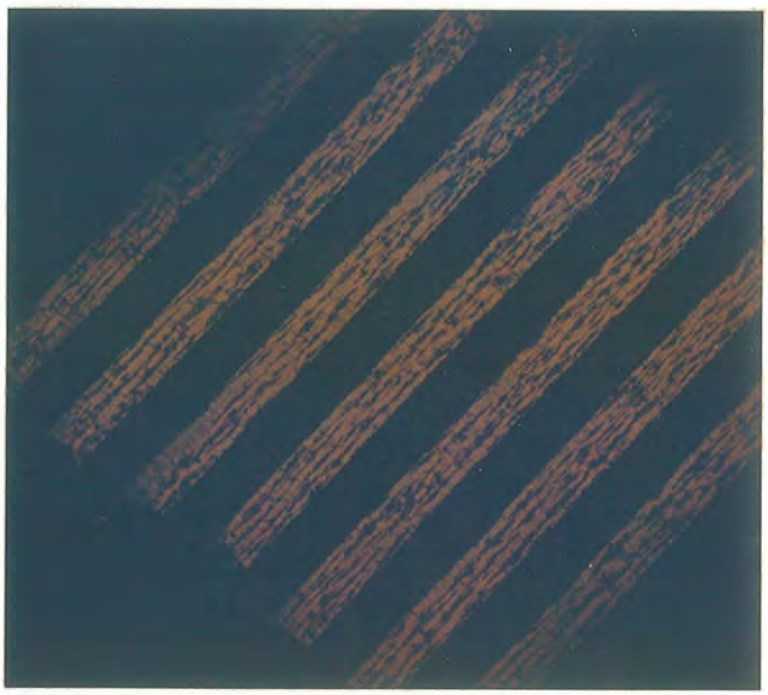

FIGURE 7.10(b)
The texture of GN3/14 dyed with 3% D102 is shown here 24 hours after alignment with 140V, 3 kHz sine wave, applied between interdigitated electrodes (60x magnification).

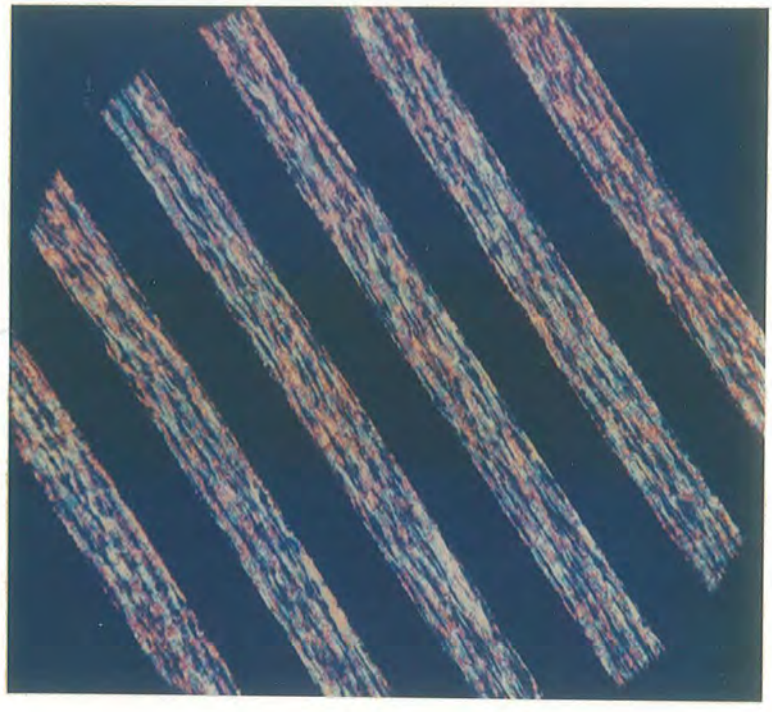

FIGURE 7.10(c)
The texture of GN3/14 dyed with 3% D102 is shown here 3 months after alignment with 140V, 3 kHz sine wave, applied between interdigitated electrodes (80x magnification).

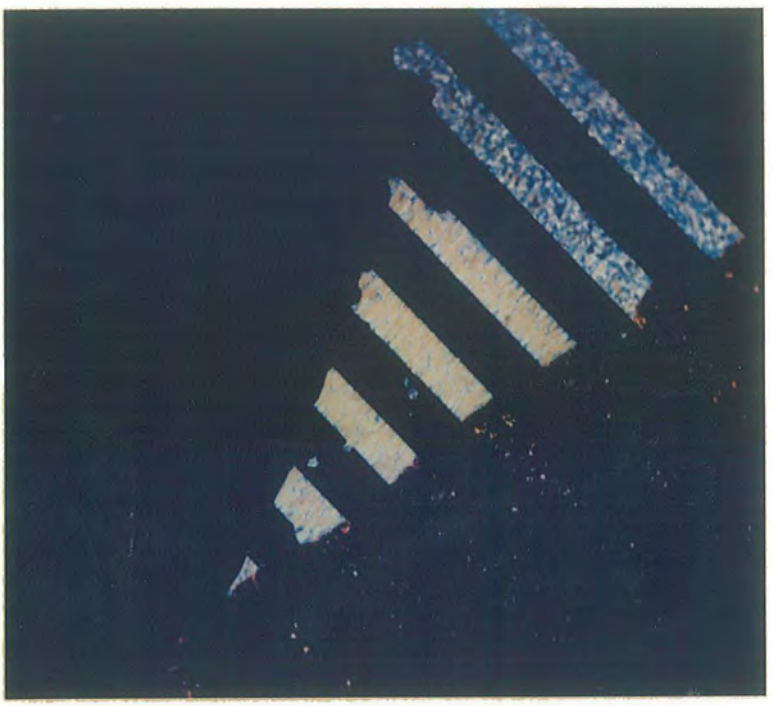

FIGURE 7.11(a)
The texture of GN4/19 dyed with 3% F512 is shown here 24 hours after alignment with 160V, 3 kHz sine wave, applied between interdigitated electrodes (60x magnification).

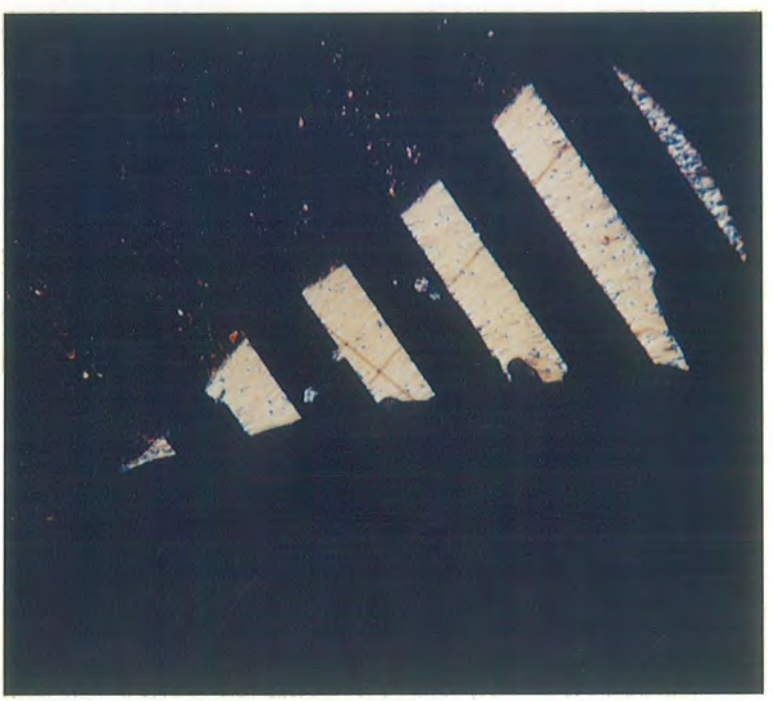

FIGURE 7.11(b)
The texture of GN4/19 dyed with 3% F512 is shown here 3 months after alignment with 160V, 3 kHz sine wave, applied between interdigitated electrodes (80x magnification).

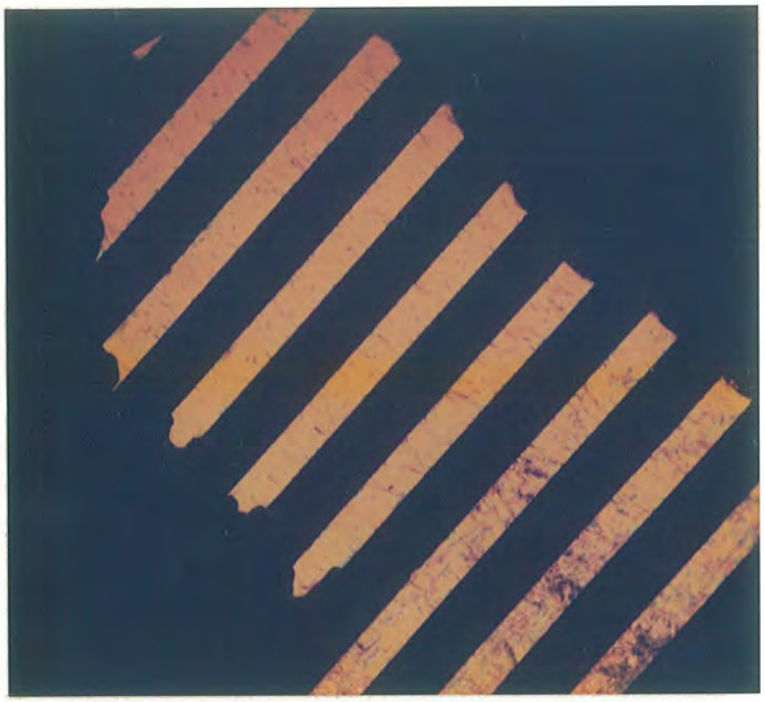

FIGURE 7.12(a)
The texture of undyed GN3/14 is shown here after alignment with 140V, 3 kHz sine wave, applied between interdigitated electrodes (60x magnification).

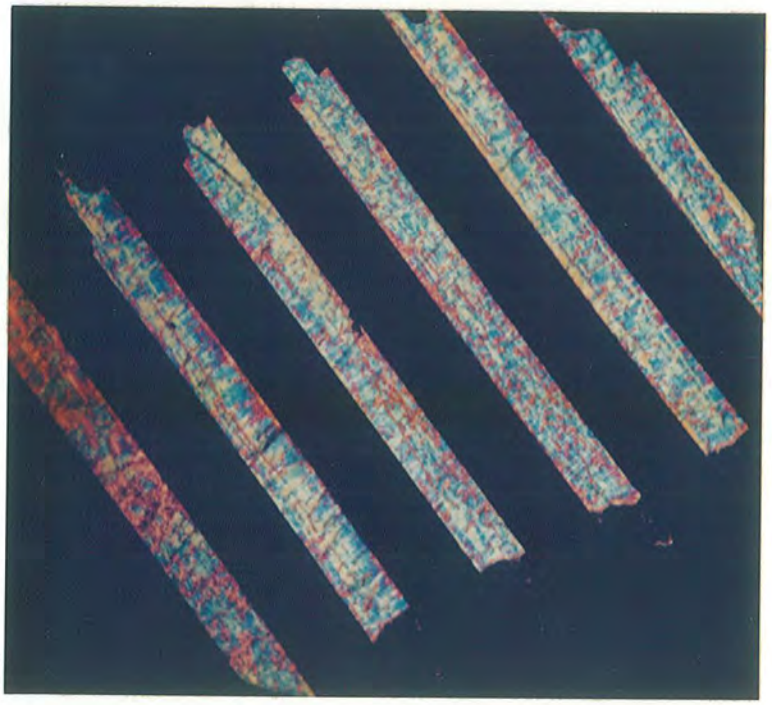

FIGURE 7.12(b)
The texture of undyed GN3/14 is shown here 3 months after alignment with 140V, 3 kHz sine wave, applied between interdigitated electrodes (80x magnification).

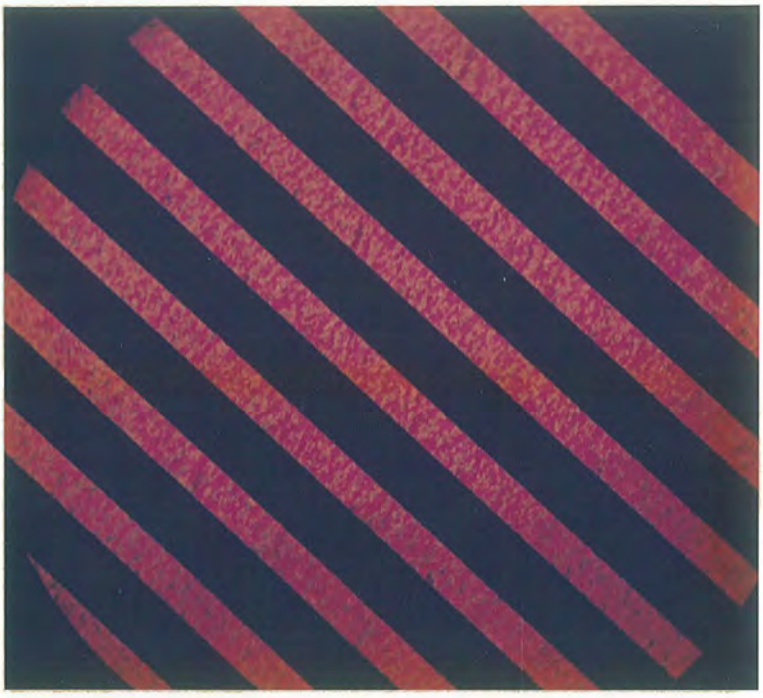

FIGURE 7.13(a)
The texture of undyed GN3/3 immediately after alignment with 140V, 3 kHz sine wave, applied between interdigitated electrodes (60x magnification).

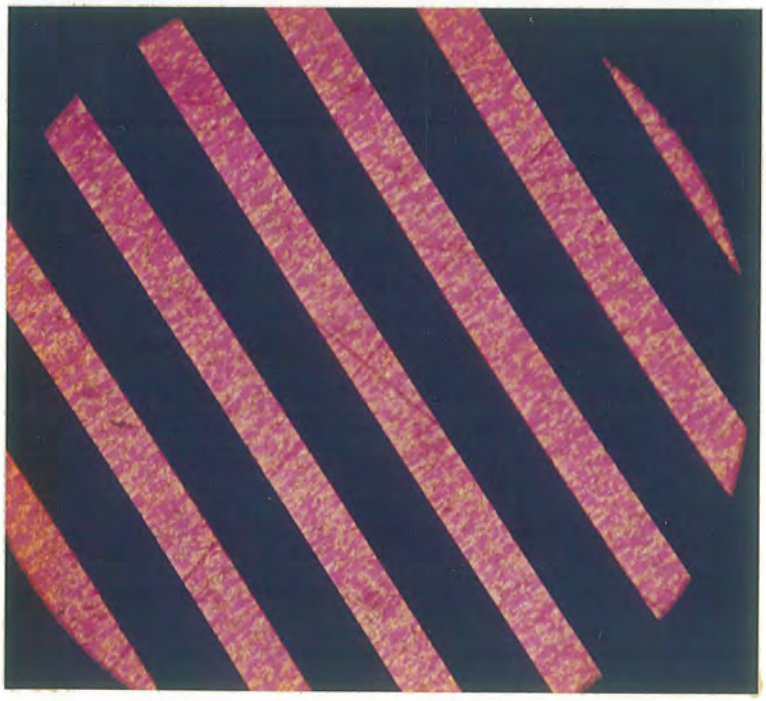

FIGURE 7.13(b)
The texture of undyed GN3/3 three months after alignment with 140V, 3 kHz sine wave, applied between interdigitated electrodes (80x magnification).

7.2.5 Summary

The optical absorption characteristics of blue pleochroic dyes have been measured and the dyes D102 (BDH Chemicals Ltd) and F512 (E Merck) were shown to have absorption maxima close to the Helium-Neon laser wavelength. F512 is probably the most suitable dye (from the selection available) for use with LCPs in laser written optical memories. The dichroic ratio was largest (which allows high resolution written information) and the high value of the parallel component of the extinction coefficient, $\epsilon_{||}$, results in the efficient absorption of laser energy.

Interdigitated electrodes were also used to produce homogeneous alignment over small areas of positive dielectric anisotropy LCPs. These regions were used to study the time and temperature stability of alignment. Generally there was little evidence of degradation with temperature up to 50°C and with time over a three month period, except in the case of GN3/14 when the alignment appeared to be rapidly corrupted.

Chapter Eight

Recommendations for Future Work

The main emphasis of the work described in this thesis has been a study of the electrical properties of side chain polysiloxane liquid crystal polymers. The separation into "dielectric" and "bulk conduction" properties followed in part from the extensive discussion of the dielectric behaviour of mesogenic materials in the literature which acted as the groundwork for this detailed study of individual LCPs. In contrast, electrical conduction in LCPs has not been studied in such depth elsewhere so a broad investigation of the mechanisms of, and influences on, conductivity was more appropriate here. These different emphases to the investigations result in different types of recommendations for the development of the results. The optical and viscosity studies described in Chapter 7 were very brief preliminary investigations so there are obviously many developments which are still to be pursued in these areas. Brief summaries of the results from the dielectric studies, electrical conductivity measurements and the viscosity and optical investigations are given in Sections 5.7, 6.4, 7.1.5 and 7.2.5, respectively.

The proposed application for these LCPs as the active media in optical storage devices required them to have both high dielectric anisotropy and low microviscosity to allow rapid switching in an electric field. It has been shown that to some extent these properties are not compatible since the lower viscosity methyl-copolymer LCPs (Table 2.2) do not possess a high dipole density. However, there were considerable benefits to these structures over comparable homopolymers in terms of ease of handling and lower transition temperatures (therefore lower energy input requirements during the laser writing process). A structural variation which was not available for this work but which might provide an acceptable compromise

is an LCP homopolymer having an ethyl substituted polysiloxane backbone, with a fluoro- and cyano-substituted phenyl benzoate mesogenic side group (as in GN4/17). This will have a higher dipole strength than the copolymers, but the ethyl substituent should disrupt the packing sufficiently to lower the microviscosity compared to the methyl substituted backbones. A $-(CH_2)_5O-$ spacer group would also minimise steric hindrance against reorientation of the side groups about the backbone.

The production of perfectly aligned samples was found to be more difficult than expected. Even when dielectric relaxation measurements suggested that alignment was complete, optical observations indicated that this was not so. This emphasised the value of optically transparent measuring cells. The practical benefit to device design of being able to measure $\epsilon_{||}$ reliably means that in future effort should be directed at improving this alignment technique. The methods recommended in Chapter 6 to reduce the probability of dielectric breakdown during alignment should be applied.

The study of the variation of alignment with temperature described in Section 5.4 showed that certain LCPs appeared to retain their alignment more successfully than others. This should be extended to an investigation of temperature cycling and the variations which occur with time in order to assess the durability and lifetime of an aligned film of LCP in an optical memory device.

Although Sutherland et al (1987) have used X-ray diffraction to study the layer spacing and molecular packing of a small number of these LCPs, a

more systematic survey could provide evidence to confirm some of the interpretations of molecular packing proposed here. It would also be useful to identify any structural anomalies in those LCPs which exhibited unusual conductivity behaviour.

In Chapter 6, a study of the AC conductivity of most of the LCPs available showed that a direct relationship existed between the behaviour of 12 of them. In order to explain this observation, an investigation of the conductivity in the isotropic phase of each LCP needs to be carried out.

High field DC conductivity measurements were particularly useful in determining the mechanisms of conduction in the LCP GN3/3 and the 1mmLC S2. It has been shown that Schottky emission of charge occurs at the electrodes at high temperatures due to field enhancement by space charge layers. Although these experiments were slow and fairly difficult to perform, more LCPs should be investigated in order to confirm the validity of the theory for polysiloxane LCPs in general.

The mechanism of electrical conduction through the bulk of the LCPs has not been explicitly proved to be ionic: this has been assumed to be the case on the basis of studies of 1mmLCs and classical polymers described in the literature. This could be verified by doping the LCPs with known quantities of ionic species and observing the conductivity response.

The motivation for studying the electrical conductivity here was to explain (and hopefully reduce) the tendency of samples of these LCPs to dielectric breakdown. Organic surfactants on the electrodes were shown to

reduce the build-up of space charge and it was noted that this ought to reduce the tendency to breakdown. However, a statistical analysis of carefully controlled experiments should be performed to prove that this is actually the case.

The viscosity of GN3/14 has been found by extrapolation from mixtures with S2. It would be useful to measure the viscosity of a wider range of LCPs in order to provide information for device development and to show the effects of structural variations. These results could be obtained from measurements in solution or extrapolation from mixtures, but ideally an automatic heated cone and plate rheometer would be used to allow direct measurement of the LCPs.

There are many optical studies which could usefully be performed on these LCPs. The dichroic ratio of the dyes used to absorb the laser energy ought to be measured in the LCP rather than in lmmLCs since there may be chromatic shifts due to different local field conditions. These measurements are difficult to perform in LCPs due to the need for dyed and undyed samples which have the same (good) degree of alignment. However, when the optical storage system is fine tuned for maximum sensitivity to make a commercial device, perhaps they will become necessary. Similar well aligned samples will also be necessary in order to measure the refractive indices of the LCPs. These values are important to allow optical matching with the substrate materials, so reducing reflection losses.

References

REFERENCES

Akande A R, Lowell J, J. Phys. D: Appl. Phys., 20, 565 (1987)

Araki K, Attard G S, Liquid Crystals, 1(3), 301 (1986)

Attard G S, Molecular Physics, 58, 1087 (1986)

Attard G S, Williams G, Polymer Communications, 27, 2 (1986a)

Attard G S, Williams G, Polymer Communications, 27, 66 (1986b)

Attard G S, William G, Liquid Crystals, 1(3), 253 (1986c)

Attard G S, Araki K, Williams G, J. Mol. Electron., 3, 1 (1987a)

Attard G S, Araki K, Williams G, Brit. Polymer J., 19, 119 (1987b)

Attard G S, Moura-Ramos J J, Williams G, Nestor G, White M S, Gray G W, Lacey D, Toyne K J, Makromol. Chem., 188, 2769 (1987c)

Attard G S, Moura-Ramos J J, Williams G, J. Polymer Sci: Part B, 25, 1099 (1987d)

Baird D G, Polymeric Liquid Crystals , Ed. A Blumstein (Plenum) (1985)

Barrett R, IEEE Colloquium on Optical Mass Data Storage, May (1986)

Blinov L M, Electro-Optical and Magneto-Optical Properties of Liquid Crystals, (Wiley, Chichester) (1983)

Block H, Advances in Polymer Science, 33, 93 (1979)

Blumstein A, Liquid Crystalline Order in Polymers, (Academic Press, New York) (1978)

Blythe A R, Electrical Properties of Polymers, (Cambridge University Press) (1979)

Bock F J, Kneppe H, Schneider F, Liquid Crystals, 1, 239 (1986)

Bone M F, Price A H, Clark M G, McDonnell D G, Liquid Crystals and Ordered Fluids, Ed. Giffin A C, Johnson J F, (Plenum) (1984)

Bormuth F J, Haase W, Zentel R, Mol. Cryst. Liq. Cryst., 148, 1 (1987a)

Bormuth F J, Haase W, Mol. Cryst. Liq. Cryst., 153, 207 (1987b)

Bormuth F J, Haase W, Liquid Crystals, 3 (6,7), 881 (1988)

Böttcher C J F, Bordewijk P, Theory of Electric Polarisation, Second Edition, Volume 2, (Elsevier, Amsterdam) (1978)

Boyd R H, J. Polymer Sci: Polymer Phys. Edn., 21, 505 (1983)

Boyer R F, Molecular Basis of Transitions and Relaxations Ed. Meier D J, (Gordon and Breach, New York) (1978)

Bradshaw M J, Raynes E P, Mol. Cryst. Liq. Cryst., 91, 145 (1983)

Bradshaw M J, PhD Thesis, University of Essex (1984)

Brochard F, J. Polymer Sci., 17, 1367 (1979)

Buka A, Owen P G, Price A H, Mol. Cryst. Liq. Cryst., 51, 273 (1979)

Casagrande C, Fabre P, Veyssie M, Weill C, Finkelmann H, Mol. Crys Liq. Cryst., 113, 193 (1984)

Chandrasekhar S, Liquid Crystals, (Cambridge) (1977)

Ciferri A, Krigbaum W R, Meyer R B, (Eds) Polymer Liquid Crystals, (Academic Press, New York) (1982)

Cladis P E, Phys. Rev. Lett., 35, 48 (1975)

Clark M G, Raynes R A, Tough R J A, J. Phys. D, 13, 2151 (1980)

Clark M G, Mol. Cryst. Liq. Cryst., 127, 1 (1985a)

Clark M G, Chemistry and Industry, 258, April (1985b)

Clark M G, Private Communication, (1988)

Cole K S, Cole R H, J. Chem. Phys., 9, 341 (1941)

Coles H J, Simon R, UK Patent 2.146 787A (1984)

Coles H J, Faraday Discuss. Chem. Soc., 79, 201 (1985)

Daniel V V, Dielectric Relaxtion, (Academic Press, London) (1967)

Davidson D W, Cole R H, J. Chem. Phys., 19, 1484 (1951)

De Gennes P G, Comments on Solid State Physics, 3, 35 (1970)

De Gennes P G, The Physics of Liquid Crystals, (Oxford) (1974)

De Jeu W H, Physical Properties of Liquid Crystalline Materials, (Gordon and Breach) (1980)

De Vries A, Mol. Cryst. Liq. Cryst., 131, 125 (1985)

Debye P, Polar Molecules, (Chemical Catalogue Company, New York) (1929)

Demus D, Richter L, Textures of Liquid Crystals, (Verlag Chemie, Weinham), (1978)

Dewey A G, Opt. Engng., 23, 230 (1984)

Dunmur D A, Manterfield M R, Miller W H, Dunleavy J K, Mol. Cryst. Liq. Cryst., 45, 127 (1978)

Dunmur D A, Miller W H, Mol. Cryst. Liq. Cryst. 60, 281 (1980)

Eich M, Reck B, Ringsdorf H, Wendorff J H, Proc. SPIE, 682, 93 (1986)

Eidenschink R, Kontakte (Darmstadt), 2, 25 (1984)

Endres B W, Wendorff J H, Reck B, Ringsdorf H, Makromol. Chem., 188, 1501 (1987)

Fabre P, Veyssie M, Mol. Cryst. Liq. Cryst. Lett., 4 (3-4), 99 (1987)

Finkelmann H, Happ M, Portugall M, Ringsdorf H, Makromol. Chem., 179, 2541 (1978a)

Finkelmann H, Ringsdorf H, Wendorff J H, Makromol. Chem. Rapid. Commun., 179, 273 (1978b)

Finkelmann H, Kiechle U, Rehage G, Mol. Cryst. Liq. Cryst., 94, 343 (1983)

Finkelmann H, Rehage G, Advances in Polymer Science, 60/61, 99 (1984)

Friedel G, Ann. Physique, 18, 273 (1922)

Fuoss R, Kirkwood J G, J. Am. Chem. Soc., 63, 385 (1941)

Gemmell P A, Gray G W, Lacey D, Mol. Cryst. Liq. Cryst., 122, 205 (1985)

Ginnai T M, Oxley D P, Pritchard R G, Thin Solid Films, 68, 241 (1980)

Gordon A J, Ford R A, The Chemists Companion, (Wiley, New York) (1972)

Gray G W, Molecular Crystals, 1, 333 (1966)

Gray G W, The Molecular Physics of Liquid Crystals, Ed. Luckhurst G R, Gray G W (Academic Press) (1979)

Gray G W, Phil. Trans. Roy. Soc. Lond. A, 309, 77 (1983)

Gray G W, Lacey D, Nestor G, White M S, Makromol. Chem. Rapid Commun., 7, 71 (1986)

Haase W, Pranoto H, Progress in Colloid and Polymer Science, 69, 139 (1984)

Haase W, Pranoto H, Bormuth F J, Ber. Bunsenges Chem., 89, 1229 (1985)

Haase W, Side Chain Liquid Crystal Polymers, Ed McArdle C B, (Blackie) (1989)

Hardouin F, Achard M F, Gasparoux H, Liebert L, Strzelecki L, J. Polym. Sci., 20, 975 (1982)

Harrop P J, Dielectrics, (Butterworths, London) (1972)

Haws C M, Clark M G, McArdle C B, (Poster) British Liquid Crystal Group Meeting, University of Hull (1987)

Hecht E, Zajac A, Optics, (Addison-Wesley, London) (1974)

Heilmeier G H, Zannoni L A, Appl. Phys. Lett., 13, 91 (1968)

Herino R, J. Chem. Phys. 74 (5), 3016 (1981)

Hill R M, Dissado L A, J. Phys. C, 15, 5171 (1982)

Humphries R G, Tarry H A, Bradshaw M J, Liquid Crystals, 3,(87), 1039 (1988)

Jadzyn J, Kedziora P, Mol. Cryst. Liq. Cryst., 145, 17 (1987)

Johnson J F, Cole R H, J. Am. Chem. Soc. 73, 4536 (1951)

Jonscher A K, Dielectric Relaxation in Solids, (Chelsea Dielectrics Press, London) (1983)

Klingbiel R T, Genova D J, Criswell T R, Van Meter J P, J. Am. Chem. Soc., 96 (25), 7651 (1974)

Ko A Y, Hirsch J, Solid State Commun., 39, 215 (1981)

Koide N, Mol. Cryst. Liq. Cryst., 139, 47 (1986)

Lamb D R, Electrical Conduction Mechanisms in Thin Insulating Films, (Methuen) (1967)

Legrand C, Parneix J P, Chapoton A, Nguyen H T, Destrade C, Mol. Cryst. Liq. Cryst., 124, 277 (1985)

Lehmann O, Z. Krist., 18, 464 (1890)

Lesniak M, Labno W, Szwajczak e, Szymanski A, Mol. Cryst. Liq. Cryst., 61, 241 (1980)

Lowell J, J. Phys. D: Appl. Phys., 21, 138 (1988)

Luckhurst G R, Zannoni C, Proc. R. Soc. Lond. A, 343, 389 (1975)

Mada H, Osajima K, J. Appl. Phys., 69, 3111 (1986)

Mada H, Yoshino S, Japn. J. Appl. Phys., 27(8), L1361 (1988)

Madden P A, Kivelson D, Advan. Chem. Phys., 56, 467 (1984)

Maier W, Saupe A, Z. Naturforsch, A14, 822 (1959)

Maier W, Meier G, Z. Naturforsch, A16, 262 (1961)

Major S, Bhatnager M C, Kumar S, Chopra K L J. Mater. Res., 3(4), 723 (1988)

McArdle C B, Clark M G, Haws C M, Wiltshire M C K, Parker A, Nestor G, Gray G W, Lacey D, Toyne K J, Liquid Crystals, 2(5), 253 (1987a)

McArdle C B, Clark M G, Haws C M, Proc. Eurodisplay (IOP, London) 160 (1987b)

McArdle C B, Side Chain Liquid Crystal Polymers, Ed. McArdle C B (Blackie) (1989)

Meier G, Saupe A, Mol. Cryst., 1, 515 (1966)

Meier H, Dark and Photoconductivity of Organic Solids, (Verlag Chemie) (1973)

Meredith G R, Van Dusen J G, Williams D J, Macromolecules. 15, 1385 (1982)

Miesowicz M, Bull. Intern. Acad. Polon. Ser. A, 228 (1936)

Mircea-Roussel A, Léger L, Rondelez F, Journal de Physique, 36 C1 - 93, (1975)

Möhlmann G R, Van der Vorst CPJM, Side Chain Liquid Crystal Polymers, Ed. McArdle C B (Blackie) (1989)

Movaghar B, J. Mol. Electron., 3, 183 (1987)

Nesrullaev A, Rabinovich A, Sonin A, Sov. Phys. Tech. Phys., 25, 1445 (1980)

Nestor G, White M S, Gray G W, Lacey D, Toyne K J, Makromol. Chem., 188 2759 (1987)

Nestor G, Phd Thesis, University of Hull (1988)

Nordio P G, Rigatti G, Segre U, Molecular Physics, 25 (1), 129 (1973)

Nordio P G, Segre U, The Molecular Physics of Liquid Crystals, Ed. Luckhurst G R, Gray G W, (Academic Press) Chapter 18 (1979)

O'Dwyer J J, The Theory of Electrical Breakdown in Solid Dielectrics, (Oxford) (1973)

O'Konski C T, Edwards A, Rev. Sci. Instrumen., 39 10, 1456 (1968)

Onsager L, J. Am. Chem. Soc., 58, 1486 (1936)

Parneix J P, Njeumo R, Legrand C, Le Barney P, Dubois J C, Liquid Crystals, 2(2), 167 (1987)

Pranoto H, Bormuth F J, Haase W, Kiechle U, Finkelmann H, Makromol. Chem., 187, 2453 (1986)

Reinitzer F, Montash. Chem., 9, 421 (1988)

Rhoderick E H, Metal Semiconductor Contacts, Oxford (1978)

Ringsdorf H, Zentel R, Makeromol. Chem., 183, 1245 (1982)

Sessler G M, Hahn B, Yoon D Y, J. Appl. Phys., 60, 318 (1986)

Shanks I A, Contemp. Physics, 23, 65 (1982)

Shibaev V, Platé N, Freidzon Y, Polym. Sci. Chem. Ed., 17, 1655 (1979)

Shibaev V P, Kostromin S, Plate N, Ivanov S, Yu Vetrov V, Yakovlev I, Polym. Commun., 24, 364 (1983)

Shibaev V P, Platé N A, Advances In Polymer Science, 60/61, 173 (1984)

Shibaev V P, Kostromin S, Platé N, Ivanov S, Yu Vetrov V, Yakolev I, Polym. Sci. Technol., 28, 345 (1985)

Sprokel G J, Mol. Cryst. Liq. Cryst., 22, 249 (1973)

Sprokel G J, Mol. Cryst. Liq. Cryst., 26, 45 (1974)

Sutherland H, Poster, British Liquid Crystal Group Meeting, Hull (1987)

Suzuoki Y, Muto H, Mizutani T, Ieda M, J. Phys. D: Appl. Phys., 18, 2293 (1985)

Suzuoki Y, Muto H, Mizutani T, Ieda M, J. Phy D: Appl. Phys., 20, 1053 (1987)

Sze S M, Physics of Semiconductor Devices, (Wiley) Second Edition (1981)

Szymanski A, Bak G W, J. Phys. D: Appl. Phys., 19, L25 (1986)

Szwajczak E, Szymanski A, Mol. Cryst. Liq. Cryst., 139, 253 (1986)

Tal'roze R V, Shibaev V P, Platé N A, Ploymer Science USSR, 25 (12), 2863 (1983)

Urabe T, Arai K, Ohkoshi A, J. App. Phys. 54(3), 1552 (1983)

Williams G, Watts D C, Trans. Farad. Soc., 66, 80 (1970)

Wissbrun K F, Journal of Rheology, 25(b), 619 (1981)

Yoshino K, Yamashiro K, Tabuchi Y, Inuishi Y., Proc. Conf. Dielectric Materials, Measurements and Applications, Cambridge, 295, 21-25 July (1975)

Zentel R, Strobl G R, Ringsdorf H, Macromolecules, 18, 960 (1985)

Appendices

APPENDIX I

MANUFACTURING PROCESS OF GLASS SANDWICH CELLS

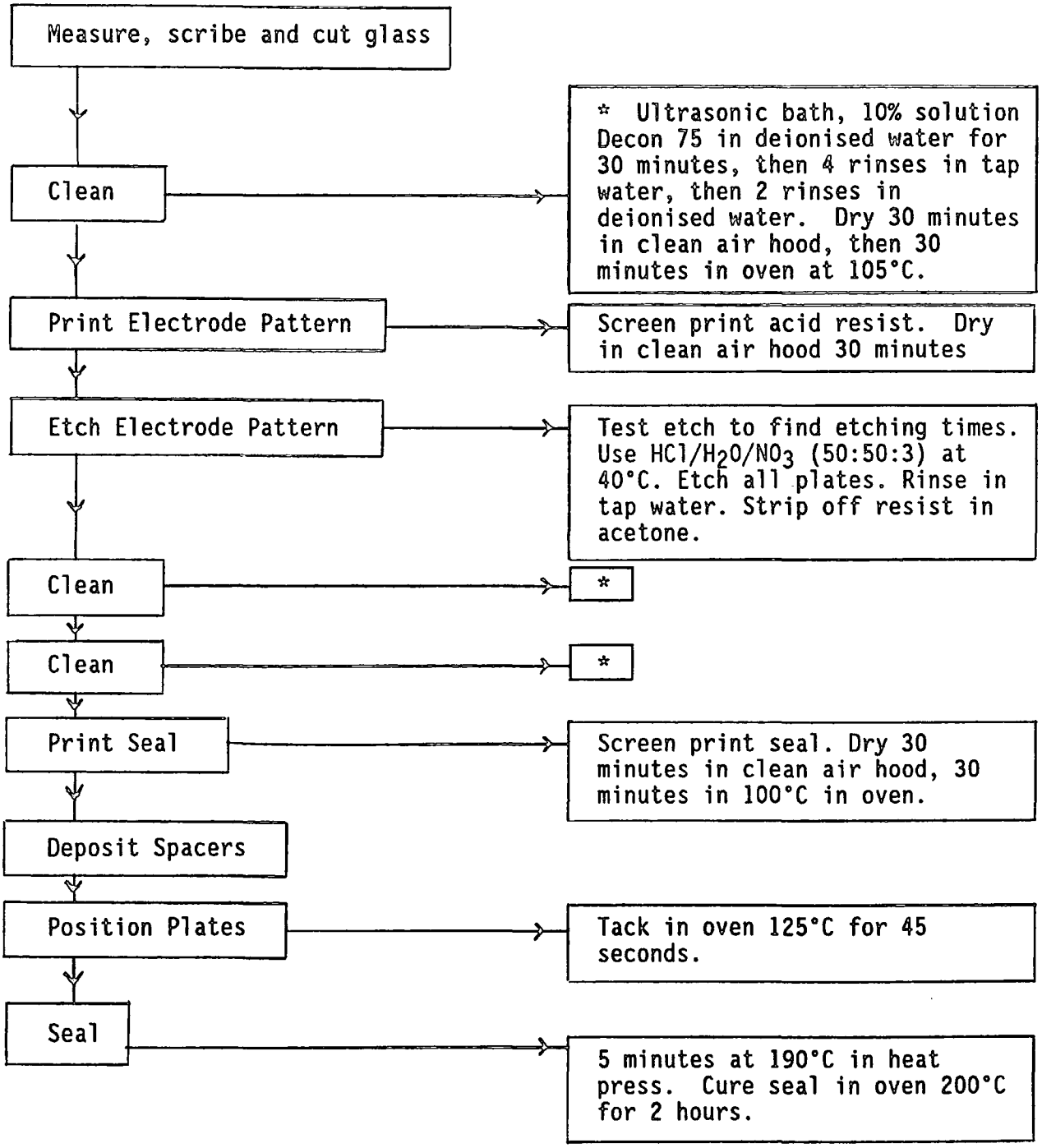

APPENDIX II

THE DEPOSITION OF SURFACTANTS ON INDIUM TIN OXIDE COATED GLASS PLATES

Silicon Monoxide

A coating of silicon monoxide was deposited by the thermal evaporation of SiO granules in a vacuum chamber. The thickness of the film was monitored by a quartz crystal oscillator and was generally about 300 Å. The angle of the plate was either 90° (i.e. perpendicular) to the beam or 60° to the beam. This latter orientation is commonly used to produce a layer which aligns 1mmLCs homogeneously with zero surface tilt.

Organosilane Barrier Layer

"Liquicoat Si" is supplied by E Merck for use in liquid crystal displays as an insulating and hardening layer. It is a silicon dioxide solution which is deposited by spin coating. A solution of 2:3:3 parts of this barrier layer:iso-propanol:butanol was filtered using a 0.2 μm filter before spin coating at 300 rpm for 30 seconds. The coating was dried at 100°C for 10 minutes before being baked at 450°C for 6 hours.

UV Curable Epoxy

The epoxy "Optic Adhesive 63" is supplied by Norland as a sealant for liquid crystal displays. Films of this UV curable epoxy were deposited by spin coating. A solution of 1% of the epoxy in cyclopentanone was spun at 3000 rpm for 30 seconds. The coating was dried at 120°C for 30 minutes and then cured in a UV box for 20 minutes.

Polyimide

Buffed polyimide is commonly used as an alignment layer in liquid crystal displays. An adhesion promoter was spun onto the plate initially and then a solution of 10% polyimide in NMP was spun at 3000 rpm for 30 seconds. The coating was dried at 125°C for 30 minutes and then ramped to 300°C over a two hour period. In some cases, plates were then buffed using a velvet roller, as in liquid crystal display manufacture.

APPENDIX III

CALCULATION OF THEORETICAL DIPOLE MOMENTS OF LCPS

Dipole moments of the mesogenic side groups have been included in the calculation of the LCP effective dipole moments used in Tables 5.3 and 5.4. The method described by Klingbiel et al (1974) has been used together with the dipole moment values shown in Table III. The calculation of the effective dipole moment of GN3/ 3 is shown overleaf to illustrate this method.

i	μ_i	μ_i (Debye)	$\mu_{II,i}$ (Debye)	$\mu_{\perp,i}$ (Debye)
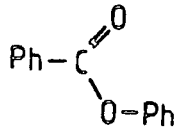		1.90	0.89	1.68
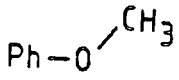		1.28	-0.40	1.22
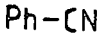		4.18	4.18	0
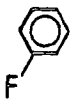		2.19*	-1.1	1.89
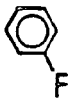		2.19*	1.1	1.89
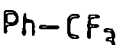		2.39	1.02	2.16

Table III

Dipole moment values used in the calculation of the effective dipole moments of the mesogenic side groups of LCPs. The values were taken from Klingbiel et al (1974) except for those marked * which are from Gordon and Ford (1972).

GN3/3

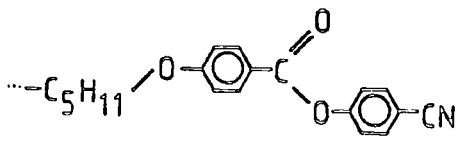

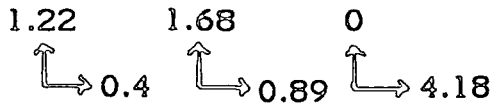

$$\mu_{eff}^2 = \sum \mu_{i,\perp}^2 + \left(\sum \mu_{i,\parallel}\right)^2$$

So

$$\mu_{eff}^2 = (1.22^2 + 1.68^2) + (0.4 + 0.89 + 4.18)^2$$

$$\underline{\mu_{eff} = 5.85 D}$$

$$\underline{\mu_{eff} = 19.5 \times 10^{-30} Cm}$$

APPENDIX IV

STRUCTURES AND TRANSITION DATA OF MATERIALS USED IN THIS WORK (NOT LCPs DESCRIBED IN TABLES 2.2 TO 2.5)

Polymer I

(Attard and Williams, 1986c)

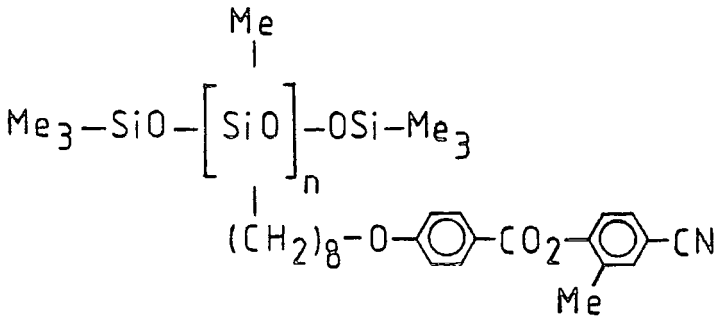

n ~ 50

G 1°C S_A 90°C I

Polymer II

(Araki and Attard, 1986)

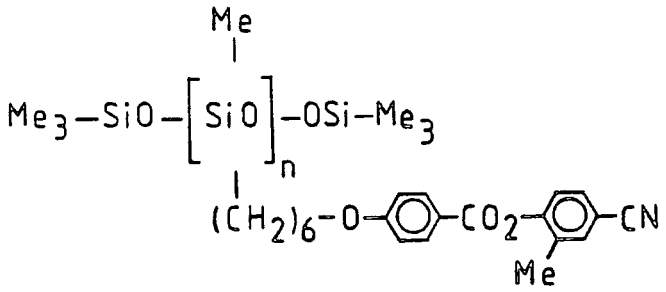

n ~ 35

G 2°C N 41°C I

P^{6}_{50}

(Fabre et al, 1987)

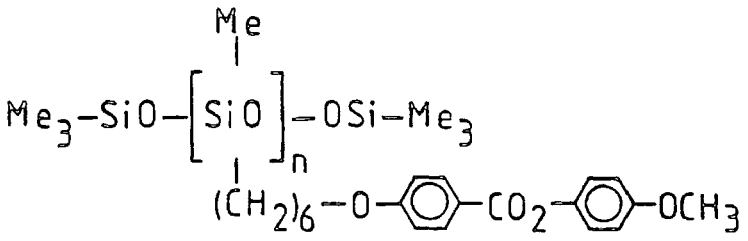

n ~ 50
G 7°C N 106°C I

C6CN

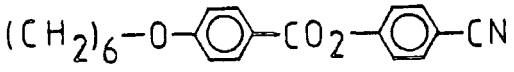

K 69°C N 83°C I

Low Molar Mass Liquid Crystals

Commerical mixtures supplied by BDH Chemicals Ltd

E7	k	-10°C	N	60.5°C	I			
S2	k	-1°C	S_A	48°C	N	49°C	I	
S5	k	1°C	S_A	55.5-55.7°C	N	57.5-61.0°C	I	

Mixtures

These mixtures were prepared for this research. The transition temperatures were measured by polarised light microscopy.

25% GN3/14	:	75% S2	S_A (54.9-59.6°C) I
50% GN3/14	:	50% S2	S_A (68-75.5°C) I
75% GN3/14	:	25% S2	S_A (76.7-84.1°C) I

Blue Pleochroic Dyes

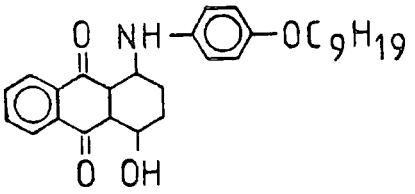

D16

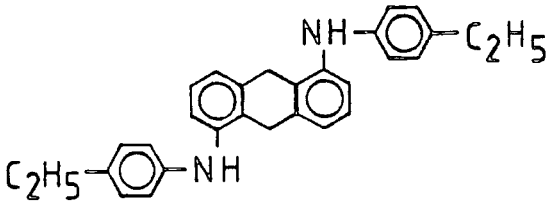

D35

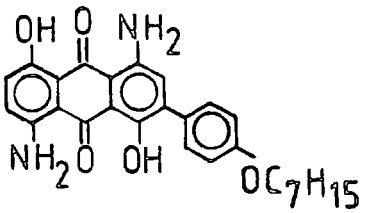

D102